Quantitative pharmacology approaches to inform treatment strategies against tuberculosis

Mehta, K.

Quantitative Pharmacology Approaches to Inform Treatment Strategies Against Tuberculosis

Krina Mehta

Quantitative Pharmacology Approaches to Inform Treatment Strategies Against Tuberculosis

Krina Mehta

Krina Mehta

Quantitative Pharmacology Approaches to Inform Treatment Strategies Against Tuberculosis

PhD Thesis, Leiden University, Leiden, The Netherlands 2024

ISBN: 978-94-6506-056-9

Cover design: Joey Roberts | www.ridderprint.nl
Layout and printing: Ridderprint | www.ridderprint.nl

Quantitative Pharmacology Approaches to Inform Treatment Strategies Against Tuberculosis

Proefschrift

ter verkrijging van
de graad van doctor aan de Universiteit Leiden, op gezag van
rector magnificus prof.dr.ir. H. Bijl,
volgens besluit van het college voor promoties
te verdedigen op donderdag 30 mei 2024
klokke 13:45 uur

door

Krina Mehta

geboren te
Bhavnagar, Gujarat, India
in 1983

Promotores:
Prof. dr. J.G.C. van Hasselt
Prof. dr. P.H. van der Graaf

Promotiecommissie:
Prof. dr. H. Irth
Prof.dr. E.C.M. de Lange
Prof.dr. C.A.J. Knibbe
Dr E.M. Svensson, Uppsala University, Uppsala, Sweden
Prof. dr. R.E. Aarnoutse, Radboud University Medical Center, Netherlands

TABLE OF CONTENTS

Section I.

Introduction

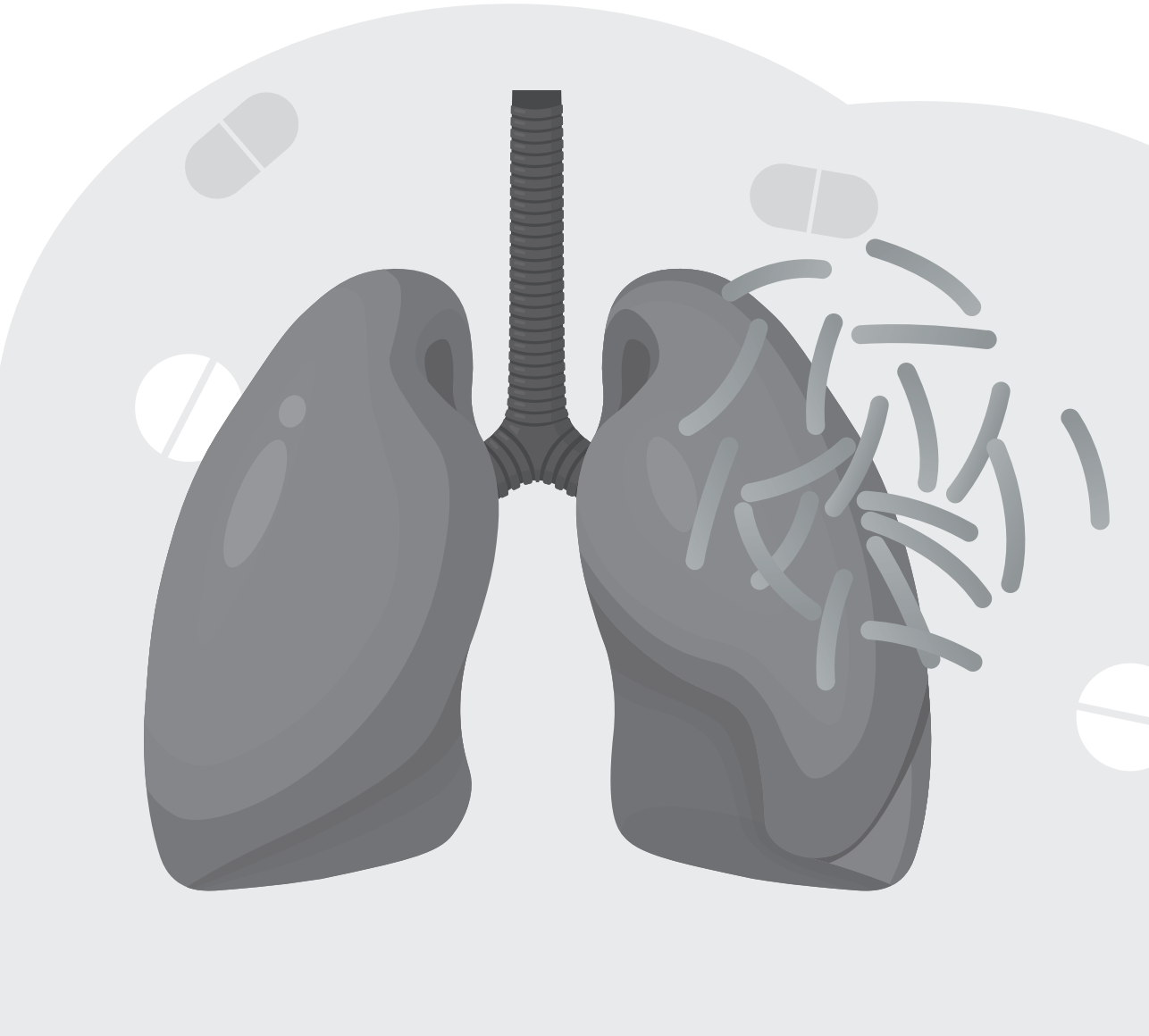

Chapter 1

Introduction and scope of the thesis

Tuberculosis treatment landscape

Tuberculosis (TB) is an infectious disease caused by *Mycobacterium tuberculosis* (Mtb). TB is the oldest known infectious disease with the first documentation dating back to 3300 years ago although it is believed to be that Mtb existed even 70,000 years back[1]. The first isolation of Mtb by Dr. Robert Koch in 1882 marked a key step in the fight against Mtb. Today, more than 140 years later, Mtb infections are still associated with approximately 1.5 – 2 million deaths annually[2]. Initiation of TB infection occurs through the respiratory route by inhalation of aerosols containing Mtb bacteria. In the first few days, Mtb invades pulmonary alveoli of the host and alveolar resident macrophages will ingest Mtb via phagocytosis followed by induction of the host immune response against Mtb. The host immune response will lead to the formation of granulomas that contain Mtb bacilli, where Mtb may remain in a dormant state, also known as latent TB. If granulomas are unable to contain Mtb because they have multiplied significantly, an active TB infection can develop. Approximately 5-10% of individuals with latent TB develop active TB[3]. Individuals with a weakened immune response, i.e., patients with co-morbid conditions, such as HIV, diabetes, and patients taking immunosuppressants are at higher risk of developing active TB. Current first-line treatment of drug-sensitive TB includes a weight-based fixed-dose combination of four antibiotic agents, isoniazid, rifampin, pyrazinamide, and ethambutol. First discovered and developed in the 1960s through early 1970s, isoniazid and rifampin have been the most important drugs in the treatment of patients with TB[4]. Isoniazid is a potent bactericidal drug that inhibits mycolic acid synthesis leading to cell wall synthesis in Mtb **(Figure 1.1)**. Rifampin is also bactericidal against Mtb and inhibits Mtb ribonucleic acid (RNA) polymerase. Pyrazinamide and ethambutol add to the anti-bacterial activity of rifampin and isoniazid and act through Mtb plasma membrane disruption and inhibition of cell wall synthesis, respectively. Overall, this first-line combination treatment regimen results in a reasonable cure rate in patients with drug-sensitive TB; however, various challenges remain as discussed further **(Figure 1.2)**.

Figure 1.1 Mechanism of action of anti-tuberculosis drugs. Adapted based on Zumla et al., 2013[4]. Figure created with biorender.com.

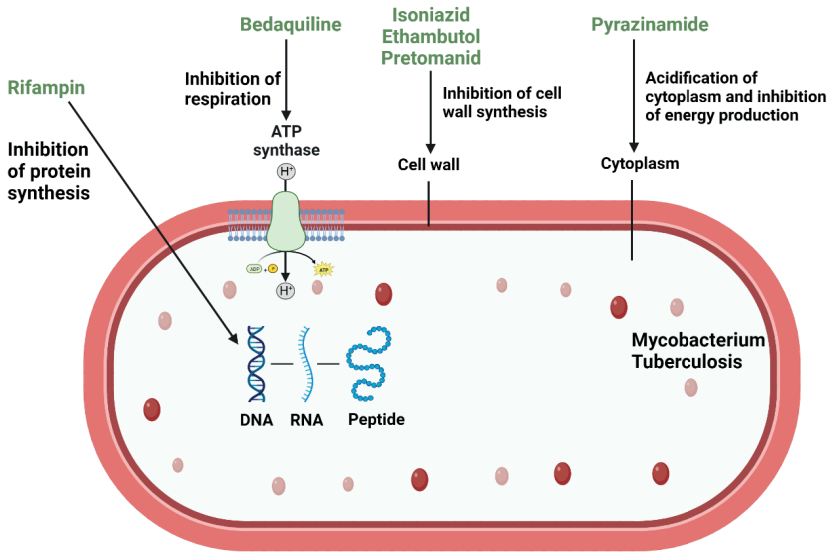

Current challenges of tuberculosis therapeutics

Mtb has evolved and developed resistance mechanisms. The key mechanism of resistance development against antibiotics includes a subpopulation of Mtb, persisters, which are phenotypically resistant against the drugs without genetic mutations.[5,45,46] Factors contributing to Mtb developing phenotypic resistance against drugs include interruptions in treatment, suboptimal drug concentrations, and poor host immune response against Mtb. Over time, phenotypic resistance leads to the development of genetic mutations resulting in the proliferation and transmission of drug-resistant Mtb strains.[5,45,46] Various forms of drug-resistant TB exist, including, rifampin-resistant TB (RR-TB), rifampin- and isoniazid-resistant TB (known as multi-drug resistant TB (MDR-TB)), and extensive form of MDR-TB (XDR-TB) that is resistant to rifampin, isoniazid, and one or more additional anti-TB drugs. Together, drug-resistant TB constitutes 450,000 TB cases globally in 2021. As such, drug-resistant TB is a major global health challenge[6].

Figure 1.2 Current challenges against the treatment of tuberculosis.

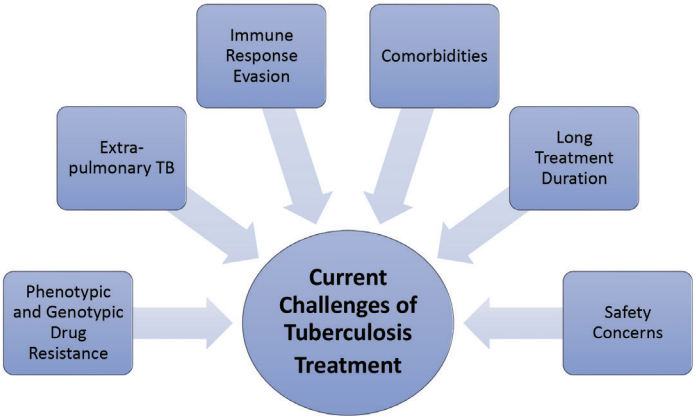

Prior to availability of bedaquiline and other newer anti-TB drugs, standard regimens for MDR-TB included a combination of five or more drugs. These combination regimens against MDR-TB were associated with toxicity issues and had poor efficacy outcomes with approximately 20% cure rate only. Bedaquiline, the first newly approved anti-TB drug in 40 years, is a diarylquinoline and inhibits Mtb adenosine triphosphate synthesis to exert its bactericidal effect[7]. Bedaquiline-containing regimens have shown reasonable efficacy in MDR-TB patients[8,9]. Increased prevalence of RR-TB and MDR-TB cases and bedaquiline development was followed by a revival in anti-TB research leading to the development and approvals of nitroimidazoles, pretomanid and delamanid, in the last decade[10]. The new, all-oral, combination regimen of bedaquiline, pretomanid, and linezolid (BPaL) showed approximately 90% cure rate and is now endorsed by the WHO for the treatment of MDR-TB[11,12]. Additional drug combinations including these newer drugs are being evaluated for the treatment of various forms of drug-resistant TB[47-49].

TB primarily affects the lungs; however, Mtb may get disseminated into the lymphatics, distribute through systemic circulation, and infect other organs leading to extrapulmonary TB. Extrapulmonary TB is generally difficult to diagnose and treat. The most severe form of extrapulmonary TB is TB meningitis (TBM) affecting the central nervous system (CNS). TBM is associated with high morbidity and mortality with approximately half the patients suffering from severe neurologic disability or death[13]. Treatment of TB meningitis is especially challenging due to poor penetration of anti-TB drugs, especially rifampin, into CNS[14]. Standard treatment of TBM patients remains the same as the first-line treatment of pulmonary TB patients; however, high morbidity and mortality rates remain. As

such, the efficacy and safety of intensified dosing schedules are being evaluated for the treatment of patients with TBM. There has been an increasing trend in the prevalence of drug resistance amongst TBM patients[15–18]. Currently, no standard treatment recommendations for drug-resistant TBM, and treatment approaches are generally selected by treating physicians based on individual patient factors often including extensive treatment with more than 5 drugs. Safety concerns about extensive treatments and high mortality rate (69-100%) amongst drug-resistant TBM patients persist[15].

Mtb has developed several mechanisms to evade host immune-mediated eradiation to allow its survival and virulence in the host, such as inhibition of autophagy and apoptosis, inhibition of antigen presentation, inducing changes in host transcriptomics and cytokine balance, development of resistance against anti-Mtb treatment, etc. Understanding the mechanistic details of host-pathogen interactions is essential to develop new treatment approaches against Mtb. Comorbidities, especially human immunodeficiency virus (HIV) infections or type II diabetes mellitus, are associated with higher morbidity and mortality in TB patients due to their immunosuppressive nature[19,20]. HIV co-infection has also been associated with decreased exposures to several key anti-TB drugs[21–23]. Treatment of the comorbidities further increases the likelihood of drug-drug interactions[24]. Additional studies are needed to develop treatment and patient management plans for TB patients with comorbidities[25]. Current treatment duration ranges from 6 to 9 months for the majority of patients, with some patients, especially with MDR-TB and XDR-TB, requiring treatment up to 18 to 24 months[11]. Such long treatment duration leads to safety issues, increased economic burden, and treatment adherence issues, and significantly affects patients' quality of life[26]. Several studies have evaluated potential shorter combination treatment regimens but have yielded variable results[26,27,50]. It has been suggested that the required duration of TB treatment is highly dependent on various patient and disease factors. Overall, further evaluations are needed to develop innovative, shorter, efficacious, and safer treatment optimization approaches against pulmonary, extra-pulmonary, drug-sensitive, drug-resistant Mtb infections.

Quantitative pharmacology approaches for anti-tuberculosis therapeutics

The current challenges in the fight against Mtb infections call for innovative drug development and treatment approaches. Quantitative pharmacology combines concepts from biology, pharmacology, mathematics, statistics, and data science to inform drug development and treatment decisions across various therapeutic areas, including TB[28,29]. Various quantitative approaches, ranging from population pharmacokinetic (PopPK) and population pharmacokinetic-pharmacodynamic (PopPKPD) modeling to quantitative systems pharmacology (QSP) approaches, have been employed to streamline and optimize anti-TB drug development and treatment approaches[30–32]. Extensive work using PopPK and PopPKPD approaches for anti-TB therapeutics has been performed to date[33–36]. These models allowed thorough characterization of PK and PD of various anti-TB drugs using rich clinical trial data. Population models have enabled the exploration and identification of the roles of covariates, i.e., intrinsic and extrinsic factors, on PK and PD of anti-TB drugs. Such models have played a key role in determining dosing regimens for many anti-TB drugs. Semi-mechanistic models including target site compartments allowed the quantification of biodistribution of several anti-TB drugs into lungs and TB lesions in lungs[37–39]. Semi-mechanistic multi-state tuberculosis pharmacometrics (MTP) models describing dynamics of fast-, slow-, and non-replicating Mtb populations have been developed utilizing in vitro, mouse, and clinical data[30,32]. Such models allowed predictions of drug effects on the sub-population of Mtb rifampin[35,40]. The MTP model combined with PD models have been used to translate treatment effects from preclinical experiments to patients. The MTP model combined with PD interaction models to estimate optimal doses of individual drugs in combination therapy have been evaluated[41]. Physiologically-based pharmacokinetic (PBPK) models of anti-TB have been developed to perform drug metabolism and drug-drug interaction evaluations[42,43]. Extended PBPK models including multi-compartment lungs have also been developed to further understand the target site distribution of drugs[44]. QSP models of capturing the dynamics of bacterial and key immune response markers following Mtb infections have also been developed and combined with PK-PD models of first-line anti-TB drugs to explore the impact of immune effects on treatment outcomes[31]. These examples highlight how quantitative pharmacology has influenced the development and optimization of anti-TB therapeutics. However, several key challenges still persist, for example, translation of PK and efficacy from preclinical to patients, emergence of drug resistance, long treatment duration, poor treatment outcome in some patients especially with drug-resistant TB, extrapulmonary TB, and/or comorbidities, safety and adherence concerns, etc. **(Figure 1.2)**. Due to the

multifaceted nature of TB disease and the current challenges in its treatment, there is a necessity for increased efforts utilizing quantitative pharmacology approaches. These efforts can play a crucial role in the development of treatment strategies that are both more effective and safer.

Scope of the thesis

The main objective of this thesis was to employ different quantitative pharmacology approaches to evaluate treatment optimization strategies for anti-TB therapeutics. In section II and III, we demonstrated applications of modeling and simulations to optimize treatment of first-line anti-TB therapeutics and newer anti-TB therapeutics, respectively by accounting for target site exposures, patient covariates, translational aspects, etc. In section IV, we discuss the utilization of QSP modeling to guide the development of host-directed therapies against Mtb infections. Lastly, in section V, we discuss a summary of our quantitative pharmacology analyses and discuss future perspectives to help eradicate TB. In Section II, we focus on quantitative pharmacology approaches for first-line anti-TB therapeutics, ethambutol, rifampin, and isoniazid. In **Chapter 2**, PopPK analysis of ethambutol in TB patients co-infected with HIV was performed. Covariate analysis was performed to evaluate the impact of HIV infection on the PK of ethambutol in pulmonary TB patients. PK target attainment simulations were performed to recommend alternative ethambutol dosing in TB patients co-infected with HIV. In **Chapter 3**, a whole-body PBPK modeling approach was used to evaluate the role of patient pharmacogenetic variability in determining the site of action target attainment in TBM patients. Rifampin and isoniazid PBPK models that included SLCO1B1 and NAT2 effects on exposures respectively were developed and validated using available cerebrospinal-fluid (CSF) concentrations from TB patients. Simulations were conducted to evaluate the combined effects of pharmacogenetic and Mtb minimum inhibitory concentrations (MIC) variability on target attainment at the site of action, brain, in TBM patients. In Section III, we focused on applying quantitative pharmacology approaches for newer anti-TB treatment regimens, including bedaquiline and pretomanid. In **Chapter 4**, bedaquiline and pretomanid translational mPBPK models were developed to predict site-of-action exposures and the probability of target attainment in TB patients. The probability of target attainment was calculated by comparing predicted target-site concentrations with minimal bactericidal concentrations (MBC) reported in the literature. In **Chapter 5**, a mechanistic framework was developed for a new combination regimen, bedaquiline, pretomanid, and linezolid (BPaL). The framework included key components that play a role in the overall response to the

therapy, such as patient body weight, TB lesion volume, target-site drug exposures, and individual patient and drug MICs. Simulations were conducted to predict anti-bacterial activity following BPaL current and alternative dosing strategies in virtual drug-resistant TB patients. In **Chapter 6**, a whole-body PBPK model with a CNS compartment was developed for bedaquiline and its active metabolite, M2, using bedaquiline and M2 PK data from plasma and CSF of TB patients. Simulations were conducted to predict target site drug concentrations to evaluate the feasibility of bedaquiline-containing regimens as a treatment option for MDR-TBM patients. In Section IV, we discuss innovative treatment approaches of host-directed therapies (HDT) for the treatment of TB. In **Chapter 7**, we review key host-pathogen interaction mechanisms as the basis of HDTs against Mtb. We introduce the components and utility of QSP approaches to support the identification and optimization of host-directed treatment targets, to facilitate preclinical to human translation, and to design combination treatment strategies including host-directed therapies. In **Chapter 8**, we developed a quantitative systems pharmacology (QSP) framework to evaluate the effects of metformin-associated autophagy induction in combination with first-line anti-TB therapy in patients. Simulations were conducted for adjunctive HDT therapy with metformin in newly diagnosed TB patients. In Section V, we discuss a summary of the evaluations and discuss future perspectives in utilizing quantitative pharmacology approaches for optimization of treatment approaches for TB therapeutics to eradicate TB.

References

1. Barberis I, Bragazzi NL, Galluzzo L, Martini M. The history of tuberculosis: from the first historical records to the isolation of Koch's bacillus. *J Prev Med Hyg*. 2017;58(1):E9-E12.
2. Nahid P, Dorman SE, Alipanah N, et al. Executive Summary: Official American Thoracic Society/Centers for Disease Control and Prevention/Infectious Diseases Society of America Clinical Practice Guidelines: Treatment of Drug-Susceptible Tuberculosis. *Clinical Infectious Diseases*. 2016;63(7):853-867. doi:10.1093/cid/ciw566
3. World Health Organization. Consolidated Operational Guidelines on Handbook Tuberculosis.; 2020.
4. Zumla A, Nahid P, Cole ST. Advances in the development of new tuberculosis drugs and treatment regimens. *Nature Reviews Drug Discovery*. 2013;12(5):388-404. doi:10.1038/nrd4001
5. Zhang Y, Yew WW. Mechanisms of drug resistance in Mycobacterium tuberculosis: update 2015. *Int J Tuberc Lung Dis*. 2015;19(11):1276-1289. doi:10.5588/ijtld.15.0389
6. WHO Consolidated Guidelines on Tuberculosis Module 4: Treatment Drug-Resistant Tuberculosis Treatment Module 4: Treatment WHO Operational Handbook on Tuberculosis Drug-Resistant Tuberculosis Treatment.; 2020. http://apps.who.int/bookorders.
7. van Heeswijk RPG, Dannemann B, Hoetelmans RMW. Bedaquiline: A review of human pharmacokinetics and drug-drug interactions. *Journal of Antimicrobial Chemotherapy*. 2014;69(9):2310-2318. doi:10.1093/jac/dku171
8. Pym AS, Diacon AH, Tang SJ, et al. Bedaquiline in the treatment of multidrug- and extensively drug-resistant tuberculosis. *Eur Respir J*. 2016;47(2):564-574. doi:10.1183/13993003.00724-2015
9. Khoshnood S, Goudarzi M, Taki E, et al. Bedaquiline: Current status and future perspectives. *Journal of Global Antimicrobial Resistance*. 2021;25:48-59. doi:10.1016/j.jgar.2021.02.017
10. Mudde SE, Upton AM, Lenaerts A, Bax HI, De Steenwinkel JEM. Delamanid or pretomanid? A Solomonic judgement! *Journal of Antimicrobial Chemotherapy*. 2022;77(4):880-902. doi:10.1093/jac/dkab505
11. WHO operational handbook on tuberculosis. Module 4: treatment - drug-resistant tuberculosis treatment, 2022 update. Published online December 15, 2022. Accessed December 6, 2023. https://www.who.int/publications/i/item/9789240065116
12. Conradie F, Diacon AH, Ngubane N, et al. Treatment of Highly Drug-Resistant Pulmonary Tuberculosis. *New England Journal of Medicine*. 2020;382(10):893-902. doi:10.1056/nejmoa1901814
13. Navarro-Flores A, Fernandez-Chinguel JE, Pacheco-Barrios N, Soriano-Moreno DR, Pacheco-Barrios K. Global morbidity and mortality of central nervous system tuberculosis: a systematic review and meta-analysis. *J Neurol*. 2022;269(7):3482-3494. doi:10.1007/s00415-022-11052-8
14. Dooley KE. High-Dose Rifampin: Shall We Be Bolder? *Am J Respir Crit Care Med*. 2018;198(5):558-560. doi:10.1164/rccm.201806-1140ED
15. Evans EE, Avaliani T, Gujabidze M, et al. Long term outcomes of patients with tuberculous meningitis: The impact of drug resistance. *PLoS One*. 2022;17(6):e0270201. doi:10.1371/journal.pone.0270201
16. Vinnard C, Winston CA, Wileyto EP, Macgregor RR, Bisson GP. Isoniazid resistance and death in patients with tuberculous meningitis: retrospective cohort study. *BMJ (Clinical research ed)*. 2010;341:c4451. doi:10.1136/bmj.c4451
17. Vinnard C, King L, Munsiff S, et al. Long-term mortality of patients with tuberculous meningitis in New York city: A cohort study. *Clinical Infectious Diseases*. 2017;64(4):401-407. doi:10.1093/cid/ciw763
18. Gopalaswamy R, Dusthackeer VNA, Kannayan S, Subbian S. Extrapulmonary Tuberculosis—An Update on the Diagnosis, Treatment and Drug Resistance. *Journal of Respiration*. 2021;1(2):141-164. doi:10.3390/jor1020015

19. Cáceres G, Calderon R, Ugarte-Gil C. Tuberculosis and comorbidities: treatment challenges in patients with comorbid diabetes mellitus and depression. *Ther Adv Infect Dis*. 2022;9:20499361221095831. doi:10.1177/20499361221095831

20. Ronacher K, Joosten SA, van Crevel R, Dockrell HM, Walzl G, Ottenhoff THM. Acquired immunodeficiencies and tuberculosis: focus on HIV/AIDS and diabetes mellitus. *Immunol Rev*. 2015;264(1):121-137. doi:10.1111/imr.12257

21. Vinnard C, Ravimohan S, Tamuhla N, et al. Isoniazid clearance is impaired among human immunodeficiency virus/tuberculosis patients with high levels of immune activation. *British Journal of Clinical Pharmacology*. 2017;83(4):801-811. doi:10.1111/bcp.13172

22. Vinnard C, Ravimohan S, Tamuhla N, et al. Markers of gut dysfunction do not explain low rifampicin bioavailability in HIV-associated TB. *Journal of Antimicrobial Chemotherapy*. 2017;72(7):2020-2027. doi:10.1093/jac/dkx111

23. Mehta K, Ravimohan S, Pasipanodya JG, et al. Optimizing ethambutol dosing among HIV/tuberculosis co-infected patients: a population pharmacokinetic modelling and simulation study. *J Antimicrob Chemother*. 2019;74(10):2994-3002. doi:10.1093/jac/dkz265

24. Pooranagangadevi N, Padmapriyadarsini C. Treatment of Tuberculosis and the Drug Interactions Associated With HIV-TB Co-Infection Treatment. *Frontiers in Tropical Diseases*. 2022;3. https://www.frontiersin.org/articles/10.3389/fitd.2022.834013

25. Dzinamarira T, Imran M, Muvunyi CM. The Management of Infectious Diseases in Comorbidity with Tuberculosis. *Medicina (Kaunas)*. 2022;58(10). doi:10.3390/medicina58101406

26. Aggarwal AN. Quality of life with tuberculosis. *J Clin Tuberc Other Mycobact Dis*. 2019;17:100121. doi:10.1016/j.jctube.2019.100121

27. de Miranda Silva C, Hajihosseini A, Myrick J, et al. Effect of Moxifloxacin plus Pretomanid against Mycobacterium tuberculosis in Log Phase, Acid Phase, and Nonreplicating-Persister Phase in an In Vitro Assay. *Antimicrobial Agents and Chemotherapy*. 2019;63(1). doi:10.1128/AAC.01695-18

28. Wilkins JJ, Svensson EM, Ernest JP, Savic RM, Simonsson USH, McIlleron H. Pharmacometrics in tuberculosis: progress and opportunities. *International Journal of Antimicrobial Agents*. 2022;60(3). doi:10.1016/j.ijantimicag.2022.106620

29. Dooley KE, Hanna D, Mave V, Eisenach K, Savic RM. Advancing the development of new tuberculosis treatment regimens: The essential role of translational and clinical pharmacology and microbiology. *PLoS Med*. 2019;16(7):e1002842. doi:10.1371/journal.pmed.1002842

30. Ernest JP, Strydom N, Wang Q, et al. Development of New Tuberculosis Drugs: Translation to Regimen Composition for Drug-Sensitive and Multidrug-Resistant Tuberculosis. *Annual Review of Pharmacology and Toxicology*. 2021;61:495-516. doi:10.1146/annurev-pharmtox-030920-011143

31. Fors J, Strydom N, Fox WS, Keizer RJ, Savic RM. Mathematical Model and Tool to Explore Shorter Multi-Drug Therapy Options for Active Pulmonary Tuberculosis. Vol 16.; 2020. doi:10.1371/journal.pcbi.1008107

32. Bartelink IH, Zhang N, Keizer RJ, et al. New Paradigm for Translational Modeling to Predict Long-term Tuberculosis Treatment Response. *Clinical and Translational Science*. 2017;10(5):366-379. doi:10.1111/cts.12472

33. Sturkenboom MGG, Märtson AG, Svensson EM, et al. Population Pharmacokinetics and Bayesian Dose Adjustment to Advance TDM of Anti-TB Drugs. *Clinical Pharmacokinetics*. 2021;60(6):685-710. doi:10.1007/s40262-021-00997-0

34. McLeay SC, Vis P, Van Heeswijk RPG, Green B. Population pharmacokinetics of bedaquiline (TMC207), a novel antituberculosis drug. *Antimicrobial Agents and Chemotherapy*. 2014;58(9):5315-5324. doi:10.1128/AAC.01418-13

35. Svensson RJ, Simonsson USH. Application of the multistate tuberculosis pharmacometric model in patients with rifampicin-treated pulmonary tuberculosis. *CPT: Pharmacometrics and Systems Pharmacology*. 2016;5(5):264-273. doi:10.1002/psp4.12079

36. Lyons MA. Pharmacodynamics and Bactericidal Activity of Combination Regimens in Pulmonary Tuberculosis: Application to Bedaquiline-Pretomanid-Pyrazinamide. *Antimicrobial Agents and Chemotherapy*. 2022;66(12). doi:10.1128/aac.00898-22

37. Strydom N, Gupta SV, Fox WS, et al. Tuberculosis Drugs' Distribution and Emergence of Resistance in Patient's Lung Lesions: A Mechanistic Model and Tool for Regimen and Dose Optimization. Vol 16.; 2019. doi:10.1371/journal.pmed.1002773

38. Tucker EW, Guglieri-Lopez B, Ordonez AA, et al. Noninvasive (11)C-rifampin positron emission tomography reveals drug biodistribution in tuberculous meningitis. *Sci Transl Med*. 2018;10(470). doi:10.1126/scitranslmed.aau0965

39. Ordonez AA, Wang H, Magombedze G, et al. Heterogeneous Drug Exposures in Pulmonary Lesions. *HHS Public Access*. 2020;26(4):529-534. doi:10.1038/s41591-020-0770-2.Dynamic

40. Wicha SG, Huisinga W, Kloft C. Translational pharmacometric evaluation of typical antibiotic broad-spectrum combination therapies against Staphylococcus aureus exploiting in vitro information. *CPT: Pharmacometrics and Systems Pharmacology*. 2017;6(8):515-522. doi:10.1002/psp4.12197

41. Susanto BO, Wicha SG, Hu Y, Coates ARM, Simonsson USH. Translational Model-Informed Approach for Selection of Tuberculosis Drug Combination Regimens in Early Clinical Development. *Clinical Pharmacology and Therapeutics*. 2020;108(2):274-286. doi:10.1002/cpt.1814

42. Hanke N, Frechen S, Moj D, et al. PBPK Models for CYP3A4 and P-gp DDI Prediction: A Modeling Network of Rifampicin, Itraconazole, Clarithromycin, Midazolam, Alfentanil, and Digoxin. *CPT: Pharmacometrics and Systems Pharmacology*. 2018;7(10):647-659. doi:10.1002/psp4.12343

43. Cordes H, Thiel C, Aschmann HE, Baier V, Blank LM, Kuepfer L. A physiologically based pharmacokinetic model of isoniazid and its application in individualizing tuberculosis chemotherapy. *Antimicrobial Agents and Chemotherapy*. 2016;60(10):6134-6145. doi:10.1128/AAC.00508-16

44. Gaohua L, Wedagedera J, Small BG, et al. Development of a Multicompartment Permeability-Limited Lung PBPK Model and Its Application in Predicting Pulmonary Pharmacokinetics of Antituberculosis Drugs. *CPT: Pharmacometrics and Systems Pharmacology*. 2015;4(10):605-613. doi:10.1002/psp4.12034

45. Allué-Guardia A, Garcia-Vilanova A, Olmo-Fontánez AM, et al. Host- and age-dependent transcriptional changes in Mycobacterium tuberculosis cell envelope biosynthesis genes after exposure to human alveolar lining fluid. Int J Mol Sci. 2022;23(2). https:// www. mdpi. com/ 1422- 0067/ 23/2/983.

46. Chesov E, Chesov D, Maurer FP, et al. Emergence of bedaquiline resistance in a high tuberculosis burden country. Eur Respir J. 2022;59(3):1–10. https:// doi. org/ 10. 1183/ 13993 003. 00621- 2021.

47. Guglielmetti L, Ardizzoni E, Atger M, et al. Evaluating newly approved drugs for multidrug-resistant tuberculosis (endTB): study protocol for an adaptive, multi-country randomized controlled trial. Trials. 2021 Sep 25;22(1):651. doi: 10.1186/s13063-021-05491-3.

48. Seung KJ, Khan P, Franke MF, et al. Culture Conversion at 6 Months in Patients Receiving Delamanid-containing Regimens for the Treatment of Multidrug-resistant Tuberculosis. Clin Infect Dis. 2020 Jul 11;71(2):415-418. doi: 10.1093/cid/ciz1084. Erratum in: Clin Infect Dis. 2023 Jan 13;76(2):374.

49. Tweed CD, Dawson R, Burger DA, , et al. Bedaquiline, moxifloxacin, pretomanid, and pyrazinamide during the first 8 weeks of treatment of patients with drug-susceptible or drug-resistant pulmonary tuberculosis: a multicentre, open-label, partially randomised, phase 2b trial. Lancet Respir Med. 2019 Dec;7(12):1048-1058. doi: 10.1016/S2213-2600(19)30366-2.

50. Pranay Sinha, Karen R Jacobson, C Robert Horsburgh, Carlos Acuña-Villaorduña. At Long Last: Short, All-Oral Regimens for Multidrug-Resistant Tuberculosis in the United States, Open Forum Infectious Diseases, Volume 10, Issue 4, April 2023, ofad177, https://doi.org/10.1093/ofid/ofad177.

Section II.

Quantitative Pharmacology Approaches for First-Line Anti-Tuberculosis Therapeutic

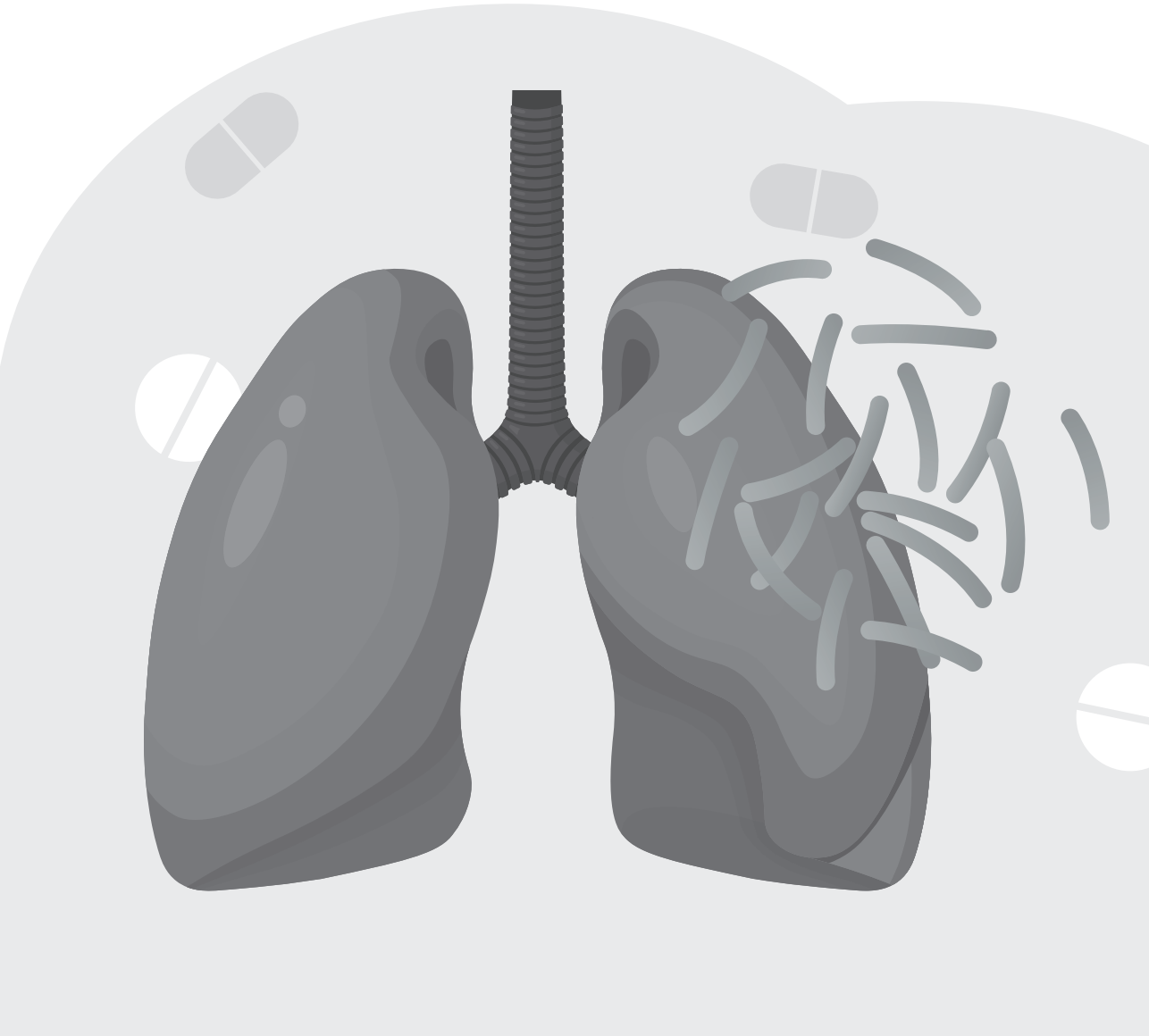

Chapter 2

Optimizing ethambutol dosing among HIV/tuberculosis co-infected patients: a population pharmacokinetic modelling and simulation study

Krina Mehta, Shruthi Ravimohan, Jotam G. Pasipanodya, Shashikant Srivastava, Chawangwa Modongo, Nicola M. Zetola, Drew Weissman, Vijay Ivaturi, Tawanda Gumbo, Gregory P. Bisson, and Christopher Vinnard

J Antimicrob Chemother. 2019 Oct 1;74(10):2994-3002

Abstract

Background: Reduced ethambutol serum concentrations are commonly observed among tuberculosis (TB) patients co-infected with human immunodeficiency virus (HIV) and may lead to treatment failure.

Objectives: To perform a population pharmacokinetic study of ethambutol in HIV/TB patients, and to evaluate an intensified ethambutol weight-based dosing strategy to support pharmacokinetic target attainment.

Methods: We conducted a prospective study of ethambutol pharmacokinetics among HIV/TB patients administered first-line TB treatment in Botswana, with study visits before and after initiation of antiretroviral therapy (ART). Clinical and disease status markers, including HIV-associated systemic immune activation and gut dysfunction biomarkers, were evaluated as covariates of ethambutol pharmacokinetic parameters in non-linear mixed effects analysis. Monte Carlo simulations were performed to compare pharmacokinetic target attainment under standard and intensified weight-based ethambutol dosing strategies.

Results: We studied 40 HIV/TB patients prior to initiation of ART, of whom 24 returned for a second visit a median of 33 days following ART initiation. Ethambutol serum concentrations were best explained by a two-compartment model with first-order elimination, with a significant improvement in oral bioavailability following ART initiation. In Monte Carlo simulations, a supplementary ethambutol dose of 400mg daily led to >2-fold improvements in pharmacokinetic target attainment probabilities in lung tissue, both before and after ART initiation.

Conclusions: Low serum ethambutol concentrations were commonly observed among HIV/TB patients in Botswana, and the oral bioavailability of ethambutol increased following ART initiation. Supplementary ethambutol dosing among HIV/TB patients may provide a strategy to optimize anti-TB treatment regimens in this high-risk population.

Introduction

Ethambutol is a key drug in the first-line TB treatment regimen worldwide, protecting companion drugs against acquired drug resistance and acting synergistically with rifampicin for sterilizing effect in a concentration-dependent fashion.[1-3] More recently, ethambutol has also demonstrated utility in second-line treatment regimens for multi-drug resistant TB (MDR-TB) (caused by Mycobacterium tuberculosis resistant to both isoniazid and rifampicin) in the shortened WHO regimen.[4] Ethambutol demonstrates high partitioning into the center and walls of tuberculous cavities, which likely contributes to its sterilizing effect.[5] Efficacy advantages are counter-balanced by the potential for toxicity, in particular an optic neuritis that is driven by cumulative exposures in a dose-dependent manner.[6-7] However, the mechanism of ethambutol-induced optic neuritis remains undefined, and consequently the optimal strategy for ethambutol dosing among TB patients is uncertain.

Weight-based dosing strategies using fixed-dose combinations of anti-TB drugs are the mainstay of the WHO Global TB Program. These combination regimens were largely developed before the emergence of the HIV epidemic. Administered as daily therapy, ethambutol weight-based dosing bands center around 15–25 mg/kg, without dose adjustment for HIV co-infection or other comorbid diseases. Some, but not all, clinical studies have demonstrated that HIV co-infection is associated with low ethambutol concentrations in peripheral blood.[8-12] Mycobacterial killing by ethambutol is concentration dependent, while prevention of resistance is driven by the proportion of time that ethambutol concentrations persist above the minimum inhibitory concentrations (MIC).[13,14] Thus, low ethambutol exposures may increase the risk of TB treatment failure and the emergence of drug resistance, outcomes that are more commonly observed among TB patients co-infected with HIV.[15,16]

We conducted a prospective study to evaluate the pharmacokinetics of the first-line anti-TB drugs (rifampicin, isoniazid, pyrazinamide and ethambutol) administered via fixed-dose combinations among HIV/TB co-infected patients in Botswana. Here, we report the population pharmacokinetic model of ethambutol, followed by Monte Carlo simulations to identify target attainment probabilities in lung tissue under standard and intensified weight-based dosing strategies.

Methods

Ethics

The study was approved by institutional review boards of the Ministry of Health of Botswana and the University of Pennsylvania. Written informed consent was obtained from all participants.

Study design

We identified ethambutol pharmacokinetic parameters among HIV/TB patients in Gaborone, Botswana, using an intensive pharmacokinetic sampling design. The population pharmacokinetic models for rifampicin, isoniazid and pyrazinamide identified in this study cohort have been previously reported. We measured clinical and disease status markers, including measures of HIV-associated immune activation and gut dysfunction, before and after initiation of ART.

Study population

A detailed description of the study population has been reported.[17] In brief, we enrolled HIV-infected patients >21 years of age who were naive to ART and newly diagnosed with pulmonary TB. We included patients initiated on the standard first-line TB regimen, dosed according to weight-based bands as recommended in WHO guidelines, consistent with the policy of the Botswana National TB Program. Ethambutol was administered as daily therapy according to standard weight-based dosing bands (550 mg if <40kg, 825 mg if 41–55 kg, 1100 mg if 55–70kg, 1375 mg if >70 kg). Exclusion criteria included pregnancy, renal insufficiency (defined as a creatinine clearance (CL_{CR}) <50mL/min) and hepatic dysfunction (defined as either alanine transaminase (ALT) or aspartate transaminase (AST) greater than three times the upper limit of normal).

Data collection

Study procedures included one or two pharmacokinetic study visits for each enrolled patient. The first visit occurred 5–28 days after initiation of standard TB therapy and was performed in each instance prior to the initiation of ART. All participants were eligible to complete a second pharmacokinetic study visit after ART had been initiated. The procedures at both study visits (i.e., pre- and post-ART) were identical. After an overnight fast, the anti-TB drugs were administered by directly observed therapy. Blood samples (10mL) were drawn at 0, 0.3, 0.9, 2.2, 4.5

and 8 h post-dosing, with these timepoints selected according to optimal sampling theory.[20] Clinical and demographic information included age, gender, weight, BMI, serum creatinine, HIV viral load and CD4+ T cell count.

We evaluated additional HIV disease markers as potential covariates related to ethambutol pharmacokinetic variability, including systemic immune activation, microbial translocation and gut dysfunction. HIV associated systemic immune activation was measured as the percentage of CD38+ T cells co-expressing HLA-DR and CD38 (%CD38+DR+CD8+).[21] Other systemic inflammatory markers included plasma levels of neopterin, IL-6 and C-reactive protein (CRP). We also evaluated markers of gut dysfunction related to HIV-associated immune activation, including soluble CD14 (sCD14), a marker of macrophage activation in the LPS pathway,[22] and intestinal fatty acid-binding protein (I-FABP), a measure of intestinal damage.[23]

Analytical methods

Markers of immune activation and gut damage

Blood samples were transported to the Botswana Harvard Partnership Laboratory. We performed plasma and PBMC isolation using Ficoll-Paque Plus (GE Healthcare) density gradient centrifugation. Plasma assays for sCD14, IL-6, neopterin, CRP and I-FABP were performed using previously described methods.[17-19] All assays were performed according to the manufacturers' protocols.

Serum ethambutol concentrations

Cryopreserved serum samples for each timepoint were shipped to the Center for Infectious Diseases Research and Experimental Therapeutics at the Baylor Research Institute (Dallas, TX, USA). We used a previously published stable-isotope dilution LC-electrospray ionization-MS/MS method to determine ethambutol concentrations in the serum.[5] Ethambutol dihydrochloride and the stable isotope (2S,20S)-ethambutol-d10 (1,1,1',1',2,2'-d6; ethylene-d4) were purchased from Sigma–Aldrich (St Louis, MO, USA) and CDN isotopes (Quebec, Canada), respectively. All chemicals used in the assay were chromatographic or LC-MS/MS grade. Calibrators, controls and internal standards (ethambutol-d10) were included in each analytical run for quantification. Quality control samples were prepared by spiking human serum with stock standards (calibration range 0.125–4 mg/L). The lower limit of quantification of this method was 0.16 mg/L with 3.4% intra-day precision.

Statistical analysis

Population pharmacokinetic modelling of ethambutol among HIV/TB patients

Phoenix NLME software 7 (Certara USA, Inc., Princeton, NJ, USA) was used for pharmacokinetic analysis. Summary statistics were obtained for each timepoint, separately for pre- and post-ART visits, and used to explore mean concentration–time plots. Non-compartmental analysis was performed to obtain initial estimates for the pharmacokinetic parameters. The first-order conditional estimation-extended least squares method was used for all population model runs. For nested models, a reduction in the objective function value of >3.84 was considered statistically significant ($P<0.05$), corresponding to a χ^2 distribution with one degree of freedom. We visually examined model goodness of fit by plotting the observed serum ethambutol concentrations versus population-predicted concentrations, observed versus individual-predicted concentrations, individual weighted residuals versus population-predicted concentrations, and conditional weighted residuals versus time.

Standard population pharmacokinetic modelling methodology was applied for model development and evaluations. Oral bioavailability was included in the structural model and fixed to 65% for the first study visit (pre-ART) based on previous findings in HIV/TB-co-infected patients. Prior clinical studies have linked observed variability in ethambutol oral bioavailability to body weight, food intake, genetic factors and disease status. Because we were unable to estimate oral bioavailability in the absence of intravenous dosing data, we fixed this parameter to a previously reported value and estimated interindividual variability (IIV) from this fixed parameter value. This approach allowed us to compare the relative oral bioavailability from one patient to another, even though the absolute bioavailability could not be estimated directly from the data. First-order absorption with lag time (Tlag), transit compartment absorption models and distributional delay models were evaluated. We explored proportional and additive models to describe residual unexplained variability and exponential models to describe IIV. To capture the covariate effect of body weight on ethambutol pharmacokinetic parameters, allometric exponents were either fixed to theoretical values, 0.75 for disposition-related parameters and 1.0 for distribution related parameters, or directly estimated from the data.[24]

Selection of the final population pharmacokinetic model to be used for simulations was based on the Akaike information criterion (AIC), diagnostic plots, plausibility and precision. To evaluate the performance of the final population pharmacokinetic

model, both visual predictive checks and bootstrapping were performed. For the visual predictive checks, the distributions of stochastic simulated ethambutol concentrations (including median and 5th and 95th percentiles) were compared with distributions of the observed concentrations. Differences and overlap of the simulated and original distributions indicated the accuracy of the final model. In the bootstrap analysis, 500 datasets were sampled from the original study dataset. Each of the simulated datasets was fitted to the final model to evaluate variation in predicted parameter estimates (as described by the median and associated 90% CI). Finally, we performed an external validation of the final population pharmacokinetic model, comparing model-simulated serum concentrations with observations from an independent study of 48 HIV/TB patients (not used in model development) treated with daily ethambutol according to standard weight-based dosing guidelines, with the median and range of ethambutol concentrations reported for 2, 6 and 10 h post-dosing.[10]

Monte Carlo simulations of pharmacokinetic target attainment probabilities

Monte Carlo simulations were performed using the RStudio 1.1.383 (RStudio, Boston, MA, USA) platform for software R 3.4.1 (The R Foundation, Vienna, Austria) and R package mrgsolve.[25] Using the pharmacokinetic parameter estimates from the final population pharmacokinetic model (with associated variability), we performed simulations to identify pharmacokinetic target attainment under standard and intensified weight-based dosing strategies.[26] The simulated population contained 1000 virtual patients with normal body weight distribution with mean 55 kg and SD 10 kg.[17] Using the final population model, pharmacokinetic simulations were performed for the standard weight-based dosing regimen as well as an intensified dosing strategy that consisted of a supplementary 400 mg dose across each body weight group, also administered as daily therapy. We selected this intensified treatment strategy based on the ready availability of ethambutol 400 mg oral formulations in TB control programs worldwide. For each virtual patient, we determined AUC0–24 with noncompartmental analysis. Based on prior published data on ethambutol partitioning into pulmonary TB lesions, we estimated a 10-fold increase in lung tissue drug exposures relative to serum drug exposures.[27] We defined the AUC_{0-24}/MIC target ratio in lung tissue as 119, corresponding to EC_{90} in an inhibitory sigmoid E_{max} model of ethambutol pharmacodynamics.[14,28] Since the toxicodynamic relationships of systemic ethambutol exposures remain undefined, we examined the distributions of ethambutol serum C_{max} under standard and intensified dosing strategies in relation to the recommended 'target' ethambutol serum Cmax range of 2–6 mg/L.

Results

A total of 40 patients were enrolled and completed the first pharmacokinetic study visit. Twenty-four patients (60%) returned for a second pharmacokinetic study visit conducted a median of 33 days (range 5–44 days) after starting ART. Among 240 samples collected pre-ART, 8 (3.3%) were below the lower limit of quantification; post-ART, 4 of 144 samples (2.8%) were below the lower limit of quantification. At the time of the second visit, the median duration of anti-TB therapy was 74 days (range 33–118 days). Clinical characteristics for study participants grouped by body weight are shown in **Table 2.1**. Based on the recommended weight-based ethambutol dosing, the first study visit included 1 patient dosed with 550 mg (14.75 mg/kg), 19 patients dosed with 825mg (range 11.77–19.64 mg/kg), 17 patients dosed with 1100 mg (range 16.17–22.92 mg/kg) and 3 patients dosed with 1375 mg (range 17.73–19.31 mg/kg). Serum ethambutol concentration–time profiles, sorted by dose and visit (i.e., pre- or post-ART initiation), are presented in **Figure 2.1**.

Figure 2.1 Individual ethambutol serum concentration–time curves by weight group and study visit, before and after initiation of ART. The weight group 55 kg or lower includes one patient with body weight <40 kg. The horizontal line corresponds to the proposed target range for serum ethambutol Cmax (2–6 mg/L).

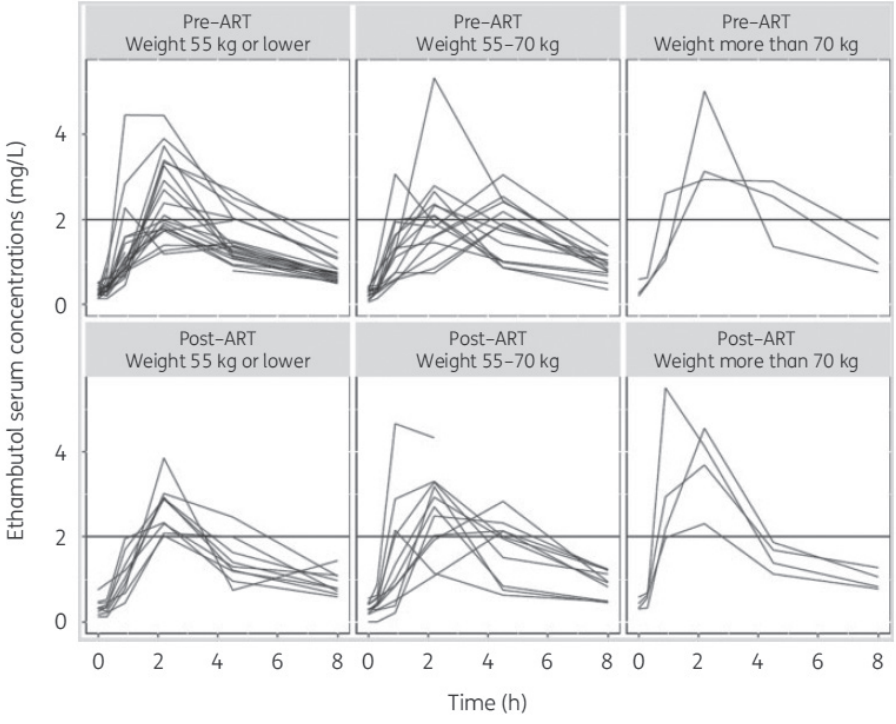

Serum ethambutol concentrations were best described by a two-compartment pharmacokinetic model with first-order absorption with lag time, linear elimination and IIV in the volume of distribution for the central compartment (V1), CL and oral bioavailability. Estimates of IIV in volume of distribution for the peripheral compartment (V2), inter-compartment transfer (Q) and absorption rate constant (ka) were small (<0.0001) and shrinkage in random effects was high, and we did not include IIV in these parameters moving forward in model development. The inclusion of a covariance term between the central compartment volume and CL showed improvement in the model fit based on AIC criteria. A proportional residual variability model adequately described unexplained residual variability. The pharmacokinetic model with fixed allometric exponents on pharmacokinetic parameters (1 for volume parameters, 0.75 for CL parameters) yielded lower AIC values (474.67) than the model with estimated allometric exponents (479.89). Thus, theoretical fixed allometric scaling was used to describe the covariate effect of weight on distribution and CL parameters. Oral bioavailability at the pre-ART study visit was fixed to 0.65[9] and IIV was estimated. Based on the plot of visit effect on IIV in oral bioavailability (S2.1), we evaluated study visit (i.e., pre- or post-ART initiation) as a categorical covariate on oral bioavailability. Interestingly, this effect was found to be statistically significant (-Δ2LL=3.92), and therefore was retained in the final model. We sequentially evaluated serum creatinine, HIV viral load, CD4+ T cell count, % CD8+CD38+DR+, neopterin, IL-6, CRP, sCD14 and I-FABP as covariates on CL and oral bioavailability. None of these covariate effects reached our pre-defined criteria for statistical significance, and thus were not retained in the final model. Parameter estimates from the final population pharmacokinetic model are shown in **Table 2.2**. Overall, parameter estimates were plausible and comparable to those previously reported in other studies[9,11,24] with a coefficient of variation, 25% for most parameters. The goodness of fit of the final model was supported by diagnostic plots (S2.2).

Table 2.1 Summary of clinical characteristics (median and IQR) by body weight group.

	HIV/TB patient body weight category		
	>55 kg (n=22)[a]	**55–70 kg (n=15)**	**<70 kg (n=3)**
Creatinine (μmol/L)	64.7 (55.4–69.1)	69.0 (60.9–73.2)	64.3 (58.0–65.1)
Age (years)	32 (27.2–43.5)	31 (27–34)	46 (39–47)
IL6 (pg/mL)	15.1 (9.15–29.1)	16.6 (8.2–26.7)	4.6 (4.4–5.9)
sCD14 (μg/mL)	2.5 (2.0–3.8)	3.2 (2.8–4.0)	3.1 (3.0–3.3)
I-FABP (pg/mL)	407.7 (188.4–573.8)	179.9 (74.9–506.6)	327.2 (306.5–424.4)
CD4 count (cells/mm^3)	217 (94.75–320)	237 (139.5–305)	352 (301–425)
Neopterin (ng/mL)	10.9 (6.68–14.8)	10.7 (7.0–20.1)	7.1 (6.3–7.8)
CRP (μg/mL)	15.2 (3.5–35.7)	7.5 (4.0–12.8)	8.3 (6.0–9.7)
CD8+CD38+DR+ (%)	38.5 (28.1–45.7)	38.5 (27.7–53.3)	27.6 (27.4–31.5)
Viral load (log_{10} copies/mL)	11.4 (10.3–13.0)	11.3 (10.0–13.3)	10.4 (10.1–12.1)
Female gender, n (%)	10 (45%)	5 (33%)	3 (100%)

[a] Includes one patient with body weight ,40 kg.

Table 2.2 Parameter estimates from the final ethambutol population pharmacokinetic model.

Population pharmacokinetic parameters	**Typical value (% SE)**	**Median (95% CI)[a]**
k_a (h$^{\#1}$)	0.44 (19.80)	0.42 (0.31–0.59)
T_{lag} (h)	0.25 (3.09)	0.26 (0.24–0.27)
Oral bioavailability for pre-ART visit (*F*)	0.65 (fixed)	0.65 (fixed)
Change in oral bioavailability post-ART	0.12 (54.45)	0.13 (0.00052–0.25)
V_1 (L)	110.23 (20.78)	107.05 (71.52–151.35)
CL (L/h)	35.42 (4.64)	35.56 (32.73–38.20)
V_2 (L)	512.52 (54.01)	634.82 (313.46–3784.53)
Q (L/h)	27.25 (16.08)	25.66 (19.62–34.28)
Weight exponent for CL and *Q*	0.75 (fixed)	0.75 (fixed)
Weight exponent for V_1 and V_2	1 (fixed)	1 (fixed)
IIV		
in *F* (%)	10.00 (13.61)	11.09 (9.04–12.91)
in V_1 (%)	55.67 (23.35)	54.27 (29.89–78.11)
in CL (%)	14.14 (5.65)	13.41 (11.92–14.89)
Residual unexplained variability		
proportional (%)	36.00 (6.10)	35.16 (31.32–39.31)

[a] Obtained from bootstrap of 1000 replicates.

Visual predictive checks from the final model demonstrate adequate model fit with the observed data (S2.3). Once the final pharmacokinetic model was identified,

we performed Monte Carlo simulations of serum ethambutol concentration–time profiles. We first simulated ethambutol serum concentrations under the standard-of-care weight-based dosing scheme. For each virtual patient, we sampled from distributions of body weight, assigning ethambutol dose based on WHO guidelines, as described above. We performed an external validation of the pharmacokinetic model by comparing simulated serum ethambutol concentrations at 2, 6 and 10 h post-dosing with observed serum ethambutol concentrations at these timepoints, as reported in a separate pharmacokinetic study among HIV/TB patients that was not used in model development.[10] The overlap between distributions of simulated and observed serum ethambutol concentrations at these timepoints supported the use of the pharmacokinetic model for simulation purposes **(Figure 2.2)**.

Figure 2.2 External validation of pharmacokinetic model, comparing simulated and observed distributions of serum ethambutol concentrations at 2, 6 and 10 h post-dosing with observed values reported in a cohort of 48 HIV/tuberculosis patients.[10] The box represents the 25th–75th quartiles, the solid horizontal line in the box represents the arithmetic mean, and the error bars represent 1.5%IQR. The floating bars represent the range of observed serum ethambutol concentrations at each timepoint.

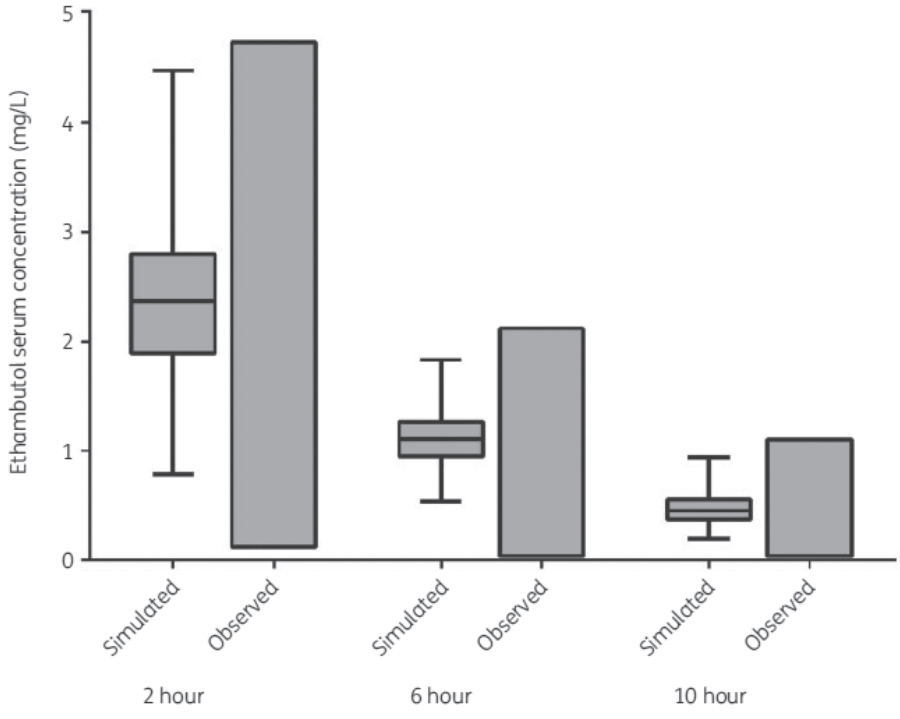

Next, we estimated probabilities of ethambutol pharmacokinetic target attainment in lung tissue according to ethambutol MIC values, under standard and intensified dosing strategies. The lung tissue AUC0–24 was estimated from the reported partitioning of ethambutol into pulmonary lesions[27] and the ethambutol MIC for the infecting *Mycobacterium tuberculosis* (Mtb) strain was sampled from a previously reported MIC distribution of ethambutol-susceptible strains.[30] The probabilities of successful pharmacokinetic target attainment at each MIC level, defined as a ratio of ethambutol AUC0–24/MIC in lung tissue >119, are shown in **Figure 2.3**. We separately compared probabilities of pharmacokinetic target attainment under standard and intensified dosing strategies among HIV/TB patients pre-ART **(Figure 2.3a)** and post-ART **(Figure 2.3b)**.

Figure 2.3 Probability of pharmacokinetic target attainment under standard and intensified ethambutol dosing strategies (n=1000 per simulation). The pharmacokinetic target was defined as an AUC0–24/MIC ratio in lung tissue .119. Circles/solid line, standard dosing regimen; squares/dashed line, intensified dosing regimen. (a) Before initiation of ART. (b) After initiation of ART.

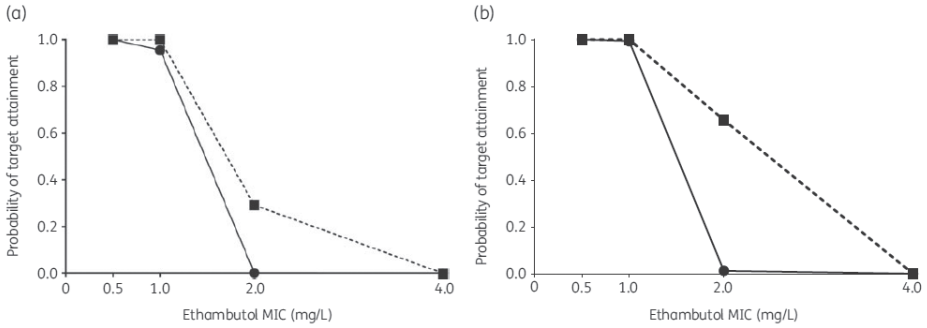

Figure 2.4 Comparison of ethambutol (EMB) pharmacokinetic target attainment probabilities by body weight category, before (a) and after (b) initiation of ART (n=1000 per simulation).

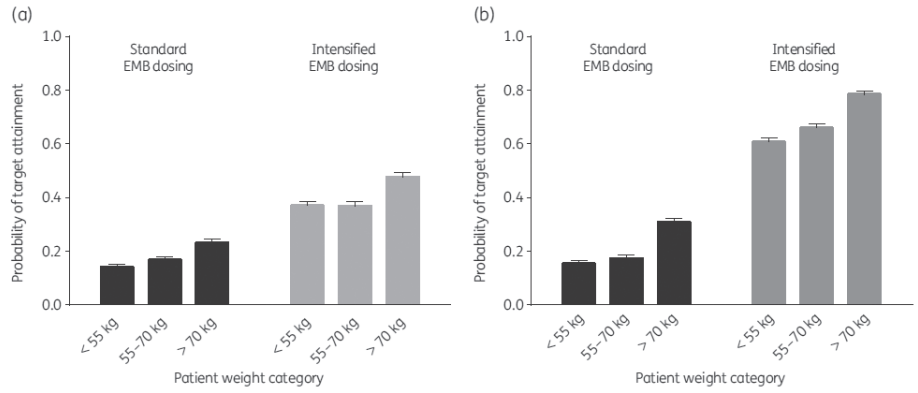

The cumulative fraction of response pre-ART under standard dosing was 15.8% and under intensified dosing was 37.6%. Post-ART initiation, the cumulative fraction of response was 17.2% under standard dosing and 64.1%with intensified dosing. Notably, at the ethambutol MIC level of 4mg/L, the PTA was <1% across all scenarios. Patients in the lowest body weight category (under 55 kg) were least likely to demonstrate pharmacokinetic target attainment under each simulation scenario, both before (**Figure 2.4a)** and after **(Figure 2.4b)** ART initiation. Finally, in order to characterize the safety of intensified ethambutol dosing, we determined the proportion of virtual patients achieving ethambutol serum Cmax between 2 and 6mg/L, the recommended range for clinicians in the context of therapeutic drug monitoring.[29] Under an intensified dosing strategy, the ethambutol serum Cmax fell between 2 and 6mg/L for 94% of virtual patients pre-ART initiation and 97% post-ART initiation. Among the 9% of virtual patients with ethambutol serum Cmax outside the target range post-ART initiation, 8% were, 2mg/L and 1% were .6mg/L, with similar proportions in each body weight category **(Figure 2.5)**. Thus, this intensified dosing strategy did not lead to supratherapeutic serum ethambutol exposures in these simulations, as defined by the recommended range of peak serum concentrations.

Figure 2.5 Simulation-based evaluation of the proportion of virtual HIV/TB patients with serum ethambutol Cmax within the proposed target range under an intensified dosing strategy, according to body weight category (n=1000 per simulation). The grey and black lines correspond to simulated patients with peak serum ethambutol within and outside of the target range, respectively.

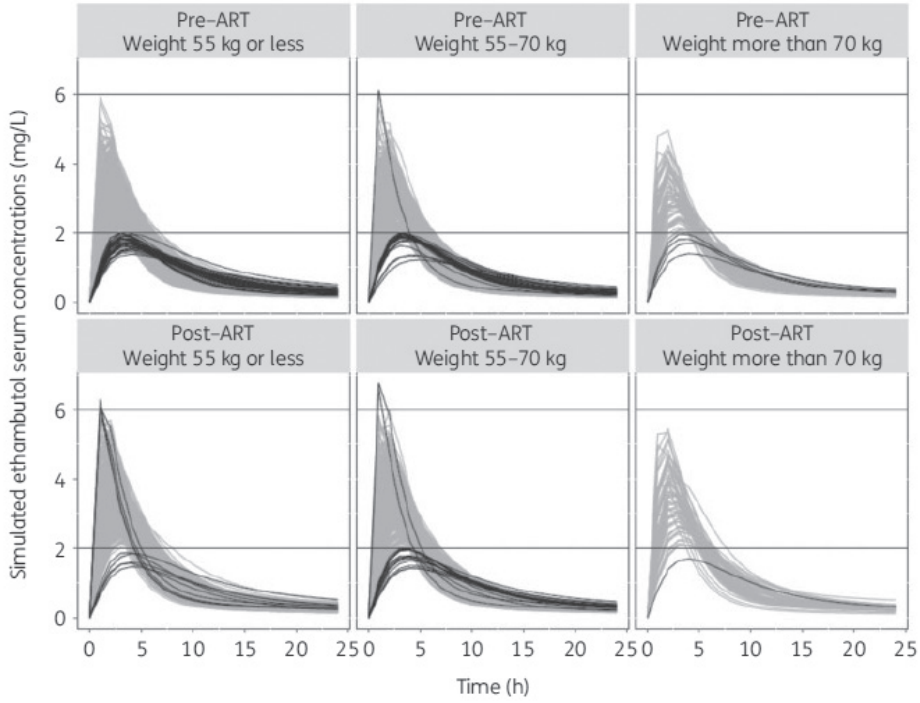

Discussion

Ethambutol remains a key drug in the first-line treatment regimen for TB. Prior work has demonstrated that HIV co-infection exerts a negative effect on ethambutol oral bioavailability, with a 15% reduction in oral bioavailability among TB patients co-infected with HIV, compared with HIV-uninfected TB patients.[9] Our work builds on these findings with the novel observation that ART initiation restores, at least partially, ethambutol oral bioavailability among HIV/TB patients treated with standard dosing regimens. We were unable to identify a specific HIV disease biomarker that was associated with improvement in oral bioavailability, among virological, immunological or gut-specific measures of HIV disease. Indeed, we cannot rule out that an overall improvement in health status, as a consequence of HIV and TB treatment, led to the increase in oral bioavailability. Broadly, these findings support efforts to identify the optimal strategy for managing HIV/TB patients who are ART naive at the time of TB treatment initiation.[31] Future work should identify mechanisms for the observed effect of ART initiation on ethambutol

oral bioavailability, whether driven by drug–drug interactions (for example, effects of ART) or drug–disease interactions (as we have demonstrated with effects of HIV-associated immune activation on the CL of isoniazid[17] and pyrazinamide[18]).

Monte Carlo simulations with our population pharmacokinetic model demonstrated that an intensified dosing strategy, comprising a supplementary dose of 400mg across all body weight groups, led to improvements in pharmacokinetic target attainment in lung tissue (measuring efficacy) while maintaining the serum Cmax range within the recommended range (approximating safety). The benefit of intensified ethambutol dosing was most notable for Mtb strains at an ethambutol MIC of 2mg/L, with an increase in target attainment probability from ,1% to 29% (pre-ART), and from 1% to 65% (post-ART). Based on these findings, the combination of early ART and intensified ethambutol dosing appears essential to achieve >50% probability of efficacious exposures to ethambutol in infected lung tissue among HIV/TB patients.

An additional finding of the current work was that the ethambutol MIC of 4mg/L provided an unattainable pharmacokinetic target for HIV/TB patients (both pre- and post-ART) under both the standard and intensified dosing strategies. This is particularly notable given the increasing recognition that the susceptibility breakpoints for anti-TB drugs should reflect the probability of pharmacokinetic target attainment during treatment.[28,32] These findings should be validated in prospective cohorts of HIV/TB patients, in order to relate these pharmacokinetic/pharmacodynamic indices to clinical endpoints (such as time to sterilization of sputum samples).[33]

A previous pharmacokinetic study conducted among healthy volunteers demonstrated that the ethambutol AUC0–24 was significantly lower among obese (BMI 25–40 kg/m^2) and extremely obese (BMI>40 kg/ m^2) individuals compared with individuals with a BMI <25 kg/m^2.[2.24] Although we were unable to characterize the effects of obesity on ethambutol pharmacokinetics given the body weight distribution of the study population, the current WHO weight-based bands for ethambutol dosing may require further optimization among patients with increased BMI in order to reach serum targets. Similarly, the absence of patients with significant kidney disease in the study cohort constrained our ability to study this covariate effect on CL, even though ethambutol is renally eliminated. The effects of BMI and kidney disease on ethambutol pharmacokinetics require further investigation given the merging of HIV, diabetes mellitus and TB epidemics, and the increasing need to treat overweight or obese patients with optimized ethambutol dosing.[34]

Our study had several limitations. First, the study was not designed to evaluate safety endpoints such as optic neuritis that may be associated with increasing ethambutol exposures,[6,7,35] and serum Cmax values within a recommended range were used as an approximate measure of the safety of an intensified dosing scheme. Although many of the early clinical studies of ethambutol included much higher dosing than currently used (up to 50mg/kg), optic neuritis can develop with doses as low as 15mg/kg and may occur more commonly among patients with nutritional deficiencies.[36] As with the other first-line anti-TB drugs, delineating toxicodynamic relationships will be essential to support intensified dosing strategies among high-risk patients.[37] In addition, we estimated lung tissue drug exposure relative to serum based on the rabbit model of tuberculous lung lesions[27], which may overestimate ethambutol exposures at the center of lung cavities and underestimate ethambutol exposures in alveolar cells.[38] Furthermore, the ethambutol MIC demonstrates regional variability in tuberculous lung lesions,[5] which adds additional complexity to the likelihood of AUC0–24/MIC target attainment. Although the pharmacodynamic target was identified in the hollow-fiber system, which provides the basis for dose selection in TB drug development guidance from both the FDA and EMA, emerging clinical data should validate this target. Finally, because pharmacokinetic sampling was limited to the central compartment, we were unable to incorporate additional IIV in ethambutol partitioning into lung tissue in Monte Carlo simulations of target attainment probabilities. Strengths of the study include the multifaceted characterization of HIV disease status (including immunological, virological and gut-specific assays) and the repeated measures study design, supporting the formal investigation of the effects of ART initiation on ethambutol pharmacokinetics during TB treatment.

In summary, we present the novel finding that ART initiation among HIV/TB-co-infected patients was associated with an improvement in ethambutol oral bioavailability and provide evidence in support of the efficacy and safety of an intensified ethambutol dosing strategy to optimize ethambutol use among HIV/TB patients. Given the critical role of ethambutol in TB treatment regimens, emerging knowledge regarding the pharmacokinetic/pharmacodynamic indices of ethambutol safety and efficacy will support further refinement of treatment strategies among high-risk TB patient populations.

References

1. Nahid P, Dorman SE, Alipanah N et al. Official American Thoracic Society/Centers for Disease Control and Prevention/Infectious Diseases Society of America Clinical Practice Guidelines: Treatment of Drug-Susceptible Tuberculosis. Clin Infect Dis 2016; 63: e147–e95.
2. Mitchison DA. Role of individual drugs in the chemotherapy of tuberculosis. Int J Tuberc Lung Dis 2000; 4: 796–806.
3. Chigutsa E, Pasipanodya JG, Visser ME et al. Impact of nonlinear interactions of pharmacokinetics and MICs on sputum bacillary kill rates as a marker of sterilizing effect in tuberculosis. Antimicrob Agents Chemother 2015; 59: 38–45.
4. Caminero JA, Sotgiu G, Zumla A et al. Best drug treatment for multidrug-resistant and extensively drug-resistant tuberculosis. Lancet Infect Dis 2010; 10: 621–9.
5. Dheda K, Lenders L, Magombedze G et al. Drug penetration gradients associated with acquired drug resistance in tuberculosis patients. Am J Respir Crit Care Med 2018; 198: 1208–19.
6. Leibold JE. The ocular toxicity of ethambutol and its relation to dose. Ann N Y Acad Sci 1966; 135: 904–9.
7. Harcombe A, Kinnear W, Britton J et al. Ocular toxicity of ethambutol. Respir Med 1991; 85: 151–3.
8. Sahai J, Gallicano K, Swick L et al. Reduced plasma concentrations of anti- tuberculosis drugs in patients with HIV infection. Ann Intern Med 1997; 127: 289–93.
9. Jonsson S, Davidse A, Wilkins J et al. Population pharmacokinetics of ethambutol in South African tuberculosis patients. Antimicrob Agents Chemother 2011; 55: 4230–7.
10. Perlman DC, Segal Y, Rosenkranz S et al. The clinical pharmacokinetics of rifampin and ethambutol in HIV-infected persons with tuberculosis. Clin Infect Dis 2005; 41: 1638–47.
11. Denti P, Jeremiah K, Chigutsa E et al. Pharmacokinetics of isoniazid, pyrazinamide, and ethambutol in newly diagnosed pulmonary TB patients in Tanzania. PLoS One 2015; 10: e0141002.
12. Van Oosterhout JJ, Dzinjalamala FK, Dimba A et al. Pharmacokinetics of antituberculosis drugs in HIV-positive and HIV-negative adults in Malawi. Antimicrob Agents Chemother 2015; 59: 6175–80.
13. Deshpande D, Srivastava S, Meek C et al. Ethambutol optimal clinical dose and susceptibility breakpoint identification by use of a novel pharmacokinetic-pharmacodynamic model of disseminated intracellular Mycobacterium avium. Antimicrob Agents Chemother 2010; 54: 1728–33.
14. Srivastava S, Musuka S, Sherman C et al. Efflux-pump-derived multiple drug resistance to ethambutol monotherapy in Mycobacterium tuberculosis and the pharmacokinetics and pharmacodynamics of ethambutol. J Infect Dis 2010; 201: 1225–31.
15. Li J, Munsiff SS, Driver CR et al. Relapse and acquired rifampin resistance in HIV-infected patients with tuberculosis treated with rifampin- or rifabutin- based regimens in New York City, 1997-2000. Clin Infect Dis 2005; 41: 83–91.
16. Korenromp EL, Scano F, Williams BG et al. Effects of human im- munodeficiency virus infection on recurrence of tuberculosis after rifampin-based treatment: an analytical review. Clin Infect Dis 2003; 37: 101–12.
17. Vinnard C, Ravimohan S, Tamuhla N et al. Isoniazid clearance is impaired among human immunodeficiency virus/tuberculosis patients with high levels of immune activation. Br J Clin Pharmacol 2017; 83: 801-11.
18. Vinnard C, Ravimohan S, Tamuhla N et al. Pyrazinamide clearance is impaired among HIV/tuberculosis patients with high levels of systemic immune activation. PLoS One 2017; 12: e0187624.
19. Vinnard C, Ravimohan S, Tamuhla N et al. Markers of gut dysfunction do not explain low rifampicin bioavailability in HIV-associated TB. J Antimicrob Chemother 2017; 72: 2020.
20. Tam VH, Preston SL, Drusano GL. Optimal sampling schedule design for populations of patients. Antimicrob Agents Chemother 2003; 47: 2888–91.

21. Giorgi JV, Liu Z, Hultin LE et al. Elevated levels of CD38! CD8! T cells in HIV infection add to the prognostic value of low CD4+ T cell levels: results of 6 years of follow-up. The Los Angeles Center, Multicenter AIDS Cohort Study. JAcquir Immune Defic Syndr 1993; 6: 904–12.

22. Sandler NG, Wand H, Roque A et al. Plasma levels of soluble CD14 inde- pendently predict mortality in HIV infection. J Infect Dis 2011; 203: 780–90.

23. Perkins MR, Bartha I, Timmer JK et al. The interplay between host genetic variation, viral replication, and microbial translocation in untreated HIV- infected individuals. J Infect Dis 2015; 212: 578–84.

24. Hall RG 2nd, Swancutt MA, Meek C et al. Ethambutol pharmacokinetic variability is linked to body mass in overweight, obese, and extremely obese people. Antimicrob Agents Chemother 2012; 56: 1502–7.

25. Baron KT, Gastonguay MR, Simulation from ODE-based population PK/PD and systems pharmacology models in R with mrgsolve. J Pharmacokinet Pharmacodyn 2015; W-23: S84–5.

26. Pasipanodya J, Gumbo T. An oracle: antituberculosis pharmacokinetics-pharmacodynamics, clinical correlation, and clinical trial simulations to predict the future. Antimicrob Agents Chemother 2011; 55: 24–34.

27. Zimmerman M, Lestner J, Prideaux B et al. Ethambutol partitioning in tuberculous pulmonary lesions explain its clinical efficacy. Antimicrob Agents Chemother 2017; 61: e00924-17.

28. Gumbo T. New susceptibility breakpoints for first-line antituberculosis drugs based on antimicrobial pharmacokinetic/ pharmacodynamic science and population pharmacokinetic variability. Antimicrob Agents Chemother. 2010; 54: 1484–91.

29. Alsultan A, Peloquin CA. Therapeutic drug monitoring in the treatment of tuberculosis: an update. Drugs 2014; 74: 839–54.

30. Schon T, Jure´en P,Giske CGet al. Evaluation ofwild-type MIC distributions as a tool for determination of clinical breakpoints for Mycobacteriumtuberculosis. J Antimicrob Chemother 2009; 64: 786–93.

31. US Department of Health and Human Services. Guidelines for the Use of Antiretroviral Agents in Adults and Adolescents Living with HIV. https://aidsinfo.nih.gov/contentfiles/ lvguidelines/AdultandAdolescentGL.pdf.

32. Gumbo T, Angulo-Barturen I, Ferrer-Bazaga S. Pharmacokinetic-pharmacodynamic and dose–response relationships of antituberculosis drugs: recommendations and standards for industry and academia. J Infect Dis 2015; 211: S96–S106.

33. Magombedze G, Pasipanodya JG, Srivastava S et al. Transformation morphisms and time-to-extinction analysis thatmap therapy duration from preclinical models to patients with tuberculosis: translating from apples to oranges. Clin Infect Dis 2018; 67: S349–S358.

34. Jeon CY,MurrayMB. Diabetes mellitus increases the risk of active tuberculosis: a systematic review of 13 observational studies. PLoS Med 2008; 5: e152.

35. Ezer N, Benedetti A, Darvish-Zargar M et al. Incidence of ethambutol related visual impairment during treatment of active tuberculosis. Int J Tuberc Lung Dis 2013; 17: 447–55.

36. Koul PA. Ocular toxicity with ethambutol therapy: timely recaution. Lung India 2015; 32: 1–3.

37. Srivastava S, Deshpande D, Magombedze G et al. Efficacy versus hepatotoxicity of high-dose rifampin, pyrazinamide, and moxifloxacin to shorten tuberculosis therapy duration: there is still a fight in the old warriors yet! Clin Infect Dis 2018; 67: S359–S364.

38. Conte JE, Golden JA, Kipps J et al. Effects of AIDS and gender on steady-state plasma and intrapulmonary ethambutol concentrations. Antimicrob Agents Chemother 2001; 45: 2891–6.

Supplementary Materials

Figure S2.1. IIV (Eta) in bioavailability by visits, before (Figure 1a) and after (Figure 1b) the inclusion of study visit as a covariate on oral bioavailability. The box represents 25th and 75th quartiles, solid horizontal line in box represent arithmetic mean, dashed horizontal line in box represent median, and the error bars represent 1.5 x interquartile range.

(a)

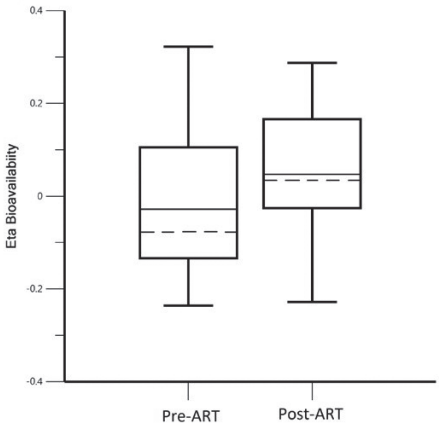

(b)

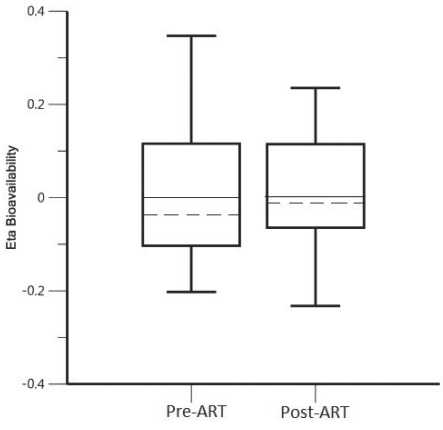

Figure S2.2. Diagnostics plots from final ethambutol population pharmacokinetic model. (a) observed versus individual predicted concentrations, Black dots: Observed, Solid line: linear regression line; (b) conditional weighted residuals versus individual variable (time after dose), Black dots: Observed, Solid line: Loess regression; (c) conditional weighted residuals versus population predicted concentrations, Black dots: Observed, Solid line: loess regression.

(a)

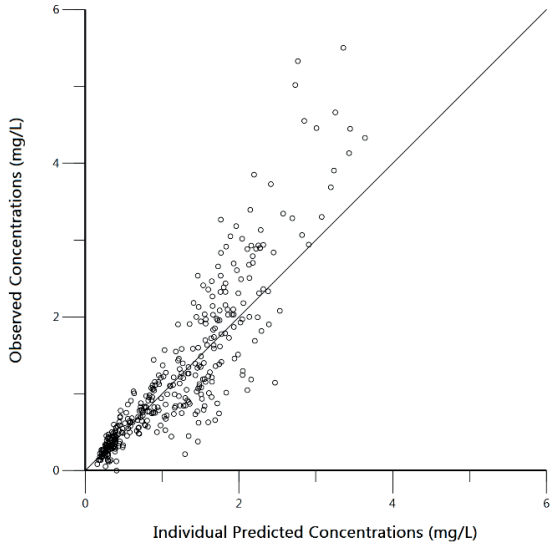

(b)

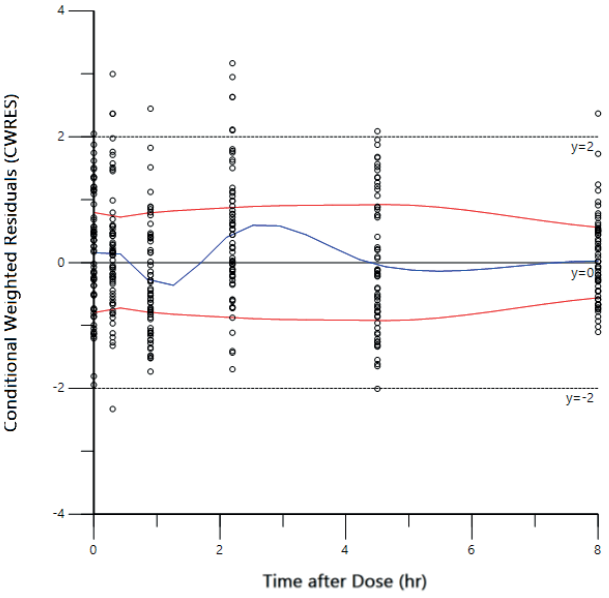

(c)

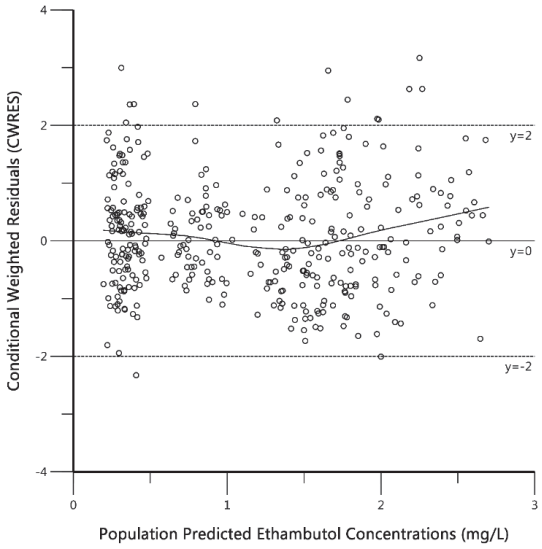
Conditional Weighted Residuals (CWRES)
Population Predicted Ethambutol Concentrations (mg/L)
y=2
y=0
y=-2
4
2
0
-2
-4
0
1
2
3

Figure S2.3. Prediction corrected visual predictive checks from 500 replicates of final ethambutol population pharmacokinetic model. Gray dots: observed, Gray lines: observed 5th, 50th, 95th quantiles; black dotted lines: 95% CI for predicted quantiles (5th, 50th, and 95th), black solid and dashed lines: 50th quantiles of respective predicted quantiles.

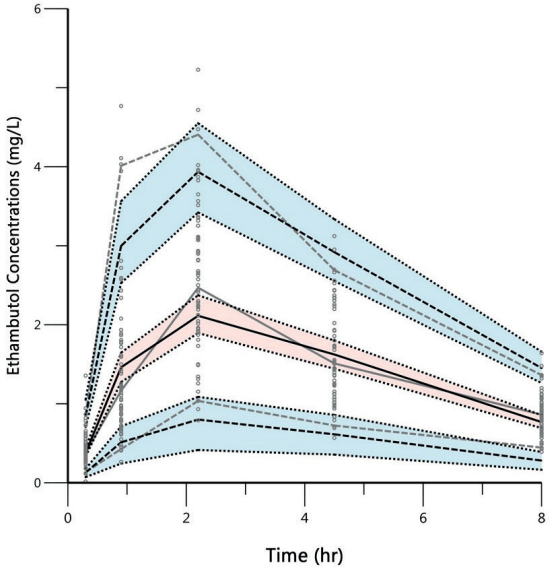

Chapter 3

Pharmacogenetic variability and the probability of site of action target attainment during tuberculosis meningitis treatment: A physiologically based pharmacokinetic modeling and simulations study

Krina Mehta, Navaneeth Narayanan, Scott Heysell, Gregory P Bisson, Selvakumar Subbian, Natalia Kurepina, Barry N. Kreiswirth, Christopher Vinnard

Tuberculosis. Volume 137, December 2022, 102271.

Abstract

Objective and Methods: Our objective was to investigate the role of patient pharmacogenetic variability in determining site of action target attainment during tuberculous meningitis (TBM) treatment. Rifampin and isoniazid PBPK model that included *SLCO1B1* and NAT2 effects on exposures respectively were obtained from literature, modified, and validated using available cerebrospinal-fluid (CSF) concentrations. Population simulations of isoniazid and rifampin concentrations in brain interstitial fluid and probability of target attainment according to genotypes and *M. tuberculosis* MIC levels, under standard and intensified dosing, were conducted.

Results: The rifampin and isoniazid model predicted steady-state drug concentration within brain interstitial matched with the observed CSF concentrations. At MIC level of 0.25 mg/L, 57% and 23% of the patients with wild type and heterozygous *SLCO1B1* genotype respectively attained the target in CNS with rifampin standard dosing, improving to 98% and 91% respectively with 35 mg/kg dosing. At MIC level of 0.25 mg/L, 33% of fast acetylators attained the target in CNS with isoniazid standard dosing, improving to 90% with 7.5 mg/kg dosing.

Conclusion: In this study, the combined effects of pharmacogenetic and *M. tuberculosis* MIC variability were potent determinants of target attainment in CNS. The potential for genotype-guided dosing during TBM treatment should be further explored in prospective clinical studies.

Introduction

Central nervous system infection is the most severe manifestation of TB, with approximately one-half of affected patients suffering severe neurologic disability or death[1,2]. In the absence of known or suspected drug-resistant disease, TB treatment guidelines recommend standard dosing of isoniazid and rifampin as part of the first-line regimen[3]. Clinical trials of intensified dosing of rifampin for tuberculosis meningitis (TBM) have yielded mixed results[4–6], perhaps owing to differences in the dosing regimen of the intensified arm[7]. There still remains considerable uncertainty regarding the optimal initial treatment of TBM patients[6].

For the treating clinician, limited information is available to guide the selection of a drug regimen for a TBM patient. The susceptibility of *M. tuberculosis* to a given anti-TB drug is typically established with phenotypic resistance testing at a "breakpoint" MIC, with a delay of several weeks after cultures are obtained[8]. While these breakpoint MIC values have been interrogated in the treatment of pulmonary TB[9], the relationship between MIC breakpoint and clinical response in the treatment of TBM patients is less examined[2]. Furthermore, there is an emerging understanding of the contribution of host genetics to the pharmacokinetic (PK) variability of both isoniazid and rifampin[10]. For isoniazid, this source of variability is primarily driven by the metabolizing enzyme responsible for isoniazid elimination, the N-acetyltransferase-2 (*NAT2)* gene[11]. More recently, pharmacogenetic variability in the hepatic OATP1B1 uptake transporter gene (*SLCO1B1*) has been identified as a driver of rifampin PK variability, as individuals who possessed the variant allele demonstrated increased rifampin clearance compared to individuals with the homozygous wild-type gene[12,13].

For both isoniazid and rifampin, the pharmacodynamic effect is based on achieving PK exposure at the site of infection, defined by the area under the concentration-versus-time profile (AUC), that is sufficiently greater than the MIC of the infecting *M. tuberculosis* strain[14,15]. Prior work has examined the impact of phenotypic drug resistance on the clinical outcomes of TBM, demonstrating that initial isoniazid and/or rifampin resistance is associated with death before treatment completion[16,17]. We sought to extend this work by examining the likelihood of target attainment among TBM patients with putative drug-susceptible disease, as defined by MIC levels for isoniazid and rifampin below the CLSI breakpoint[18]. We hypothesized that sub-breakpoint MIC levels would correspond to unattainable targets among TBM patients with genotypes of *SLCO1B1* (for rifampin) or *NAT2* (for isoniazid) that correspond with lower systemic exposures.

Methods

Rifampin and isoniazid PBPK modeling with genotype effects of SLCO1B1 and NAT2

A previously developed rifampin whole-body PBPK model was used as the base model[19]. The rifampin PBPK model included metabolism by enzyme arylacetamide deacetylase (AADAC), transport by organic anion-transporting polypeptide transporter (OATP1B1) and P-glycoprotein, along with the auto-induction of AADAC, OATP1B1, P-glycoprotein, and CYP3A4. Partition-coefficients from plasma to various tissues, including brain interstitial and intracellular compartments, were calculated based on Rodgers and Rowland method20. The model included efflux transporter, P- glycoprotein, mediated passive transport through blood-brain barrier[19]. The model also included the effect of hepatic OATP1B1 (encoded by the gene *SLCO1B1*) on rifampin clearance (S3.1).

To quantify the effects of *SLCO1B1* pharmacogenetic variability on rifampin exposure, we first reviewed the available literature. A clinical study that included rifampin PK and *SLCO1B1* genotypes identified an association of SLCO1B1 SNP c.463CC (rs11045819 wild type) or c.463CA (rs11045819 heterozygous) with plasma concentrations of rifampin in TB patients (n=72 pulmonary TB patients from Africa, North America, and Spain)[13]. We performed a comparison of this SNP with data collected in a prospective cohort study of 40 HIV/TB patients in Botswana and also identified an association between SLCO1B1 rs11045819 and rifampin exposure[12]. As such, only SLCO1B1 rs11045819 heterozygous vs. wild type categories were selected for evaluations in our PBPK study. The rifampin PBPK model was calibrated using data from literature[13] and the proportional effect of heterozygous category on the maximum transport rate ($Vmax_{OATP1B1}$) was estimated, with all other parameters kept unchanged from the original model. Next, we performed an external validation of the expanded rifampin PBPK model using the PK data from our Botswana study[12]. Patients in the validation dataset were categorized into heterozygous or wild-type groups based on the rs11045819 SNP (S3.2). We validated this expanded rifampin PBPK model by overlaying the model-predicted rifampin concentrations, stratified by SLCO1B1 genotype, with the observed PK data for both genotype categories. Once validated, we performed a sensitivity analysis of the expanded rifampin PBPK model. The sensitivity of the estimates in exposure metrics, including the AUC, C_{max}, and half-life were examined, after introducing 10% variation in absorption and clearance parameters.

We utilized a previously published and validated whole-body PBPK model of isoniazid to simulate PK profiles in CNS compartments during TB treatment[21]. This model incorporated a complex metabolic network, including metabolism of isoniazid by N-acylethanolamine-hydrolyzing acid amidase (NAAA) and NAT2 enzymes, along with further metabolism and transport of the metabolites by various processes. Partition-coefficients from plasma to various tissues, including brain interstitial and intracellular compartments, were calculated based on PK-Sim standard method as incorporated in the software[22].

Additional external validation of the rifampin and isoniazid for the purpose of our analysis was performed by comparing brain interstitial drug predictions against observed drug concentrations measured in cerebrospinal fluid (CSF) collected from TB patients who received various doses of rifampin and isoniazid[5,23,24]. Upon completion of the external validations, the rifampin and isoniazid PBPK model, which included *SLCO1B1* and NAT2 covariate effects on drug exposures, respectively, were used for simulations and CNS target attainment evaluations.

Model codes

The isoniazid PBPK model was unchanged from the previously published version[21] and is available at the GitHub repository https://github.com/HenrikCordes/isoniazid-PBPK-model. The updated rifampin PBPK model with SLCO1B1 genotype effect is available at the GitHub repository https://github.com/krinaj/RIF-INH-PBPK-Models. Additional details about the isoniazid and rifampin PBPK model development, validation, and parameter estimates are available in literature [19,20].

Observed MIC distributions in M. tuberculosis isolates cultured from CSF in TBM patients

To understand the potential benefit of intensified dosing regimens at the population level, we directly measured the rifampin and isoniazid MIC levels in collection of *M. tuberculosis* isolates that had been obtained from TBM patients in the U.S. state of New Jersey over a 12-year period. In support of statewide molecular epidemiology efforts, the Kreiswirth laboratory routinely performs DNA fingerprinting on all *M. tuberculosis* isolates across the state of New Jersey, recording the anatomic site of culture for each of isolate in the collection[25]. Among those *M. tuberculosis* isolates that had been cultured from CSF and previously determined to be susceptible to both rifampin and isoniazid (n=34), we determined the MIC for rifampin and isoniazid by agar diffusion[26].

Target attainment under standard and intensified dosing schemes of isoniazid and rifampin

Isoniazid and rifampin concentrations in venous blood plasma and brain interstitial fluids were simulated using PBPK models. The simulated population contained 1,000 virtual adult TBM patients with body weight sampled from prior distribution of body weight from TB patients[12]. Additionally, other physiological and anatomical parameters were varied as described previously to generate the virtual population[21]. Next, we performed separate simulations (n=1,000) for each *NAT2* (slow, intermediate, and fast acetylators) and *SLCO1B1* (wild-type and heterozygous) genotype[27]. Under each dosing scheme (standard or intensified), the isoniazid or rifampin $AUC_{0\text{-}24}$ following the 10^{th} dose was calculated for brain interstitial fluid compartment.

Next, we calculated the $AUC_{0\text{-}24}$/MIC ratio corresponding to each MIC value for the infecting *M. tuberculosis* strain. Since all MIC values were falling below the breakpoint that defines drug susceptibility or resistance, we also calculated target attainment at higher MIC referring to drug-resistant strains[23]. For each MIC value, we estimated probabilities of target attainment in brain interstitial fluid for both drugs, under standard and intensified dosing strategies. For rifampin, the target was defined as an $AUC_{0\text{-}24}$/MIC ratio of 30, corresponding to a 1 $\log_{10}$ CFU/mL decrease in *M. tuberculosis* bacterial load[28]. Based on the same criteria, the isoniazid target was defined as an $AUC_{0\text{-}24}$/MIC ratio of 43.5[14]. We selected intensified dosing strategies based on published clinical trial experiences[23,24,29]. Additionally, based on observed MIC distributions at the population level, cumulative fraction of response under standard and intensified dosing strategies was estimated by sampling from observed distribution of MIC values in CSF of TB patients.

Software

Physiologically-based PK modeling and simulation was performed in PK-Sim® and Mobi® (Open Systems Pharmacology Suite, v8.0, www.open-systems-pharmacology.org). Statistical analysis and plots were generated in R (R for Windows, v4.1, https://www.r-project.org/) using RStudio (RStudio, v1-554, www.rstudio.com/).

Results

Extension of rifampin PBPK model with SLCO1B1 genotype effects

The rifampin and isoniazid PBPK models included all major contributing factors affecting systemic and CNS exposures, including, protein binding, active and passive transports into various tissues, and relevant metabolism networks. As such, these models were selected for the purpose of our analysis. The updated rifampin PBPK model described observed plasma concentrations for both patients with both wild type and heterozygous SLCO1B1 genotypes **(Figure 3.1a)**. The model suggested a 3% proportional increase in OATP1B1 V_{max} among heterozygous genotype patients, compared to wild-type genotype patients (OATP1B1 V_{max} WT = 0.37 µmol/L/min vs. OATP1B1 V_{max} WT = 0.39 µmol/L/min)[13]. All other parameters, other than OATP1B1 V_{max}, remained unchanged from the literature-based model[19]. In an external validation exercise, the simulated plasma concentration-time profile agreed well with observed rifampin PK data (R^2=0.96 and 0.93, respectively, p-value<0.0001) for both *SLCO1B1* genotypes **(Figure 3.1b)**. With a 10% change in parameter estimates, the sensitivity for key rifampin PK parameters was low (between -1 and 1), which further supported the reliability of the rifampin expanded PBPK model.

Model-predicted isoniazid and rifampin exposures in CNS, stratified by genotype

The rifampin and isoniazid PBPK models predicted steady-state drug concentration within brain interstitial compartment matched well with observed CSF drug concentrations **(Figure 3.2, Figure 3.4)**. With the standard rifampin dose of 10 mg/kg orally once daily, the mean AUC_{0-24} ratio for brain interstitial fluid: plasma was predicted to be approximately 0.36 and 0.24 for wild-type and heterozygous groups, respectively. For the standard isoniazid dose (5 mg/kg), the mean AUC_{0-24} ratio for brain interstitial fluid: plasma was predicted to be approximately 0.76 for fast acetylators and 0.78 for both intermediate and slow acetylators.

Figure 3.1 Development and validation of an expanded rifampin PBPK model to include SLCO1B1 genotype. (A) Development of the model to include SLCO1B1 covariate effects (n=72 patients from Weiner et al, 2010[13]. (B) Validation of the expanded rifampin PBPK model (n=40 patients from Vinnard et al, 2017[12]. Rifampin PBPK model described plasma concentrations time profiles for both SLCO1B1 wild type and heterozygous groups well. Black points with error bars represent mean and SD of observed data, black points represent individual concentrations data, black line represent median of predicted, and grey shading represent 95% confidence interval of the predictions.

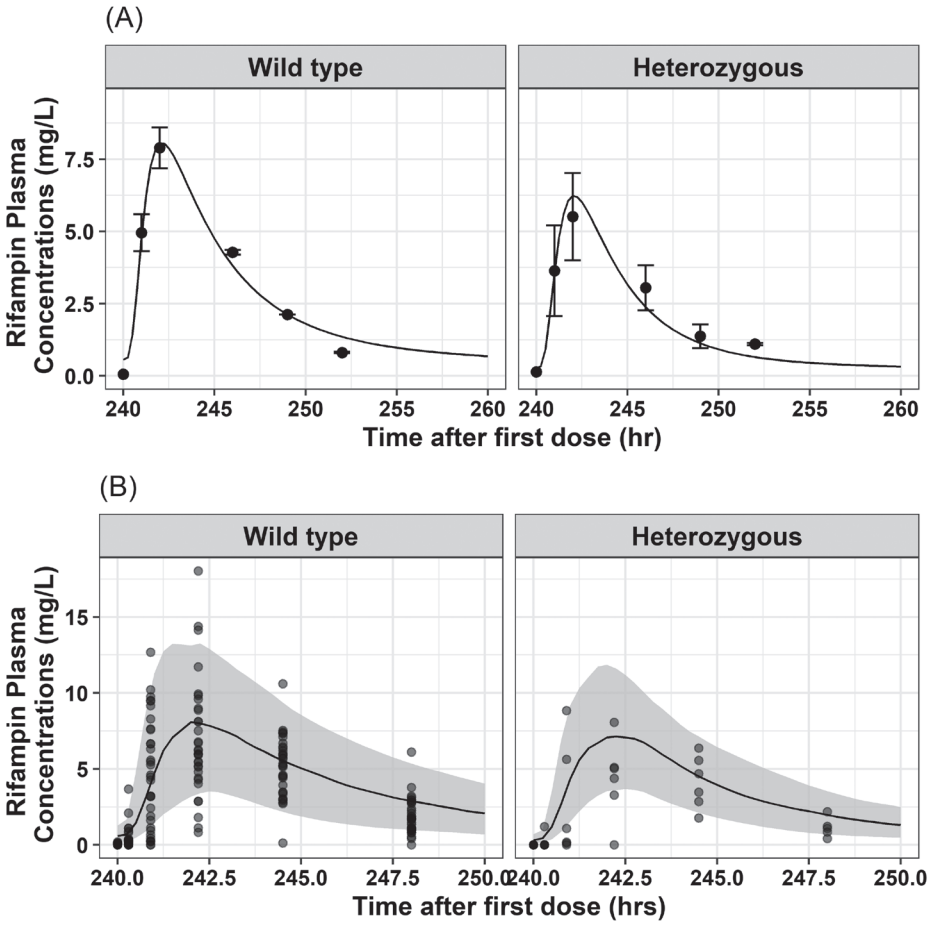

Figure 3.2 Validation of the rifampin and isoniazid PBPK models for predictions of drug exposures in the CSF. The PBPK models predicted rifampin and isoniazid steady-state concentrations in brain interstitial compartment matched well with the observed concentrations data from CSF of TB patients[23,24].

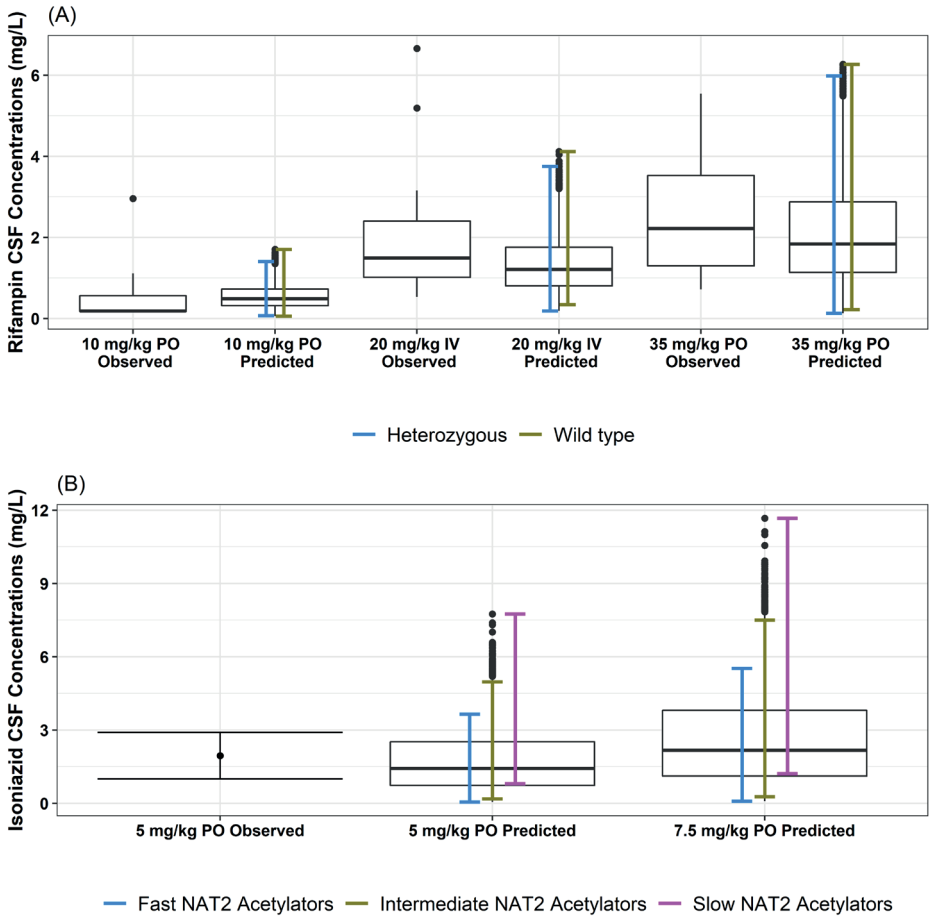

Figure 3.3 Distribution of minimum inhibitory concentration levels of isoniazid and rifampin among M. tuberculosis isolates that were cultured from CSF in New Jersey over a 12 -year period.

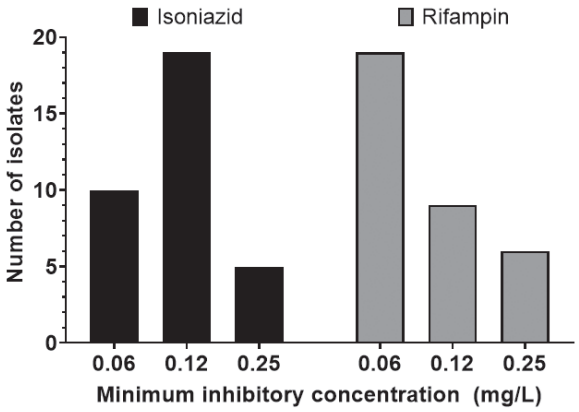

Probability of target attainment in CNS under standard and intensified treatments

Distribution of MIC levels for rifampin and isoniazid in a collection of *M. tuberculosis* isolates that had been cultured from the CSF of patients is presented in **Figure 3.3**. With standard and intensified rifampin dosing, the probabilities of successful rifampin target attainment in brain interstitial fluid are shown in **Figure 3.5A.** At rifampin MIC level of 0.125 mg/L, 92% of patients with wild-type *SLCO1B1* genotype attained the rifampin target in brain interstitial fluid, compared with 86% of the patients with heterozygous *SLCO1B1* genotype. At a rifampin MIC level of 1 mg/L, none of the patients with either *SLCO1B1* genotype were predicted to achieve rifampin target in brain interstitial fluid. With intensified rifampin dosing of 35 mg/kg and MIC level of 1 mg/L, 42% and 21% of patients with wild-type and heterozygous *SLCO1B1* genotype, respectively, attained the rifampin target in brain interstitial fluid. With standard and intensified rifampin dosing, the probabilities of successful isoniazid target attainment in brain interstitial fluid are shown in **Figure 3.5B**. At an isoniazid MIC level that is less than or equal to 0.125 mg/L, nearly all TBM patients regardless of *NAT2* genotypes attained the target in brain interstitial fluid at the standard dosing. At an isoniazid MIC level of 1 mg/L, none of the fast or intermediate acetylators and only 12% of slow acetylator patients attained the target in brain interstitial fluid at the standard dosing. At the same MIC, intensified dosing predicted to provide target attainment in none of the fast acetylators, 2% of intermediate acetylators, and 68% of slow acetylators.

Figure 3.4 Predicted steady state rifampin and isoniazid AUC_{0-24} (mg·hr/L) in the CNS compartments stratified by dosing regimen and genotype. (A) rifampin brain interstitial, (B) isoniazid brain interstitial, (C) rifampin brain intracellular, (D) rifampin brain interstitial. All dosing regimens were administered once daily.

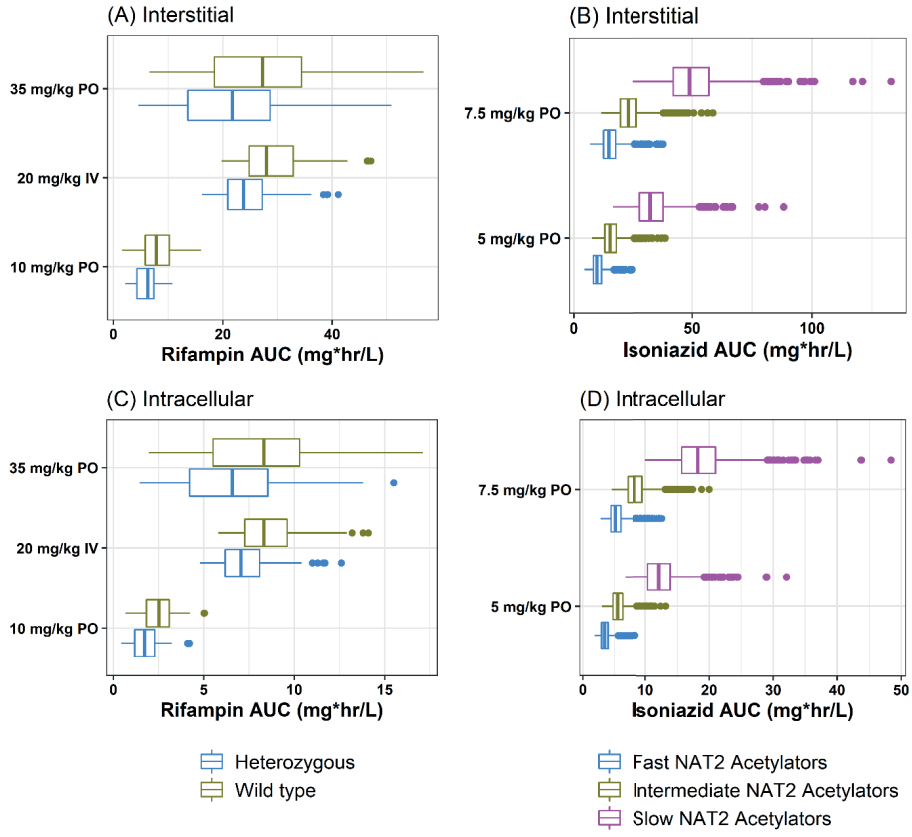

Based on observed MIC distributions at the population level **(Figure 3.3)**, cumulative fraction of response under standard and intensified dosing strategies was estimated by sampling MIC values from observed distribution of MIC values in CSF of TB patients to calculate target attainment probabilities. For the drug-susceptible strains, there was 86% and 99% overall probability of PD target attainment in brain interstitial fluid with standard dosing and intensified dosing of rifampin, respectively. Similarly, for the drug-susceptible strains, there was a 92% and 99% overall probability of target attainment in brain interstitial fluid with standard dosing and intensified dosing of isoniazid, respectively.

Figure 3.5 Target attainment probabilities in brain interstitial compartment under standard and intensified dosing regimens for rifampin and isoniazid stratified by *SLCO1B1* and NAT2 genotypes, respectively. All dosing regimen assumed once daily therapy.

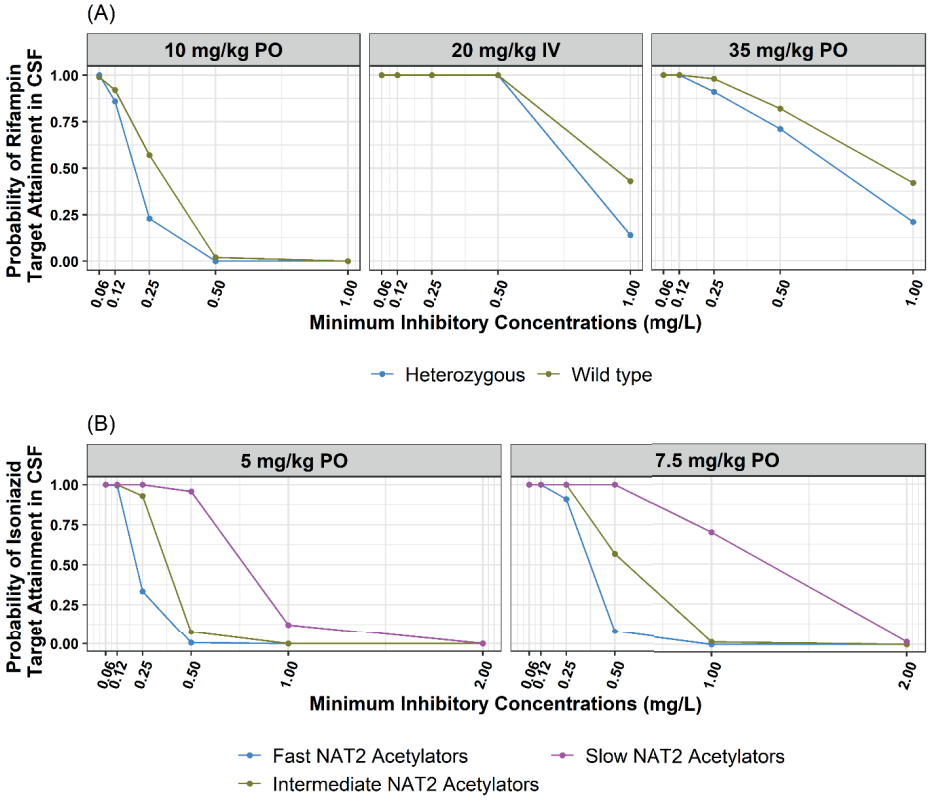

Discussion

Our objective was to evaluate the probability of target attainment in the CNS during TBM treatment with a first-line regimen that includes isoniazid and rifampin. We used a PBPK modeling approach to incorporate two independent sources of variability: host pharmacogenetics and pathogen MIC levels. Using this approach, we tested the hypothesis that sub-breakpoint MIC levels for isoniazid and rifampin would correspond to essentially unattainable targets among patients with fast elimination genotypes. While our findings support this hypothesis, they also demonstrate that the clinical benefit of intensified dosing regimens are concentrated at certain MIC levels for the infecting *M. tuberculosis* strain.

Adequate PK exposures of anti-TB drugs in the CNS are crucial for treatment success for TBM patients[30]. Current bioanalytical sampling methods do not allow measurements of drug exposure from various CNS sites of TB lesions, such as brain intracellular tuberculomas, and CSF drug concentrations may be used as a summary measure of CNS drug exposure[31]. The whole-body PBPK model that was used in this analysis includes blood cells, plasma, interstitial space, and tissue space for each organ/compartment; drug partitioning into these spaces is based on physicochemical parameters of the drug and physiological parameters of the species. Furthermore, the rifampin PBPK model also includes P-glycoprotein transporter effects at the blood-brain barrier[19]. As such, our PBPK model-based approach in this analysis is useful to predict anti-TB drug target attainment at CNS sites of action in TBM patients, and advances prior understandings based on CSF concentration-time profiles[32–34].

In clinical trials of pulmonary TB patients, intensified dosing of rifampin (up to 50 mg/kg oral) led to fast sterilization activity increasing toxicity[23,29,35]. In TBM patient populations, clinical trials of intensified rifampin dosing have shown mixed results. Rifampin doses up to 15 mg/kg did not show improved survival in a study conducted in Vietnamese patients (n=817)[4]. In contrast, a clinical trial of intensified rifampin dosing among Indonesian TBM patients (n=122) led to improvements in mortality without an increased rate of adverse events, with dose increases up to 30 mg/kg[5]. A model-based meta-analysis has found that even doses beyond 30 mg/kg may be expected to improve clinical response[33]. Our work also suggests that unmeasured MIC variability may be a major driver of clinical response, with an additional contribution of *SLCO1B1* pharmacogenetic variability in some populations. Importantly, the MIC variability in the current study was entirely sub-breakpoint, meaning that these isolates would be classified as drug-susceptible by the clinical laboratory. With the PBPK model-based simulations, we were able to demonstrate that standard dosing would achieve markedly low probabilities for target attainment for drug-resistant strains by setting MIC to higher values. We propose that future prospective clinical trials of TBM treatment regimens prioritize the capacity for secondary analyses based on these additional sources of variability.

As patient genotyping methods advance to reach a greater number of bedsides in geographic areas with a high burden of TB disease, the potential tradeoffs between personalized medicine and standardized treatment regimens will require greater consideration, regarding incremental benefits and resource utilization. Much attention has been focused on the support of clinical decision-making provided

by DNA sequencing of *M. tuberculosis* strains, for example to identify mutants likely to confer phenotypic drug resistance[36]. Yet parallel efforts are underway to identify the patient's genotypic determinants of TB treatment response, including the use of the *LTA4H* genotype to select patients for adjunctive corticosteroid treatment[37], currently studied in a prospective clinical trial[38]. Our findings suggest that these patient genotyping efforts should be expanded to evaluate prospectively the impact of SNPs related to *NAT2* and/or *SLCO1B1* activity during TBM treatment. This information could be combined with *M. tuberculosis* mutational analysis to identify those patients most likely to benefit from intensified drug therapy, and perhaps to guide further the selection of the intensified dose in the regimen.

A key finding of the current work was the difference in drug exposures between brain interstitial fluid and brain intracellular. According to one model of TBM pathogenesis, the early bloodstream dissemination of *M. tuberculosis* may lead to foci of infection established in the meninges and brain parenchyma, following a vascular distribution[39]. As these tubercles enlarge, there is potential for rupture into the sub-arachnoid space, leading to the signs and symptoms of meningitis, most commonly in a basilar distribution[40]. Yet the tubercles themselves are found in the brain or meningeal tissue, and enlargement without rupture leads to the formation of tuberculomas, which may become clinically apparent as space-occupying lesions. Delayed sterilization of deep CNS anatomic sites during TB treatment, as a consequence of sub-optimal PK exposures, could contribute to the observed risk of paradoxical reaction during TBM treatment[41]. The current PBPK model calculated brain interstitial to intracellular partition coefficients based on standard PBPK modeling methods[42]. As such, the model may not contain all relevant mechanistic details pertaining drug penetration in the brain intracellular compartment. Although further work may be needed to implement all relevant mechanisms of brain intracellular penetration for anti-tuberculosis drugs, our relatively simple adaptation of whole-body PBPK model provide a quantitative estimate of the PK exposures of isoniazid and rifampin in brain intracellular, relative to brain interstitial fluid.

Our study had several notable limitations. The pharmacogenetic association of *SLCO1B1* variability with lower rifampin exposures was based on analysis from two independent clinical studies, and we recognize that heterozygous alleles at additional loci likely relate to rifampin PK variability[43]. In pharmacogenetic studies that were reported subsequent to the work used in our PBPK model development and validation, the rs11045819 allele was found to be rare in certain populations[44]. Linkage disequilibrium analyses, both between- and within- populations, will be

essential to improve understanding of the SNPs tags that correspond to gene function[45]. For simplicity, we assigned the drug dose (mg) based on body weight (kg), rather than using dosing bands that allow for fixed-dose combination, and the additional impact of weight-based dosing bands would be of interest in a future study[46]. Furthermore, recent clinical trials have also studied even higher rifampin doses than we selected for simulation purposes, up to 50 mg/kg[47]. Strengths of our approach included the utilization of previously validated PBPK models for each drug, the formal validation of the *SLCO1B1* genotype as a novel covariate effect in the rifampin PBPK model, and the additional measurements of MIC distributions for isoniazid and rifampin among *M. tuberculosis* isolates cultured from TBM patients.

In summary, our PBPK-based approach demonstrated that the likelihood of target attainment during TBM treatment is jointly influenced by host pharmacogenetics and pathogen MIC variability. Within a PK-PD framework, the combination of these factors also identifies those patients most likely to benefit from intensified drug therapy. We propose that prospective clinical trials of TBM therapies should routinely capture these determinants of clinical response.

References

1. Seddon JA, Wilkinson R, van Crevel R, Figaji A, Thwaites GE, Aarnoutse RE, et al. Knowledge gaps and research priorities in tuberculous meningitis. Wellcome Open Res. 2019;4:1–18.
2. Mezochow A, Thakur K, Vinnard C. Tuberculous Meningitis in Children and Adults: New Insights for an Ancient Foe. Curr Neurol Neurosci Rep. 2017;17(11).
3. Nahid P, Dorman SE, Alipanah N, Barry PM, Brozek JL, Cattamanchi A, et al. Executive Summary: Official American Thoracic Society/ Centers for Disease Control and Prevention/ Infectious Diseases Society of America Clinical Practice Guidelines: Treatment of Drug-Susceptible Tuberculosis. Clin Infect Dis. 2016;63(7):853–67.
4. Heemskerk AD, Bang ND, Mai NTH, Chau TTH, Phu NH, Loc PP, et al. Intensified Antituberculosis Therapy in Adults with Tuberculous Meningitis. N Engl J Med. 2016;374(2):124–34.
5. Dian S, Yunivita V, Ganiem AR, Pramaesya T, Chaidir L, Wahyudi K, et al. Double-blind, randomized, placebo-controlled phase II dose-finding study to evaluate high-dose rifampin for tuberculous meningitis. Antimicrob Agents Chemother. 2018;62(12):1–12.
6. Cresswell F V, Te Brake L, Atherton R, Ruslami R, Dooley KE, Aarnoutse R, et al. Intensified antibiotic treatment of tuberculosis meningitis. Expert Rev Clin Pharmacol. 2019 Mar;12(3):267–88.
7. Donald PR. Chemotherapy for Tuberculous Meningitis. N Engl J Med [Internet]. 2016;374(2):179–81. Available from: https://doi.org/10.1056/NEJMe1511990
8. Cox H, Mizrahi V. The Coming of Age of Drug-Susceptibility Testing for Tuberculosis. N Engl J Med. 2018;379(15):1474–5.
9. Gumbo T, Angulo-Barturen I, Ferrer-Bazaga S. Pharmacokinetic-Pharmacodynamic and Dose-Response Relationships of Antituberculosis Drugs: Recommendations and Standards for Industry and Academia. J Infect Dis. 2015;211(Suppl 3):S96–106.
10. Naidoo A, Chirehwa M, Ramsuran V, McIlleron H, Naidoo K, Yende-Zuma N, et al. Effects of genetic variability on rifampicin and isoniazid pharmacokinetics in South African patients with recurrent tuberculosis. Pharmacogenomics. 2019;20(4):224–40.
11. Vinnard C, Ravimohan S, Tamuhla N, Ivaturi V, Pasipanodya J, Srivastava S, et al. Isoniazid clearance is impaired among human immunodeficiency virus/tuberculosis patients with high levels of immune activation. Br J Clin Pharmacol. 2017;83(4):801–11.
12. Vinnard C, Ravimohan S, Tamuhla N, Pasipanodya J, Srivastava S, Modongo C, et al. Markers of gut dysfunction do not explain low rifampicin bioavailability in HIV-associated TB. J Antimicrob Chemother. 2017;72(7):2020–7.
13. Weiner M, Peloquin C, Burman W, Luo CC, Engle M, Prihoda TJ, et al. Effects of tuberculosis, race, and human gene SLCO1B1 polymorphisms on rifampin concentrations. Antimicrob Agents Chemother. 2010;54(10):4192–200.
14. Jayaram R, Gaonkar S, Kaur P, Suresh BL, Mahesh BN, Jayashree R, et al. Pharmacokinetics-pharmacodynamics of rifampin in an aerosol infection model of tuberculosis. Antimicrob Agents Chemother. 2003;47(7):2118–24.
15. Gumbo T, Pasipanodya JG, Nuermberger E, Romero K, Hanna D. Correlations between the hollow fiber model of tuberculosis and therapeutic events in tuberculosis patients: Learn and confirm. Clin Infect Dis. 2015;61(Suppl 1):S18–24.
16. Vinnard C, King L, Munsiff S, Crossa A, Iwata K, Pasipanodya J, et al. Long-term mortality of patients with tuberculous meningitis in New York city: A cohort study. Clin Infect Dis. 2017;64(4):401–7.
17. Vinnard C, Winston CA, Wileyto EP, Macgregor RR, Bisson GP. Isoniazid resistance and death in patients with tuberculous meningitis: retrospective cohort study. BMJ. 2010 Sep;341:c4451.
18. Woods GL, Brown-Elliott BA, Conville PS, Desmond EP, Hall GS, Lin G, et al. 2nd edition. Wayne (PA): Clinical and Laboratory Standards Institute; 2011 Mar. Report No.: M24-A2. [Internet]. Wayne (PA); 2011. Available from: https://www.ncbi.nlm.nih.gov/books/NBK544374/
19. Hanke N, Frechen S, Moj D, Britz H, Eissing T, Wendl T, et al. PBPK Models for CYP3A4 and P-gp DDI Prediction: A Modeling Network of Rifampicin, Itraconazole, Clarithromycin, Midazolam, Alfentanil, and Digoxin. CPT Pharmacometrics Syst Pharmacol. 2018;7(10):647–59.

20. Rodgers T, Rowland M. Physiologically based pharmacokinetic modelling 2: predicting the tissue distribution of acids, very weak bases, neutrals and zwitterions. J Pharm Sci. 2006 Jun;95(6):1238–57.

21. Cordes H, Thiel C, Aschmann HE, Baier V, Blank LM, Kuepfer L. A physiologically based pharmacokinetic model of isoniazid and its application in individualizing tuberculosis chemotherapy. Antimicrob Agents Chemother. 2016;60(10):6134–45.

22. Lippert J, Burghaus R, Edginton A, Frechen S, Karlsson M, Kovar A, et al. Open Systems Pharmacology Community—An Open Access, Open Source, Open Science Approach to Modeling and Simulation in Pharmaceutical Sciences. CPT Pharmacometrics Syst Pharmacol. 2019;8(12):878–82.

23. Cresswell F V., Meya DB, Kagimu E, Grint D, Te Brake L, Kasibante J, et al. High-Dose Oral and Intravenous Rifampicin for the Treatment of Tuberculous Meningitis in Predominantly Human Immunodeficiency Virus (HIV)-Positive Ugandan Adults: A Phase II Open-Label Randomized Controlled Trial. Clin Infect Dis. 2021;73(5):876–84.

24. Kaojarern S, Supmonchai K, Phuapradit P, Mokkhavesa C, Krittiyanunt sarinee. Effect of steroids on CSF penetration of antituberculous drugs in tuberculous meningitis. Clin Pharmacol Ther. 1991;49(1):6–12.

25. Brown TS, Narechania A, Walker JR, Planet PJ, Bifani PJ, Kolokotronis SO, et al. Genomic epidemiology of Lineage 4 Mycobacterium tuberculosis subpopulations in New York city and New Jersey, 1999-2009. BMC Genomics [Internet]. 2016;17(1):1–11. Available from: http://dx.doi.org/10.1186/s12864-016-3298-6

26. Woods GL, Brown-Elliott BA, Conville PS, Desmond EP, Hall GS, Lin G, et al. Susceptibility Testing of Mycobacteria, Nocardiae, and Other Aerobic Actinomycetes. 2nd editio. Wayne (PA): Clinical and Laboratory Standards Institute; 2011.

27. Rajman I, Knapp L, Hanna I. Genetic Diversity in Drug Transporters: Impact in African Populations. Clin Transl Sci. 2020 Sep;13(5):848–60.

28. Gumbo T, Louie A, Liu W, Brown D, Ambrose PG, Bhavnani SM, et al. Isoniazid bactericidal activity and resistance emergence: Integrating pharmacodynamics and pharmacogenomics to predict efficacy in different ethnic populations. Antimicrob Agents Chemother. 2007;51(7):2329–36.

29. Boeree MJ, Diacon AH, Dawson R, Narunsky K, Du Bois J, Venter A, et al. A dose-ranging trial to optimize the dose of rifampin in the treatment of tuberculosis. Am J Respir Crit Care Med. 2015;191(9):1058–65.

30. Davis A, Meintjes G, Wilkinson RJ. Treatment of Tuberculous Meningitis and Its Complications in Adults. Curr Treat Options Neurol. 2018;20(3).

31. Nau R, Djukic M, Spreer A, Eiffert H. Bacterial meningitis: new therapeutic approaches. Expert Rev Anti Infect Ther [Internet]. 2013;11(10):1079–95. Available from: https://doi.org/10.1586/14787210.2013.839381

32. Ruslami R, Gafar F, Yunivita V, Parwati I, Ganiem AR, Aarnoutse RE, et al. Pharmacokinetics and safety/tolerability of isoniazid, rifampicin and pyrazinamide in children and adolescents treated for tuberculous meningitis. Arch Dis Child. 2021;70–7.

33. Svensson EM, DIan S, Te Brake L, Ganiem AR, Yunivita V, Van Laarhoven A, et al. Model-Based Meta-analysis of Rifampicin Exposure and Mortality in Indonesian Tuberculous Meningitis Trials. Clin Infect Dis. 2020;71(8):1817–23.

34. Ding J, Thuy Thuong Thuong N, Pham T Van, Heemskerk D, Pouplin T, Tran CTH, et al. Pharmacokinetics and Pharmacodynamics of Intensive Antituberculosis Treatment of Tuberculous Meningitis. Clin Pharmacol Ther. 2020;107(4):1023–33.

35. Velásquez GE, Brooks MB, Coit JM, Pertinez H, Vásquez DV, Garavito ES, et al. Efficacy and safety of high-dose rifampin in pulmonary tuberculosis a randomized controlled trial. Am J Respir Crit Care Med. 2018;198(5):657–66.

36. Gliddon HD, Frampton D, Munsamy V, Heaney J, Pataillot-Meakin T, Nastouli E, et al. A Rapid Drug Resistance Genotyping Workflow for Mycobacterium tuberculosis, Using Targeted Isothermal Amplification and Nanopore Sequencing. Microbiol Spectr. 2021;9(3):1–12.

37. van Crevel R, Avila-Pacheco J, Thuong NTT, Ganiem AR, Imran D, Hamers RL, et al. Improving host-directed therapy for tuberculous meningitis by linking clinical and multi-omics data. Tuberculosis [Internet]. 2021;128:102085. Available from: https://www.sciencedirect.com/science/article/pii/S1472979221000354

38. Donovan J, Phu NH, Thao LTP, Lan NH, Mai NTH, Trang NTM, et al. Adjunctive dexamethasone for the treatment of hiv-uninfected adults with tuberculous meningitis stratified by leukotriene a4 hydrolase genotype (LAST ACT): Study protocol for a randomised double blind placebo controlled non-inferiority trial [version 1; r. Wellcome Open Res. 2018;3:1–19.

39. Donald PR, Schaaf HS, Schoeman JF. Tuberculous meningitis and miliary tuberculosis: the Rich focus revisited. J Infect. 2005 Apr;50(3):193–5.

40. Rock RB, Olin M, Baker CA, Molitor TW, Peterson PK. Central nervous system tuberculosis: Pathogenesis and clinical aspects. Clin Microbiol Rev. 2008;21(2):243–61.

41. Singh AK, Malhotra HS, Garg RK, Jain A, Kumar N, Kohli N, et al. Paradoxical reaction in tuberculous meningitis: Presentation, predictors and impact on prognosis. BMC Infect Dis [Internet]. 2016;16(1):1–11. Available from: http://dx.doi.org/10.1186/s12879-016-1625-9

42. Thiel C, Schneckener S, Krauss M, Ghallab A, Hofmann U, Kanacher T, et al. A systematic evaluation of the use of physiologically based pharmacokinetic modeling for cross-species extrapolation. J Pharm Sci. 2015 Jan;104(1):191–206.

43. Thomas L, Miraj SS, Surulivelrajan M, Varma M, Sanju CSV, Rao M. Influence of single nucleotide polymorphisms on rifampin pharmacokinetics in tuberculosis patients. Antibiotics. 2020;9(6):1–15.

44. Sloan DJ, McCallum AD, Schipani A, Egan D, Mwandumba HC, Ward SA, et al. Genetic determinants of the pharmacokinetic variability of rifampin in Malawian adults with pulmonary tuberculosis. Antimicrob Agents Chemother. 2017;61(7):1–9.

45. Tishkoff SA, Reed FA, Friedlaender FR, Ehret C, Ranciaro A, Froment A, et al. The genetic structure and history of Africans and African Americans. Science (80-). 2009;324(5930):1035–44.

46. Sekaggya-Wiltshire C, Chirehwa M, Musaazi J, Von Braun A, Buzibye A, Muller D, et al. Low antituberculosis drug concentrations in HIV-tuberculosis-coinfected adults with low body weight: Is it time to update dosing guidelines? Antimicrob Agents Chemother. 2019;63(6):1–11.

47. Wasserman S, Davis A, Stek C, Chirehwa M, Botha S, Daroowala R, et al. Plasma pharmacokinetics of high-dose oral versus intravenous rifampicin in patients with tuberculous meningitis: a randomized controlled trial. Antimicrob Agents Chemother. 2021;65(8).

Supplementary Materials

S3.1. Generic Structure and Relevant Mechanistic Details of the PBPK Models for Rifampin and Isoniazid. The whole-body PBPK models for isoniazid and rifampin contains the relevant organs that play key roles in pharmacokinetics of drugs[1]. The organs are represented by their volume and connected with each other by arterial and venous blood flows. Each organ, including brain, is further divided into blood, interstitial, and intracellular compartments. Reproduced from Thiel et al., 2015 and Kuepfer et al., 2016 under Creative Commons Attribution[2,3.] Additionally, the rifampin and isoniazid PBPK models included all major contributing factors affecting systemic and CNS exposures, including, protein binding, active diffusion, passive transport, and relevant distribution and metabolism networks[4,5].

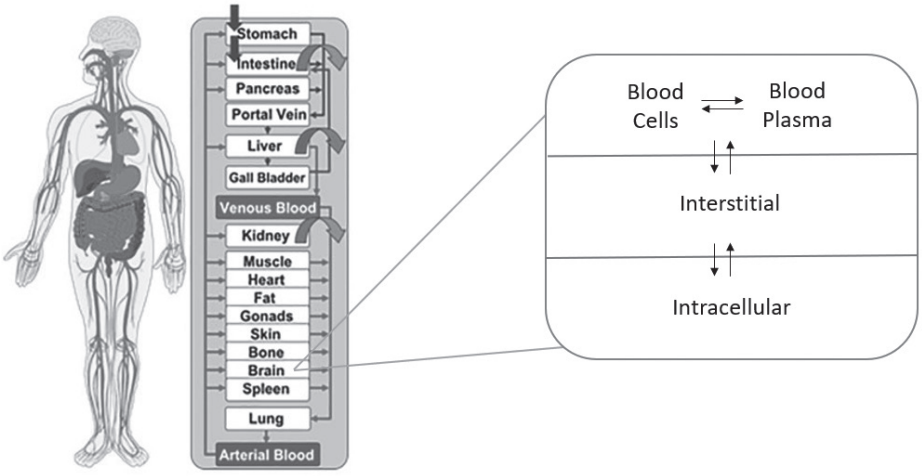

S3.2. Selection of the SNP Variant for Inclusion in Rifampin PBPK Analysis. Prior work has identified association of SLCO1B1 c.463CC (rs11045819 wild type) or c.463CA (rs11045819 heterozygous) genotypes with serum concentrations of rifampin in TB patients[6]. In our study, all SNPs identified in SLCO1B1 recognized in were evaluated for each subject[7]. Here, we performed a linkage disequilibrium analysis to characterize the association between various SLCO1B1 SNPs observed in our study data. A total of 32/40 patients had at least one heterozygous SNP. Four patients had heterozygous rs11045819 which was previously associated with lower rifampin Cmax. We identified other SNPs that were possibly associated with rs11045819 via linkage disequilibrium analysis. Two patients who did not have heterozygous rs11045819 SNP, but one or more associated SNP also had lower rifampin Cmax values in our dataset Additionally, two patients who had heterozygous rs4149080 had lower rifampin Cmax. Previously, Sloan et al., 2017 observed that rs4149032 to be possibly associated with lower rifampin exposure however, our study did not demonstrate similar finding[8]. Patients who had rs11045819 heterozygous SNP were flagged in our dataset as SLCO1B1 heterozygous for evaluation in the PBPK model.

Linkage Disequilibrium Heatmap for SLCO1B1 SNPs

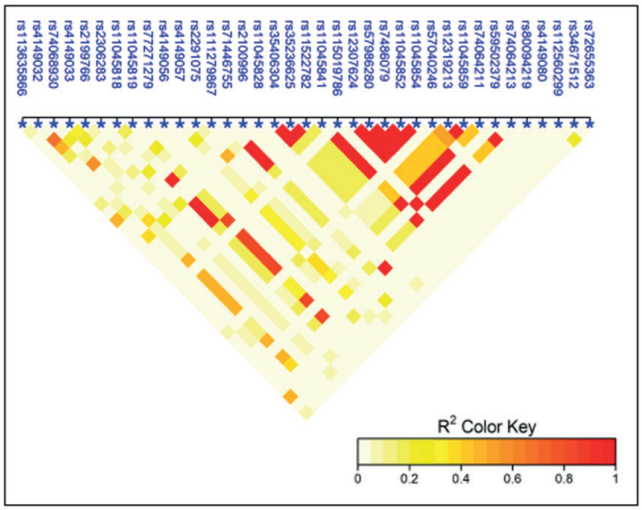

Table S3.3. List of SLCO1B1 SNPs associated with RS11045819

SLCO1B1 SNPs	rs11045819 (r^2)
rs11045841	0.82
rs11045852	0.82
rs11045854	0.82
rs12307624	0.82
rs57986280	0.82
rs74064211	0.82
rs74064213	0.82
rs74068930	0.57
rs7486079	0.82

S3.4. Observed Cmax Stratified by SLCO1B1 SNP Groups

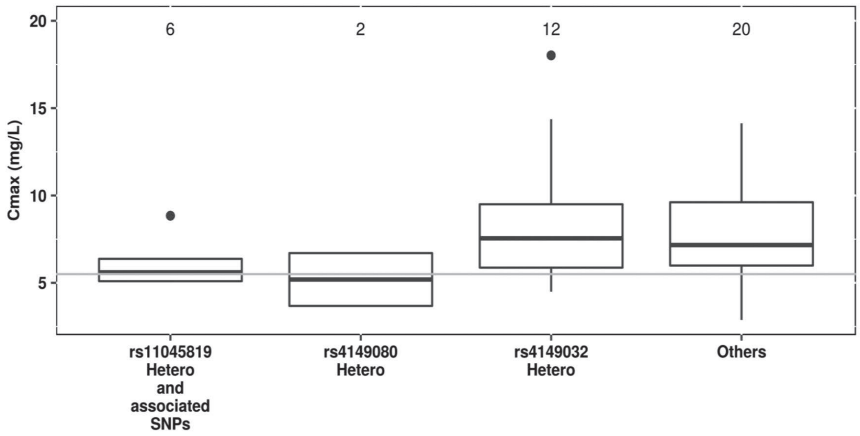

References

1. Lippert J, Burghaus R, Edginton A, Frechen S, Karlsson M, Kovar A, et al. Open Systems Pharmacology Community—An Open Access, Open Source, Open Science Approach to Modeling and Simulation in Pharmaceutical Sciences. CPT Pharmacometrics Syst Pharmacol. 2019;8(12):878–82.
2. Thiel C, Schneckener S, Krauss M, Ghallab A, Hofmann U, Kanacher T, et al. A systematic evaluation of the use of physiologically based pharmacokinetic modeling for cross-species extrapolation. J Pharm Sci. 2015 Jan;104(1):191–206.
3. Kuepfer L, Niederalt C, Wendl T, Schlender JF, Willmann S, Lippert J, et al. Applied Concepts in PBPK Modeling: How to Build a PBPK/PD Model. CPT Pharmacometrics Syst Pharmacol. 2016;5(10):516–31.
4. Hanke N, Frechen S, Moj D, Britz H, Eissing T, Wendl T, et al. PBPK Models for CYP3A4 and P-gp DDI Prediction: A Modeling Network of Rifampicin, Itraconazole, Clarithromycin, Midazolam, Alfentanil, and Digoxin. CPT Pharmacometrics Syst Pharmacol. 2018;7(10):647–59.
5. Cordes H, Thiel C, Aschmann HE, Baier V, Blank LM, Kuepfer L. A physiologically based pharmacokinetic model of isoniazid and its application in individualizing tuberculosis chemotherapy. Antimicrob Agents Chemother. 2016;60(10):6134–45.
6. Weiner M, Peloquin C, Burman W, Luo CC, Engle M, Prihoda TJ, et al. Effects of tuberculosis, race, and human gene SLCO1B1 polymorphisms on rifampin concentrations. Antimicrob Agents Chemother. 2010;54(10):4192–200.
7. Vinnard C, Ravimohan S, Tamuhla N, Pasipanodya J, Srivastava S, Modongo C, et al. Markers of gut dysfunction do not explain low rifampicin bioavailability in HIV-associated TB. J Antimicrob Chemother. 2017;72(7):2020–7.
8. Sloan DJ, McCallum AD, Schipani A, Egan D, Mwandumba HC, Ward SA, et al. Genetic determinants of the pharmacokinetic variability of rifampin in Malawian adults with pulmonary tuberculosis. Antimicrob Agents Chemother. 2017;61(7):1–9.

Section III.

Quantitative Pharmacology Approaches for Newer Anti-Tuberculosis Therapeutics

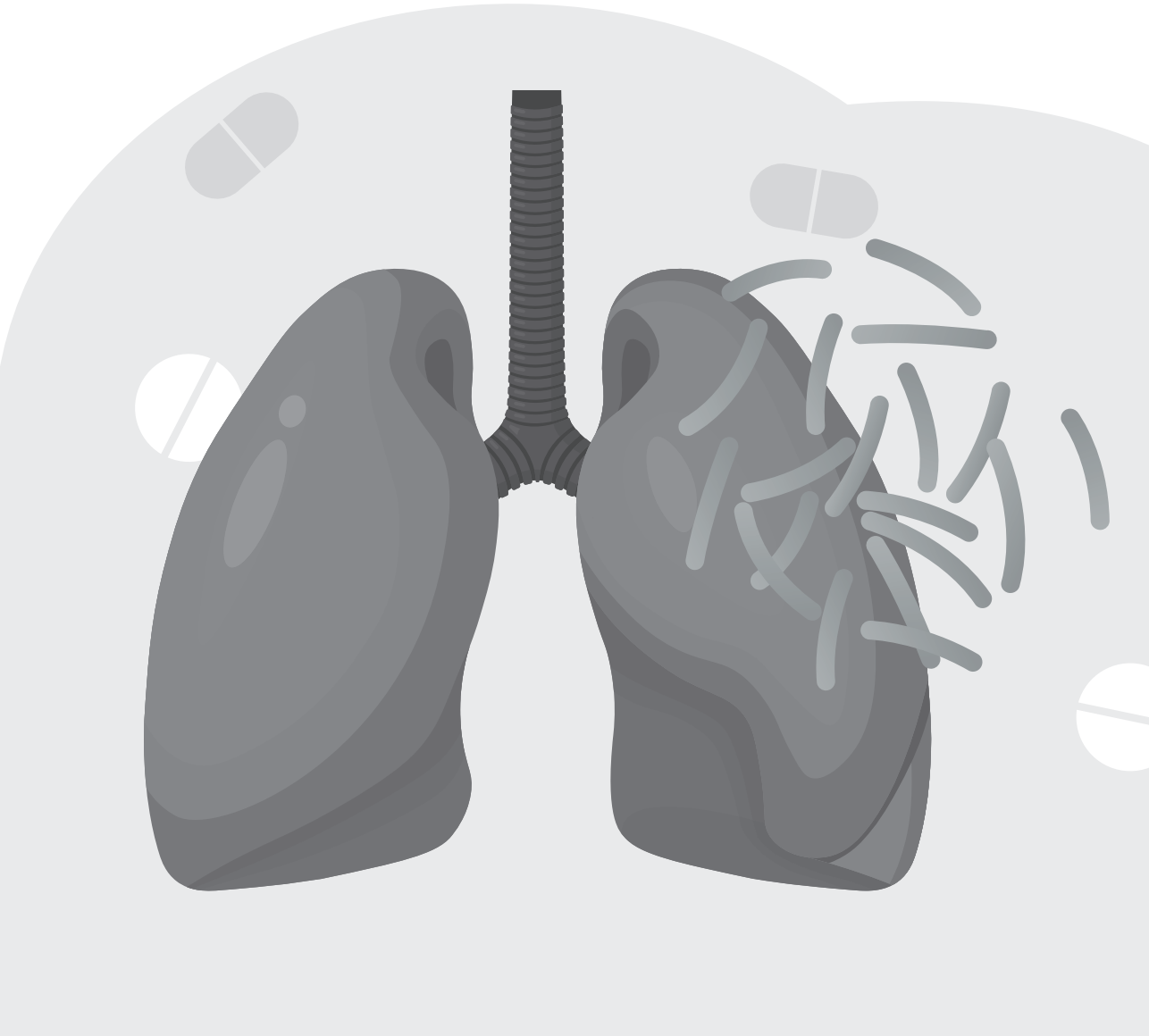

Chapter 4

Predictions of bedaquiline and pretomanid target attainment in lung lesions of tuberculosis patients using translational minimal physiologically based pharmacokinetic modeling

Krina Mehta, Tingjie Guo, Piet H van der Graaf, J G Coen van Hasselt

Clin Pharmacokinet, 2023 Mar, 62(3):519-532

Abstract

Background: Site-of-action concentrations for bedaquiline and pretomanid from tuberculosis patients are unavailable. The objective of this work was to predict bedaquiline and pretomanid site-of-action exposures using a translational minimal physiologically-based pharmacokinetic (mPBPK) approach to understand the probability of target attainment (PTA).

Methods: A general translational mPBPK framework for the prediction of lung and lung lesion exposure was developed and validated using pyrazinamide site-of-action data from mice and humans. We then implemented the framework for bedaquiline and pretomanid. Simulations were conducted to predict site-of-action exposures following standard bedaquiline and pretomanid, and bedaquiline QD dosing. Probabilities of average concentrations within lesions and lungs greater than the minimum bactericidal concentration for non-replicating (MBC_{NR}) and replicating (MBC_{R}) bacteria were calculated. Effects of patient-specific differences on target attainment were evaluated.

Results: The translational modeling approach was successful in predicting pyrazinamide lung concentrations from mice to patients. We predicted that 94% and 53% of patients would attain bedaquiline C_{avg}-lesion>MBC_{NR} during the extensive phase of bedaquiline standard (2 weeks) and QD (8 weeks) dosing, respectively. Less than 5% of patients were predicted to achieve C_{avg}-lesion>MBC_{NR} during the continuation phase of bedaquiline or pretomanid treatment. More than 80% of patients were predicted to achieve C_{avg}-lung>MBC_{R} for all simulated dosing regimens of bedaquiline and pretomanid.

Conclusions: The translational mPBPK model predicted that the standard bedaquiline continuation phase and standard pretomanid dosing may not achieve optimal exposures to eradicate non-replicating bacteria in most patients.

Introduction

Tuberculosis (TB) continues to be a global health challenge. Rifampin and isoniazid are two key first-line antibiotics against *Mycobacterium tuberculosis* (Mtb). Increasing levels and frequency of resistance against rifampin and isoniazid over time necessitated the discovery of new anti-TB antibiotics[1]. Within the last decade, two promising second-line antibiotics, bedaquiline and pretomanid, were developed as a result of increased efforts to tackle drug-resistant TB[2,3]. A combination regimen containing bedaquiline, pretomanid, and linezolid showed Mtb clearance as measured by negative culture status in 90% of patients with drug-resistant TB after 6-months of therapy[4]. BPaL is now recommended for the treatment of rifampin-resistant TB and multidrug-resistant TB patients[1].

Drug exposures at the site-of-action, within lungs, and especially within cavitary lesions, are correlated with bactericidal and sterilizing activities against Mtb. Anaerobic conditions within the necrotic region of the lesion microenvironment, caseum, provide a survival niche for nonreplicating but persistent Mtb[5]. Inadequate exposures within cavitary lesions can lead to resistance development. Measuring drug PK within the lungs and lesions of TB patients usually requires invasive methods to obtain samples and therefore is not readily possible. Preclinical animal models have traditionally been used to evaluate drug penetration at sites of action. These results require accounting for interspecies differences in physiological, pathological, and drug-specific aspects to translate to the patients[6]. Newer methods, such as, PET-imaging methods are increasingly being implemented to measure drug penetration at the site-of-action following intravenous administration of radiolabeled drugs to measure the relative fraction of drug penetration at the site-of-action[7]. A key benefit of this method is that it can be performed in the patients and as such can allow evaluations of tissue-specific PK with patient-specific covariates.

In-silico approaches allow the incorporation of available data for the development of predictive models for optimal decision-making. Population pharmacokinetics (PopPK) modeling approaches have been previously applied to quantify the relationship between plasma and lesion PK for several first-line and second-line TB antibiotics; however, this approach can only be applied when sites of action measurements are available from the patients[8,9]. Minimal physiologically-based pharmacokinetics (mPBPK) models are well suited for translational predictions of the relationship between drugs' PK in blood plasma and at sites of action and. Such models can account for known species-related differences and incorporate patient covariates and expected interindividual variability and uncertainty in the

parameter estimate to allow population simulations. The probability of target attainment (PTA) can then be predicted by defining target attainment to the desired breakpoint based on experimental data[5]. In general, several experimental methods exist to understand drug exposures at site-of-action. These methods should be used in combination with in-silico approaches to rationally predict overall treatment response in the TB patients.

Bedaquiline and its primary metabolite M2 exposures at the current standard dosing regimen (400 mg once daily (QD) for 14 days followed by 200 mg three times a week) have the potential for safety concerns related to QTc interval prolongation and hepatic adverse events[10–12]. Alternative QD dosing (200 mg QD for 8 weeks followed by 100 mg QD) of bedaquiline is of interest to increase patient adherence to obtain optimal efficacy[12]. Pretomanid has overall acceptable clinical safety profiles; however, pretomanid combination with bedaquiline and linezolid can have additive effects leading to an increased potential of certain adverse effects[13]. As such, understanding drug exposures within the systemic circulation and at sites of action is crucial to evaluate combination treatment strategies to ensure the attainment of adequate exposures to maximize efficacy, avoid resistance development, and minimize safety issues.

The main objective of this work was to predict bedaquiline and pretomanid lung- and lesion- exposures in TB patients to understand the probability of target attainment and the impact of patient covariates, body weight and cavity size, on PTA. To this end, we developed and validated a translational mPBPK modeling approach that allowed to predict bedaquiline and pretomanid PK at standard and alternative QD dosing and calculation of PTA in lungs and lesions using preclinical data.

Methods

A general translational mPBPK framework including lung and lesion was first developed and was validated using available lung PK data in mice and humans for pyrazinamide. The framework was then implemented for the development and assessments of bedaquiline and pretomanid models. Simulations were conducted to predict site-of-action exposures at standard bedaquiline and pretomanid dosing, and an alternative bedaquiline dosing. Then, the simulations were compared against critical concentration estimates to evaluate the effects of body weight and cavity size on lesion PTA.

General modeling approach

mPBPK model structure

The model development for all drugs was based on a general mPBPK structural model containing central and lung compartments[14]. The mPBPK models were parameterized using species-specific physiological parameters, such as body weight, cardiac output, lung and other tissue volumes, and volume of blood in systemic circulation[15]. Drug-specific parameters, such as blood-to-plasma ratio and plasma protein binding were obtained from the literature. Other drug-specific parameter estimates, such as absorption rates, partition coefficients, and apparent clearance (CL) were estimated using the data from PK studies in mice (S4.1). Additional structural components were evaluated in a stepwise manner as suggested by the available data and prior knowledge. For instance, plasma concentrations of the primary metabolite of bedaquiline, M2, are of importance due to its relevance to safety concerns[16,17]. Therefore, mechanistic representation of metabolism of bedaquiline to M2 was described using a liver compartment represented by the well-stirred liver model. Although in vitro and mice experimental studies have demonstrated lower anti-Mtb activity of M2 compared to bedaquiline, its site-of-action exposures can be useful to evaluate its overall impact on bacterial load in TB patients using PK-PD models; therefore, M2 lungs and lesion compartments were included in the model and the relevant parameters were estimated using mice M2 lung and lesion data. Different absorption models, i.e., multiple-site absorption, transit compartment absorption model, and dose-dependent bioavailability were evaluated.

Drug uptake in lung lesions and uninvolved lungs was described using the effect compartment structural model as described previously[18]. Rates of drug transport between systemic circulation and lesions and uninvolved lungs compartments were described by blood flow rates to these compartments calculated based on the approximate lesion and total lung volumes. The volume of lesions and uninvolved lungs were calculated based on the mean total lesion volume reported in the literature for cavitary TB patients and species-specific total lung volumes[19].

$$d/dt(Ci) = ki \times (Cbld \times Ri - Ci)$$

$$ki = Qc/Vi$$

$$Vi = Vlung \times VFi$$

Here, i represents compartments, i.e., lesion or uninvolved lungs; Ci represents drug concentration in the respective compartment; Cbld is drug concentration in systemic circulation; ki is the transfer rate constant to the respective compartment; Ri is penetration ratio for the respective compartment; Qc is cardiac output;

Vlung is the total volume of lungs; VFi is the fractional volume of the respective compartment; and Vi is the volume of the respective compartment. Mean volume of lesions (VF_{le}) was assumed 0.0216 calculated based on the mean total lesion volume, approximately 14 mL, reported in the literature for cavitary TB patients[20]. VF_{ul} was calculated as 1-VF_{le}.

Translation of the mpbpk models to tb patients

The mice mPBPK models developed using mice data were scaled to TB patients considering physiological differences between the species. Physiological parameters such as cardiac output and volumes of compartments for humans were obtained from the literature[15]. Drug-specific parameter, CL, was scaled from mice to humans using a previously known allometric exponent 0.75 for CL[21]. For the absorption rate parameter, ka, plasma PK predictions using the models scaling using allometric exponent of -0.25 and models without any scaling were compared with the observed data for each drug prior to selecting whether or not to scale ka from mice to humans. The same estimated partition coefficients and penetration ratios for each drug and compartment from mice were assumed for TB patients. To simulate a standard TB population, body weights for 500 virtual patients were sampled from the body weight distribution from clinical trial data (S4.1). Cavity presence or absence was also sampled from observed distribution from the clinical trials dataset. For virtual patients with a cavity, cavity size was simulated considering normal distribution using reported mean and standard deviation of total lesion volume in cavitary TB patients[19]. Log-normally distributed IIV of 25-40% was added in the relevant parameters. To account for uncertainty in the parameter estimates, 50 trials with the estimated RSE were simulated for each of the 500 virtual patients. All parameters for both mice and humans, including variability and RSE, are presented in **Table 4.1**.

Evaluation of the modeling approach using pyrazinamide data

An external evaluation of the predictability of our overall approach was performed using pyrazinamide plasma, lungs, and lesions PK data from mice and TB patients22,23. Therefore, preclinical mice data for pyrazinamide were digitized from the literature and were used in the pyrazinamide mPBPK model development22. Next, pyrazinamide clinical studies data were compiled from the literature23 and the Platform for Aggregation of Clinical TB Studies (TB-PACTS; https://c-path.org/programs/tb-pacts/). Simulated lesion and uninvolved lungs PK profiles of pyrazinamide were compared against available observed data in TB patients23 (S4.1).

Bedaquiline and pretomanid model development and assessment

Bedaquiline and pretomanid model development was conducted using PK data from mice. PK data from plasma, liver, and lung including both lung lesions and uninvolved lungs of mice for bedaquiline and its primary metabolite M2 were extracted from literature[22,24]. Plasma PK data from mice treated with oral pretomanid were also digitized[25]. PK concentrations from PET imaging of plasma, lung lesions, and uninvolved lungs of mice that were administered a single intravenous dose of radioactive 18F-pretomanid were also digitized[26]. The PK concentrations obtained using the PET imaging were represented as relative units (i.e., % of injected dose per mL (%ID/mL)); therefore, relevant doses were set to 100% in the analysis dataset. Model development was performed using the mPBPK generic structure as described above. Evaluations of additional drug-specific components were guided by data and the parameters were estimated using a model fitting to mice data. Model development and final model selection were guided by objective function value (OFV), the goodness of fit (predictions vs. observed) plots, physiological plausibility of parameter estimates, and precision (RSE) of the estimates.

Assessment of bedaquiline and pretomanid mice to human translated models was conducted using PK data from TB patients. Individual level PK, body weight, and cavity presentation data from various clinical studies were retrieved from the TB-PACTS database. Data from relevant dose levels and clinical studies were compiled for bedaquiline and pretomanid. Simulated plasma PK profiles for bedaquiline and pretomanid in TB patients were compared against observed data to evaluate the translated mPBPK model performance in TB patients. No lesion or uninvolved lungs PK data were available from human subjects for bedaquiline or pretomanid. Local sensitivity analysis was conducted to evaluate the impact of the parameters on steady-state plasma drug exposure was examined by introducing 10% variation in the parameters one at a time and running the simulations for 50 times.

Pharmacokinetics and target attainment predictions of bedaquiline and pretomanid at the site of action

Predictions of bedaquiline and pretomanid exposures in the lesions and uninvolved lungs were performed for 500 virtual humans using the body weight and cavity volume distributions from TB patients using the final translated mPBPK models (Table 4.1). Bedaquiline simulations included currently approved oral dosing of 400 mg QD for 14 days followed by 200 mg three times a week. The alternative bedaquiline dosing regimen included in the simulations was 200 mg QD for 8 weeks followed by 100 mg QD. Pretomanid simulations included oral dosing of 200 mg QD. Plots of the predicted lesion and uninvolved lungs PK and drug exposure matrices were prepared. Next, predicted bedaquiline and pretomanid concentrations and exposures at the site-of-action following either standard or alternative bedaquiline or standard pretomanid dosing were compared against critical concentration estimates based on in vitro experiments obtained from the literature. The range for bedaquiline and pretomanid minimum inhibitory concentrations (MIC) for MDR-TB strains, minimal bactericidal concentrations for replicating bacteria (MBC_R), and minimal bactericidal concentrations for non-replicating bacteria (MBC_{NR}) were obtained from the literature (Table 4.1)[5,27.] Plots of predicted PK exposures within lesions and lungs were plotted and compared against the MDR-TB MIC range, MBC_R, and MBC_{NR} for both drugs. Attainment of target exposures in the lesions was defined as average daily PK exposure within lesions (C_{avg}-lesion) greater than MBC_{NR} to ensure bactericidal activity against persisting, non-replicating bacteria. Body weight and cavity size from the virtual patient population were binned and PTA was calculated for each bin.

Software

All analyses were conducted in R (R for Windows, v4.1, https://www.r-project.org/) using RStudio (RStudio, v1-554, www.rstudio.com/). Data management and plotting were performed using the tidyverse package. Parameter optimization and model simulations were conducted using nlmixr and RxODE packages. Final model codes are provided in the supplementary materials (S4.2).

Figure 4.1 Final Model Structures, (A) Bedaquiline, (B) Pretomanid. The mPBPK models for bedaquiline and pretomanid contain the relevant compartments, including lung and lung lesions. Blood, liver, lungs, and lung lesions are represented by their volumes and the rest of the body is lumped into tissue compartment(s). Compartments are connected with each other by blood flows. CL=plasma clearance, DoseF=dose-dependent bioavailability, Eh=hepatic extraction ratio, F1=bioavailability of depot1, ka1=absorption rate from depot1, ka2=absorption rate from depot2, Kp=partition coefficient for tissue compartments, Qh=blood flow to liver, Qle=blood flow rate to lung lesions, Qt=blood flow to tissues, QUL=blood flow rate to unaffected lungs, Rle=penetration ratio for lung lesion, RUL=penetration ratio for unaffected lungs, Vblood=volume of blood reservoir, Vliver=volume of liver, Vtissues=volume of tissue compartment.

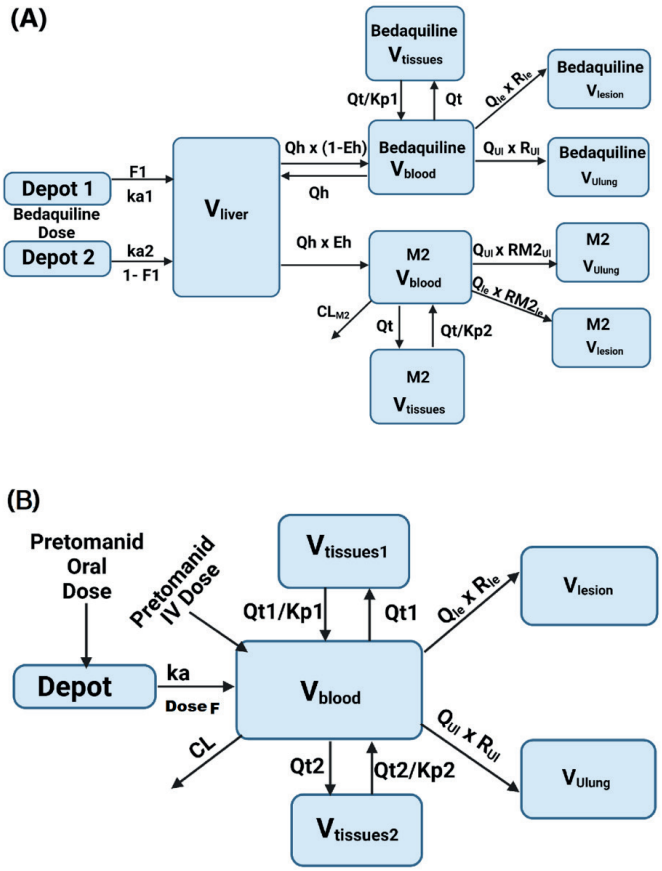

Results

Evaluation of the modeling approach using pyrazinamide data

The pyrazinamide mPBPK model was first developed using mice PK data to evaluate the predictability of our translational mPBPK approach. Pyrazinamide plasma, lung lesion, and uninvolved lungs PK data from mice were best described by the mPBPK structural model with first-order absorption and first-order elimination (S4.3). The addition of a tissue compartment and evaluations of other absorption models did not improve the model fit. The parameters describing plasma PK were estimated with good precision (RSE < 20%). The parameters R_{le} and R_{ul} were associated with an RSE of 52% and 102%, respectively (Table 4.1). The scaled mPBPK model appropriately described pyrazinamide plasma, lung lesions, and uninvolved lungs concentrations at steady-state from TB patients using allometric exponents of -0.25 for ka and 0.75 for CL **(Table 4.1, Figure 4.1)**. Overall, the pyrazinamide model predictions showed good agreement with the observed data from mice and TB patients suggesting the reliability of our translational mPBPK approach for other TB antibiotics.

Figure 4.2 Evaluation of the modeling approach using Pyrazinamide PK profiles in TB patients. Pyrazinamide model predictions showed good agreement with the observed data from TB patients suggesting the reliability of our mPBPK framework for other TB antibiotics. Pyrazinamide 1500 mg oral dosing was simulated and compared against observed data from plasma, lungs, and lesions of TB patients[23,29,39] accessed through TB-Pacts. Both observed and simulations for lung and lesion represent one dosing cycle at steady-state. Blue points=observed data, solid grey line=median of the simulations, shaded grey area=95% prediction interval (PI) of the simulations.

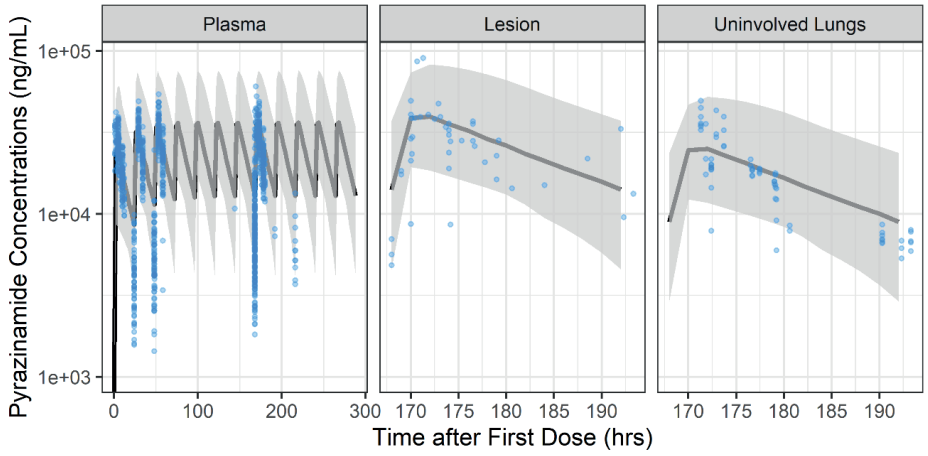

Table 4.1 Parameter estimates of Bedaquiline, Pretomanid, and Pyrazinamide mPBPK models

Parameter (Units)	Description	Parameter Estimate		%RSE	Source
		Mice	Humans		
Physiological					
Qc (L/hr)	Cardiac output	0.839	312 (for 70 kg)		15
Qh (fraction of Qc)	Blood flow to liver	0.161	0.227		
Vliv (fraction of body weight)	Volume of liver	0.0549	0.0549		
Vbl (fraction of body weight)	Volume of blood reservoir	0.077	0.077		
Bedaquiline					
fup (%)	Unbound fraction	0.1	0.1		28
BP	Blood-to-plasma ratio	1	1	-	35
ka1 (1/hr)	Absorption rate from depot1	1.3	1.3	37.8	Estimated
ka2 (1/hr)	Absorption rate from depot2	0.00501	0.00501	9.13	
CLint (L/hr)	Intrinsic clearance	1.21	60.3	16.7	
KpT	Partition coefficient for tissue compartments	4.45	4.45	15.3	
CLM2 (L/hr)	Clearance for M2	0.0119	45.9	13.6	
KpTM2	Partition coefficient for tissue compartments for M2	9.54	9.54	18.4	
R_{le}	Penetration ratio for lung lesion	11	11	10.7	
R_{ul}	Penetration ratio for uninvolved lungs	10.2	10.2	10.9	
$R_{le}M2$	Penetration ratio for lung lesion for M2	88.4	88.4	5.72	
$R_{ul}M2$	Penetration ratio for uninvolved lungs for M2	88.8	88.8	5.53	
frc	Fraction going through fast absorption (depot1)	0.609	0.609	11.9	
IIV for ka1, ka2, CLint, CLM2, KpT, and KpTM2 (%)	Lognormally distributed random variability in bedaquiline parameters for human simulations	-	40	-	
MBC_{NR}	Minimum bactericidal concentration for non-replicating bacteria (ng/mL)	-	17760	-	5
MBC_{R}	Minimum bactericidal concentration for replicating bacteria (ng/mL)	-	5500	-	5
MIC Range	Minimum inhibitory concentration range (ng/mL)	-	60-250	-	41

Parameter (Units)	Description	Parameter Estimate		%RSE	Source
		Mice	Humans		
Pretomanid					
BP	Blood-to-plasma ratio	1.65	1.65		[13]
ED50 (mg)	Dose at which bioavailability is 50% of the maximum which was assumed 1	7.59	554	14.8	Mice estimated, Humans [42]
ka (1/hr)	Absorption rate	0.3	0.3	23.3	Estimated
CL (L/hr)	Apparent clearance	0.016	4.42	3.78	
KpT	Partition coefficient for tissue compartment 1	36.3	36.3	3.77	
FT1	Fraction going to tissue compartment 1	0.97	0.97	9.72	
KpT1	Partition coefficient for tissue compartment 2	0.483	0.483	14	
R_{le}	Penetration ratio for lung lesion	1.05	1.05	145	
R_{ul}	Penetration ratio for uninvolved lungs	1.75	1.75	13.8	
IIV for ka, ED50, CL, KpT, and KpT2 (%)	Lognormally distributed random variability in pretomanid parameters for human simulations	-	40	-	
MBC_{NR}	Minimum bactericidal concentration for non-replicating bacteria (ng/mL)	-	6300	-	[13]
MBC_{R}	Minimum bactericidal concentration for replicating bacteria (ng/mL)	-	20	-	[13]
MIC Range	Minimum inhibitory concentration range (ng/mL)	-	8 - 4000	-	[13]
Pyrazinamide					
BP	Blood-to-plasma ratio	0.79	0.79	-	[43]
ka (1/hr)	Absorption rate	0.30	0.05[a]	7.25	Estimated
CL (L/hr)	Apparent clearance	0.014	3.5	3.04	
R_{le}	Penetration ratio for lung lesion	1.37	1.37	52.2	
R_{ul}	Penetration ratio for uninvolved lungs	0.85	0.85	102	
IIV for ka and CL (%)	Lognormally distributed random variability in pyrazinamide parameters for human simulations (%)	-	40	-	

[a] allometrically scaled from mice to humans using exponent -0.25; Estimated residual errors in model fitting to mice data were as following: combined bedaquiline plasma, liver, and M2 plasma = proportional 43 %; bedaquiline and M2 lesion and lungs = proportional 53%, pretomanid plasma= proportional 12 %, pretomanid lesion = proportional 6% and additive 2.24 ng/mL, pretomanid lungs = proportional 12 % and additive 0.239 ng/mL, pyrazinamide combined plasma, lungs, and lesion= proportional 35%. Residual errors were not included in the human simulations.

Model development and assessment for bedaquiline and pretomanid

Bedaquiline and M2 PK data from plasma, liver, lung lesions, and uninvolved lungs of Mtb infected mice was best described by the mPBPK structural model containing parallel first-order two absorptions that are in alignment with prior bedaquiline PopPK models, parent-metabolite well-stirred liver compartment, tissue compartments for both bedaquiline and M2, first-order elimination of M2, and lung lesion and uninvolved lungs compartments **(Figure 4.1A)**. Other components that were evaluated but did not provide improvements in the model fit included only one first-order absorption, transit compartment absorption, and saturable conversion of bedaquiline to M2. All parameters were estimated with reasonable precision (RSE < 40%) **(Table 4.1)**, and the model predictions showed good agreement with the observed data in mice **(Figure 4.3A,** S4.4A**)**.

Slight under-predictions of bedaquiline and over-predictions of M2 plasma concentrations were noted when the mPBPK model was directly scaled from mice to humans using only allometric scaling. This was assumed to be due to the species difference between mice and humans in bedaquiline and M2 metabolism and has been previously noted[24,28]. To account for this difference, calibration of two parameters, intrinsic clearance (CLint) and clearance of M2 (CLM2) was performed by fitting to median rich concentrations-time profiles from TB patients for one dose group (400 mg on day1, 300 mg on day2, and 200 mg day3-14)[29]. The updated model predicted both bedaquiline and M2 plasma concentrations time profiles well for all dose groups in the dataset **(Table 4.2, Figure 4.4)**. With a 10% or 50% variation in parameter estimates, the mean sensitivity index was low (between -1 and 1) for both bedaquiline and M2 with the exception of absorption rate of depot2 (ka2) that showed high sensitivity for both bedaquiline and M2 plasma concentrations (S4.6). Overall, this mPBPK model for bedaquiline and M2 was deemed reliable for predictions of exposures at the site-of-action, within lung lesions, in TB patients.

Pretomanid oral absorption was best described by a first-order absorption model with dose-dependent bioavailability. Transit compartment absorption was evaluated but did not provide improvements in the model fits. Pretomanid plasma PK after oral dosing, and F18-pretomanid plasma, lung lesion, and uninvolved lungs PK after F18-pretomanid IV dosing were best described by the mPBPK structural model with two tissue compartments and first-order elimination **(Figure 4.2B)**. All parameters were estimated with reasonable precision (RSE < 45%) except that R_{le} was estimated with RSE of 145% due to limited lesion PK data **(Table 4.1)**. Overall, the model predictions showed good agreement with the observed data

from mice following either F18-pretomanid IV or pretomanid oral dosing **(Figure 4.3B)**. Reasonable agreement between observed data and scaled-up human model predictions was noticed for plasma PK data for pretomanid from TB patients, although some underpredictions were noted at 1000 mg and 1200 mg doses **(Table 4.2, Figure 4.4)**. With a 10% change in parameter estimates, the sensitivity for key pretomanid PK parameters was relatively low (between -2.5 and 2.5) with the exception of partition coefficient for tissue compartment 1 (kpT1) that showed moderate sensitivity for pretomanid plasma concentrations. This further supported the reliability of the model (S4.6). Overall, the mPBPK model for pretomanid was deemed reliable for predictions of exposures at the site-of-action, within lung lesions, following clinically-relevant doses in TB patients.

Figure 4.3 Predicted vs. observed PK profiles in mice, (A) Bedaquiline, (B) Pretomanid. The model predictions for plasma, lung, and lesion bedaquiline and pretomanid agreed well with the observed data for mice. Bedaquiline 25 mg/kg was administered orally[22]. Pretomanid was administered orally at varying doses between 18 mg/kg to 486 mg/kg[25,26]. Radioactive 18F pretomanid was administered intravenously and the % of the injected dose was measured in plasma, lungs, and lesions of mice. Blue points=observed data, black line=model fit predictions, %ID= percent of injected dose, pretomanid concentrations for oral dosing unit=ng/mL, 18F-pretomanid concentrations for IV dosing=%ID/mL.

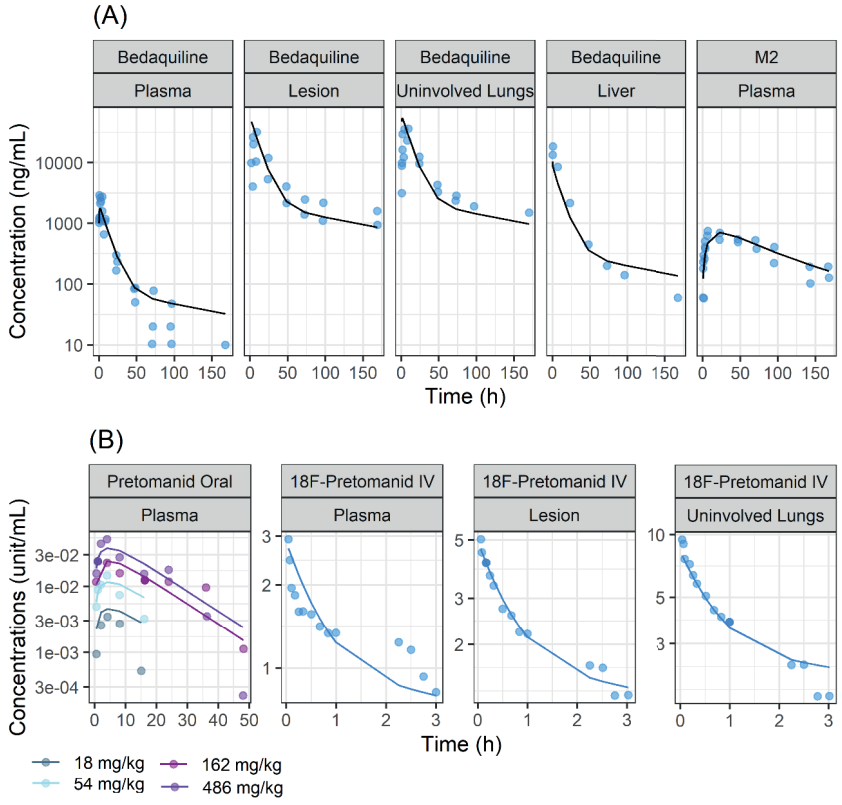

Figure 4.4 Predicted and observed plasma PK profiles in TB patients for Bedaquiline, M2, and Pretomanid. The model predictions for plasma bedaquiline, M2, and pretomanid agreed well with the observed data for TB patients from clinical trials at various doses[29,40]. Blue points=observed data, solid grey line=median of the simulations, shaded grey area=95% prediction interval (PI) of the simulations. Panel titles represent bedaquiline or pretomanid doses in mg. Bedaquiline was administered as an increasing daily dose, i.e., panel 1 represents a group that received 200 mg on day1 and 100 mg on day2 onwards.

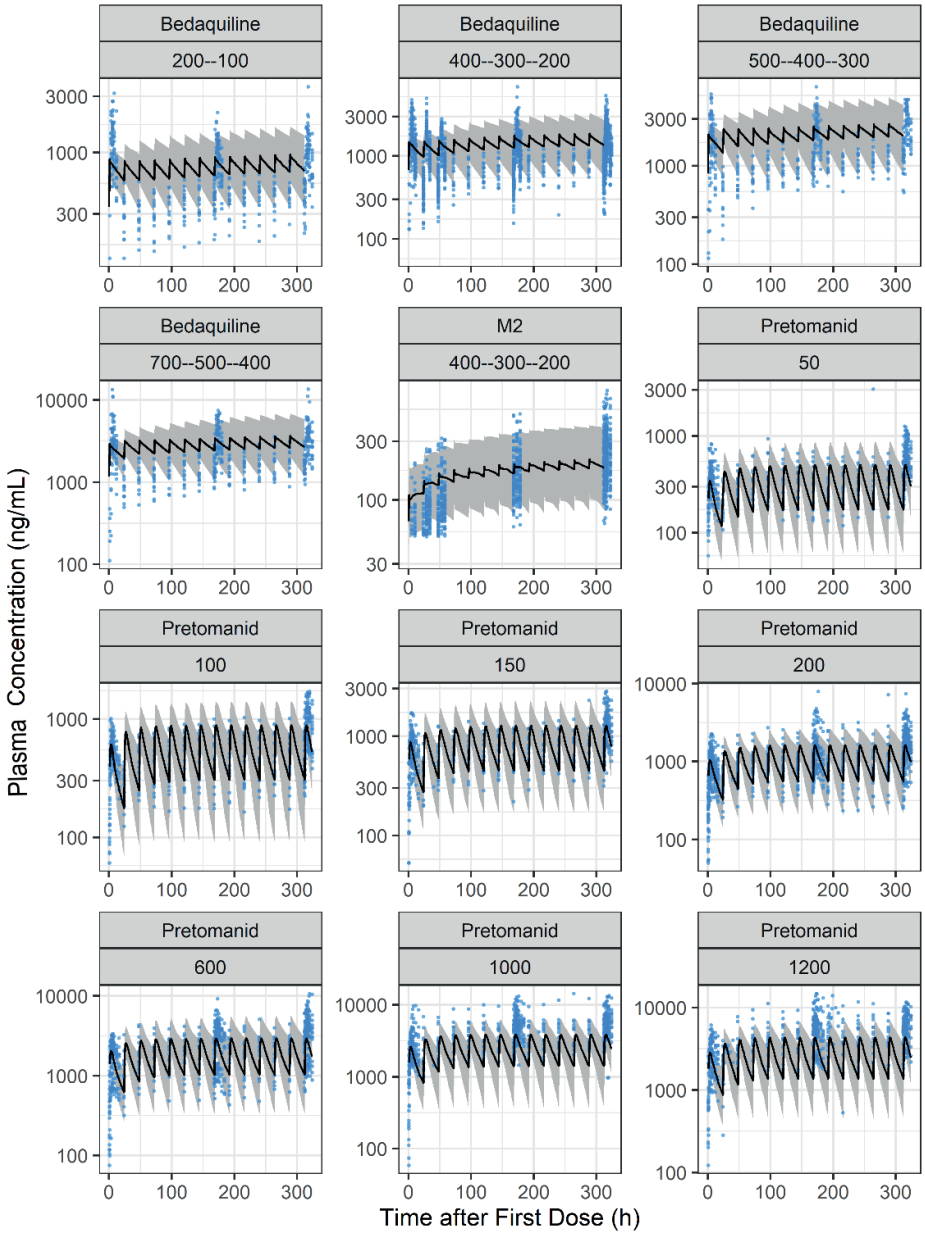

Pharmacokinetics and target attainment predictions of bedaquiline and pretomanid at the site of action

The simulations suggested good penetration for both bedaquiline in lung lesions and uninvolved lungs **(Figure 4.5A)**. The predicted bedaquiline median (95% prediction interval) lesion-to-plasma ratio was 11.0 (10.5-11.4) and uninvolved-lungs-to-plasma was 10.2 (9.8-10.5). Bedaquiline lesions and uninvolved lungs concentrations were predicted to remain above the MIC range observed for MDR-TB isolates at standard dosing and alternative QD dosing[27]. Bedaquiline lesion and uninvolved lungs concentrations were predicted to be slightly above MBC_R for all virtual patients throughout the treatment period during extensive phase of standard dosing and alternative QD dosing **(Figure 4.5A)**[5,27]. At standard bedaquiline dosing, a total of 94% of virtual patients were predicted to have Cavg-lesion > MBC_{NR} after extensive dosing (400 mg QD) for the first 14 days of treatment, but <5% of virtual patients were predicted to have Cavg-lesion > MBC_{NR} throughout the continuation phase of treatment when dosing was reduced to 200 mg three times a week. At alternative QD bedaquiline dosing, a total of 86% of virtual patients were predicted to have Cavg-lesion > MBC_{NR} during extensive phase (200 mg QD) for the 8 weeks of treatment, but <5% of virtual patients were predicted to have Cavg-lesion > MBC_{NR} throughout the continuation phase of treatment when dosing was reduced to 100 mg QD. The simulations also suggested relatively similar M2 exposures at site-of-action to those of bedaquiline **(Figure 4.5)**. Simulated plasma M2 concentrations were below reported M2 EC50 concentrations for QTcF prolongation for 83% of virtual patients during extensive phase of standard bedaquiline treatment, and for all virtual patients during continuation phase of standard bedaquiline and both phases of alternative QD dosing (S4.4B). It should be noted that although the probability of target attainment is higher with bedaquiline standard dosing during the extensive phase, the period of extensive phase in standard dosing vs. alternative QD dosing is shorter (2 vs. 8 weeks) which may have a large impact on overall efficacy. The probability of Cavg-lesion >MBC_{NR} was predicted to increase with an increase in body weight for both dosing scenarios **(Figure 4.6)**. Cavity size was predicted to not affect the attainment of average lesion concentrations above MBC_{NR}.

Pretomanid predicted median (95% prediction interval) lesion-to-plasma ratio was 2.6 (2.5-2.8) and uninvolved-lung-to-plasma ratio was 2.9 (2.7-3.1) (Figure 4.5B). Predicted lesion concentrations after pretomanid 200 mg daily dosing were predicted to remain above the pretomanid MIC range observed for MDR-TB isolates for 18% of virtual patients[13]. Pretomanid lesions and uninvolved lungs concentrations were predicted to remain well above (MBC_R) for all patients. Less than 1% of patients were predicted to have pretomanid Cavg-lesion> MBC_{NR} **(Figure 4.5B)**[13].

Table 4.2 Observed vs. predicted exposure comparison for Bedaquiline and Pretomanid at standard dosing at steady-state.

Exposure Metric (mg/L)	Bedaquiline 400 mg QD		Bedaquiline 200 mg Thrice a Week		Pretomanid 200 mg QD	
	Observed [28]	Predicted	Observed [28]	Predicted	Observed [13]	Predicted
$Cavg_{ss}$	2.696 (0.865) [a] 1.371 (0.529) [b]	3.24 (0.497)	0.584 (0.197)	0.68 (0.108)	1.26 (0.16)	1.06 (0.143)
$Cmax_{ss}$	5.502 (2.965) [a] 2.763 (1.185) [b]	6.29 (1.45)	1.267 (0.435)	1.57 (0.404)	1.7 (0.29)	3.06 (0.61)
$Cmin_{ss}$	1.448 (0.437) [a] 0.728 (0.257) [b]	1.07 (0.322)	0.356 (0.170)	0.174 (0.062)	0.5 (0.08)	0.149 (0.06)

[a] Drug-susceptible TB patients, [b] MDR-TB patients. All values are presented as mean (standard deviation)

Figure 4.5 Simulated PK profiles at sites of action in TB patients: (A) Bedaquiline standard and QD dosing, and (B) Pretomanid. Bedaquiline standard dosing included 400 mg QD for 14 days followed by 200 mg three days a week. Bedaquiline QD dosing included 200 mg QD for 8 weeks followed by 100 mg QD. Pretomanid dosing included 200 mg QD. The model predicted that lung and lesion concentrations of bedaquiline and pretomanid would remain above MIC (for rifampin and/or isoniazid drug-resistant TB strains) and MBCR at current clinically-relevant doses. Although it was predicted that 94% and 53% of patients would achieve target exposures at standard and alternative QD bedaquiline dosing, respectively; it should be noted that alternative QD dosing provides higher target attainment for a longer duration (2 vs. 8 weeks). M2 target attainment was predicted to be slightly higher than those of bedaquiline. It should be noted that M2 MBC and MICs were assumed the same as those of bedaquiline[41]. MIC= minimum inhibitory concentrations, MDR= multi-drug resistant tuberculosis, MBCR = minimum bactericidal concentrations for replicating bacteria, MBCNR = minimum bactericidal concentrations for non-replicating bacteria. Blue or black lines=median of the simulations, shaded blue or grey area=95% prediction interval (PI) of the simulations.

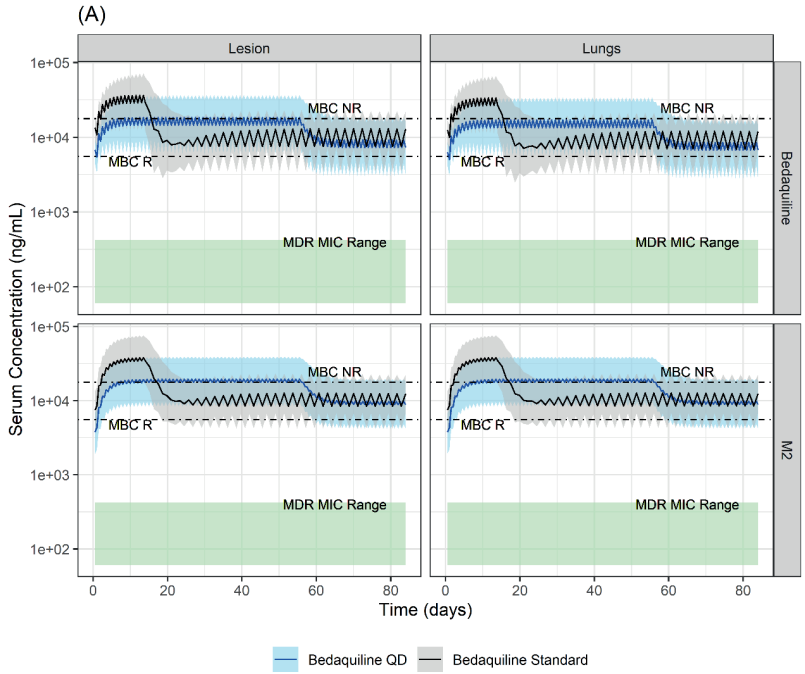

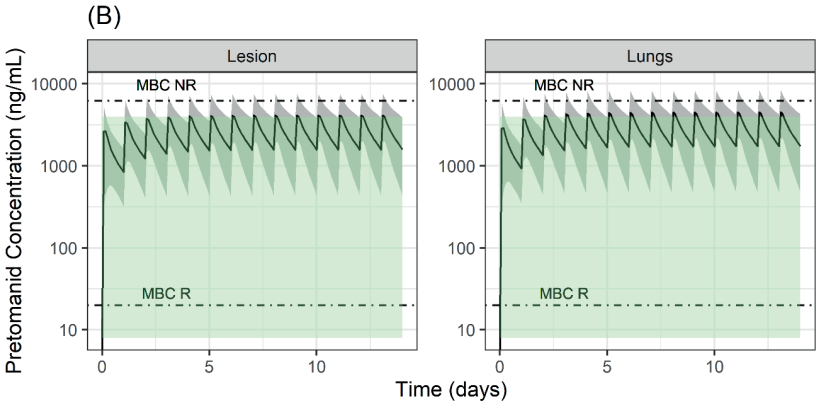

Figure 4.6 Predicted probability of average Bedaquiline concentrations above MBCNR in TB patients by body weight. Body weight was predicted to have an impact on lesion PTA. PTA was defined as Cavg-lesion > MBC NR. MBCNR = minimum bactericidal concentrations for non-replicating bacteria. PTA were calculated at steady-state for each dosing group.

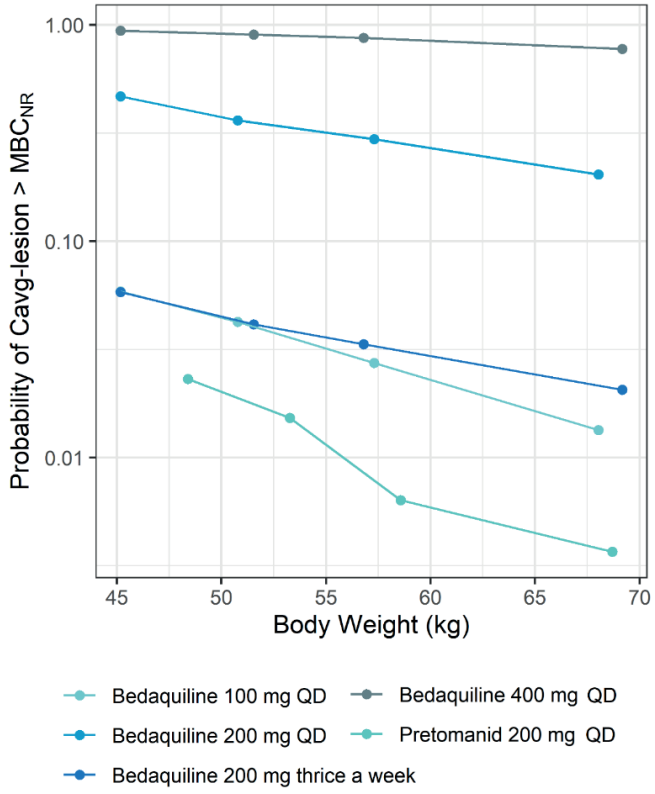

Discussion

In this work, we developed translational mPBPK models for bedaquiline and pretomanid containing lungs including cavitary lesions compartments using physiological parameters describing blood flows and volumes of lesions and uninvolved lungs. The mPBPK models adequately described plasma, lungs, and lesion PK data from mice well. The translational mPBPK models adequately described dose-ranging plasma PK data from TB patients. The mPBPK models allowed predictions of bedaquiline and pretomanid exposures and target attainment in the lungs and lesions of TB patients.

One of the concerns against the newer antibiotics, bedaquiline and pretomanid, is the development of resistance[30]. A key mechanism of resistance development against antibiotics includes a subpopulation of Mtb, persisters, developing phenotypic tolerance against the drugs without genetic mutations. This process is reversible; however, sub-optimal drug exposures within cavitary lesions where persisters dwell, allow them to survive. This eventually allows Mtb strains to develop genotypic mutation and allow replication of genetically resistant strains against antibiotics[31]. As such, it is crucial to optimize therapeutic strategies to eliminate the non-replicating persistent Mtb population during the treatment phase. Our mPBPK models can be combined with various types of experimental in vitro and in vivo bacterial-kill dynamics and resistance development data to construct mechanistic PK-PD models that can be used to further evaluate optimal strategies against Mtb, especially against persisters within lesions[32].

Our predictions suggested that PTA decrease with an increase in patients' body weight for both bedaquiline and pretomanid. The current dosing regimen for bedaquiline is associated with safety risks of QTcF prolongation and hepatic adverse events; therefore, an increase in bedaquiline dosing may not be a viable approach for all patients. Further efficacy and safety evaluations of bodyweight-based dose optimization for bedaquiline may be useful. The model also captured the pharmacokinetics of the bedaquiline metabolite M2 within plasma and at site-of-action. To further evaluate the contribution of M2 on Mtb clearance using the developed mPBPK framework, M2-specific pharmacodynamic parameters such as derived in an in vitro experiment would be required. Model-informed precision dosing approaches can be employed to ensure maximum risk-benefit balance for most patients considering totality of information[33,34]. The current dosing regimen for pretomanid is considered safe. The mechanistic PK-PD model can be used

to predict the effects of alternative dosing of pretomanid in combination with bedaquiline and/or other antibiotics on clearance of persisting Mtb from lesion.

Previously, standard compartmental models combined with effect compartment structural models or whole-body PBPK modeling combined with mechanistic lung models have been developed for mostly first-line TB antibiotic[8,9,35]. Middle-out approaches, such as mPBPK models, allow the balance between empirical compartmental models and rigorous whole-body PBPK models[36]. Our mPBPK model construct included standard physiological parameters, such as blood flow rates and volume for lungs. A key component of our structural model is the parameter describing flow rates to lesions that were calculated based on total blood flow rates and volume fraction of cavitary lesion. As such, this approach suggests a simple technique to evaluate the impact of cavitary lesion size on target exposure attainment within lesions for anti-TB agents. Our simulations suggested no significant impact of total lesion volume on PTA within lesions for bedaquiline and pretomanid given other variability and uncertainty in the parameters that were estimated using limited preclinical data. Additional model-based analyses using our structural model and longitudinal PET-imaging data from lesions of varying sizes from TB patients[7] may allow further insights into understating the impact of cavity size on bedaquiline and pretomanid target attainment within lesions to further optimize treatment strategies.

In vitro experimental evaluations of MIC and MBC values for antimicrobials are usually performed using free drug. As such, the role of plasma protein binding may be important for in vitro – in vivo response comparisons if plasma drug concentrations are used for predictions of response in vivo. Generally, only unbound drug from the systemic circulation is available for diffusion into the tissues. Both bound and unbound drug can penetrate the tissues via active transport; however, as distribution equilibrium is achieved, unbound plasma and unbound tissue concentrations reach equilibrium[37,38]. The previously described empirical model structure for tissue penetration that was fitted to the observed lung and lesion concentrations data allows estimation of lung and lesion distribution parameters relative to plasma drug concentrations, and may empirically account for the contributions of the plasma protein binding[8,18]. Following drug penetration to the lung tissue, the fraction of drug available to exert the effect depends on the tissue content and drug physicochemical properties, such as lipophilicity, solubility, tissue protein binding, and acidity[37,38]. Therefore, accounting for fraction unbound in tissue for predictions of PK-PD relationship may be important[5]. In this work, we did not directly correct site of action exposures for protein or tissue binding process

as uncertainty exists in the overall impact of these parameters on the PK-PD relationship for bedaquiline and pretomanid. Evaluations of these relationships may be of interest in future studies.

Our mPBPK models were calibrated to mice PK data. The models were translated to TB patients using allometric scaling and were compared and qualified against dose-ranging plasma concentrations data from clinical studies. Although our translational models provided reasonable agreement with the observed plasma concentrations data for all three drugs, this work did not include evaluations of best structural model fit to the clinical data or estimation of individual parameter estimation. The sensitivity analysis identified the most sensitive parameters. The future work may consider estimation of individual parameters using the mPBPK model structure, including further evaluations of the role of the sensitive parameters on exposure using clinical data. Mechanistic understanding included in the mPBPK construct combined with Bayesian estimation using our final parameter estimates as priors may provide thorough understanding of individual variability and covariate-parameter relationships towards the goal of treatment optimization, especially against persisting Mtb.

Although the validation of our translational approach for predictions of lesion and lung concentrations using pyrazinamide give confidence in the applied approach, our model predictions for lesion and lung concentrations for bedaquiline and pretomanid cannot be compared to observed data from TB patients as such data are not available to date. Our models may be further validated or further developed in the future when such data is available. In general, the current construct of mPBPK models for bedaquiline and pretomanid are relevant for our primary objective, i.e., to predict exposures in the lungs and lesions of TB patients using preclinical data. Additionally, the good performance of our translational mPBPK approach for pyrazinamide gives confidence that similar translational performance may be expected for other drugs, such as, bedaquiline and pretomanid.

To conclude, we present the first translational mPBPK models for bedaquiline and pretomanid allowing comprehensive predictions of lungs and lesions exposures in patients. Both extensive and continuation phase of current standard bedaquiline dosing were predicted to achieve target exposures within lungs and cavitary lesions to elicit bactericidal activity against replicating bacteria; however, only extensive phase treatment was predicted to achieve target exposures to elicit minimum bactericidal activity against non-replicating bacteria. Standard pretomanid dosing was predicted to achieve target exposures to elicit bactericidal

activity against replicating bacteria but not against non-replicating bacteria for most patients. These models can also be further developed to be combined with pharmacodynamics, efficacy, or safety measures to optimize or individualize combination treatment strategies.

References

1. World Health Organization. Consolidated Operational Guidelines on Handbook Tuberculosis. 2020. 132 p.
2. Khoshnood S, Goudarzi M, Taki E, Darbandi A, Kouhsari E, Heidary M, et al. Bedaquiline: Current status and future perspectives. J Glob Antimicrob Resist [Internet]. 2021;25:48–59. Available from: https://doi.org/10.1016/j.jgar.2021.02.017
3. Stancil SL, Mirzayev F, Abdel-Rahman SM. Profiling pretomanid as a therapeutic option for tb infection: Evidence to date. Drug Des Devel Ther. 2021;15:2815–30.
4. Conradie F, Diacon AH, Ngubane N, Howell P, Everitt D, Crook AM, et al. Treatment of Highly Drug-Resistant Pulmonary Tuberculosis. N Engl J Med. 2020;382(10):893–902.
5. Sarathy JP. Caseum : a Niche for Mycobacterium tuberculosis Drug-Tolerant.
6. Ernest JP, Strydom N, Wang Q, Zhang N, Nuermberger E, Dartois V, et al. Development of New Tuberculosis Drugs: Translation to Regimen Composition for Drug-Sensitive and Multidrug-Resistant Tuberculosis. Annu Rev Pharmacol Toxicol. 2021;61:495–516.
7. Ordonez AA, Wang H, Magombedze G, Ruiz-CA, Srivastava S, Chen A, et al. Heterogeneous Drug Exposures in Pulmonary Lesions. HHS Public Access. 2020;26(4):529–34.
8. Kjellsson MC, Via LE, Goh A, Weiner D, Low KM, Kern S, et al. Pharmacokinetic evaluation of the penetration of antituberculosis agents in rabbit pulmonary lesions. Antimicrob Agents Chemother. 2012 Jan;56(1):446–57.
9. Strydom N, Gupta S V., Fox WS, Via LE, Bang H, Lee M, et al. Tuberculosis drugs' distribution and emergence of resistance in patient's lung lesions: A mechanistic model and tool for regimen and dose optimization. Vol. 16, PLoS Medicine. 2019.
10. Dooley KE, Rosenkranz SL, Conradie F, Moran L, Hafner R, von Groote-Bidlingmaier F, et al. QT effects of bedaquiline, delamanid, or both in patients with rifampicin-resistant tuberculosis: a phase 2, open-label, randomised, controlled trial. Lancet Infect Dis [Internet]. 2021 Jul 1;21(7):975–83. Available from: https://doi.org/10.1016/S1473-3099(20)30770-2
11. Cohen K, Maartens G. A safety evaluation of bedaquiline for the treatment of multi-drug resistant tuberculosis. Expert Opin Drug Saf [Internet]. 2019;18(10):875–82. Available from: https://doi.org/10.1080/14740338.2019.1648429
12. Tanneau L, Karlsson MO, Rosenkranz SL, Cramer YS, Shenje J, Upton CM, et al. Assessing Prolongation of the Corrected QT Interval with Bedaquiline and Delamanid Coadministration to Predict the Cardiac Safety of Simplified Dosing Regimens. Clin Pharmacol Ther. 2022;0(0):1–9.
13. FDA, Center For Drug Evaluation and Research. Center for Drug Evaluation and Research Application Number: 211810Orig1s000: MULTI-DISCIPLINE REVIEW. 2016;1–264. Available from: https://www.accessdata.fda.gov/drugsatfda_docs/nda/2019/212862Orig1s000MultidisciplineR.pdf
14. Jermain B, Hanafin PO, Cao Y, Lifschitz A, Lanusse C, Rao GG. Development of a Minimal Physiologically-Based Pharmacokinetic Model to Simulate Lung Exposure in Humans Following Oral Administration of Ivermectin for COVID-19 Drug Repurposing. J Pharm Sci. 2020 Dec;109(12):3574–8.
15. Brown RP, Delp MD, Lindstedt SL, Rhomberg LR, Beliles RP. Physiological parameter values for physiologically based pharmacokinetic models. Toxicol Ind Health. 1997;13(4):407–84.
16. Ngwalero P, Brust JCM, van Beek SW, Wasserman S, Maartens G, Meintjes G, et al. Relationship between plasma and intracellular concentrations of bedaquiline and its m2 metabolite in South African patients with rifampin-resistant tuberculosis. Antimicrob Agents Chemother. 2021;65(11).
17. Tanneau L, Svensson EM, Rossenu S, Karlsson MO. Exposure–safety analysis of QTc interval and transaminase levels following bedaquiline administration in patients with drug-resistant tuberculosis. CPT Pharmacometrics Syst Pharmacol. 2021;10(12):1538–49.
18. Gobburu JVS, Tammara V, Lesko L, Jhee SS, Sramek JJ, Cutler NR, et al. Pharmacokinetic-pharmacodynamic modeling of rivastigmine, a cholinesterase inhibitor, in patients with Alzheimer's disease. J Clin Pharmacol [Internet]. 2001 Oct 1;41(10):1082–90. Available from: https://doi.org/10.1177/00912700122012689

19. Chen RY, Yu X, Smith B, Liu X, Gao J, Diacon AH, et al. Radiological and functional evidence of the bronchial spread of tuberculosis: an observational analysis. The Lancet Microbe [Internet]. 2021;2(10):e518–26. Available from: http://dx.doi.org/10.1016/S2666-5247(21)00058-6

20. Chen RY, Yu X, Smith B, Liu X, Gao J, Diacon AH, et al. Radiological and functional evidence of the bronchial spread of tuberculosis: an observational analysis. The Lancet Microbe. 2021 Oct;2(10):e518–26.

21. Mahmood I, Balian JD. The Pharmacokinetic Principles Behind Scaling from Preclinical Results to Phase I Protocols. Clin Pharmacokinet [Internet]. 1999;36(1):1–11. Available from: https://doi.org/10.2165/00003088-199936010-00001

22. Irwin SM, Prideaux B, Lyon ER, Zimmerman MD, Brooks EJ, Schrupp CA, et al. Bedaquiline and Pyrazinamide Treatment Responses Are Affected by Pulmonary Lesion Heterogeneity in Mycobacterium tuberculosis Infected C3HeB/FeJ Mice. ACS Infect Dis. 2016;2(4):251–67.

23. Prideaux B, Via LE, Zimmerman MD, Eum S, Sarathy J, O'Brien P, et al. The association between sterilizing activity and drug distribution into tuberculosis lesions. Nat Med. 2015;21(10):1223–7.

24. Rouan MC, Lounis N, Gevers T, Dillen L, Gilissen R, Raoof A, et al. Pharmacokinetics and pharmacodynamics of TMC207 and its N-desmethyl metabolite in a murine model of tuberculosis. Antimicrob Agents Chemother. 2012;56(3):1444–51.

25. Ahmad Z, Peloquin CA, Singh RP, Derendorf H, Tyagi S, Ginsberg A, et al. PA-824 exhibits time-dependent activity in a murine model of tuberculosis. Antimicrob Agents Chemother. 2011;55(1):239–45.

26. Filipa Mota, PhD, Camilo Ruiz-Bedoya, MD, Elizabeth Tucker, MD, Patricia De Jesus, BS, Kelly Flavahan, Mitchell Turner, BA, Clara Erice, PhD, Melissa Bahr, BA, John Kim, BA, Farina Mahmud, PhD, Charles A Peloquin, Pharm.D, Charles A Peloquin, Pharm.D, Alvaro A Ordonez, MD, Sanjay K Jain, MD, Sanjay K Jain, MD, 1411. Noninvasive Assessment of Intralesional Antimicrobial Concentration-Time Profiles in Pulmonary and Central Nervous System Tuberculosis using Dynamic 18F-Pretomanid Positron Emission Tomography, Open Forum Infectious Diseases, Volume 8, Issue Supplement_1, November 2021, Pages S789–S790, https://doi.org/10.1093/ofid/ofab466.1603

27. Ismail NA, Omar S V., Joseph L, Govender N, Blows L, Ismail F, et al. Defining Bedaquiline Susceptibility, Resistance, Cross-Resistance and Associated Genetic Determinants: A Retrospective Cohort Study. EBioMedicine [Internet]. 2018;28:136–42. Available from: https://doi.org/10.1016/j.ebiom.2018.01.005

28. van Heeswijk RPG, Dannemann B, Hoetelmans RMW. Bedaquiline: A review of human pharmacokinetics and drug-drug interactions. J Antimicrob Chemother. 2014;69(9):2310–8.

29. Diacon AH, Dawson R, Von Groote-Bidlingmaier F, Symons G, Venter A, Donald PR, et al. Bactericidal activity of pyrazinamide and clofazimine alone and in combinations with pretomanid and bedaquiline. Am J Respir Crit Care Med. 2015;191(8):943–53.

30. Chesov E, Chesov D, Maurer FP, Andres S, Utpatel C, Barilar I, et al. Emergence of bedaquiline resistance in a high tuberculosis burden country. Eur Respir J [Internet]. 2022;59(3):1–10. Available from: http://dx.doi.org/10.1183/13993003.00621-2021

31. Allué-Guardia A, Garcia-Vilanova A, Olmo-Fontánez AM, Peters J, Maselli DJ, Wang Y, et al. Host- and Age-Dependent Transcriptional Changes in Mycobacterium tuberculosis Cell Envelope Biosynthesis Genes after Exposure to Human Alveolar Lining Fluid. Int J Mol Sci [Internet]. 2022;23(2). Available from: https://www.mdpi.com/1422-0067/23/2/983

32. Drusano GL, Kim S, Almoslem M, Schmidt S, D'Argenio DZ, Myrick J, et al. The funnel: A screening technique for identifying optimal two-drug combination chemotherapy regimens. Antimicrob Agents Chemother. 2021;65(2).

33. Jarugula P, Scott S, Ivaturi V, Noack A, Moffett BS, Bhutta A, et al. Understanding the Role of Pharmacometrics-Based Clinical Decision Support Systems in Pediatric Patient Management: A Case Study Using Lyv Software. J Clin Pharmacol. 2021 Jun;61 Suppl 1:S125–32.

34. Hughes JH, Tong DMH, Lucas SS, Faldasz JD, Goswami S, Keizer RJ. Continuous Learning in Model-Informed Precision Dosing: A Case Study in Pediatric Dosing of Vancomycin. Clin Pharmacol Ther. 2021;109(1):233–42.

35. Humphries H, Almond L, Berg A, Gardner I, Hatley O, Pan X, et al. Development of physiologically-based pharmacokinetic models for standard of care and newer tuberculosis drugs. CPT Pharmacometrics Syst Pharmacol. 2021;10(11):1382–95.

36. Cao Y, Jusko WJ. Applications of minimal physiologically-based pharmacokinetic models. J Pharmacokinet Pharmacodyn. 2012;39(6):711–23.

37. Rowland M, Tozer TN. Clinical Pharmacokinetics and Pharmacodynamics: Concepts and Applications. In 1980.

38. Shargel L, Wu-Pong S, Yu ABC. Chapter 10. Physiologic Drug Distribution and Protein Binding. In: Applied Biopharmaceutics & Pharmacokinetics, 6e [Internet]. New York, NY: The McGraw-Hill Companies; 2012. Available from: http://accesspharmacy.mhmedical.com/content.aspx?aid=56603200

39. Diacon AH, Dawson R, von Groote-Bidlingmaier F, Symons G, Venter A, Donald PR, et al. 14-day bactericidal activity of PA-824, bedaquiline, pyrazinamide, and moxifloxacin combinations: a randomised trial. Lancet [Internet]. 2012 Sep 15;380(9846):986–93. Available from: https://doi.org/10.1016/S0140-6736(12)61080-0

40. The global alliance for tb drug development. Evaluation of Early Bactericidal Activity in Pulmonary Tuberculosis (TMC207-CL001). https://clinicaltrials.gov/show/NCT01215110. 2017.

41. Kim S, Yamada WM, Duncanson B, Nole J, Rogers S, Parker S, et al. Building Optimal Three-Drug Combination Chemotherapy Regimens To Eradicate Mycobacterium tuberculosis in Its Slow-Growth Acid Phase. Antimicrob Agents Chemotherapy. 2021;65(10):e00693-21. Available from: https://journals.asm.org/doi/abs/10.1128/AAC.00693-21

42. Lyons MA. Pretomanid dose selection for pulmonary tuberculosis: An application of multi-objective optimization to dosage regimen design. CPT Pharmacometrics Syst Pharmacol. 2021;10(3):211–9.

43. Muliaditan M, Della Pasqua O. Evaluation of pharmacokinetic-pharmacodynamic relationships and selection of drug combinations for tuberculosis. Br J Clin Pharmacol. 2021 Jan;87(1):140–51.

Supplementary Materials

S4.1. Summary of the time course data used for model development and validation

Drug Name	Study Details	Source
Model Development		
Bedaquiline	Bedaquiline concentrations from blood plasma and liver of mice after a single oral dose of 25 mg/kg bedaquiline	[1]
	Bedaquiline and M2 concentrations from blood plasma, lesion, and uninvolved lungs of mice after a single oral dose of 25 mg/kg bedaquiline	[2]
Pretomanid	Pretomanid concentrations from blood serum of mice after single oral doses of either 6-, 18-, 54-, 162-, or 486- mg/kg pretomanid	[3]
	F18-pretomanid plasma, lesion, and uninvolved lungs concentrations were measured by PET imaging after IV dosing of F18-pretomanid	[4]
Pyrazinamide	Pyrazinamide concentrations from blood plasma, lesions, and uninvolved lungs of mice after a single oral dose of 150 mg/kg pyrazinamide	[2]
Model Validation		
Bedaquiline	Bedaquiline and M2 concentrations from blood serum of pulmonary TB patients after bedaquiline doses ranging between 100 mg – 700 mg.	[5,6]
Pretomanid	Pretomanid serum concentrations from pulmonary TB patients after pretomanid doses ranging between 50 mg – 1200 mg.	[5,7,8]
Pyrazinamide	Pyrazinamide serum concentrations from pulmonary TB patients after 1500 mg daily dosing of pretomanid	[5]
Pyrazinamide	Pyrazinamide steady-state concentrations from lesions, and uninvolved lungs of pulmonary TB patients	[9]

S4.2. Final Model Codes for Bedaquiline and Pretomanid mPBPK.

```
BDQparams <- c(TVka1=1.3, TVka2=0.00501, TVCLint=60.3,
KpT=4.45, TVCLM2=45.9, KpTM2=18.4, Rles=11,
RUL=10.2, RlesM2=88.4, RULM2=88.8, TVfrc=0.609, fup=0.1 )
BDQmod <- RxODE({

################ Drug-specific Parameters Estimated and Translated to Humans
ka1=TVka1*exp(eta.ka1) ;
ka2 =TVka2*exp(eta.ka2) ;
CLint=TVCLint*((BW/70)^0.75)*exp(eta.CLint) ;
CLM2=TVCLM2*((BW/70)^0.75) *exp(eta.CLM2) ;
logit_frc = log(TVfrc/(1 - TVfrc)) ;

frc = (1 / (1 + exp(-logit_frc))) ;
################ Human System specific parameters ################
#Cardiac output
Qc = 312*(BW/70)^0.75 ; # Cardiac output (Brown 1997 table 22; calculated based on 5200 ml/min)
Qh = Qc*0.227 ; # Blood flow to liver as fraction of Qc (Brown1997 table 23)
Qt = Qc - Qh ;

# Volumes
VLiv = 0.0257*BW ; # Volume of liver (L) (Brown1997 table 7)
VLu = 0.0076*BW ; # Volume of lungs (L) (Brown1997 table 7)
Dblv = 0.0514 ; # Volume veins per kg BW (L/kg)
Dbla = 0.0257 ; # Volume arteries per kg BW (L/kg)
Dbl = Dblv + Dbla ; # Volume blood resovior per kg BW (L/kg)
Vbl = Dbl*BW ; # volume of blood resovioir (L)
Vt = BW - VLu - Vbl - VLiv ; # Residual body volume (L)

# Lesion volume calculation
# Median total lesion volume in cavitary TB patients = 14 mL (PMID: 34617068)
# 14 mL = 0.014 L represents ~2.16 % of total lung volume (total lung volume 0.532 L in 70 kg human)
# Assume comparable extent of lesions in Mtb infected mice
# VLeF = 0.014/0.53 ; # Volume of lung lesions (fraction of lung volume)
VULF = 1 - VLeF ; # Volume of lung lesions (fraction of lung volume)
VLe = VLeF*VLu ; # Absolute volume of lesion (L)
```

```
VUL = VLu - VLe ; # Volume of uninvolved lung (L)
QLe = Qc/VLe ; # Blood flow to lesion (1/hr)
QUL = Qc/VUL ; # Blood flow to uninvolved lungs (1/hr)

# Secondary parameters
Eh = (fup*CLint)/(Qh + (fup*CLint)) ;
Cbld = blood/Vbl ;
CbldM2 = M2blood/Vbl ;

################################## ODEs ################
d/dt(depot1) = -ka1*depot1 ; # Input
d/dt(depot2) = -ka2*depot2 ; # Input
d/dt(liver) = frc*ka1*depot1 + (1-frc)*ka2*depot2 - # Input
Qh*Eh*liver/VLiv - # conversion to M2
Qh*(1-Eh)*liver/VLiv + # outflow to blood
Qh*blood/Vbl ; # inflow from blood
d/dt(blood) = Qh*(1-Eh)*liver/VLiv - # absorption
Qh*blood/Vbl + # outflow to liver
tissue*Qt/(Vt*KpT) - blood*Qt/Vbl ; # in and out of tissues
d/dt(tissue) = blood*Qt/Vbl - tissue*Qt/(Vt*KpT) ;
d/dt(M2blood) = Qh*Eh*liver/VLiv - CLM2*M2blood/Vbl +
M2tissue*Qt/(Vt*KpTM2) - M2blood*Qt/Vbl ; # in and out of tissues
d/dt(M2tissue) = M2blood*Qt/Vbl - M2tissue*Qt/(Vt*KpTM2) ;
###Lesion and uninvolved lungs ODEs
d/dt(Cles) = QLe*(Cbld*Rles - Cles) ;
d/dt(CUlung) = QUL*(Cbld*RUL - CUlung) ;
d/dt(ClesM2) = QLe*(CbldM2*RlesM2 - ClesM2) ;
d/dt(CUlungM2) = QUL*(CbldM2*RULM2 - CUlungM2) ;

################ Outputs ################
C_plasma_bdq = (blood/Vbl)*1000 ; #ng/mL
C_liver_bdq = (liver/VLiv)*1000 ; #ng/mL ;
C_plasma_m2 = (M2blood/Vbl)*1000 ; #ng/mL ;
C_lesion_bdq = (Cles)*1000 ; #ng/mL ;
C_uninvolvedL_bdq = (CUlung)*1000 ; #ng/mL ;
C_lesion_m2 = (ClesM2)*1000 ; #ng/mL ;
C_uninvolvedL_m2 = (CUlungM2)*1000 ; #ng/mL ;
})
```

```
PTMparams <- c(
TVka=0.3,
TVCL=4.42,
TVED50=554,
TVKpT=36.24,
TVKpT1=0.48,
Rles=1.6,
RUL=1.76)

PTMmod <- RxODE({

################ Drug-specific Parameters Estimated and Translated to Humans #################
ka=TVka*exp(eta.ka) ;
CL=TVCL*exp(eta.CL)*(BW/70)^0.75 ;
KpT = TVKpT*exp(eta.KpT) ;
KpT1 = TVKpT1*exp(eta.KpT1) ;
ED50 = TVED50 ; #*exp(eta.ED50) ;
FT1 = 0.975 ;
BP = 1.65;

################ Human System specific parameters ################
#Cardiac output
Qc = 312*(BW/70)^0.75 ; # Cardiac output (Brown 1997 table 22; calculated based on 5200 ml/min)
Qt = Qc*(1 - FT1) ;
Qt1 = Qc*FT1 ;

# Volumes
VLu = 0.0076*BW ; # Volume of lungs (L) (Brown1997 table 7)
Dblv = 0.0514 ; # Volume veins per kg BW (L/kg)
Dbla = 0.0257 ; # Volume arteries per kg BW (L/kg)
Dbl = Dblv + Dbla ; # Volume blood resovior per kg BW (L/kg)
Vbl = Dbl*BW ; # volume of blood resovioir (L)
Vt_tot = BW - VLu - Vbl ; # Residual body volume (L)
Vt = Vt_tot*(1 - FT1) ;
Vt1 = Vt_tot*FT1 ;
```

```
# Lesion volume calculation
# Median total lesion volume in cavitary TB patients = 14 mL (PMID: 34617068)
# 14 mL = 0.014 L represents ~2.16 % of total lung volume (total lung volume 0.532
L in 70 kg human)
# Assume comparable extent of lesions in Mtb infected mice
# VLeF = 0.014/0.53 ; # Volume of lung lesions (fraction of lung volume)
VULF = 1 - VLeF ; # Volume of lung lesions (fraction of lung volume)
VLe = VLeF*VLu ; # Absolute volume of lesion (L)
VUL = VLu - VLe ; # Volume of uninvolved lung (L)
QLe = Qc/VLe ; # Blood flow to lesion (1/hr)
QUL = Qc/VUL ; # Blood flow to uninvolved lungs (1/hr)
Cbld = blood/Vbl ;

################################## ODEs #################
d/dt(depot) = -ka*depot ;
Fmax = 1 ;
doseIn = Fmax*dose/(1 + (dose/ED50)) ;
f(depot) = doseIn/dose ;
d/dt(blood) =ka*depot - CL*blood/Vbl + tissue*Qt/(Vt*KpT) - blood*Qt/Vbl +
tissue1*Qt1/(Vt1*KpT1) - blood*Qt1/Vbl ;
d/dt(tissue) = blood*Qt/Vbl - tissue*Qt/(Vt*KpT) ;
d/dt(tissue1) = blood*Qt1/Vbl - tissue1*Qt1/(Vt1*KpT1) ;
###Lesion and uninvolved lungs ODEs
d/dt(Cles) = QLe*(Cbld*Rles - Cles) ;
d/dt(CUlung) = QUL*(Cbld*RUL - CUlung) ;

################ Outputs #################
C_plasma = (Cbld/BP)*1000 ; #ng/mL
C_lesion = (Cles)*1000 ; #ng/mL
C_Ulung = (CUlung)*1000 ; #ng/mL})
```

S4.3. Pyrazinamide mPBPK model in mice. (A) Model structure, (B) Model fit. blue points=observed data, black line=model fit predictions.

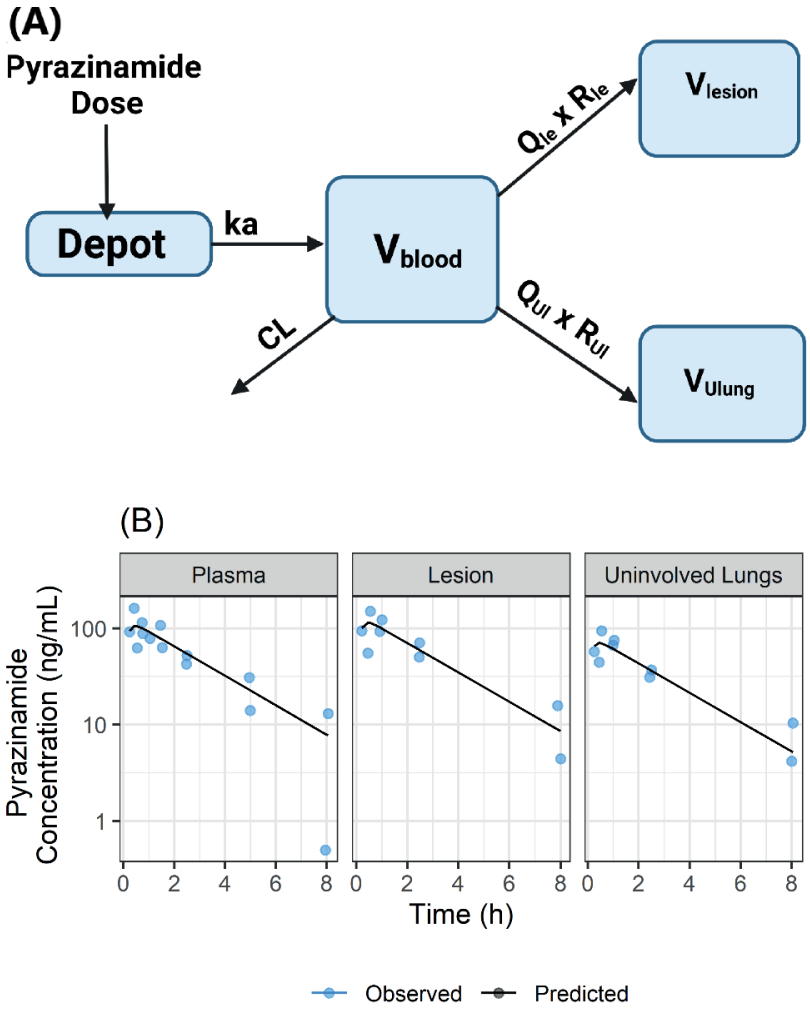

S4.4. Time course of Bedaquiline Metabolite, M2, concentrations, (A) Plasma, lungs, and lesion observed vs. model predictions in mice, (B) Plasma in TB patients. The model predictions for bedaquiline well with the observed data for mice and TB patients from clinical trials at clinically-relevant doses. Bedaquiline was administered orally as 25 mg/kg in mice and 400 mg on day1, 300 mg on day2, and 100 mg QD on day3 onwards in patients[5]. Red horizontal line refers to half-maximal M2 concentrations for QTcF prolongation[10].

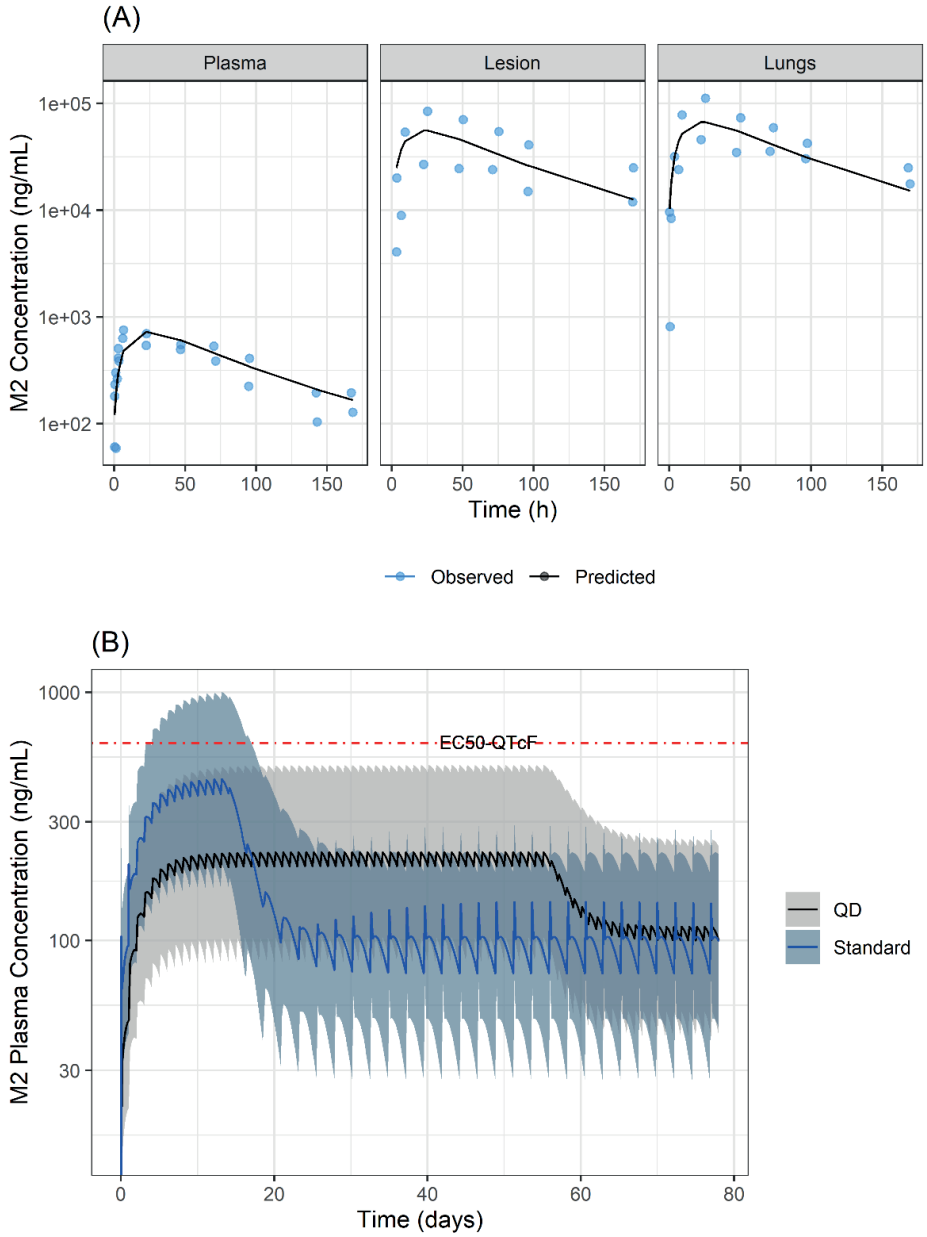

S4.5. Predicted and observed plasma steady-states PK pProfiles in TB patients for Bedaquiline, M2, and Pretomanid. Blue points=observed data, solid grey line=median of the simulations, shaded grey area=95% confidence interval (CI) of the simulations. Panel titles represent bedaquiline or pretomanid doses in mg. Bedaquiline was administered as an increasing daily dose, i.e., panel 1 represents a group that received 200 mg on day1 and 100 mg on day2 onwards.

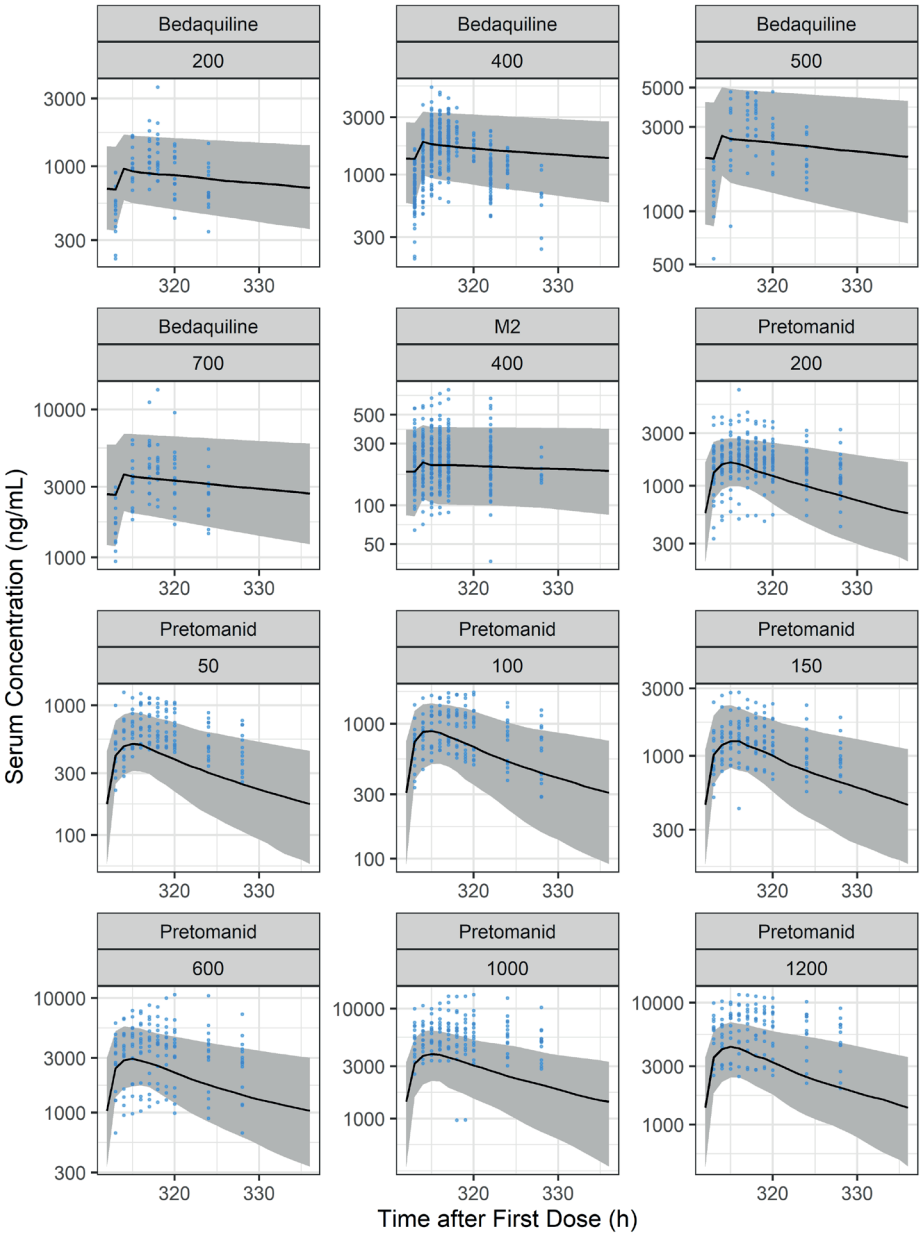

S4.6. Local sensitivity Analysis. The sensitivity of the parameter estimates on steady-state plasma drug exposure was examined by introducing 10% or 50% variation in the parameters one at a time and running the simulations for 50 times. Overall, the mean sensitivity index was low (between -2.5 and 2.5) for both bedaquiline and pretomanid with the exception of ka2 of bedaquiline that showed high sensitivity to affect both bedaquiline and M2 plasma concentrations, and kpT1 showed relatively moderate sensitivity to affect pretomanid plasma concentrations. Points and error bars represent mean (95% CI) of the sensitivity index.

10%

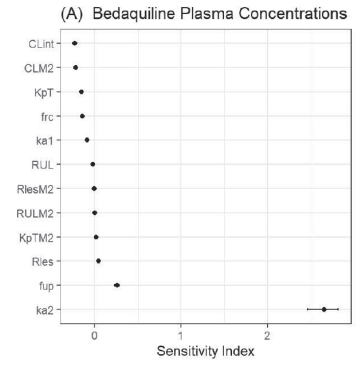

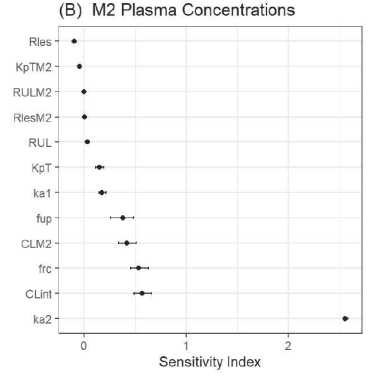

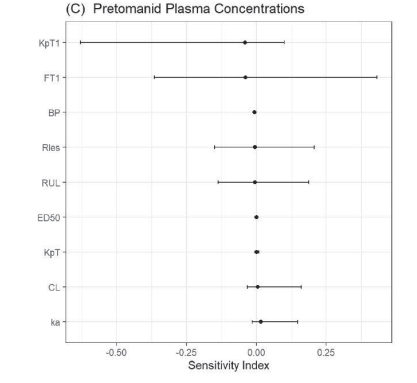

50%

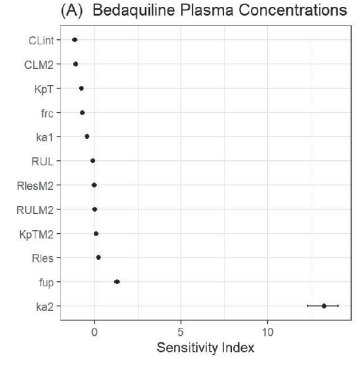

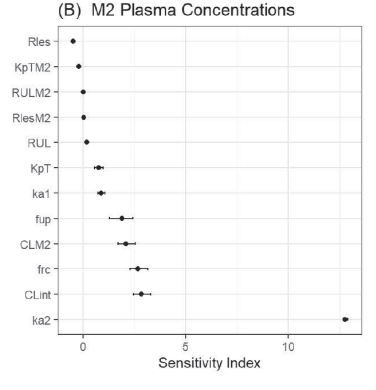

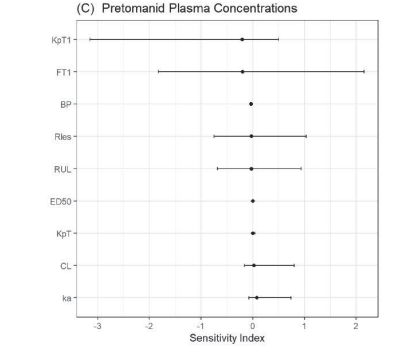

References

1. Rouan MC, Lounis N, Gevers T, Dillen L, Gilissen R, Raoof A, et al. Pharmacokinetics and pharmacodynamics of TMC207 and its N-desmethyl metabolite in a murine model of tuberculosis. Antimicrob Agents Chemother. 2012;56(3):1444–51.
2. Irwin SM, Prideaux B, Lyon ER, Zimmerman MD, Brooks EJ, Schrupp CA, et al. Bedaquiline and Pyrazinamide Treatment Responses Are Affected by Pulmonary Lesion Heterogeneity in Mycobacterium tuberculosis Infected C3HeB/FeJ Mice. ACS Infect Dis. 2016;2(4):251–67.
3. Ahmad Z, Peloquin CA, Singh RP, Derendorf H, Tyagi S, Ginsberg A, et al. PA-824 exhibits time-dependent activity in a murine model of tuberculosis. Antimicrob Agents Chemother. 2011;55(1):239–45.
4. Mota F, Ruiz-Bedoya C, Tucker E, De Jesus P, Flavahan K, Turner M E, C, Bahr M, Kim J, Farina M, Peloquin CA, Ordonez A JS. Noninvasive Assessment of Intralesional Antimicrobial Concentration- Time Profiles in Pulmonary and Central Nervous System Tuberculosis using Dynamic 18F-Pretomanid Positron Emission Tomography. OFID 20218 Sess P-80 Tuberc other Mycobact Infect. 2021;789–90.
5. Diacon AH, Dawson R, Von Groote-Bidlingmaier F, Symons G, Venter A, Donald PR, et al. Bactericidal activity of pyrazinamide and clofazimine alone and in combinations with pretomanid and bedaquiline. Am J Respir Crit Care Med. 2015;191(8):943–53.
6. The global alliance for tb drug development. Evaluation of Early Bactericidal Activity in Pulmonary Tuberculosis (TMC207-CL001). https://clinicaltrials.gov/show/NCT01215110. 2017.
7. Diacon AH, Dawson R, Du Bois J, Narunsky K, Venter A, Donald PR, et al. Phase II dose-ranging trial of the early bactericidal activity of PA-824. Antimicrob Agents Chemother. 2012;56(6):3027–31.
8. Dawson R, Diacon AH, Everitt D, van Niekerk C, Donald PR, Burger DA, et al. Efficiency and safety of the combination of moxifloxacin, pretomanid (PA-824), and pyrazinamide during the first 8 weeks of antituberculosis treatment: a phase 2b, open-label, partly randomised trial in patients with drug-susceptible or drug-resistant pul. Lancet [Internet]. 2015 May 2;385(9979):1738–47. Available from: https://doi.org/10.1016/S0140-6736(14)62002-X
9. Prideaux B, Via LE, Zimmerman MD, Eum S, Sarathy J, O'Brien P, et al. The association between sterilizing activity and drug distribution into tuberculosis lesions. Nat Med. 2015;21(10):1223–7.
10. Tanneau L, Karlsson MO, Rosenkranz SL, Cramer YS, Shenje J, Upton CM, et al. Assessing Prolongation of the Corrected QT Interval with Bedaquiline and Delamanid Coadministration to Predict the Cardiac Safety of Simplified Dosing Regimens. Clin Pharmacol Ther. 2022;0(0):1–9.

Chapter 5

Model-based dose optimization framework for bedaquiline, pretomanid, and linezolid for the treatment of drug-resistant tuberculosis

Krina Mehta, Tingjie Guo, Piet H van der Graaf, J G Coen van Hasselt

Br J Clin Pharmacol.2023 Oct;1–12

Abstract

Aim: Bedaquiline, pretomanid, and linezolid combination (BPaL) treatment against *Mycobacterium tuberculosis* is promising yet safety and adherence concerns exist that motivates exploration of alternative dosing regimens. We developed a mechanistic modeling framework to compare the efficacy of the current and alternative BPaL treatment strategies.

Methods: Pharmacodynamic models for each drug in the BPaL combination treatment were developed using in vitro time-kill data. These models were combined with pharmacokinetic models, incorporating bodyweight, lesion volume, site-of-action distribution, bacterial susceptibility, and pharmacodynamic interactions to assemble the framework. The model was qualified by comparing the simulations against the observed clinical data. Simulations were performed evaluating bedaquiline and linezolid approved (bedaquiline 400mg once daily (QD) 14-days followed by 200mg three times a week, linezolid 1200mg QD) and alternative dosing regimens (bedaquiline 200mg QD, linezolid 600mg QD).

Results: The framework adequately described the observed anti-bacterial activity data in patients following monotherapy for each drug and approved BPaL dosing. The simulations suggested a minor difference in median time to colony forming units (CFU)-clearance state with the bedaquiline alternative compared to the approved dosing and the linezolid alternative compared to the approved dosing. Median time to non-replicating-clearance state was predicted to be 15-days from the CFU-clearance state.

Conclusion: The model-based simulations suggested that comparable efficacy can be achieved using alternative bedaquiline and linezolid dosing, which may improve safety and adherence in drug-resistant tuberculosis patients. The framework can be utilized to evaluate treatment optimization approaches, including dosing regimen and duration of treatment predictions to eradicate both replicating- and non-replicating bacteria from lung and lesions.

Introduction

Emergence of resistance to commonly used anti-tuberculosis (TB) drugs has been a global health challenge[1]. Historically, drug-resistant TB treatment regimens were associated with poor efficacy and safety outcomes. The new combination regimen of bedaquiline, pretomanid, and linezolid (BPaL) showed high efficacy in patients with multi-drug resistant TB (MDR-TB) and is now endorsed by the world health organization for the treatment of MDR-TB2,3. The current approved BPaL dosing is based on a combination of bedaquiline 400 mg once daily (QD) for 14 days followed by 200 mg three times a week, pretomanid 200 mg QD, and linezolid 1200 mg QD. The current linezolid dose is associated with safety concerns including peripheral and optic neuropathy and myelosuppression4,5. Moreover, the unconventional, three times a week, bedaquiline dosing schedule leads to patient non-adherence which ultimately affects treatment efficacy and emergence of resistance6. To overcome these safety and adherence concerns associated with approved BPaL dosing regimen, alternative treatment optimization approaches are being evaluated, including bedaquiline 200 mg QD for 8 weeks followed by 100 mg QD and linezolid 600 mg QD7,8. The recently completed ZeNix study evaluating the suggested alternative bedaquiline and linezolid dosing demonstrated overall improved benefit-risk ratio following alternative, simplified and lower, bedaquiline and linezolid dosing regimen compared to approved dosing regimen8. Although the alternative linezolid dosing schedule was associated with overall improved benefit-risk ratio, slightly higher percentage (5%) of favorable outcome was reported at approved dosing compared to the alternative dosing. Additionally, precise treatment effect could not be assessed in the ZeNix study due to several limitations, such as smaller sample size and lack of comparator arm. Overall, it is evident that the current BPaL dosing regimen may not be optimal for all patients, and improvements are needed to ensure that every patient can receive the maximum benefits with minimal risks.

The BPaL treatment is associated with variable efficacy and safety outcomes across MDR-TB patients[3,8,9]. Mechanistic understanding of the relationship between patient- or disease-related factors and treatment outcome can help rationalize BPaL treatment optimization approaches to increase favorable treatment outcomes. Standard recommended BPaL treatment duration is 6-9 months with extension allowed as needed for up to 26 weeks[3,8,10]. Although the majority (~90%) of the patients achieve culture conversion during the first two months of therapy but some patients have also relapsed or had treatment failure after 26 months of therapy[3,8]. Mechanistically, relapse can be attributed to non-replicating

persisting *mycobacterium tuberculosis* (Mtb) subpopulation. TB patients' treatment response is measured in sputum samples. Non-replicating Mtb subpopulation persists within cavitary lung lesions of TB patients and as such often are not measurable. Thus, predictions of BPaL treatment response on non-replicating Mtb within cavitary lesions can help rationalize BPaL treatment duration to avoid relapse. To this end, a mechanistic pharmacokinetic (PK) – pharmacodynamic (PD) - response modeling framework that includes patient-, disease-, and drug-related factors to enable predictions of BPaL anti-bacterial efficacy on replicating and non-replicating Mtb subpopulation is needed. Such a framework can help evaluate treatment optimization and individualization approaches for BPaL combination dosing regimen, schedule, and duration selection based on the relevant factors in MDR-TB patients.

To date, quantitative pharmacology approaches have exploited some relationships between patient- and disease-related covariates, PK and response for bedaquiline, pretomanid, and linezolid individually[11–14]. These models however did not include several key mechanistic components, such as Mtb susceptibility, target site drug exposures, and PD interactions between the BPaL combination regimen. In this work, we aimed to combine the relevant mechanistic components to develop a quantitative framework for BPaL combination, including, dynamics of replicating and non-replicating Mtb, patient-related and other covariates and their effects on drug exposures, target site drug exposures, individual drug effects, and PD drug interactions. The developed framework was then applied to perform anti-Mtb activity predictions for both replicating and non-replicating Mtb following the current approved and alternative BPaL dosing regimens in MDR-TB patients.

Methods

The development of the mechanistic PK-PD framework for BPaL combination treatments was performed in four main steps. We first fit the multi-state tuberculosis model to in vitro time-kill data for bedaquiline, pretomanid, and linezolid for fast- and slow-replicating subpopulations of Mtb separately. Then, the individual drug effect models were translated to TB patients by accounting for patient body weight, TB lesion volume in patient lungs, drug exposure predictions within lungs and lesions, and Mtb susceptibility profiles (i.e., minimum inhibitory concentrations (MIC)). Next, the PD interaction parameters were incorporated. Lastly, the model was combined with a previously developed model for correlation between two anti-Mtb activity measures, colony forming units (CFU) and time to

positivity (TTP) to allow for predictions of both outcome measures. Combination treatment simulations were performed for approved and alternative treatment schedules, and the results were compared against the observed clinical data. The overall process for the construction of the quantitative framework for BPaL combination therapy is illustrated in **Figure 5.1**.

Mechanistic PD models

The published multi-state tuberculosis model which describes the growth dynamics of fast-, slow-, and non-replicating Mtb population was reproduced and used to describe bacterial growth dynamics in TB patients[15]. We digitized longitudinal bacterial CFU data from in vitro fast-multiplying (log-phase) and semi-dormant Mtb time-kill experiments at various concentrations of bedaquiline, pretomanid, and pretomanid[16–21]. Experiment-specific growth rate parameters, fast-multiplying bacterial growth rate (kG), and system carrying capacity (Bmax), were estimated using the untreated control data. Next, drug effects for bedaquiline, pretomanid, and linezolid were separately estimated (S5.1). Linear and nonlinear drug-induced kill functions on fast-, slow-, and non-replicating Mtb populations were evaluated. As no data for slow-replicating bacteria were available, the drug effect models for non-replicating Mtb were applied to the slow-replicating Mtb population. Models were selected based on objective function value, visual inspections of observed vs. predictions plots, and plausibility and precision of the parameter estimates.

Figure 5.1 Overview of the BPaL Quantitative Framework Development Process. BDQ=bedaquiline, CFU=colony-forming unit of Mtb, Cavgd=daily average concentrations of drug d at the site of action of TB patients (bedaquiline, pretomanid, or linezolid), Concd=in vitro concentrations of drug d, EBA=early-bactericidal activity, $Effect_{di}$=bacterial killing effect of drug d for Mtb population i (fast-, slow-, or non-replicating), Fu_{lung}=fraction unbound in lungs, LZD=linezolid, MDR=multi-drug resistant TB, MIC=minimum inhibitory concentrations, MTP=multistate tuberculosis pharmacometrics model[11,15], PD=pharmacodynamic, PK=pharmacokinetic, PTM=pretomanid, TB=tuberculosis, TTP=time to liquid culture positivity. Figure created with Biorender.com.

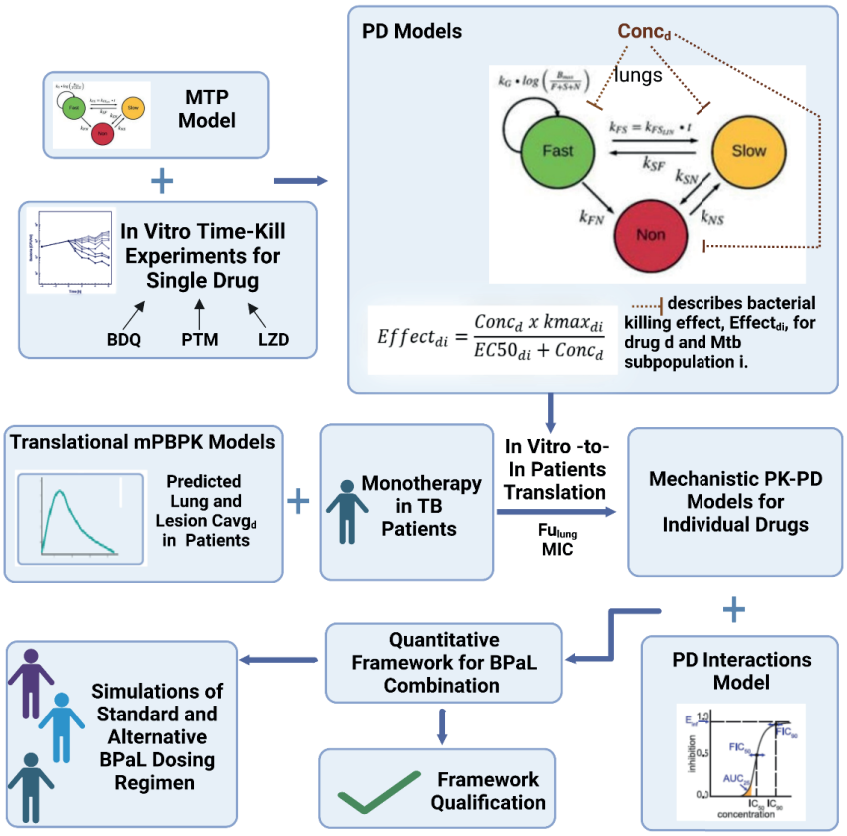

Mechanistic PK-PD models

Sputum CFU data from bedaquiline, pretomanid, and linezolid early bactericidal activity (EBA) studies, i.e., clinical studies that evaluated monotherapy 14-day anti-Mtb effects, in pulmonary tuberculosis patients were obtained from the Platform for Aggregation of Clinical TB Studies (TB-PACTS; https://c-path.org/programs/tb-pacts/) database[12,22–24]. PK models and parameter estimates for bedaquiline and pretomanid from our prior work were used to simulate plasma and site of action,

lungs and lesions, and concentration-time profiles[14]. A PK model for linezolid was reproduced from the literature to simulate plasma, lungs, and lesion concentration-time profiles[25]. Body weights were sampled for the virtual patients from observed TB patients' body weight distribution from the data. TB lung lesion volumes were simulated using observed TB patients cavity volume from the literature.26 We simulated the PK of bedaquiline, pretomanid, and linezolid monotherapy for various dose groups that were evaluated in the monotherapy clinical studies (n=500 patients per simulated dose group), and target site exposure metrics for each virtual subject, daily average lung concentrations ($C_{avg\text{-}lung}$), and average lesion concentrations ($C_{avg\text{-}lesion}$) were calculated to use in the simulations of anti-Mtb activities. The multistate tuberculosis pharmacometrics model, PK, and PD models were combined for all three drugs for the simulations[13,15].

Drug effects were introduced in the simulations at 150 days post-infection when the bacterial population was assumed to have reached a steady state. Drug effects were assumed to be driven by $C_{avg\text{-}lung}$ for fast- and slow-replicating Mtb and $C_{avg\text{-}lesion}$ for non-replicating Mtb. A lung tissue binding factor (Fu_{lung}) was incorporated to calculate free drug exposure at target sites to exert an anti-Mtb effect. Parameter estimates for Fu_{lung} were obtained from the literature[27,28]. Bacterial load, i.e., CFU, simulations were performed according to the dosing schedules tested in the corresponding studies. CFU was calculated as sum of predicted fast- and slow-replicating Mtb population within lungs. The plots of predicted change in bacterial load were compared against the observed change in CFU over 14 days of monotherapy treatment for all three drugs.

The models for each drug used to perform monotherapy simulations were then combined to construct the framework for the simulation of combination therapies. PD interactions between each two-drug combination of the three drugs were incorporated using the adapted version of the Bliss independence model structure[29,30]. The parameter estimates were obtained from in vitro experiments-derived fractional inhibition coefficients for each two-drug combination[31] **(Table 5.1).**

Table 5.1 Parameter Estimates of Bedaquiline, Pretomanid, and Linezolid Semi-Mechanistic PK–PD Models

Parameter	Description	Estimate	%RSE or Assumption
Bedaquiline [a]			
BDQkmaxfst	Maximum kill rate for fast-replicating Mtb (1/day)	8.76	2.61
BDQkmaxS, BDQkmaxN	Maximum kill rate for slow- and non-replicating Mtb (1/day)	3.39	25.6
BDQEC50fst	Bedaquiline concentrations needed for half-maximum response for fast-replicating Mtb (mg/L)	0.12	11.7
BDQEC50S, BDQEC50N	Bedaquiline concentrations needed for half-maximum response for slow and non-replicating Mtb (mg/L)	3.49	64.2
BDQTau	Delay in start of bedaquiline activity (days)	5.3	15.0
Fu_{lung}BDQ	Lung tissue binding factor	0.01	[28]
bdqm2-scaling	Bedaquiline to M2 antibacterial effect scaling factor	0.2	Assumed 5-fold lower efficacy of M2 as compared to bedaquiline
Pretomanid [b]			
PTMkmaxfst	Maximum kill rate for fast-replicating Mtb (1/day)	2.97	8.34
PTMkmaxS, PTMkmaxN	Maximum kill rate for slow- and non-replicating Mtb (1/day)	0.709	36.4
PTMEC50fst	Pretomanid concentrations needed for half-maximum response for fast-replicating Mtb (mg/L)	0.156	21.3
PTMEC50S, PTMEC50N	Pretomanid concentrations needed for half-maximum response for slow- and non-replicating Mtb (mg/L)	12.5	69.2
Fu_{lung}PTM	Lung tissue binding factor	1	Assumed
Linezolid [c]			
LZDkmaxfst	Maximum kill rate for fast-replicating Mtb (1/day)	0.65	35.6
LZDkmaxS, LZDkmaxN	Maximum kill rate for slow- and non-replicating Mtb (1/day)	0.41	47.1
LZDEC50fst	Linezolid concentrations needed for half-maximum response for fast-replicating Mtb (mg/L)	0.8	58.3
LZDEC50S, LZDEC50N	Linezolid concentrations needed for half-maximum response for slow- and non-replicating Mtb (mg/L)	1.1	48.5
Fu_{lung}LZD	Lung tissue binding factor	0.29	[28]
Pharmacodynamic Interactions			
FICBP	Interaction bedaquiline-pretomanid (synergy)	0.89	[31]
FICBL	Interaction bedaquiline-linezolid (antagonism)	1.13	
FICPL	Interaction pretomanid-linezolid (antagonism)	1.86	

The Multi-state tuberculosis model structure and parameter estimated were fixed to the published estimates to describe Mtb growth dynamics[15]. The PK model structure and parameters were fixed to the published estimates to predict serum and lung site concentrations[14,25]. [a] kG = 1.52 day^{-1} and Bmax = 6.5e+07 mL^{-1} were estimated by fitting the Multi-state tuberculosis model to combined log-phase Mtb growth data in absence of bedaquiline.; b Bmax = 8.25e+09 mL^{-1} was estimated by fitting the Multi-state tuberculosis model to combined log-phase Mtb growth data in absence of pretomanid.; [c] Linezolid hollow-fiber experiment showed no increase in Mtb load for the controls group for the duration of the study; therefore, linezolid controls data were best described by first-order natural death rates 0.542 day^{-1} and 0.275 day^{-1} for fast- and non-replicating bacteria, respectively.

BPaL quantitative framework

Clinical studies often measure anti-microbial activity using solid culture (CFU) or liquid culture time to positivity (TTP). Therefore, a CFU-TTP correlation model has been previously developed by fitting a Gompertz model structure to the matched CFU and TTP clinical data from TB patients treated with rifampin[32]. We reproduced the CFU-TTP correlation model and added it within the quantitative frame to allow for simulations of CFU and TTP. As no in vitro time-kill experiments for M2 were available, M2 maximum kill rates for each bacterial sub-population were assumed to be 5-fold lower than that of bedaquiline based on the literature[33]. Sensitivity analysis was conducted to evaluate the impact of bedaquiline-M2 effect scaling parameter (bdqm2scaling) by varying scaling parameter and plotting typical CFU predictions (S5.2). Overall, the final quantitative framework for BPaL included the dynamics of TB disease progression, drug distribution and available effective fraction into lung and lesions, individual drug effects, patient-related and other covariates, and PD drug interactions.

Virtual patient (n=500) MICs for bedaquiline, pretomanid, and linezolid were simulated by sampling from the observed MIC distribution for each drug from the Nix-TB study data from the TB-Pacts database[3]. Patient-specific covariates, PK, multistate tuberculosis pharmacometrics model, and PD parameters were simulated in a similar manner as monotherapy simulations described above. Then, drug effect parameters, kmax and EC50, were adjusted for MIC by taking the ratio between the in-patient vs. in vitro MIC for each drug and multiplying it with the parameter value[29]. Bacterial growth simulations were generated for up to 150 days using the above-mentioned parameters. To qualify the quantitative framework, observed changes in microbiological measure, EBA-TTP from 0-14 day ($EBA\text{-}TTP_{0\text{-}14day}$) and 0-28 day ($EBA\text{-}TTP_{0\text{-}28day}$) following BPaL combination therapy were compared against the simulations for the dosing regimen studied in the Nix-TB study[3]. For the qualification task, typical Bmax was set to match observed baseline median TTP in the study.

Simulations of the approved and alternative bpal dosing regimen

The BPaL quantitative framework including the same simulated virtual population was used to perform simulations of the current approved and three alternative dosing scenarios. The alternative bedaquiline and linezolid dosing scenarios proposed in the literature were included in the simulations[7,8]. Overall, the following four dosing scenarios were simulated for 500 virtual subjects each: (1)

Bedaquiline 400 mg QD 14days followed by 200 mg three times a week (three times a week), pretomanid 200 mg QD, linezolid 600 mg BID; (2) Bedaquiline 200 mg QD, pretomanid 200 mg QD, linezolid 600 mg BID; (3) Bedaquiline 400 mg QD 14days followed by 200 mg three times a week, pretomanid 200 mg QD, linezolid 600 mg QD; and (4) Bedaquiline 200 mg QD, pretomanid 200 mg QD, linezolid 600 mg QD. Simulations were conducted for up to 14 weeks. Plots of bacterial load, CFU (total of fast- and slow-replicating Mtb), and non-replicating separately, over time following the start of treatment were generated. The time scales on the plots were selected for optimal presentation of the overall results. Time-to-Mtb-clearance, defined as <1 CFU mL^{-1} or <1 non-replicating Mtb mL^{-1}, and proportions of virtual patients achieving Mtb clearance were calculated for each virtual patient and dosing combination.

Software

All analyses were conducted in R (R for Windows, v4.1, https://www.r-project.org/) using RStudio (RStudio, v1-554, www.rstudio.com/). Data management and plotting were performed using the tidyverse package. Parameter optimization and model simulations were conducted using nlmixr and RxODE packages.

Results

Development of mechanistic pd models for in vitro time-kill data

The multi-state tuberculosis model was used as a base model structure to evaluate the drug effects of bedaquiline, pretomanid, and linezolid using in vitro anti-Mtb activity data. Prior to adding drug effects, experiment-specific Mtb growth curves were estimated using controls data. Estimation of both kG and Bmax for bedaquiline experiments, and only Bmax for pretomanid experiments best described the in vitro control data. Estimation of kG for pretomanid controls experiment was evaluated but resulted in a similar parameter estimate to that previously reported in the literature and was therefore fixed to the previously reported value[15]. Additionally, data from the hollow-fiber infection model were used for linezolid experiments, and the control data for the linezolid experiments were described by a first-order natural death term and the published multi-state TB model growth parameters[20].

Figure 5.2 Model fitting of the semi-mechanistic PD models to In Vitro anti-Mtb activity data, (A) Bedaquiline, (B) Pretomanid, (C) Linezolid. The model described the observed in vitro experimental data well. Lines show the predicted data and points show observed data.

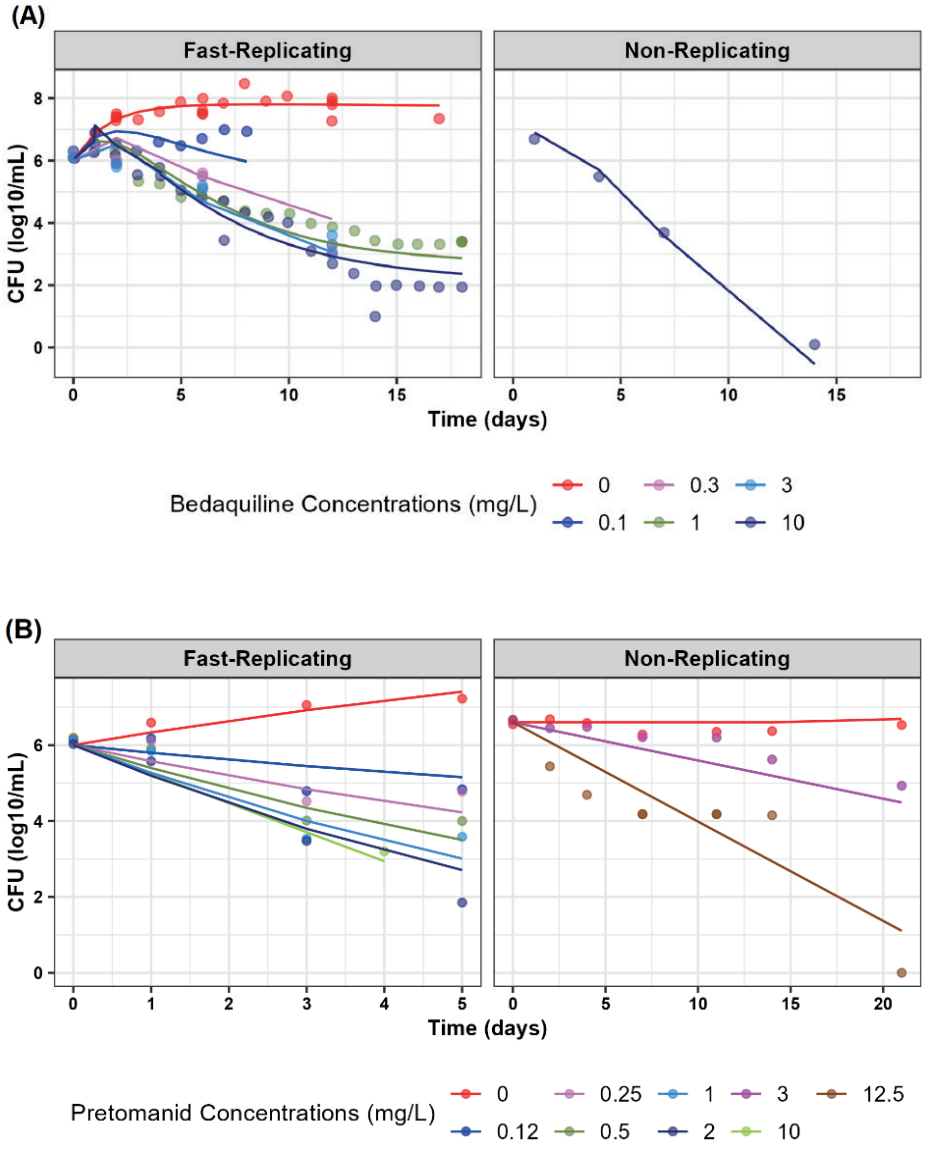

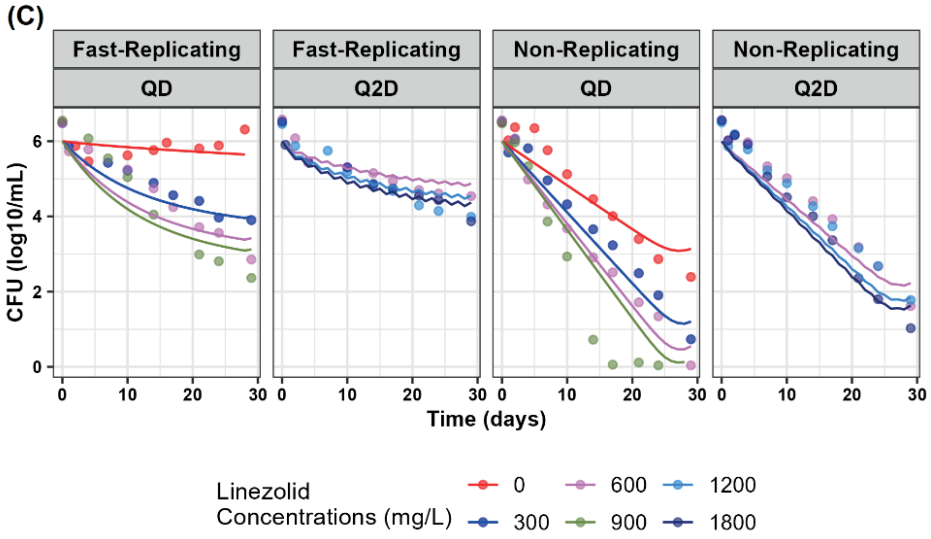

The non-linear model with separate drug-induced effects for each drug on fast-replicating and non-replicating Mtb provided improved fits than the linear models for all three drugs. No data for slow-replicating bacteria was available. Parameterization of drug effects was attempted separately for slow- and non-replicating Mtb population using a multi-state tuberculosis model construct; however, the parameters were estimated with very high relative standard errors (RSEs). Thus, the model was simplified, and the same PD models and parameter estimates were applied to the slow-replicating and non-replicating Mtb population. Delay in the induction of the bedaquiline effect has been previously described[18]. Therefore, a lag time in the bedaquiline model was evaluated and further improved the fit. The PD parameters for fast-replicating bacteria for all three drugs were estimated with good precision (%RSE < 40%). However, relatively large RSEs were noted for the parameters for slow- or non-replicating bacteria due to the limited data **(Table 5.1)**. Overall, the models described the available data reasonably well **(Figure 5.2)**.

Mechanistic PK-PD models for individual drugs

Previously developed mechanistic PK models for bedaquiline, pretomanid, and linezolid were combined with the PD models that were developed using the in vitro data to construct the mechanistic PK-PD framework. The framework was first used to simulate PK-EBA in TB patients at various doses of bedaquiline, pretomanid, and linezolid separately (S5.1). For the EBA simulations, the PD parameters were not adjusted for MICs because all patients in the EBA studies for all three drugs

had MIC ≤ lower limit of detection. The translated model over-predicted the anti-Mtb activity of bedaquiline. As bedaquiline strongly binds to plasma proteins and is widely distributed in tissues, a lung tissue binding factor parameter was introduced and estimated to be 0.01[33] **(Table 5.1)**. The final model described the median 14-day EBA data for bedaquiline at various doses well **(Figure 5.3)**. The lung tissue binding factor of 1 and 0.29 for pretomanid and linezolid, respectively described the median EBA data for both drugs well[27]. The simulations confirmed that the developed framework predicts the central tendency in bedaquiline, pretomanid, and linezolid EBA in TB patients separately well. The framework was deemed reliable for the evaluation of the next steps of the analysis, i.e., to simulate anti-Mtb activity following treatment with BPaL combination in MDR-TB patients.

BPaL quantitative framework

The final quantitative framework for the BPaL combination that included a multi-state TB model, drug effect models for all three drugs, PD interactions between the three drugs, scaling of the drug effect for MIC, and CFU-TTP correlations model was used for the simulations of combination drug effect to compare against Nix-TB observed data. Overall, the framework reasonably described the observed antibacterial activity following BPaL combination therapy (**Table 5.2**, S5.3). Median (95% PI) time to CFU-clearance status following the approved BPaL dosing was predicted as 38 (23-53) days which is in reasonable alignment with the reported median time to culture-negative status in the Nix-TB study (42 days) **(Figure 5.4)**. Overall, this modeling framework was deemed appropriate to simulate anti-Mtb activity following approved and alternative BPaL dosing regimens.

Figure 5.3 Evaluation of the Bedaquiline, Pretomanid, and Linezolid semi-mechanistic PK-PD models using early bactericidal activity studies data from pulmonary Tuberculosis patients. The in vitro to in vivo translated, semi-mechanistic PK-PD models recapitulate the early bactericidal activity in TB patients. Bedaquiline was administered with an increasing daily dose, i.e., panel 1 represents a group that received 200 mg on day 1 and 100 mg on day 2 onwards. Lines represent median.

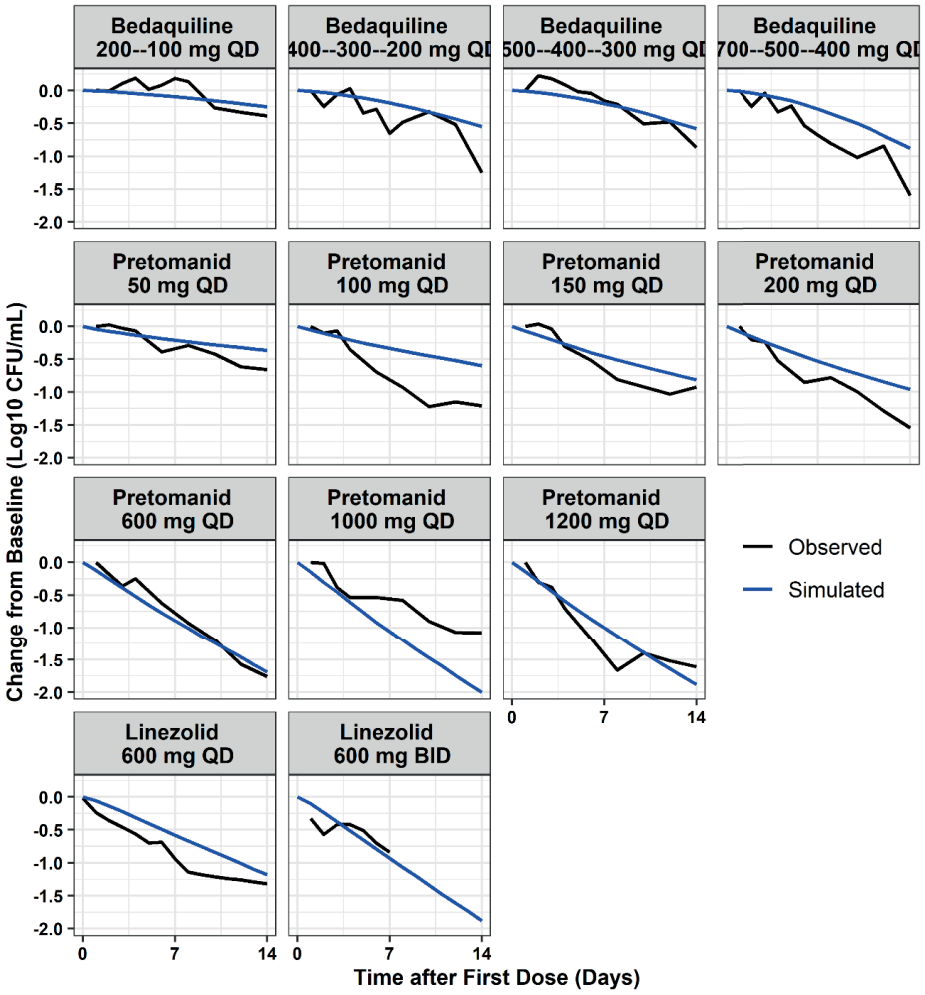

Table 5.2 Observed and predicted early bactericidal activity as measured by time to culture positivity (EBA-TTP) (1/day) following Bedaquiline, Pretomanid, and Linezolid combination therapy.

Linezolid Treatment Group	Metric	Observed Median (95% CI)	Simulated Median (95% PI)
600 mg BID	$EBA\text{-}TTP_{0\text{-}14days}$	-0.68 (-2.40 to 0.14)	-0.85 (-0.94 to -0.71)
	$EBA\text{-}TTP_{0\text{-}28days}$	-0.58 (-0.97 to -0.40)	-0.51 (-0.52 to -0.41)
1200 mg QD	$EBA\text{-}TTP_{0\text{-}14days}$	-0.63 (-1.42 to -0.07)	-0.85 (-0.93 to -0.75)
	$EBA\text{-}TTP_{0\text{-}28days}$	-0.45 (-0.92 to -0.12)	-0.51 (-0.52 to -0.46)

Simulations of anti-mtb activity following bpal at approved and alternative dosing in mdr-tb patients

The BPaL quantitative framework was used to perform and compare simulations of the current approved and three alternative dosing scenarios for up to 9 weeks **(Figure 5.4, Figure 5.5)**. Bedaquiline QD dosing (bedaquiline 200 mg QD for 9 weeks followed by 100 mg QD) was predicted to achieve slightly faster CFU clearance when compared to approved bedaquiline dosing (400 mg QD for 14-days followed by 200 mg QD) (Median (95% PI) time to <1 $CFUmL^{-1}$ = 38 (23-53) vs. 40 (27-56) days). Linezolid 600 mg BID was predicted to yield slightly faster Mtb clearance as compared to linezolid 600 mg QD dosing (Median (95% PI) time to <1 CFU mL^{-1} = 45 (26-58) vs. 43 (30-57) days). Overall clearance of non-replicating Mtb from the lesion was correlated with CFU clearance (combined fast- and slow-replicating Mtb). Median time to <1 non-replicating Mtb mL^{-1} was predicted to be additional 15 days from the CFU clearance state **(Figure 5.4)**. No clear correlation was predicted in time to Mtb clearance and individual MIC following BPaL combination therapy at the approved regimen (S5.4).

Figure 5.4 Spaghetti plots of anti-Mtb activity simulations using the BPaL quantitative framework for the approved and alternative dosing regimens. Each BPaL combination dosing regimen was simulated for 500 virtual patients and bacterial load time course predictions are plotted for each virtual patient. CFU represents total fast- and slow-multiplying Mtb, BID=twice daily, QD=once daily, three times a week=three times a week. Dashed line represent 1 CFU or non-replicating Mtb mL^{-1}. Minor difference was predicted in Mtb clearance with Bedaquiline QD dosing when compared to approved bedaquiline dosing. Similarly, minor difference was predicted in Mtb clearance following linezolid 600 mg BID as compared to linezolid 600 mg QD dosing. Median time to <1 non-replicating Mtb mL^{-1} was predicted to be additional 15 days from the CFU clearance state.

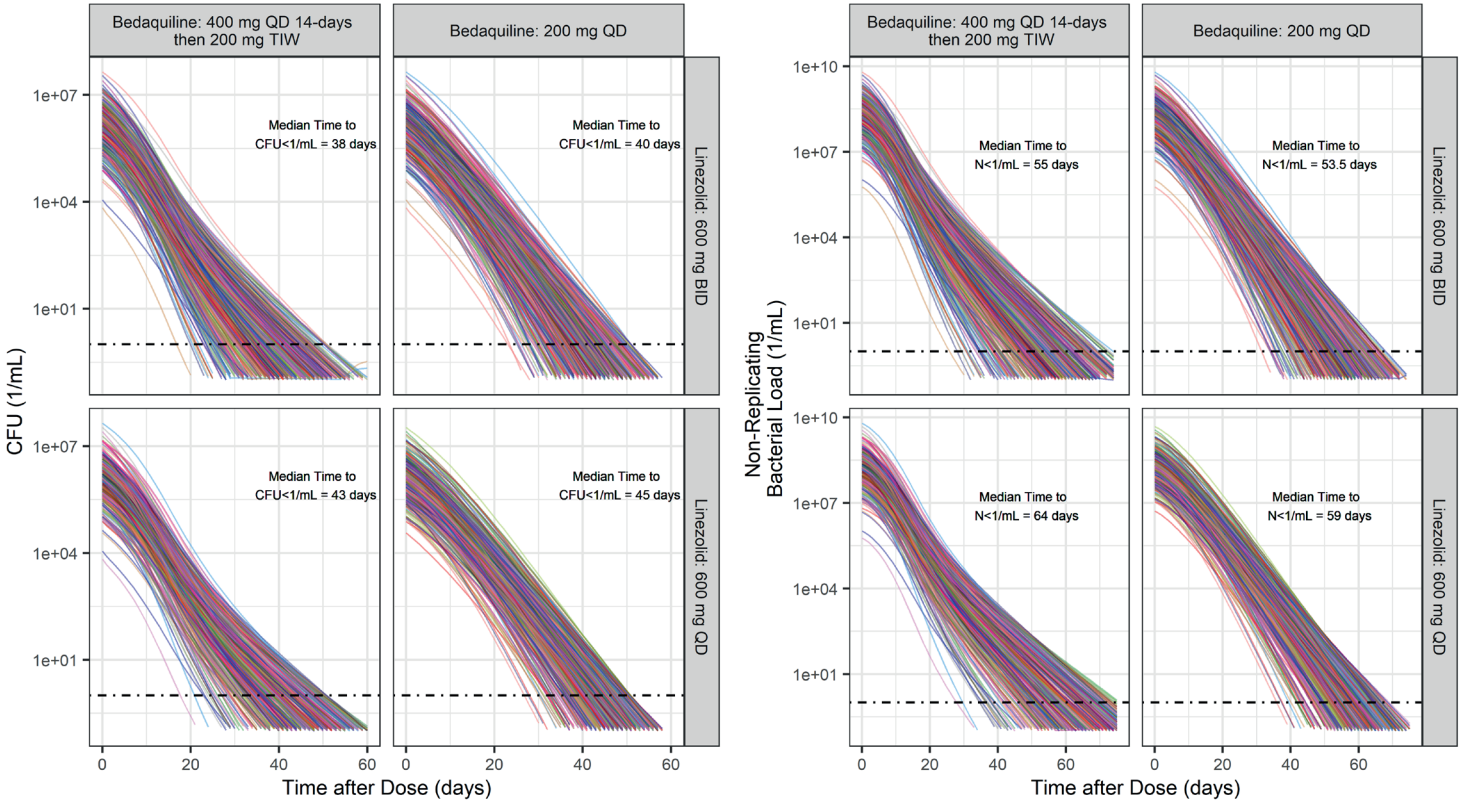

Figure 5.5 Predicted proportions of patients with CFU and non-replicating Mtb < 1 mL^{-1}. Comparable proportions of patients were predicted to achieve Mtb clearance following bedaquiline QD dosing vs. bedaquiline approved dosing. Similarly, comparable proportions of patients were predicted to achieve Mtb clearance following linezolid QD dosing vs. linezolid approved dosing.

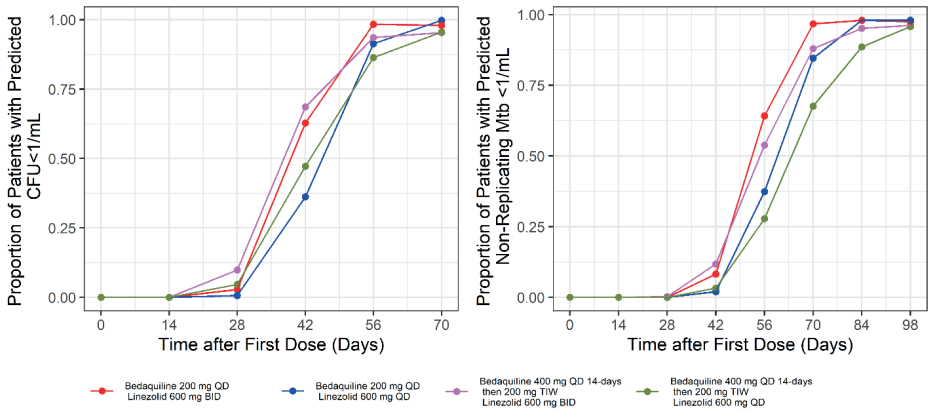

Discussion

In this work, we developed a quantitative framework for the BPaL combination that included key components that play role in the overall response to the therapy. The framework reasonably described anti-Mtb activity data for monotherapy of each drug in pulmonary TB patients and BPaL combination therapy in MDR-TB patients. We applied the framework to predict the treatment effects of the approved and alternative BPaL dosing scenarios.

The BPaL quantitative framework can be used for the rational design of BPaL dose optimization strategies in TB patients, including MDR-TB. The approved bedaquiline dose in the BPaL regimen includes 400 mg QD for 14 days followed by 200 mg three times a week for at least 6-9 weeks. This unconventional, three times a week, dosing schedule and long treatment duration may lead to patient non-adherence[34]. Additionally, bedaquiline has been reported to have delayed onset of anti-Mtb activity. Therefore, bedaquiline alternative dosing, 200 mg QD for 9 weeks followed by 100 mg QD has been proposed. Prior analyses predicted comparable safety concerns associated with bedaquiline alternative dosing and approved dosing[35]. Our simulations suggested a minor difference in Mtb clearance following bedaquiline QD dosing compared to the approved dosing. Linezolid has been a key drug in more than five drug combination regimens and was widely used for the treatment of MDR-TB

before the availability of bedaquiline and pretomanid. Despite the reasonable efficacy against MDR-TB, linezolid has high toxicity potential[2]. Our simulations suggested a slightly slower Mtb clearance following BPaL administration including linezolid 600 mg QD when compared to 600 mg BID. These simulations are in alignment with the ZeNix study, where 89% and 84% of the patients had favorable outcomes following BPaL including 1200 mg QD and 600 mg QD linezolid, respectively. In the same study, fewer adverse events and dose modifications were reported in the group with linezolid 600 mg compared to 1200 mg QD[8]. Altogether, this suggests that alternative BPaL dosing including bedaquiline 200 mg QD and linezolid 600 mg QD may be appropriate for most but some MDR-TB patients.

Our modeling framework incorporates predictions of drug penetration within lungs and cavitary lesions where drug concentrations within lungs drive fast- and slow-replicating Mtb killing, and drug concentrations within lesions drive non-replicating Mtb killing. Our model-based predictions for the effects of BPaL combination on non-replicating Mtb suggested approximately additional 15 days of BPaL therapy to achieve a non-replicating-clearance state from the CFU-clearance state. Thus, additional clinical evaluations of the BPaL regimen for longer treatment period after the CFU-negative state and its impact on tolerance, resistance, or relapse rate can be beneficial[36].

We assumed that M2 target site exposures driven maximum kill rate for all three Mtb subpopulations is 5-fold lower than that of bedaquiline[33]. Observed plasma M2-bedaquiline exposures ratio has been reported to be 0.25-0.32[33]. Based on our translational mPBPK model, plasma, lungs, and lesion M2-bedaquiline exposures ratios were predicted to be 0.18, 1.11 and 1.02, respectively[14]. These results provide an overview of the relative role of M2 as compared to bedaquiline on Mtb-clearance.

In our model, we used synergistic PD interaction between bedaquiline and pretomanid, and antagonist PD interaction between linezolid and bedaquiline as well as linezolid and pretomanid based on the robust DiaMOND drug interaction evaluation methodology from literature[31]. Previously, mixed results have been reported for type of PD interactions between each two-drug combination of bedaquiline, pretomanid, and linezolid perhaps owing to different experimental conditions[37–39]. Our model predictions agree with the consistently reported experimental and clinical findings that reported three-drug combination, BPaL, to be synergistically effective against Mtb.

A key assumption in our model was that we assumed the same drug effect parameters for the slow- or non-replicating Mtb population for all three drugs as in vitro time-kill data were not available for the slow-replicating Mtb population in literature. Such data are often not measured, and simpler bacterial growth models with two Mtb populations have been developed using murine experimental data[40]. Since our model was calibrated using multi-state tuberculosis model construct and parameterization and in vitro data from fast-replicating and slow-replicating Mtb experiments, our parameter estimates and thus simulations capture relative contributions of treatment on the killing of each Mtb subpopulations (S5.5). Future work on the development and validation of two Mtb subpopulation models using in vitro data, and on the development of bioanalytical methods to enable measurements of all three Mtb subpopulations can be useful.

Bedaquiline and pretomanid pulmonary drug concentration data from TB patients are not available to date; therefore, lung and lesion penetration of these two drugs were obtained using translational mPBPK models[14]. Additionally, lung tissue content and drug physicochemical properties affect the fraction of drug available at target sites to exert the anti-Mtb effect. Anti-bacterial activity data following monotherapy agreed well with the predictions for bedaquiline and linezolid by accounting for unbound drug fractions in lungs that were measured experimentally[27]. However, a similar approach for pretomanid underpredicted the drug effects. Therefore, this parameter was assumed to be 1 for pretomanid which provided a reasonable fit to the data. Overall, although the lung and lesion penetration component of our framework could not be qualified against observed data, our model is qualified against observed anti-Mtb activity data following the monotherapy of each drug.

Our BPaL quantitative framework includes key factors that play role in treatment outcome, such as patient body weight, plasma PK, TB lesion volume, drug penetration and available effective fraction into lung and lesion, Mtb susceptibility, and PD interactions amongst all three drugs. Thus, the framework can be utilized to further explore the relationship between these factors and individual parameter estimates to understand the key factors affecting treatment outcomes. The mechanistic understanding included in this quantitative framework combined with data-driven estimation approaches, such as Bayesian estimation, may provide a thorough understanding of individual variability towards the goal of treatment individualization. Model-informed therapeutic drug monitoring approaches have been proposed and are being evaluated for precision dosing approaches to account for variability in PK to enable optimal plasma drug exposures in the treatment of TB patients[41,42]. Additionally, variability in disease-related and treatment-response-related factors may affect treatment response[9]. Further data-driven, model-informed evaluations using our mechanistic framework as a foundation can provide insights into such factors and help identify patients at higher risk of poor treatment response and factors affecting poor treatment response[9]. Understanding such relationships can help develop further dose optimization or individualization algorithms.

In conclusion, we present a quantitative framework for predicting dosing regimens of BPaL combination treatment in TB patients, including MDR-TB patients. Our quantitative framework adequately described the observed anti-Mtb activity data following monotherapy for each drug and the BPaL combination regimen. The simulations suggested a minor difference in median time-to-Mtb-clearance with the bedaquiline alternative compared to the approved dosing (40 vs. 38 days). Similarly, the simulations suggested a minor difference in median time-to-Mtb-clearance with the linezolid alternative compared to the approved dosing (45 vs. 43 days). Overall, these results suggest that relatively comparable efficacy can be achieved using alternative bedaquiline and linezolid dosing that may improve safety and adherence in MDR TB patients. Median time to <1 non-replicating mL^{-1} was predicted to be approximately 15 days from the CFU-clearance state. These predictions can be utilized to evaluate treatment duration to eradicate non-replicating bacteria from lung lesions to avoid relapse and emergence of resistance.

References

1. Ou ZJ, Yu DF, Liang YH, et al. Trends in burden of multidrug-resistant tuberculosis in countries, regions, and worldwide from 1990 to 2017: results from the Global Burden of Disease study. *Infectious Diseases of Poverty*. 2021;10(1):24. doi:10.1186/s40249-021-00803-w
2. WHO Consolidated Guidelines on Tuberculosis Module 4: Treatment Drug-Resistant Tuberculosis Treatment Module 4: Treatment WHO Operational Handbook on Tuberculosis Drug-Resistant Tuberculosis Treatment.; 2020. http://apps.who.int/bookorders.
3. Conradie F, Diacon AH, Ngubane N, et al. Treatment of Highly Drug-Resistant Pulmonary Tuberculosis. *New England Journal of Medicine*. 2020;382(10):893-902. doi:10.1056/nejmoa1901814
4. van de Berg SEJ, Pelzer PT, van der Land AJ, et al. Acceptability, feasibility, and likelihood of stakeholders implementing the novel BPaL regimen to treat extensively drug-resistant tuberculosis patients. *BMC Public Health*. 2021;21(1):1404. doi:10.1186/s12889-021-11427-y
5. Imperial MZ, Nedelman JR, Conradie F, Savic RM. Proposed Linezolid Dosing Strategies to Minimize Adverse Events for Treatment of Extensively Drug-Resistant Tuberculosis. *Clinical Infectious Diseases*. 2022;74(10):1736-1747. doi:10.1093/cid/ciab699
6. Bloemberg GV, Keller PM, Stucki D, et al. Acquired Resistance to Bedaquiline and Delamanid in Therapy for Tuberculosis. *N Engl J Med*. 2015;373(20):1986-1988. doi:10.1056/NEJMc1505196
7. Salinger DH, Nedelman JR, Mendel C, Spigelman M, Hermann DJ. Daily dosing for bedaquiline in patients with tuberculosis. *Antimicrobial Agents and Chemotherapy*. 2019;63(11). doi:10.1128/AAC.00463-19
8. Conradie F, Bagdasaryan TR, Borisov S, et al. Bedaquiline–Pretomanid–Linezolid Regimens for Drug-Resistant Tuberculosis. *New England Journal of Medicine*. 2022;387(9):810-823. doi:10.1056/nejmoa2119430
9. Solans BP, Imperial MZ, Olugbosi M, Savic RM. Analysis of Dynamic Efficacy Endpoints of the Nix-TB Trial. *Clinical Infectious Diseases*. Published online June 8, 2023. doi:10.1093/cid/ciad051
10. Oelofse S, Esmail A, Diacon AH, et al. Pretomanid with bedaquiline and linezolid for drug-resistant TB: A comparison of prospective cohorts. *International Journal of Tuberculosis and Lung Disease*. 2021;25(6):453-460. doi:10.5588/ijtld.21.0035
11. Svensson RJ, Simonsson USH. Application of the multistate tuberculosis pharmacometric model in patients with rifampicin-treated pulmonary tuberculosis. *CPT: Pharmacometrics and Systems Pharmacology*. 2016;5(5):264-273. doi:10.1002/psp4.12079
12. Lyons MA. Modeling and simulation of pretomanid pharmacodynamics in pulmonary tuberculosis patients. *Antimicrobial Agents and Chemotherapy*. 2019;63(12):1-24. doi:10.1128/AAC.00732-19
13. Svensson EM, Karlsson MO. Modelling of mycobacterial load reveals bedaquiline's exposure-response relationship in patients with drug-resistant TB. *Journal of Antimicrobial Chemotherapy*. 2017;72(12):3398-3405. doi:10.1093/jac/dkx317
14. Mehta K, Guo T, van der Graaf PH, van Hasselt JGC. Predictions of Bedaquiline and Pretomanid Target Attainment in Lung Lesions of Tuberculosis Patients using Translational Minimal Physiologically Based Pharmacokinetic Modeling. *Clin Pharmacokinet*. 2023;62(3):519-532. doi:10.1007/s40262-023-01217-7
15. Clewe O, Aulin L, Hu Y, Coates ARM, Simonsson USH. A multistate tuberculosis pharmacometric model: A framework for studying anti-tubercular drug effects in vitro. *Journal of Antimicrobial Chemotherapy*. 2016;71(4):964-974. doi:10.1093/jac/dkv416
16. Andries K, Verhasselt P, Guillemont J, et al. A diarylquinoline drug active on the ATP synthase of Mycobacterium tuberculosis. *Science*. 2005;307(5707):223-227. doi:10.1126/science.1106753
17. Koul A, Vranckx L, Dendouga N, et al. Diarylquinolines are bactericidal for dormant mycobacteria as a result of disturbed ATP homeostasis. *Journal of Biological Chemistry*. 2008;283(37):25273-25280. doi:10.1074/jbc.M803899200

18. Koul A, Vranckx L, Dhar N, et al. Delayed bactericidal response of Mycobacterium tuberculosis to bedaquiline involves remodelling of bacterial metabolism. *Nature communications*. 2014;5:3369. doi:10.1038/ncomms4369

19. Somasundaram S, Anand RS, Venkatesan P, Paramasivan CN. Bactericidal activity of PA-824 against Mycobacterium tuberculosis under anaerobic conditions and computational analysis of its novel analogues against mutant Ddn receptor. *BMC Microbiology*. 2013;13(1). doi:10.1186/1471-2180-13-218

20. Drusano GL, Myrick J, Maynard M, et al. Linezolid kills acid-phase and nonreplicative-persister-phase mycobacterium tuberculosis in a hollow-fiber infection model. *Antimicrobial Agents and Chemotherapy*. 2018;62(8). doi:10.1128/AAC.00221-18

21. Food and Drug Administration (FDA). FDA Briefing Document Pretomanid Tablet, 200 mg Meeting of the Antimicrobial Drugs Advisory Committee (AMDAC). Published online 2019:https://www.fda.gov/media/127592/download.

22. Dietze R, Hadad DJ, McGee B, et al. Early and extended early bactericidal activity of linezolid in pulmonary tuberculosis. *American Journal of Respiratory and Critical Care Medicine*. 2008;178(11):1180-1185. doi:10.1164/rccm.200806-892OC

23. Diacon AH, Dawson R, von Groote-Bidlingmaier F, et al. 14-day bactericidal activity of PA-824, bedaquiline, pyrazinamide, and moxifloxacin combinations: a randomised trial. *The Lancet*. 2012;380(9846):986-993. doi:10.1016/S0140-6736(12)61080-0

24. Diacon AH, Dawson R, Du Bois J, et al. Phase II dose-ranging trial of the early bactericidal activity of PA-824. *Antimicrobial Agents and Chemotherapy*. 2012;56(6):3027-3031. doi:10.1128/AAC.06125-11

25. Strydom N, Gupta SV, Fox WS, et al. Tuberculosis Drugs' Distribution and Emergence of Resistance in Patient's Lung Lesions: A Mechanistic Model and Tool for Regimen and Dose Optimization. Vol 16.; 2019. doi:10.1371/journal.pmed.1002773

26. Chen RY, Yu X, Smith B, et al. Radiological and functional evidence of the bronchial spread of tuberculosis: an observational analysis. *The Lancet Microbe*. 2021;2(10):e518-e526. doi:10.1016/S2666-5247(21)00058-6

27. Sarathy JP, Via LE, Weiner D, et al. Extreme drug tolerance of mycobacterium tuberculosis in Caseum. *Antimicrobial Agents and Chemotherapy*. 2018;62(2). doi:10.1128/AAC.02266-17

28. Sarathy JP, Zuccotto F, Hsinpin H, et al. Prediction of Drug Penetration in Tuberculosis Lesions. *ACS Infectious Diseases*. 2016;2(8):552-563. doi:10.1021/acsinfecdis.6b00051

29. Wicha SG, Huisinga W, Kloft C. Translational pharmacometric evaluation of typical antibiotic broad-spectrum combination therapies against Staphylococcus aureus exploiting in vitro information. *CPT: Pharmacometrics and Systems Pharmacology*. 2017;6(8):515-522. doi:10.1002/psp4.12197

30. Lill D, Kümmel A, Mitov V, et al. Efficient simulation of clinical target response surfaces. *CPT: Pharmacometrics and Systems Pharmacology*. 2022;11(4):512-523. doi:10.1002/psp4.12779

31. Cokol M, Kuru N, Bicak E, Larkins-Ford J, Aldridge BB. Efficient Measurement and Factorization of High-Order Drug Interactions in Mycobacterium Tuberculosis.; 2017. https://www.science.org

32. Bowness R, Boeree MJ, Aarnoutse R, et al. The relationship between mycobacterium tuberculosis mgit time to positivity and cfu in sputum samples demonstrates changing bacterial phenotypes potentially reflecting the impact of chemotherapy on critical sub-populations. *Journal of Antimicrobial Chemotherapy*. 2015;70(2):448-455. doi:10.1093/jac/dku415

33. van Heeswijk RPG, Dannemann B, Hoetelmans RMW. Bedaquiline: A review of human pharmacokinetics and drug-drug interactions. *Journal of Antimicrobial Chemotherapy*. 2014;69(9):2310-2318. doi:10.1093/jac/dku171

34. Nguyen TVA, Anthony RM, Bañuls AL, Vu DH, Alffenaar JWC. Bedaquiline Resistance: Its Emergence, Mechanism, and Prevention. *Clinical Infectious Diseases*. 2018;66(10):1625-1630. doi:10.1093/cid/cix992

35. Tanneau L, Karlsson MO, Rosenkranz SL, et al. Assessing Prolongation of the Corrected QT Interval with Bedaquiline and Delamanid Coadministration to Predict the Cardiac Safety of Simplified Dosing Regimens. *Clinical Pharmacology and Therapeutics*. 2022;0(0):1-9. doi:10.1002/cpt.2685

36. Evangelopoulos D, da Fonseca JD, Waddell SJ. Understanding anti-tuberculosis drug efficacy: rethinking bacterial populations and how we model them. *Int J Infect Dis*. 2015;32:76-80. doi:10.1016/j.ijid.2014.11.028

37. Khoshnood S, Goudarzi M, Taki E, et al. Bedaquiline: Current status and future perspectives. *Journal of Global Antimicrobial Resistance*. 2021;25:48-59. doi:10.1016/j.jgar.2021.02.017

38. Kim S, Yamada WM, Duncanson B, et al. Building Optimal Three-Drug Combination Chemotherapy Regimens To Eradicate Mycobacterium tuberculosis in Its Slow-Growth Acid Phase. *Antimicrobial Agents and Chemotherapy*. 2021;65(10):e00693-21. doi:10.1128/AAC.00693-21

39. EMA. Pretomanid FGK: PAR. 2020;31(June).

40. Muliaditan M, Della Pasqua O. Bacterial growth dynamics and pharmacokinetic–pharmacodynamic relationships of rifampicin and bedaquiline in BALB/c mice. *British Journal of Pharmacology*. 2022;179(6):1251-1263. doi:10.1111/bph.15688

41. Sturkenboom MGG, Märtson AG, Svensson EM, et al. Population Pharmacokinetics and Bayesian Dose Adjustment to Advance TDM of Anti-TB Drugs. *Clinical Pharmacokinetics*. 2021;60(6):685-710. doi:10.1007/s40262-021-00997-0

42. Mockeliunas L, Keutzer L, Sturkenboom MGG, et al. Model-Informed Precision Dosing of Linezolid in Patients with Drug-Resistant Tuberculosis. *Pharmaceutics*. 2022;14(4). doi:10.3390/pharmaceutics14040753

Supplementary Materials

S5.1. Summary of the time course data used for the analysis

Drug Name	Details	Source
Digitized In Vitro Anti-Mtb Activity Data from Literature		
Bedaquiline	Mtb cultures in log-growth conditions were treated with either control or bedaquiline at 0.3- or 3- mg/L. Longitudinal bacterial load data were collected.	[1]
	Longitudinal bacterial load data were collected for log-phase and non-replicating Mtb cultures in presence of bedaquiline 10 mg/L.	[2]
	Mtb cultures in log-growth conditions were treated with either control or bedaquiline at 0.1-, 1- or 10- mg/L. Longitudinal bacterial load data were collected.	[3]
Pretomanid	Mtb cultures in log-growth conditions were treated with either control or pretomanid 0.12-, 0.25-, 0.5-, 1- or 2- mg/L. Longitudinal bacterial load data were collected.	[4]
	Mtb cultures in log-growth conditions were treated with either control or pretomanid 10 mg/L. Longitudinal bacterial load data were collected.	[5]
	Longitudinal bacterial load data were collected for non-replicating Mtb cultures in presence of control or 3- and 12.5- mg/L.	[6]
Linezolid	Mtb in log-growth and non-replicating conditions in a hollow-fiber infection model were treated with control or linezolid at 300-, 600-, 900-, 1200-, or 1800- mg dose once daily or every other day. Longitudinal bacterial load data were collected.	[7]
Monotherapy Anti-Bacterial Activity Data		
Bedaquiline	This was a Phase 1 clinical trial that evaluated 14-day bacterial load data from pulmonary TB patients who were either treated with first-line TB therapy or bedaquiline at various doses for 14 days QD. Individual, longitudinal CFU data were obtained from the TB-Pacts database.	Clinical Trial: NCT01215110
Pretomanid	This was a Phase 2 clinical trial that evaluated 14-day bacterial load data from pulmonary TB patients who were either treated with first-line TB therapy or pretomanid at various doses for 14 days QD. Individual, longitudinal CFU data were obtained from the TB-Pacts database.	[8] Clinical Trials: NCT00944021 and NCT00567840
Linezolid	This study evaluated the anti-Mtb activity of linezolid in pulmonary TB patients at either 600 mg QD or 600 mg BID doses. Median profiles were digitized from the publication.	[9]
BPaL Combination Therapy Data		
Bedaquiline, Pretomanid, and Linezolid Combination	This was a phase 3 clinical trial that evaluated the efficacy and safety of the BPaL combination regimen in MDR-TB patients. Individual, longitudinal time to liquid culture positivity data were obtained from the TB-Pacts database.	[10] Clinical Trial: NCT02333799

S5.2. Impact of bedaquiline – M2 effect scaling factor on kmax and EC50 of fast-, slow-, and non-replicating Mtb. Sensitivity analysis was conducted to evaluate the impact of bedaquiline M2 effect scaling parameter (bdqm2scaling). The impact of bdqm2scaling factor on the predicted CFU following the approved BPaL dosing was evaluated by varying the parameter by a range of values and applying on kmax and EC50 one at a time. Overall, the parameter bdqm2scaling was not predicted to significantly affect overall CFU predictions.

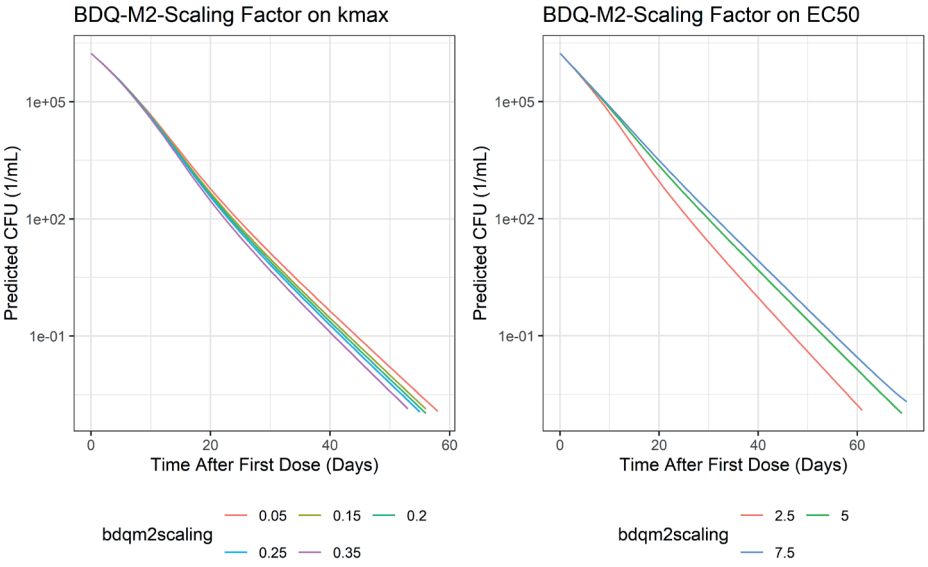

S5.3. Observed vs. Predicted $TTP_{0\text{-}14days}$ Following BPaL Combination at the Approved Dosing. Black point and error bars represent median and 95% confidence interval from the Nix-TB study[10]. Blue line and ribbon present median and 95% prediction interval.

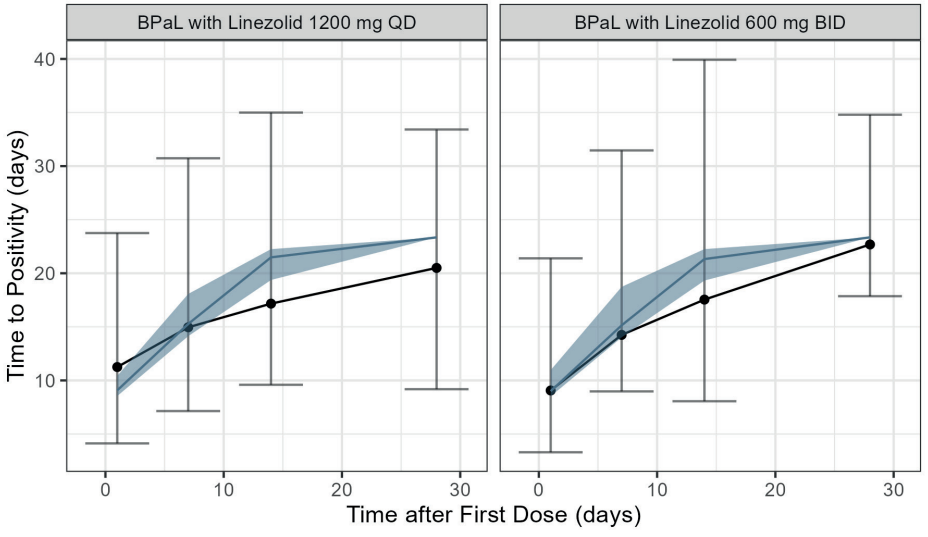

S5.4. Predicted time to Mtb clearance vs. Mtb susceptibility for each drug following BPaL combination at standard dosing regimen. Colony-forming units (CFU) represent total fast- and slow-multiplying Mtb, MIC=minimum inhibitory concentration.

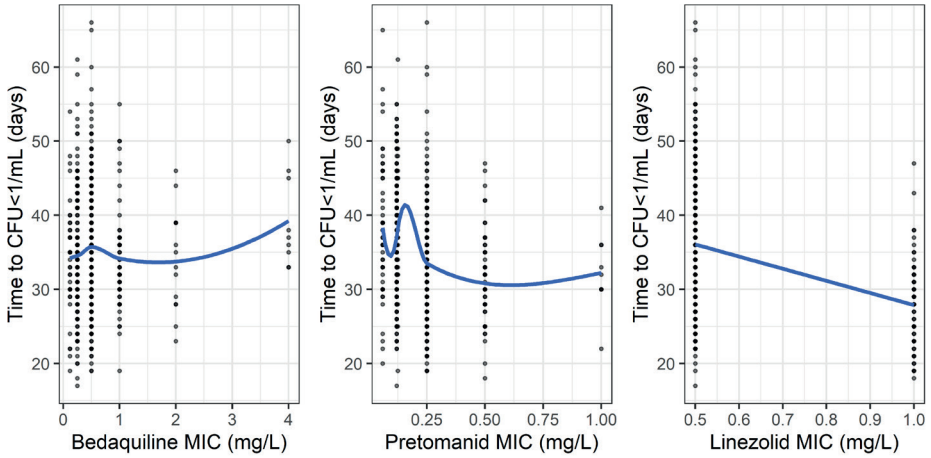

S5.5. Typical patient predictions from the BPaL quantitative framework before and after standard BPaL dosing regimen.

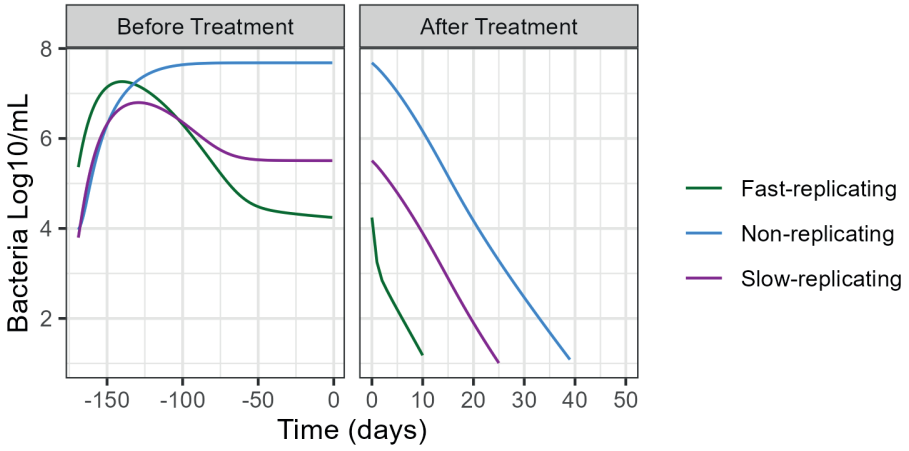

References

1. Andries K, Verhasselt P, Guillemont J, et al. A diarylquinoline drug active on the ATP synthase of Mycobacterium tuberculosis. *Science*. 2005;307(5707):223-227. doi:10.1126/science.1106753
2. Koul A, Vranckx L, Dendouga N, et al. Diarylquinolines are bactericidal for dormant mycobacteria as a result of disturbed ATP homeostasis. *Journal of Biological Chemistry*. 2008;283(37):25273-25280. doi:10.1074/jbc.M803899200
3. Koul A, Vranckx L, Dhar N, et al. Delayed bactericidal response of Mycobacterium tuberculosis to bedaquiline involves remodelling of bacterial metabolism. *Nature communications*. 2014;5:3369. doi:10.1038/ncomms4369
4. Food and Drug Administration (FDA). FDA Briefing Document Pretomanid Tablet, 200 mg Meeting of the Antimicrobial Drugs Advisory Committee (AMDAC). Published online 2019:https://www.fda.gov/media/127592/download.
5. Stover CK, Warrener P, VanDevanter DR, et al. A small-molecule nitroimidazopyran drug candidate for the treatment of tuberculosis. *Nature*. 2000;405(6789):962-966. doi:10.1038/35016103
6. Somasundaram S, Anand RS, Venkatesan P, Paramasivan CN. Bactericidal activity of PA-824 against Mycobacterium tuberculosis under anaerobic conditions and computational analysis of its novel analogues against mutant Ddn receptor. *BMC Microbiology*. 2013;13(1). doi:10.1186/1471-2180-13-218
7. Drusano GL, Myrick J, Maynard M, et al. Linezolid kills acid-phase and nonreplicative-persister-phase mycobacterium tuberculosis in a hollow-fiber infection model. *Antimicrobial Agents and Chemotherapy*. 2018;62(8). doi:10.1128/AAC.00221-18
8. Diacon AH, Dawson R, Du Bois J, et al. Phase II dose-ranging trial of the early bactericidal activity of PA-824. *Antimicrobial Agents and Chemotherapy*. 2012;56(6):3027-3031. doi:10.1128/AAC.06125-11
9. Dietze R, Hadad DJ, McGee B, et al. Early and extended early bactericidal activity of linezolid in pulmonary tuberculosis. *American Journal of Respiratory and Critical Care Medicine*. 2008;178(11):1180-1185. doi:10.1164/rccm.200806-892OC
10. Conradie F, Diacon AH, Ngubane N, et al. Treatment of Highly Drug-Resistant Pulmonary Tuberculosis. *New England Journal of Medicine*. 2020;382(10):893-902. doi:10.1056/nejmoa1901814

Chapter 6

Predictions of bedaquiline central nervous system exposure in tuberculosis meningitis patients using physiologically-based pharmacokinetic modeling

Krina Mehta, Pavel Balazki, Piet H. van der Graaf, Tingjie Guo, J. G. Coen van Hasselt

Clin Pharmacokinet. 2024 Mar 26.
doi: 10.1007/s40262-024-01363-6.

Abstract

Background: The use of bedaquiline as a treatment option for drug-resistant tuberculosis meningitis (TBM) is of interest to address the increased prevalence of resistance to first-line antibiotics. To this end, we describe a whole-body physiologically-based pharmacokinetic (PBPK) model for bedaquiline to predict central nervous system (CNS) exposure.

Methods: A whole-body PBPK model was developed for bedaquiline and its metabolite, M2. The model included compartments for brain and cerebrospinal fluid (CSF). Model predictions were evaluated by comparison to plasma PK time profiles following different dosing regimens and sparse CSF concentrations data from patients. Simulations were then conducted to compare CNS and lung exposures to plasma exposure at clinically relevant dosing schedules.

Results: The model appropriately described the observed plasma and CSF bedaquiline and M2 concentrations from pulmonary TB patients. The model predicted a high impact of tissue binding on target site drug concentrations in CNS. Predicted unbound exposures within brain interstitial exposures were comparable to unbound vascular plasma and unbound lung exposures. However, unbound brain intracellular exposures were predicted to be 7% of unbound vascular plasma and unbound lung intracellular exposures.

Conclusions: The whole-body PBPK model for bedaquiline and M2 predicted unbound concentrations in brain to be significantly lower than the unbound concentrations in the lung at clinically relevant doses. Our findings suggest that bedaquiline may result in relatively inferior efficacy against drug-resistant TBM when compared to efficacy against drug-resistant pulmonary TB.

Introduction

Tuberculosis meningitis (TBM) develops when *Mycobacterium tuberculosis* (Mtb) disseminates from the primary pulmonary site of infection to the central nervous system (CNS) including the brain[1]. TBM, the most severe form of Mtb infections, is associated with an approximately 42% mortality rate in hospitalized patient[2]. First-line treatment for drug-susceptible TBM patients remains the same as that for pulmonary tuberculosis patients, which includes a combination of rifampin, isoniazid, pyrazinamide, and ethambutol[3]. Second-line treatment for TBM patients includes streptomycin, moxifloxacin, fluoroquinolones, cycloserine, linezolid, etc. Several first-line and second-line anti-TB drugs, including, rifampin, ethambutol, and streptomycin, penetrate poorly through the blood-brain barrier (BBB) [4,43,44]. Second-line drugs, such as, moxifloxacin, fluoroquinolones, ethionamide, cycloserine and linezolid penetrate moderately through BBB[4]. Drug resistant TBM, i.e., Mtb resistant to rifampin and/or isoniazid, is challenging to diagnose and treat. Limited reporting on drug-resistant TBM is attributed to the rarity of the disease and the challenges associated with evaluation of resistance in cerebrospinal fluid (CSF). However, the prevalence of resistance aligns generally with Mtb resistance rates[5]. Currently, there are no standard treatment recommendations for drug-resistant TBM, and treatment approaches are generally selected by treating physicians based on individual patient factors often including extensive treatment with more than five antimicrobial agents. Concerns regarding safety issues of extensive treatments as well as the high mortality rate (69-100%) amongst drug-resistant TBM patients remain a clinical challenge[6].

Bedaquiline is one of the newer TB antibiotics and was the first novel anti-Mtb drug approved in over 40 years[7]. Bedaquiline has activity against Mtb strains resistant against several first-line and second-line TB therapeutics. Bedaquiline has now been evaluated in over 25 clinical trials as part of various combination regimens against Mtb infections[8]. A combination regimen containing bedaquiline, pretomanid, and linezolid (BPaL) is now recommended for the treatment of rifampin-resistant TB and multidrug-resistant TB patients[9].

Given the efficacy of BPaL and other bedaquiline-containing combination regimens against drug-resistant pulmonary TB, bedaquiline-containing regimens are being evaluated for the treatment of drug-resistant TBM[10,11]. Preclinical target site pharmacokinetic (PK) studies reported brain–to–plasma exposure ratio ranging from 2-20%)[12–14]; however, these studies do not differentiate between total and unbound exposures in the brain. In a preclinical efficacy study, combination

therapy with BPaL showed significantly inferior efficacy compared to first-line anti-TB therapy in a mice TBM model following equivalent to human clinically relevant dosing for each drug[14]. On the other hand, comparable efficacy was observed following BPaL compared to first-line anti-TB therapy in a mice pulmonary model following equivalent to human clinically relevant dosing for each drug[15,16]. In pulmonary TB patients, bedaquiline and its active metabolite, M2, concentrations in CSF have been reported to be approximately equivalent to unbound plasma concentrations[11]. No clinical data on the efficacy of bedaquiline-containing regimens for the treatment of TBM are available[14,17]. Overall, these contrary preclinical results and very limited clinical data are neither in favor of nor against the suitability of bedaquiline for the treatment of TBM.

Understanding of mechanisms behind the contradicting preclinical results can be useful in future preclinical and clinical study designs. Factors such as molecular weight, lipophilicity, protein binding, ionization, brain metabolism, and transporters play a role in drug distribution across BBB and blood-CSF-barrier (BCSFB), and the extent of unbound drug available to exert the effect. Physiologically-based pharmacokinetic (PBPK) models integrate prior knowledge about physiological processes with the drug's physicochemical and kinetic parameters to enable PK predictions of a drug within various tissue compartments. Thus, PBPK models are well suited to predict bedaquiline concentrations at the target sites-of-action, i.e., CSF, brain interstitial, and intracellular in TBM patients to evaluate its potential for the treatment of MDR TBM patients. However, a whole-body bedaquiline PBPK model with CNS compartments has not yet been developed. In this work, we aimed (1) to develop and evaluate a whole-body PBPK model for bedaquiline and M2 including CSF compartment using plasma and CSF drug and M2 concentrations data from TB patients, (2) to simulate target site concentrations for bedaquiline and M2 for currently recommended bedaquiline dosing schedules in humans.

Methods

Data

Plasma PK data from pulmonary TB patients were accessed through the Platform for Aggregation of Clinical TB Studies (TB-PACTS; https://c-path.org/programs/tb-pacts/). We first utilized bedaquiline and M2 physicochemical characteristics and plasma PK data from pulmonary TB patients from a clinical study for the model development. Mean plasma bedaquiline and M2 concentrations by nominal time following bedaquiline doses of 400 mg on Day 1, 300 mg on Day 2, and 200 mg on

Day 3 through 14 (referred to as 400-300-200 QD hereinafter) from a Phase 2 study were used for model fitting[18]. Next, the model was validated by comparing typical patient plasma PK predictions with observed data for four different dosing groups, including 200-100 mg QD, 500-400-300 mg QD, and 700-500-400 mg QD dosing in TB patients, from a Phase1 study, NCT01215110. Lastly, sparse steady-state individual (n=7) plasma and CSF PK data, one sample per patient, for bedaquiline and M2 following bedaquiline 400 mg QD followed by 200 mg three times a week at week 24 were obtained from the literature and were used for further validation of the CNS distribution component of the model[11].

Whole-body PBPK model development

The standard PK-Sim whole-body PBPK structural model for small molecules was utilized to build a combined bedaquiline and M2 model[19–21]. The standard PK-Sim whole-body PBPK model consists of key tissues and organs, including, the brain, heart, lungs, liver, kidneys, GI tract, etc., connected through vascular and arterial blood circulation. Each compartment is divided into four sub-compartments, i.e., vascular, blood cells, interstitial, and intracellular[20]. Physicochemical parameters for bedaquiline and M2 were obtained from the literature (**Table 6.1)**[22]. Different values have been reported in the literature for bedaquiline lipophilicity and fraction unbound; therefore, model evaluation using each of the reported values was conducted to select the lipophilicity and fraction unbound values that provide the best fit to bedaquiline plasma PK data[22,23]. Bedaquiline oral absorption has previously been described as atypical with delay and double peaks[24–26]. The Weibull absorption model built within the PK-Sim software was selected due to its flexibility in describing atypical absorption profiles, and the parameters were estimated by fitting to the plasma PK data. Partition coefficients and cellular permeability parameters of bedaquiline and M2 in various tissues were calculated using the PK-Sim standard method[20,27]. In PK-Sim, the standard calculation method uses lipophilicity and plasma protein binding parameters along with lipid, protein, and water fractions in each compartment and sub-compartment to calculate partition coefficients. CYP3A4 enzyme is involved in the metabolism of bedaquiline to M2[23]. Therefore, CYP3A4-mediated metabolism conversion from bedaquiline to M2 was modeled using the Michaelis-Menten equation. Experimental data also suggest contributions of CYP2C8 and CYP2C19 enzymes in the metabolism of bedaquiline to M2 and thus were evaluated in the model using the Michaelis-Menten equation. Expression profiles for all three enzymes based on the RNA-seq method were obtained from the Bgee (https://www.bgee.org/) database accessible within PK-Sim[28]. The parameter Michaelis–Menten constant (Km) for the enzymatic reactions

was obtained from literature from in vitro experiments[29]. Residual bedaquiline liver plasma clearance and M2 liver plasma clearance estimates were obtained from literature[22]. Next, the model was simultaneously fitted to bedaquiline and M2 PK data following 400-300-200 QD dosing in pulmonary TB patients to estimate Weibull absorption parameters and enzymatic reaction rates (Vmax) parameters. The combined bedaquiline – M2 plasma PK model was validated by comparing the simulations vs. observed plasma PK data for bedaquiline following 200-100 mg QD, 500-400-300 mg QD, and 700-500-400 mg QD dosing regimens (Clinical Trial: NCT01215110). M2 PK data for this study was not available.

CNS PBPK model development

The standard PK-Sim whole-body PBPK structural model included the following brain sub-compartments: plasma, blood cells, interstitial, and intracellular. Drug permeability across the blood-brain barrier (BBB) is empirically accounted for as half of the transmembrane permeability calculated from physicochemical properties to account for lipid bilayer[30]. Bedaquiline is not known to be a substrate of transporters located at BBB such as P-gp, BCRP, and MRPs[23]. Therefore, the contribution of such transporters in bedaquiline distribution to the brain was not incorporated. The model was then extended in Mobi to incorporate two CSF compartments, cranial- and spinal CSF. The processes of drug distribution to and from CSF were adapted from literature and are illustrated in **Figure 6.1 A**[31,32]. Flow rates to and from CSF were calculated based on the CSF production rate based on physiological knowledge as discussed in the literature[31,33] **(Table 6.2)**. The same permeability parameter calculated from physicochemical properties was used for diffusion across blood-CSF-barrier (BCSFB) and BBB. The partition coefficient between plasma and CSF was calculated by incorporating fractions of water, lipid, and protein albumin in CSF as shown in equation below and **Table 6.2**[27,34,35]. To validate the bedaquiline-M2 whole-body PBPK model including CNS components, plasma and brain interstitial compartment predictions for bedaquiline and M2 were compared against the observed data[11].

$$PCcsf = Fwcsf + AlbCSF : Plasma * \frac{1}{fup} - Fwplasma \quad * fup$$

Here, $Alb_{CSF:Plasma}$ = albumin CSF to plasma ratio, fup=fraction unbound in plasma, Fw_{csf} = fraction of water in CSF, Fw_{plasma} = fraction of water in plasma, PC_{csf}=Plasma-to-CSF partition coefficient.

Sensitivity analysis

A local sensitivity analysis was conducted to understand the impact of parameter uncertainty on bedaquiline and M2 plasma and brain intracellular exposure, $AUC_{0\text{-}t}$. Lipophilicity and CNS distribution-related parameters, such as partition coefficients, permeability, and flow rates, were varied 2-fold. Fraction unbound for both bedaquiline and M2 was varied 1000-fold to cover the uncertainty range. Sensitivity analyses were run in Mobi for a typical subject following clinically relevant dosing, 400 mg QD for 14 days followed by 200 mg three times a week, and a sensitivity index was calculated.

Figure 6.1. Illustration of the Bedaquiline-M2 whole-body PBPK model with CNS. The whole-body PBPK model for bedaquiline and M2 was developed in PK-Sim[19–21]. Enzymatic metabolism from bedaquiline to M2 is driven by CYP3A4 and CYP2C8. Additionally, bedaquiline is eliminated at clearance rate $CL_{other\text{-}bdq}$ and M2 is eliminated at rate CL_{M2}. There are four routes for unbound drugs to distribute within CSF and brain – (1) from plasma into brain interstitial space, from brain interstitial into brain intracellular, and (2) from plasma into cranial CSF, then into spinal CSF, (3) from cranial CSF to intracellular space, (4) from cranial and spinal CSF into venous blood plasma. Drugs in interstitial and intracellular spaces can bind to the compartment lipid and protein content. The drug goes through mass transfer driven by CSF flow within cranial and spinal sub-compartments of CSF and also to vascular blood. BBB=blood-brain barrier, BCSFB=blood-cerebrospinal fluid barrier, $CL_{other\text{-}bdq}$=additional bedaquiline hepatic clearance (other than M2-relevant clearance), CLm2=M2 clearance, CSF=cerebrospinal fluid, $PxSA_B$=permeability surface area product for BBB, $PxSA_C$=permeability surface area product for BCSFB, $PxSA_E$=permeability surface area product from brain intracellular to cranial CSF, Q_{bulk}= mass transfer flow rate from intracellular to cranial CSF, Q_{csink}=CSF flow rate from cranial CSF to peripheral venous blood, Q_{sin}=CSF flow rate from cranial CSF to spinal CSF, Q_{sout}= CSF flow rate from spinal CSF to cranial CSF, Q_{ssink}=CSF flow rate from spinal CSF to peripheral venous blood. Figure generated using Biorender.com.

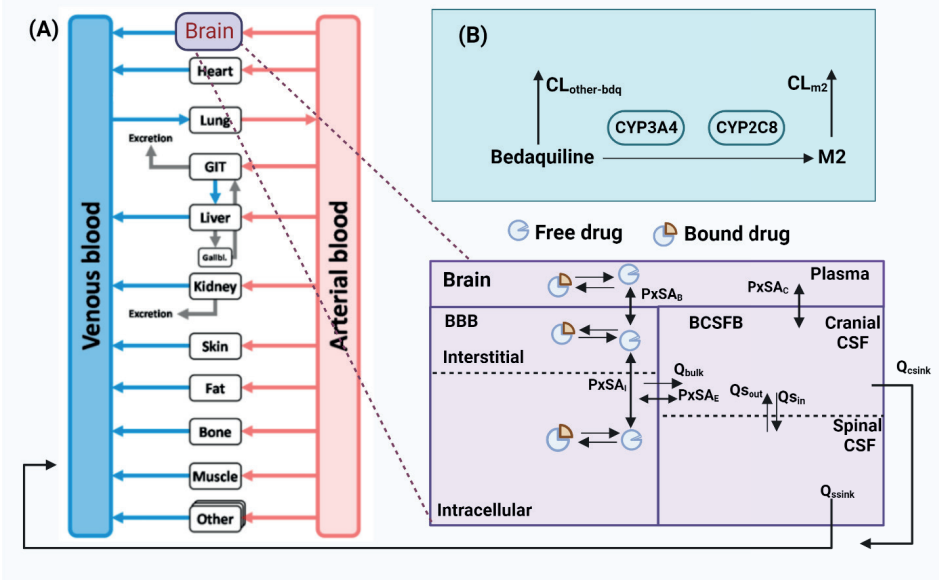

Simulations

Simulations were conducted to predict target site, brain intracellular and interstitial, concentrations for bedaquiline and M2 for clinically relevant bedaquiline dosing schedules in a typical TBM patient. A typical virtual TB patient was defined as an individual with 60 kg body weight, and 4.32 µmol/L and 2.56 µmol/L as reference concentrations of CYP4A4 and CYP2C8, respectively[18,28]. Typical virtual patient simulations were conducted for the currently approved dosing regimen and an alternative dosing regimen that was suggested to provide an improved benefit-risk ratio in patients with pulmonary TB [36]. Thus, the following dosing regimens were simulated: (1) current standard bedaquiline dosing which is 400 mg QD followed by 200 mg three times a week, and (2) alternative 200 mg QD for 8 weeks followed by 100 mg QD. Longitudinal total and unbound bedaquiline and M2 concentrations in peripheral blood plasma, lung intracellular, brain intracellular, and spinal CSF were simulated.

Software

Physiologically-based PK modeling and simulation was performed in PK-Sim® and MOBI® (Open Systems Pharmacology Suite (OSPS), v11.0, www.open-systems-pharmacology.org)[37]. Statistical analysis and plots were generated in R (R for Windows, v4.1, https://www.r-project.org/) using RStudio (RStudio, v1-554, www.rstudio.com/).

Results

The whole-body PBPK model described the observed PK data from plasma and CSF of TB patients.

The final model contained the whole-body PBPK structure with an extended CNS distribution model for both bedaquiline and M2. Multiple literature-based values have been reported in the literature for bedaquiline lipophilicity and fraction unbound, and the values that provided the best fit to observed plasma PK data were retained in the final model **(Table 6.1)**[22,23]. Enzymatic conversion of bedaquiline to M2 was first set up to be mediated by CYP3A4, CYP2C8, and CYP2C19; however, Vmax for CYP2C19-mediated reaction was estimated to be very low and thus was not retained[29]. The CNS component of the model contained the brain compartment that included plasma, interstitial, cranial CSF, spinal CSF, and intracellular sub-compartments. The parameters relevant to CNS distribution were described based on physiological and drug-specific knowledge **(Figure 6.1, Table 6.2)**[30–33].

The final bedaquiline-M2 whole-body PBPK model predictions agreed adequately with the observed plasma PK data for both bedaquiline and M2 following bedaquiline 400-300-200 QD dosing **(Figure 6.2A)** [18], as well as four different bedaquiline dosing regimens **(Figure 6.2B)**. Additionally, simulated bedaquiline and M2 PK profiles agreed very well with the observed plasma PK data in patients following current clinically recommended bedaquiline dosing **(Figure 6.3)**. At Week-24, predicted 24 hr plasma average concentrations (C_{avg}) for bedaquiline and M2 were 718 ng/mL 268 ng/mL, respectively. These results matched reasonably well with the reported 24-week plasma concentrations for both bedaquiline and M2 in literature following current clinically recommended bedaquiline dosing (median (IQR) concentrations 1264 ng/ml (910-2244) and 252 ng/ml (34-290) for bedaquiline and M2, respectively, based on data from 13 patients)[39]. At Week-8, predicted peripheral vascular blood cell to plasma concentration ratios were 0.54 and 19.5 for bedaquiline and M2, respectively **(Table 6.3)**. These results matched reasonably well with the reported peripheral blood mononuclear cells to plasma concentrations ratio in literature at Week-8 (1.1 and 22.2 for bedaquiline and M2, respectively)[40].

The model slightly underpredicted mean bedaquiline and M2 concentrations in spinal CSF; however, the CSF concentrations were within a standard deviation of the observed CSF concentrations **(Figure 6.3)**. Given that the CNS concentrations were bottom-up predictions based on physiological and drug-specific knowledge and that only sparse CSF observed data points (n=7) are available to date, the model was deemed reliable for the objectives of this study.

Table 6.1. Parameters for the Bedaquiline-M2 PBPK model with CNS distribution.

Parameter	Unit	Value	Source
Bedaquiline[a]			
Molecular Weight[b]	g/mol	555.5	PubChem Database
Lipophilicity	Log unit	5.14	[22]
Fraction unbound in plasma	Dimensionless	0.0003	[22]
pKa (Base)	Dimensionless	9.10	[22]
Weibull dissolution time (50% dissolved)	Min	125.21	Estimated
Weibull dissolution shape	Dimensionless	1.51	Estimated
Vmax CYP3A4	umol/L/min	407.85	Estimated
Km CYP3A4	umol/L	8.5	[29]
Vmax CYP2C8	umol/L/min	163.73	Estimated
Km CYP2C8	umol/L	13.1	[29]
Additional hepatic clearance	L/hr/kg	0.03	[22]
Permeability across BBB and BCSFB (assumed half of the calculated permeability from plasma-to-interstitial due to lipid bilayer in BBB and BCSFB)	dm/min	0.00217	PK-Sim Calculated
Cellular permeability from plasma to interstitial	dm/min	0.013	
Brain Interstitial-water partition coefficient	Dimensionless	0.0013	
Brain Intracellular-water partition coefficient	Dimensionless	6.2E-05	
Plasma-to-CSF partition coefficient	Dimensionless	0.0082	Calculated (see equation 1)
M2			
Molecular Weight[c]	g/mol	541	PubChem Database
Lipophilicity	Log unit	6.5	[22]
Fraction unbound in plasma	Dimensionless	0.0005	[22]
Hepatic clearance	L/hr/kg	0.14	Estimated
Permeability across BBB and BCSFB (assumed half of the calculated permeability from plasma-to-interstitial due to lipid bilayer in BBB and BCSFB)	dm/min	0.185	PK-Sim Calculated
Cellular permeability from plasma to interstitial	dm/min	0.36	
Brain Interstitial-water partition coefficient	Dimensionless	0.0013	
Brain Intracellular-water partition coefficient	Dimensionless	2.8E-06	
Plasma-to-CSF partition coefficient	Dimensionless	0.0084	Equation 1

Table 6.2. Key physiological parameters for the CNS distribution of the PBPK model.

Parameter	Unit	Value	Source
Albumin CSF-plasma ratio	Dimensionless	0.008	[35]
CSF lipid fraction	Dimensionless	0.0573	
CSF protein fraction	Dimensionless	0.005	
CSF production rate (Qcsf)[a]	mL/min	0.42	[32]
Surface area of blood-brain-barrier (BBB) (SA_B)	cm^2	150000	
Surface area of blood-CSF-barrier (BCSFB) (SA_C)	cm^2	15000	
Surface area brain interstitial – intracellular (SAi)	cm^2	3686	[41]

[a] CSF production rate was not directly used as a parameter; however, flow rates across the brain - CSF - peripheral blood were calculated based on CSF production rate as follows based on literature: Qbulk = 0.25*Qcsf, Qssink = 0.38 * ((0.75*Qcsf) + Qbulk), Qsout = 0.9*Qssink, Qsin = Qsout + Qssink, Qcsink = 0.75*(Qcsfprod + Qbulk - Qsin + Qsout); Permeability surface area product across brain intracellular to cranial CSF ($PxSA_E$) was set to high value, 300, assuming no barrier based on literature[22,23]

Figure 6.2. Predicted and observed plasma PK profiles for (A) model fitting dataset, and (B) model validation dataset. The final bedaquiline-M2 whole-body PBPK model predictions agreed well with the observed plasma PK data for both bedaquiline and M2 following bedaquiline 400-300-200 QD dosing, and four different bedaquiline dosing regimens from a Phase 1 study. Dosing regimens were administered in increasing amounts for the first three days of the therapy. I.e., 400-300-200 mg QD represents 400 mg on Day 1, 300 mg on Day 2, and 200 mg QD on Day 3 onwards.

(A)

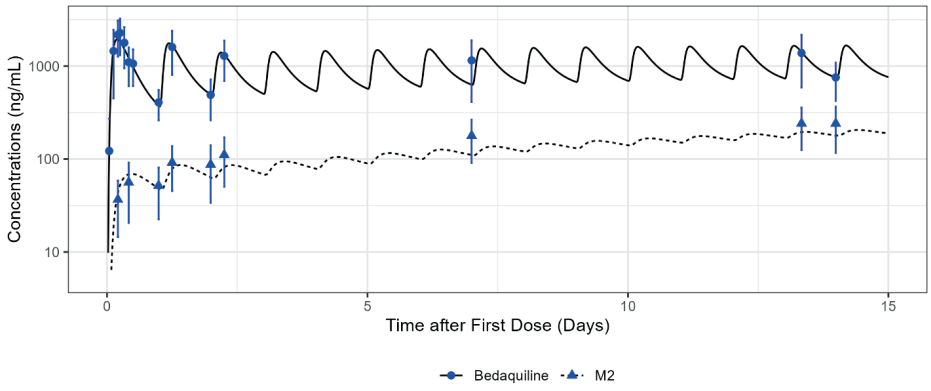

(B)

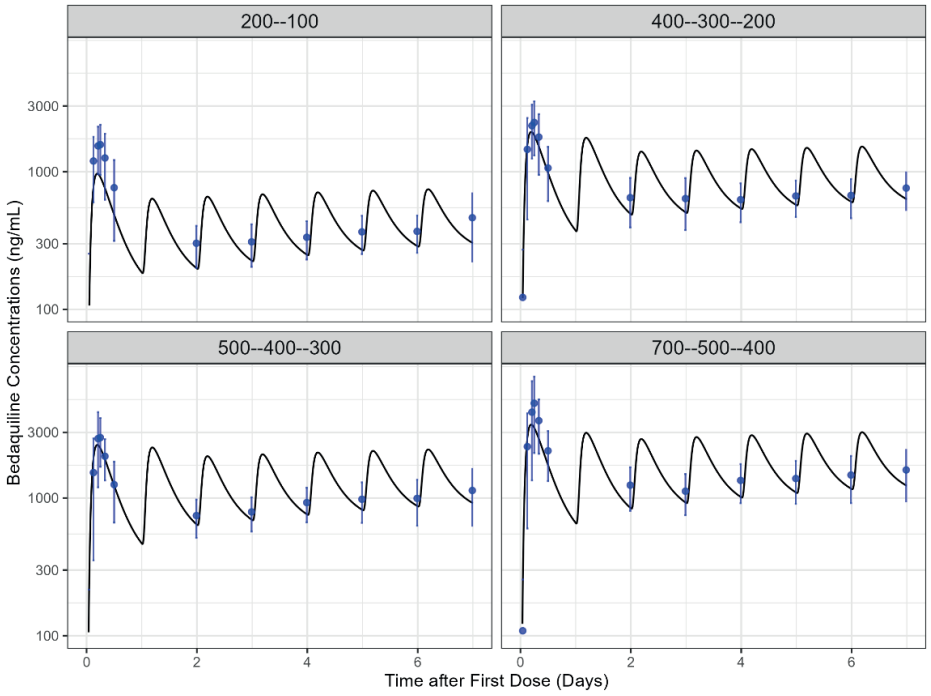

Local sensitivity analysis elucidates the influence of uncertainty in parameters on drug exposures.

The overall impact of reported uncertainties in key physicochemical parameters, lipophilicity, and plasma protein binding, on vascular plasma and CNS drug exposure ($AUC_{0\text{-}t}$) was evaluated by using local sensitivity analysis**.** A two-fold decrease in bedaquiline lipophilicity (i.e., 5.12 to 2.5) was predicted to decrease brain intracellular unbound $AUC_{0\text{-}t}$ by 65.2% and vascular plasma $AUC_{0\text{-}t}$ by 24%. A two-fold increase in albumin CSF-to-plasma ratio (i.e., 0.008 to 0.016) was predicted to increase brain intracellular total and unbound $AUC_{0\text{-}t}$ by 0.4%. A 1000-fold increase (i.e., 0.0003 to 0.3) in bedaquiline fraction unbound was predicted to decrease brain intracellular unbound $AUC_{0\text{-}t}$ by 55.2% and vascular plasma $AUC_{0\text{-}t}$ by 40.6%.

Figure 6.3. Bedaquiline and M2 observed vs. predictions for plasma and spinal CSF compartments at steady-state after 9 weeks of treatment. The model reasonably predicted the observed data. Bedaquiline dosing was 400 mg once daily (QD) for 14 days followed by 200 mg three times a week up to 9 weeks. Steady-state concentrations were measured either 3, 5, or 7 hours after the last 200 mg dose. Blue points represent the observed mean and standard deviation. Black points represent typical patients' predicted value.

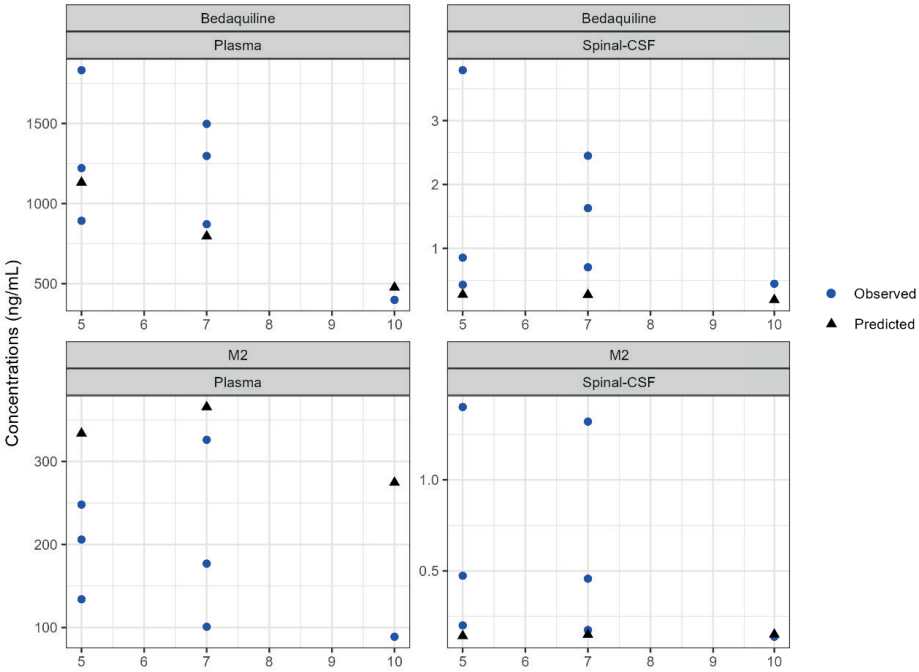

PBPK simulations predicted significantly lower bedaquiline brain concentrations in the intracellular compartment compared to peripheral blood.

Unbound bedaquiline and M2 concentrations in lung interstitial and intracellular, brain interstitial, and CSF were predicted to be comparable to unbound plasma concentrations. However, unbound bedaquiline and M2 concentrations in brain intracellular were predicted to be significantly lower than unbound plasma and unbound lung intracellular concentrations (ratio ~ 0.07 compared to unbound concentrations in plasma) **(Figure 6.4, Table 6.3)**. Additionally, our simulations suggested that 200 mg QD for 8 weeks followed by 100 mg QD would achieve relatively increased plasma concentrations for a longer duration of time when compared to 400 mg QD for 14 days followed by 200 mg three times a week **(Figure 6.4).**

Table 6.3. Predicted tissue to plasma concentrations ratio for bedaquiline and M2.

Parameter (C_{avg} ratio)	Bedaquiline	M2
Peripheral vascular blood cells / plasma	0.54	19.5
Brain Interstitial / plasma	0.36	0.38
Brain Intracellular / plasma	0.27	4.93
Brain Interstitial Unbound / plasma unbound	0.97	0.99
Brain Intracellular Unbound / plasma unbound	0.07	0.03
Spinal-CSF / plasma unbound	0.97	1.08
Lung Interstitial / plasma	0.38	0.37
Lung Intracellular / plasma	0.49	22.2
Lung Interstitial Unbound / plasma unbound	1.02	1.00
Lung Intracellular Unbound / plasma unbound	0.85	1.00

Figure 6.4. Typical patient simulations of Bedaquiline and M2 concentrations within various CNS compartments following the current and alternative Bedaquiline dosing regimens. The simulations suggested limited availability of unbound bedaquiline and M2 in brain interstitial and intracellular compartments. The model suggested relatively higher concentrations for longer duration for all compartments following the alternative dosing regimen, 200 mg QD for 8 weeks then 100 mg QD, than the current dosing regimen, 400 mg QD for 14 days followed by 200 mg three times a week.

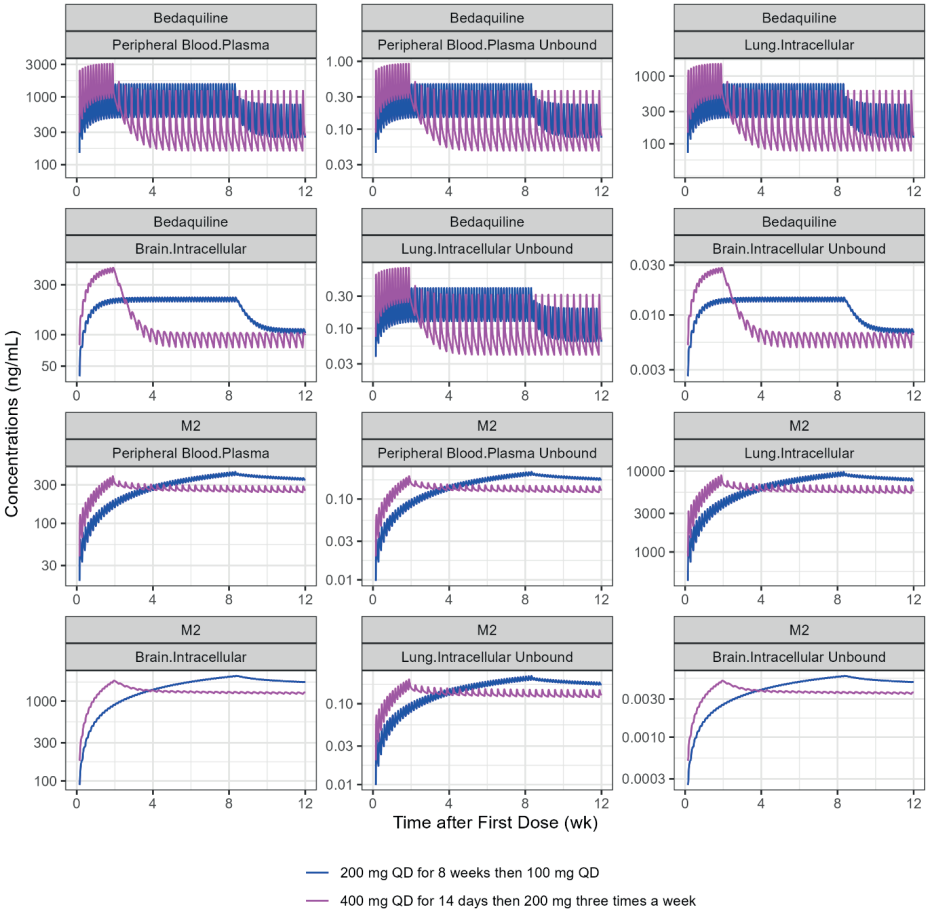

Discussion

We developed a whole-body PBPK model for bedaquiline and M2, coupled with CSF and brain compartments using clinical data. We then used the model to predict bedaquiline and M2 exposures in CNS compartments, including the brain intracellular compartment.

Our PBPK model enabled predictions of bedaquiline and M2 drug concentration-time profiles at target sites-of-action, brain interstitial and intracellular, for TBM

patients. The model predicted a total bedaquiline tissue-to-plasma concentrations ratio of 27% for brain intracellular. This predicted brain intracellular to plasma ratio is relatively comparable to the findings from preclinical studies that reported brain parenchyma to plasma concentrations ratios ranging from 2-20% following oral bedaquiline dosing suggesting the reliability of our model[12,13]. However, only unbound drug at site-of-action is assumed to be available to exert an anti-bacterial effect. The model-predicted unbound concentrations within brain intracellular compartment were drastically lower as compared to unbound concentrations in plasma and lungs (ratio ~ 0.07 compared to unbound concentrations in plasma) **(Figure 6.4)**. We predicted that sub-optimal drug concentrations would be available in brain intracellular to exert effect following bedaquiline at clinically relevant dosing in TBM patients. These predictions may support the experimental findings of inferior efficacy of BPaL combination with that of standard first-line anti-TB therapy in the TBM mouse model following dosing equivalent to human efficacious dosing for each drug[14]. Prospective studies comparing the efficacy of various combination regimens with and without bedaquiline in drug-resistant TBM models are suggested. Our model predicted no delay or non-linearity between plasma, brain, and lung tissues (S6.2). This suggests that plasma drug concentrations may be considered as surrogate for tissue concentrations considering relative ratio.

Sensitivity analysis allowed estimation of the impact of known uncertainty in protein binding and lipophilicity parameters on predictions of vascular plasma and CNS concentrations. However, it should be noted that our model was calibrated using observed vascular plasma concentrations and described observed CSF concentrations well. Thus, the estimated parameters of our model would be correlated with protein binding and lipophilicity parameters used in the model development. Therefore, it is unlikely that protein binding and lipophilicity parameters different than those used in our model development would lead to very different predictions of plasma or target site exposures.

We focused on typical TB patient simulations and did not simulate with inter-individual variability (IIV), because direct application of the IIV estimates from PopPK models to the PBPK model often does not appropriately characterize observed variability in plasma PK profiles. Previously, high IIV (>80%) in absorption-related parameters and moderate IIV (~50%) in distribution and clearance-related parameters have been estimated for bedaquiline using empirical population PK models[24,25]. These IIV estimates translate into moderate IIV in steady-state exposure ($AUC_{ss\text{-}weekly}$ interquartile range ~ 90 – 250 ug·hr/mL). Thus, the impact of observed IIV on overall

conclusions would be negligible given the fold difference between predicted total and unbound drug concentrations at the site of action for TBM patients.

Our model described plasma bedaquiline and M2 drug concentration data well for various dosing scenarios. Our typical patient CSF concentration predictions were slightly lower than the observed mean concentrations for both bedaquiline and M2 but were within the observed standard deviation range. Some uncertainty exists in observed CSF concentrations due to the small sample size (n=7, one sample for each patient) and bioanalytical challenges due to the high protein binding nature of bedaquiline. The impact of the slight underpredictions of mean CSF concentrations on overall predictions of unbound drug concentrations within the brain intracellular compartment seems negligible given the fold difference between unbound brain intracellular and CSF drug concentrations.

We did not evaluate the impact of TBM disease on bedaquiline and M2 concentrations in CNS. In our model, parameters relevant to drug penetration in CNS were calculated based on physicochemical and physiological parameters, including albumin plasma-to-CSF ratio, obtained from healthy subjects [35]. Our typical patient CSF concentration predictions were compared against the observed CSF concentrations data from pulmonary TB patients[11]. Our sensitivity analysis suggested a small impact of albumin plasma-to-CSF ratio on brain concentrations of bedaquiline. However, higher CSF protein levels are associated with increased the partition coefficient for rifampin[41]. Future studies should evaluate the impact of TBM disease on bedaquiline PK.

PBPK models including the transporters involved in BBB and BCSFB have been reported in the literature. These models included active transport processes. Key apical efflux transporters involved in blood-brain-barrier or blood-CSF-barrier are P-gp, BCRP, and MRPs[31]. Bedaquiline is not known to be a substrate of any of these transporters[23]; therefore, we did not explicitly include brain transporters in this work.

In conclusion, we present a whole-body PBPK model for bedaquiline and its active metabolite coupled with an expanded CNS distribution model, including CSF and brain sub-compartments. The model appropriately described observed plasma and CSF bedaquiline and M2 concentrations from TB patients. However, unbound concentrations in brain intracellular were predicted to be much lower than the predicted unbound concentrations in plasma and lungs. These results can be useful in designing experiments comparing the efficacy of various combination regimens with and without bedaquiline in drug-resistant TBM models.

References

1. Seddon JA, Wilkinson R, van Crevel R, et al. Knowledge gaps and research priorities in tuberculous meningitis. Wellcome Open Research. 2019;4:1-18. doi:10.12688/wellcomeopenres.15573.1
2. Navarro-Flores A, Fernandez-Chinguel JE, Pacheco-Barrios N, Soriano-Moreno DR, Pacheco-Barrios K. Global morbidity and mortality of central nervous system tuberculosis: a systematic review and meta-analysis. J Neurol. 2022;269(7):3482-3494. doi:10.1007/s00415-022-11052-8
3. Nahid P, Dorman SE, Alipanah N, et al. Executive Summary: Official American Thoracic Society/Centers for Disease Control and Prevention/Infectious Diseases Society of America Clinical Practice Guidelines: Treatment of Drug-Susceptible Tuberculosis. Clinical Infectious Diseases. 2016;63(7):853-867. doi:10.1093/cid/ciw566
4. Ramachandran R and Muniyandi M. Towards Improved Treatment Outcomes for Tuberculosis Meningitis - Rethinking the Regimen. Open access journal of neurology and neurosurgery. 2018; Volume 8, issue 2. dou: 10.19080/OAJNN.2018.08.555734.
5. Heemskerk AD, Nguyen MTH, Dang HTM, Vinh Nguyen CV, Nguyen LH, Do TDA, Nguyen TTT, Wolbers M, Day J, Le TTP, Nguyen BD, Caws M, Thwaites GE. Clinical Outcomes of Patients With Drug-Resistant Tuberculous Meningitis Treated With an Intensified Antituberculosis Regimen. Clin Infect Dis. 2017 Jul 1;65(1):20-28. doi: 10.1093/cid/cix230.
6. Evans EE, Avaliani T, Gujabidze M, et al. Long term outcomes of patients with tuberculous meningitis: The impact of drug resistance. PLoS One. 2022;17(6):e0270201. doi:10.1371/journal.pone.0270201
7. Khoshnood S, Goudarzi M, Taki E, et al. Bedaquiline: Current status and future perspectives. Journal of Global Antimicrobial Resistance. 2021;25:48-59. doi:10.1016/j.jgar.2021.02.017
8. Andries K, Verhasselt P, Guillemont J, et al. A diarylquinoline drug active on the ATP synthase of Mycobacterium tuberculosis. Science. 2005;307(5707):223-227. doi:10.1126/science.1106753
9. World Health Organization. Consolidated Operational Guidelines on Handbook Tuberculosis.; 2020.
10. Akkerman OW, Odish OFF, Bolhuis MS, et al. Pharmacokinetics of Bedaquiline in Cerebrospinal Fluid and Serum in Multidrug-Resistant Tuberculous Meningitis. Clinical Infectious Diseases. 2015;62(4):523-524. doi:10.1093/cid/civ921
11. Upton CM, Steele CI, Maartens G, Diacon AH, Wiesner L, Dooley KE. Pharmacokinetics of bedaquiline in cerebrospinal fluid (CSF) in patients with pulmonary tuberculosis (TB). J Antimicrob Chemother. 2022;77(6):1720-1724. doi:10.1093/jac/dkac067
12. Ordonez AA, Carroll LS, Abhishek S, et al. Radiosynthesis and PET Bioimaging of 76Br-Bedaquiline in a Murine Model of Tuberculosis. ACS Infectious Diseases. 2019;5(12):1996-2002. doi:10.1021/acsinfecdis.9b00207
13. Pamreddy A, Baijnath S, Naicker T, et al. Bedaquiline has potential for targeting tuberculosis reservoirs in the central nervous system. RSC Adv. 2018;8(22):11902-11907. doi:10.1039/c8ra00984h
14. Mota F, Ruiz-Bedoya CA, Tucker EW, et al. Dynamic 18F-Pretomanid PET imaging in animal models of TB meningitis and human studies. Nature Communications. 2022;13(1):7974. doi:10.1038/s41467-022-35730-3
15. Tasneen R, Betoudji F, Tyagi S, et al. Contribution of Oxazolidinones to the Efficacy of Novel Regimens Containing Bedaquiline and Pretomanid in a Mouse Model of Tuberculosis. Antimicrob Agents Chemother. 2016;60(1):270-277. doi:10.1128/AAC.01691-15
16. Food and Drug Administration (FDA). FDA Briefing Document Pretomanid Tablet, 200 mg Meeting of the Antimicrobial Drugs Advisory Committee (AMDAC). Published online 2019:https://www.fda.gov/media/127592/download.
17. Smith AGC, Gujabidze M, Avaliani T, et al. Clinical outcomes among patients with tuberculous meningitis receiving intensified treatment regimens. Int J Tuberc Lung Dis. 2021;25(8):632-639. doi:10.5588/ijtld.21.0159

18. Diacon AH, Dawson R, Von Groote-Bidlingmaier F, et al. Bactericidal activity of pyrazinamide and clofazimine alone and in combinations with pretomanid and bedaquiline. American Journal of Respiratory and Critical Care Medicine. 2015;191(8):943-953. doi:10.1164/rccm.201410-1801OC

19. Kuepfer L, Niederalt C, Wendl T, et al. Applied Concepts in PBPK Modeling: How to Build a PBPK/PD Model. CPT: Pharmacometrics and Systems Pharmacology. 2016;5(10):516-531. doi:10.1002/psp4.12134

20. Willmann S, Höhn K, Edginton A, et al. Development of a Physiology-Based Whole-Body Population Model for Assessing the Influence of Individual Variability on the Pharmacokinetics of Drugs. Journal of Pharmacokinetics and Pharmacodynamics. 2007;34(3):401-431. doi:10.1007/s10928-007-9053-5

21. Willmann S, Schmitt W, Keldenich J, Dressman JB. A Physiologic Model for Simulating Gastrointestinal Flow and Drug Absorption in Rats. Pharmaceutical Research. 2003;20(11):1766-1771. doi:10.1023/B:PHAM.0000003373.72652.c0

22. Gaohua L, Wedagedera J, Small BG, et al. Development of a Multicompartment Permeability-Limited Lung PBPK Model and Its Application in Predicting Pulmonary Pharmacokinetics of Antituberculosis Drugs. CPT: Pharmacometrics and Systems Pharmacology. 2015;4(10):605-613. doi:10.1002/psp4.12034

23. van Heeswijk RPG, Dannemann B, Hoetelmans RMW. Bedaquiline: A review of human pharmacokinetics and drug-drug interactions. Journal of Antimicrobial Chemotherapy. 2014;69(9):2310-2318. doi:10.1093/jac/dku171

24. Svensson EM, Dosne AG, Karlsson MO. Population Pharmacokinetics of Bedaquiline and Metabolite M2 in Patients with Drug-Resistant Tuberculosis: The Effect of Time-Varying Weight and Albumin. CPT: Pharmacometrics and Systems Pharmacology. 2016;5(12):682-691. doi:10.1002/psp4.12147

25. McLeay SC, Vis P, Van Heeswijk RPG, Green B. Population pharmacokinetics of bedaquiline (TMC207), a novel antituberculosis drug. Antimicrobial Agents and Chemotherapy. 2014;58(9):5315-5324. doi:10.1128/AAC.01418-13

26. Mehta K, Guo T, van der Graaf PH, van Hasselt JGC. Predictions of Bedaquiline and Pretomanid Target Attainment in Lung Lesions of Tuberculosis Patients using Translational Minimal Physiologically Based Pharmacokinetic Modeling. Clin Pharmacokinet. 2023;62(3):519-532. doi:10.1007/s40262-023-01217-7

27. Schmitt W. General approach for the calculation of tissue to plasma partition coefficients. Toxicol In Vitro. 2008;22(2):457-467. doi:10.1016/j.tiv.2007.09.010

28. Cordes H, Rapp H. Gene expression databases for physiologically based pharmacokinetic modeling of humans and animal species. CPT: Pharmacometrics & Systems Pharmacology. 2023;12(3):311-319. doi:10.1002/psp4.12904

29. Liu K, Li F, Lu J, et al. Bedaquiline metabolism: enzymes and novel metabolites. Drug Metab Dispos. 2014;42(5):863-866. doi:10.1124/dmd.113.056119

30. Yamamoto Y, Välitalo PA, van den Berg DJ, et al. A Generic Multi-Compartmental CNS Distribution Model Structure for 9 Drugs Allows Prediction of Human Brain Target Site Concentrations. Pharm Res. 2017;34(2):333-351. doi:10.1007/s11095-016-2065-3

31. Gaohua L, Neuhoff S, Johnson TN, Rostami-Hodjegan A, Jamei M. Development of a permeability-limited model of the human brain and cerebrospinal fluid (CSF) to integrate known physiological and biological knowledge: Estimating time varying CSF drug concentrations and their variability using in vitro data. Drug Metabolism and Pharmacokinetics. 2016;31(3):224-233. doi:10.1016/j.dmpk.2016.03.005

32. Saleh MAA, Loo CF, Elassaiss-Schaap J, De Lange ECM. Lumbar cerebrospinal fluid-to-brain extracellular fluid surrogacy is context-specific: insights from LeiCNS-PK3.0 simulations. J Pharmacokinet Pharmacodyn. 2021;48(5):725-741. doi:10.1007/s10928-021-09768-7

33. Verscheijden LFM, Koenderink JB, de Wildt SN, Russel FGM. Development of a physiologically-based pharmacokinetic pediatric brain model for prediction of cerebrospinal fluid drug concentrations and the influence of meningitis. PLOS Computational Biology. 2019;15(6):e1007117. doi:10.1371/journal.pcbi.1007117

34. Utsey K, Gastonguay MS, Russell S, Freling R, Riggs MM, Elmokadem A. Quantification of the impact of partition coefficient prediction methods on physiologically based pharmacokinetic model output using a standardized tissue composition. Drug Metabolism and Disposition. 2020;48(10):903-916. doi:10.1124/DMD.120.090498

35. Koch S, Donarski N, Goetze K, et al. Characterization of four lipoprotein classes in human cerebrospinal fluid. J Lipid Res. 2001;42(7):1143-1151.

36. Conradie F, Bagdasaryan TR, Borisov S, et al. Bedaquiline–Pretomanid–Linezolid Regimens for Drug-Resistant Tuberculosis. New England Journal of Medicine. 2022;387(9):810-823. doi:10.1056/nejmoa2119430

37. Lippert J, Burghaus R, Edginton A, et al. Open Systems Pharmacology Community—An Open Access, Open Source, Open Science Approach to Modeling and Simulation in Pharmaceutical Sciences. CPT: Pharmacometrics and Systems Pharmacology. 2019;8(12):878-882. doi:10.1002/psp4.12473

38. Lounis N, Vranckx L, Gevers T, Kaniga K, Andries K. In vitro culture conditions affecting minimal inhibitory concentration of bedaquiline against M. tuberculosis. Med Mal Infect. 2016;46(4):220-225. doi:10.1016/j.medmal.2016.04.007

39. Perrineau S, Lachâtre M, Lê MP, Rioux C, Loubet P, Fréchet-Jachym M, Gonzales MC, Grall N, Bouvet E, Veziris N, Yazdanpanah Y, Peytavin G. Long-term plasma pharmacokinetics of bedaquiline for multidrug- and extensively drug-resistant tuberculosis. Int J Tuberc Lung Dis. 2019 Jan 1;23(1):99-104. doi: 10.5588/ijtld.18.0042.

40. Ngwalero P, Brust JCM, van Beek SW, Wasserman S, Maartens G, Meintjes G, Joubert A, Norman J, Castel S, Gandhi NR, Denti P, McIlleron H, Svensson EM, Wiesner L. Relationship between Plasma and Intracellular Concentrations of Bedaquiline and Its M2 Metabolite in South African Patients with Rifampin-Resistant Tuberculosis. Antimicrob Agents Chemother. 2021 Oct 18;65(11):e0239920. doi: 10.1128/AAC.02399-20.

41. Svensson EM, Dian S, Te Brake L, Ganiem AR, Yunivita V, van Laarhoven A, Van Crevel R, Ruslami R, Aarnoutse RE. Model-Based Meta-analysis of Rifampicin Exposure and Mortality in Indonesian Tuberculous Meningitis Trials. Clin Infect Dis. 2020 Nov 5;71(8):1817-1823. doi: 10.1093/cid/ciz1071.

42. Van Essen DC, Donahue CJ, Glasser MF. Development and Evolution of Cerebral and Cerebellar Cortex. Brain Behav Evol. 2018;91(3):158-169. doi: 10.1159/000489943.

43. Ruslami R, Ganiem AR, Dian S, Apriani L, Achmad TH, van der Ven AJ, Borm G, Aarnoutse RE, van Crevel R. Intensified regimen containing rifampicin and moxifloxacin for tuberculous meningitis: an open-label, randomised controlled phase 2 trial. Lancet Infect Dis. 2013 Jan;13(1):27-35. doi: 10.1016/S1473-3099(12)70264-5.

44. Maranchick NF, Alshaer MH, Smith AGC, Avaliani T, Gujabidze M, Bakuradze T, Sabanadze S, Avaliani Z, Kipiani M, Peloquin CA, Kempker RR. Cerebrospinal fluid concentrations of fluoroquinolones and carbapenems in tuberculosis meningitis. Front Pharmacol. 2022 Dec 12;13:1048653. doi: 10.3389/fphar.2022.1048653.

Supplementary Materials

S6.1. Summary of the Time Course Data Used for the Analysis.

Details	Source
Model Development	
Bedaquiline and M2 concentrations from blood serum of pulmonary TB patients after bedaquiline dosing of 400 mg on Day1, 300 mg on Day2, and 200 mg QD Day 3-14	Clinical Trial: NCT 01691534
Model Validation	
Bedaquiline concentrations from blood serum of pulmonary TB patients after bedaquiline dosing of 200 mg on Day1, 100 mg QD Day 2-14	Clinical Trial: NCT01215110
Bedaquiline concentrations from blood serum of pulmonary TB patients after bedaquiline dosing of 400 mg on Day1, 300 mg on Day2, and 200 mg QD Day 3-14	
Bedaquiline concentrations from blood serum of pulmonary TB patients after bedaquiline dosing of 500 mg on Day1, 400 mg on Day2, and 300 mg QD Day 3-14	
Bedaquiline concentrations from blood serum of pulmonary TB patients after bedaquiline dosing of 700 mg on Day1, 500 mg on Day2, and 400 mg QD Day 3-14	
Steady-state concentrations of bedaquiline and M2 from blood serum and CSF of pulmonary TB patients following bedaquiline dosing of 400 mg QD for 14 days followed by 200 mg three times a week	Clinical Trial: NCT02583048

S6.2. Typical Patient Simulations of Bedaquiline and M2 Concentrations within Various Compartments Following the Current Bedaquiline Dosing Regimens. The simulations suggested limited availability of unbound bedaquiline and M2 in brain intracellular compartment. Dosing regimen, 400 mg QD for 14 days followed by 200 mg three times a week was simulated.

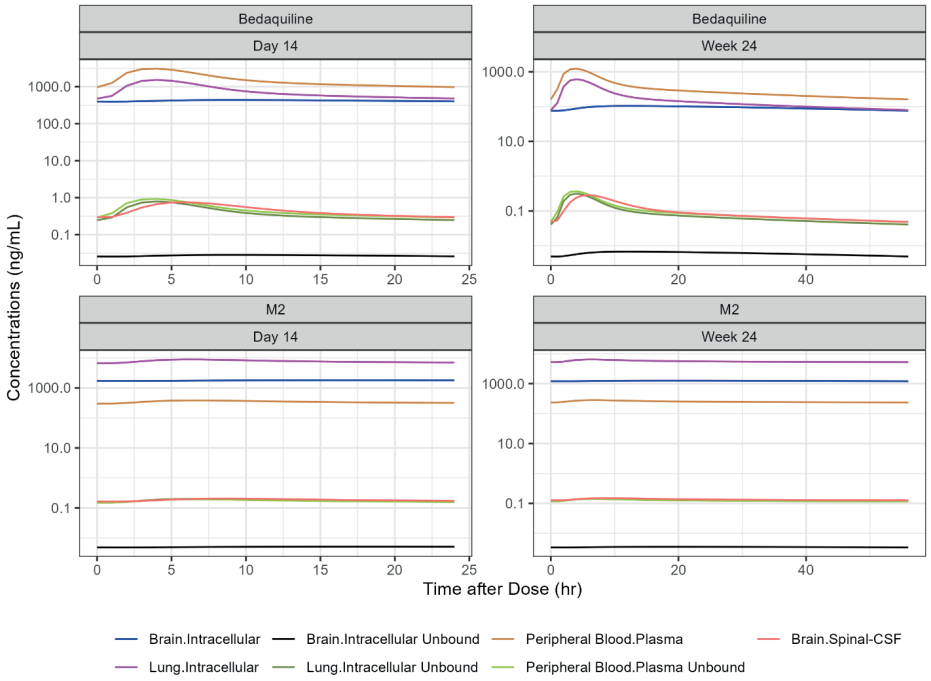

S6.3. Final model files are available to download from https://github.com/krinaj/BDQ_PBPK.

Section IV.

Host-directed therapies against tuberculosis

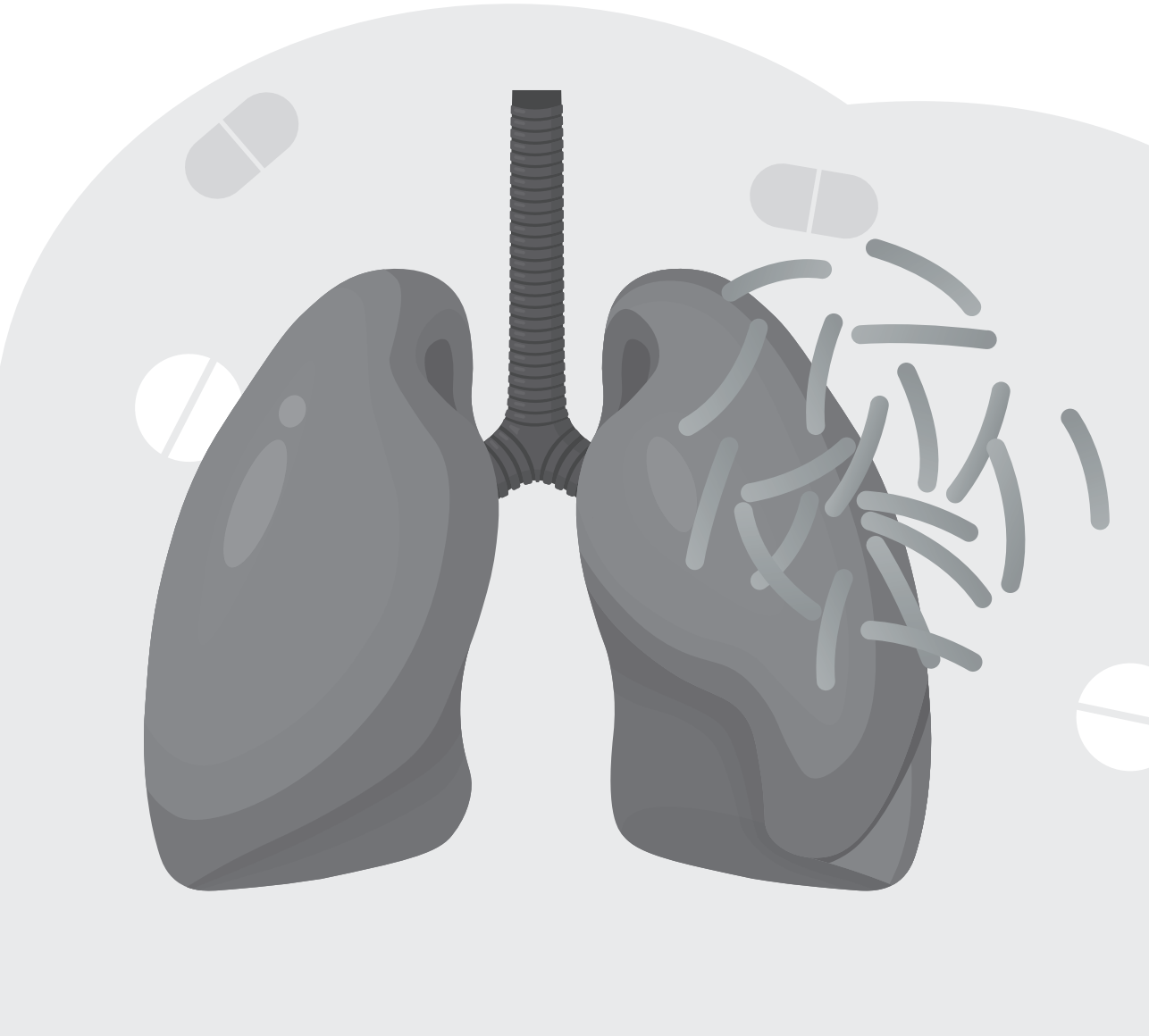

Chapter 7

Host-directed therapies for tuberculosis: quantitative systems pharmacology approaches

Krina Mehta, Herman P. Spaink, Tom H.M. Ottenhoff, Piet H. van der Graaf, J.G. Coen van Hasselt

Trends Pharmacol Sci, 2022 April, volume 43, issue 4, p293-304

Abstract

Host-directed therapies (HDT) that modulate host-pathogen interactions offer an innovative strategy to combat *Mycobacterium tuberculosis (Mtb) infections.* When combined with tuberculosis antibiotics, HDTs could contribute to improving treatment outcomes, reducing treatment duration, and preventing resistance development. Translation of the interplay of host-pathogen interactions leveraged by HDTs towards therapeutic outcomes in patients is challenging. Quantitative understanding of the multi-faceted nature of the host-pathogen interactions is vital to rationally design HDT strategies. Here, we (1) provide an overview of key Mtb host-pathogen interactions as basis for HDT strategies, and (2) discuss the components and utility of quantitative systems pharmacology (QSP) models to inform HDT strategies. QSP models can be used to identify and optimize treatment targets, to facilitate preclinical to human translation, and to design combination treatment strategies.

Glossary

Autophagy: Autophagy is an intracellular process involving the formation of a phagophore, elongation of the phagophore, autophagosome maturation, and fusion with lysosomes for degradation of the selected cellular material.

AMPK-mTOR pathway: The AMP-activated protein kinase (AMPK) and mammalian target of rapamycin (mTOR) pathway involves complex interplay between various proteins and play a key role in autophagy regulation.

HMG-CoA reductase pathway: HMG-CoA (3-hydroxy-3-methyl-glutaryl-CoA) reductase pathway is involved mainly in regulation of cholesterol synthesis but also known to be involved in regulation of autophagy[1].

Phagocytosis: Phagocytosis is a cellular process involving engulfment of large particles, including bacteria, into the cells.

PK: Pharmacokinetics (PK) describes the concentration-time profile of drugs and is determined by absorption, distribution, metabolism. and elimination processes.

PD: Pharmacodynamics (PD) describes the concentration-effect-time profile of drugs and is determined by drug pharmacology and physiology of the organism[2].

Host-directed therapies: leveraging the host immune system for treatment of tuberculosis

Mycobacterium tuberculosis (Mtb) infections are associated with approximately 1.5-2 million deaths annually worldwide. Two key challenges to successful tuberculosis (TB) treatment are long duration of treatment and emergence of drug resistant strains[3]. In the last decade, host-directed therapy (HDT) strategies have received increasing attention[4–6] to enhance treatment outcomes, shorten treatment durations, and avoid resistance development. HDTs target interactions between the host immune response and the Mtb pathogen, which reduces the likelihood for Mtb to acquire resistance against HDTs. In addition, additive effects of adjunctive HDT treatment with conventional antibiotics on bacterial elimination could help to shorten treatment duration and therefore may avoid development of resistance to conventional antibiotics[7].

The host immune response to Mtb infection is reliant on the cumulative activities of various defense mechanisms such as macrophage activation, phagocytosis (see Glossary), autophagy (see Glossary), antigen presentation, and cytokine and T-lymphocytes production. Genotypic and phenotypic changes in Mtb during infection leading to modulation of the host response allows its survival and virulence in the host[8]. Mechanistic understanding of the multiscale nature of host-pathogen interactions is essential to identify HDT targets, to design and develop new HDT drugs, and to repurpose already marketed drugs as HDT strategy.

A major challenge in the discovery and development of HDTs for TB is the prediction of treatment responses associated with specific pharmacological modulation of an immune response-associated target due to complex systems-level host-drug-pathogen interactions[4]. The translation of systems-level responses to HDT strategies from preclinical models to patients is challenged by inter-species differences in immune responses to Mtb pathogen. Quantitative systems pharmacology (QSP) modelling can serve as a valuable tool to identify relevant HDT targets, and to inform subsequent design of combination drug treatment strategies and dosing schedules[9–11]. The utility of quantitative modelling to improve treatment strategies for TB have been demonstrated for antibiotic therapies[11,12]. However, these approaches have not yet been developed to design HDTs.

Here, we review high-potential host-pathogen interactions of relevance for HDTs. We then outline how QSP modelling approaches can be used to predict optimal HDT strategies with a focus on required model components and the integration

with available data for application in target selection, inter-species translation, and treatment optimization.

Host-pathogen interactions as basis for host-directed therapy strategies

Several host-pathogen interactions of Mtb involved in its pathogenesis and immune system evasion offer potential targets for design of HDTs[6] **(Figure 7.1)** and are of relevance to capture in QSP modelling approaches.

Induction of autophagy

Autophagy plays an essential role in controlling Mtb infections and has been studied extensively as potential HDT strategy for Mtb[6]. Multiple intertwined pathways affecting glucose and cholesterol metabolism, such as AMPK-mTOR (see glossary) and HMG-CoA reductase pathway (see glossary), are involved in regulation of autophagy **(Figure 7.1)**. AMPK plays a key role in these pathways and therefore in regulation of autophagy. As an evasion mechanism, Mtb inhibits phosphorylation of AMPK protein and inhibits autophagy[13]. Apart from AMPK-mediated autophagy regulation, intracellular cholesterol is also involved in Mtb survival leading to inhibition of autophagosome maturation and autophagosome-lysosome fusion[1]. Thus, autophagy induction through inhibition of mTOR complex 1 (mTORC1) or by inhibition of HMG-CoA reductase represent a potential HDT strategy.

Figure 7.1 The Host-Pathogen interactions as basis for host-directed therapy strategies for the treatment of Mtb infections. Initiation of the host innate immune response occurs shortly after inhalation of aerosols containing Mtb bacteria and Mtb implantation in macrophages. Both resident and activated macrophages stimulate the release of pro-inflammatory cytokines, such as TNF-α and IL-1β, following phagocytosis and autophagy. Antigen presenting cells (macrophages and dendritic cells) that drain into local lymph nodes activate CD4+ and CD8+ T-cell mediated adaptive immune responses. Antigen presenting cells also stimulate the release of IL-12, which helps recruit additional CD4+ T-cells. CD4+ T-cells secrete IFN-γ that stimulate macrophage activation, IL-2, TNF-α, and IL-10 that help balance the pro-inflammatory response by deactivation of macrophages. CD8+ cells have cytotoxic activities. CD4+ T-cell secreted IL-2 drives further proliferation of CD4+ as well as CD8+ T-cells. Autophagic pathways start with parting of a section from endoplasmic reticulum, the phagophore, followed by the elongation of phagophore with engulfment of Mtb, autophagosome formation and maturation, and fusion of the autophagosome with lysosomes. Mtb activates mTORC1 and thus inhibits autophagy, while mTORC1 activates aerobic glycolysis. Intracellular cholesterol inhibits LC3, Ca2+, and LAMP3, and thus inhibits autophagy mediated Mtb killing. Mtb activates HDAC pathway and thus downregulates various genes responsible for innate and adaptive immune response. Potential host-directed therapy strategies are presented in the green text. Figure created with biorender.com.

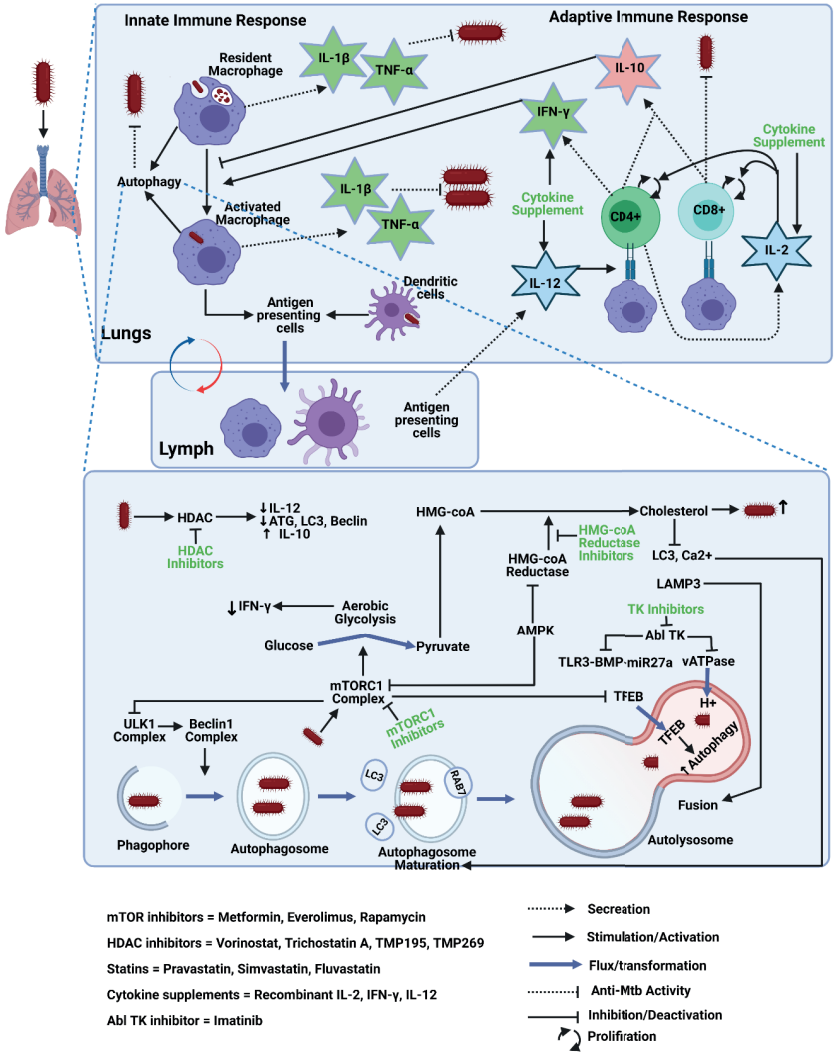

mTORC1 inhibitors

Metformin is the most evaluated mTORC1 inhibitor as potential HDT treatment for Mtb infections. Metformin inhibited the growth of intracellular Mtb in vitro and in mice[13,14]. Multiple reports suggest that metformin adjunctive therapy in diabetic TB patients improved therapy success rate and lowered mortality rate[15,16]. Adjunctive everolimus, an mTOR inhibitor, treatment with rifabutin-substituted standard TB therapy improved lung functions as measured by forced expiratory volume when compared to a control group in a randomized clinical trial[17]. A recent study identified protein kinase inhibitor ibrutinib as a potential mTORC1-mediated autophagy inducer in a mice study[18]. These results provide initial proof-of-concept and justify further evaluations of mTORC1 inhibitors in clinical trials.

HMG-CoA inhibitors

The HMG-CoA reductase pathway has been associated with intracellular cholesterol reduction and autophagy induction. Therapy with HMG-CoA inhibitors, such as simvastatin, pravastatin, and fluvastatin, as adjunctive therapy to conventional anti-TB drugs improved bacterial clearance by the host and improved the efficacy of first-line TB drugs by promoting autophagy in macrophage cell cultures and in mice[19,20]. Several retrospective clinical studies have identified that chronic use of statins reduced the risk of developing TB[21]. On the other hand, a population-based cohort analysis of data from newly diagnosed TB patients recognized no statistically significant difference in hazard ratio between patients who were using statins in addition to standard TB treatment as compared to patients who did not use statins[22]. As chronic use of statins leads to reduced risk of TB, it may be hypothesized that factors such as drug penetration in lungs and drug affinity may play a key role in determining its effectiveness as HDT. Overall, these results highlight the potential of targeting the HMG-CoA reductase pathway as autophagy induction strategy.

Regulation of host epigenetics

Infection with Mtb is associated with alterations of some gene functions important for ensuring immune response. Two key pathways known to be involved in Mtb-induced host epigenetic alterations are histone deacetylases1 (HDAC1) pathway and TLR3-BMP-miR27a pathway both of which can be pharmacologically exploited[23,24].

HDAC inhibitors

Infections with Mtb leads to upregulation of HDAC1, which leads to suppression of IL-12B gene expression leading to suppression of T-cell immunity **(Figure 7.1)**.

Additionally, HDAC1 is known to modulate autophagy associated genes[23]. HDAC inhibitors, such as Trichostatin A, TMP195, and TMP269, reduced bacterial growth in macrophage cell cultures. Vorinostat, an HDAC inhibitor, promoted immune response in macrophage cell cultures[25]. In zebrafish embryos infected with *Mycobacterium marinum* (Mm), HDAC inhibition significantly reduced microbial burden[23]. HDAC inhibition significantly inhibited Mtb growth and showed increased production of key cytokines in mice[26]. These results highlight the potential of exploiting HDAC inhibition as HDT strategy.

Abl Tyrosine Kinase Inhibitors

Protein Abl Tyrosine Kinase (ATK) is involved in entry and survival of Mtb within macrophages through TLR3-BMP-miR27a pathway. ATK also inhibits expression of vATPase pump-relevant genes, and thus inhibits acidification of autolysosomes **(Figure 7.1)**. Pharmacological inhibition of ATK using imatinib improved containment of Mtb within macrophages, induced autophagy, and decreased bacterial load in human macrophage cell cultures and in mice[6,24]. Imatinib also lead to decreased bacterial load in macrophage culture and in mice infected with rifampin-resistant Mm[27]. A clinical study assessing effects of imatinib alone and in combination with conventional anti-TB drugs in drug-resistant- and HIV co-infected- TB patients is ongoing[28]. These data suggest that imatinib may prove effective as HDT towards Mtb.

Modulation of cytokine response

The kinetics of the key cytokines, such as interferon gamma (IFN-γ), tumour necrosis alpha (TNF-α), IL-1β, IL-10, IL-4, IL-12, and IL-2, during Mtb infections have been well studied in humans and in mice. IFN-γ is one of the most important players to the host immune response and its main role is activation of macrophages **(Figure 7.1)**. Both activated and resident macrophage produce pro-inflammatory cytokines, TNF-α and IL-1β, that possess microbicidal properties against Mtb; however activated macrophage-mediated production is much more efficient[29]. Excessive production of pro-inflammatory cytokines, however, can lead to tissue damage in vivo[30]. Anti-inflammatory cytokines, IL-10 and IL-4, are also induced upon macrophage phagocytosis and balance pro-inflammatory cytokines by macrophage deactivation[30]. Excessive production of anti-inflammatory cytokines may result in limiting the immune-mediated microbicidal activities[31]. Thus, the fine balance between the pro- and anti-inflammatory cytokines may determine the overall outcome of the Mtb infection.

Adjunctive treatment with IFN-y have been evaluated in various clinical studies; however, different patient conditions, routes of administration, and dosing regimen resulted in varying outcomes[31]. Adjunctive treatment with aerosolized IFN-y showed benefits in reducing cavitary lesions and induced negative sputum conversion in TB patients in clinical studies[32]. Thus, modulation of cytokine response may be a useful HDT strategy.

Enhancing t-cell mediated host response

The innate immune reaction plays an important role in the initiation of adaptive immune response by antigen presentation and cytokines production. A few weeks after the initial infection, antigen-presenting cells (APCs) that drain into regional lymph nodes initiate adaptive T-lymphocytes-mediated immune response. Upon antigen presentation, the APCs via major histocompatibility molecules (MHC)-I and II prime CD8+ and CD4+ T-cells to initiate adaptive immune response. Both activated CD4+ and CD8+ T-cells secrete IFN-γ, IL-2, IL-17A, and IL-10. Mature dendritic cells secrete IL-12p70 which helps increasing recruitment of additional CD4+ T-cells. IL-2 play a role in further proliferation of T-cells. CD8+ cells have direct microbicidal capabilities through perforin, granzymes, and granulysin or induce apoptosis through Fas/Fas ligand interaction. Adjunctive cytokine supplementation with IL-12 and IL-2 have been evaluated in clinical studies but did not result in significant benefits. However, recombinant human IL-2 supplementation showed significant improvements in negative sputum culture conversion rates and in enhanced X-ray resolution in drug-resistant TB patients[33]. Therefore, the use of recombinant IL-2 supplementation as HDT strategy for TB should be further evaluated.

Design of host-directed therapies using quantitative systems pharmacology modelling

The overall outcome of Mtb disease and treatment is reliant on the integrated results of the molecular and cellular events, and their reflection at tissue, organ, and host level dynamics occurring at different time scales. As such, it can be challenging to predict patient responses to different HDT strategies. Species differences in immune response characteristics make it more challenging to translate the results from preclinical studies to clinical scenarios. Additionally, determination of the effects of treatments and disease progression in specific patient populations, can be challenging, i.e., in patients with weakened immune response or other conditions, patients with specific genotype known to affect certain pharmacology.

QSP modelling can address these hurdles through quantitative integration of host-pathogen interaction mechanisms with PK (see glossary) and PD (see glossary) aspects of HDTs, making it a relevant tool to guide drug discovery and development of HDTs. Development of QSP models for HDTs against TB is the requirement for large amount of mechanistic quantitative data to parametrize the model, which may concern biological system-specific data relating to immunodynamics and pathogen dynamics, as well as drug-specific model related to pharmacokinetics and drug-target interactions. Importantly, once defined, a QSP framework for specific HDT mechanisms is developed, it can be applied as platform model towards different investigational therapeutic agents. Selection of appropriate experimental approaches are important to provide quantitative understanding about components of drug-host-pathogen interactions. Here, we briefly discuss key experimental models that can be of relevance for characterization of HDTs using QSP modelling. Then, we discuss three main components of the QSP framework to evaluate HDTs for Mtb infection, (1) drug PK models, (2) host immune response models, and (3) pathogen dynamic models **(Figure 7.2)**. Lastly, we discuss applications of these models **(Figure 7.3)**.

Experimental approaches to facilitate parameterization of the qsp models

Human-derived macrophage and peripheral blood mononuclear cell cultures are extensively used to screen for the antibiotics but also identify compounds with HDT potential[14,34,35]. The in vitro hollow fiber infection model (HFIM) is commonly used to study the direct effects of antibiotics agents on Mtb, and readily allows to include co-cultures with macrophages. In HFIM, Mtb is cultured in a closed chemostat system with continuous flow of medium, while it allows simulation of concentration-time profiles of underlying PK/PD relationships of antibiotics and HDTs[36]. Several advanced cell culture systems, such as 3D cell cultures, organoids[37], and lung-on-chip[38], have been increasingly used to study host-pathogen interactions. Whilst these approaches are attractive for purposes of quantitative characterization of key mechanisms and phenotypic response profiles to be implemented in QSP models, these systems remain a simplified system that does not include all aspects related to the host immune response.

Adult zebrafish have gained increasing attention as it possess an innate immune system that is highly similar to that of mammals[39,40]. Zebrafish embryos are of interest due to their optical transparency and thus allowing the use of advanced imaging methods. Infection of zebrafish with various mycobacteria leads to

formation of granuloma structures that are highly similar to those observed in human TB patients; therefore, it has been a successful model to study the progression of TB and the effects of drug treatment[41]. Pharmacological screening of drugs to treat mycobacterial infection at a high throughput level is also possible[42]. Knockdown and overexpression experiments in zebrafish combined with translational QSP modelling would especially provide insights into contribution of certain component to overall immune response and anti-TB effects[43]. Rodents, i.e., mice, rabbits, and guinea-pigs, are commonly used as infection model for Mtb[39]. Even though these models incorporate a full immune system, differences between the human immune response remain and lead to translational challenges[11]. Non-human primates (NHP) have been widely used in immunology and vaccine research. NHP infected with Mtb are of interest in generating HDT-relevant data due to their similarities to humans in basic physiology, immunology, and disease pathology. However, the use of these models has been limited in TB treatment research due to the requirements of scientific and financial resources as well as safety issues due to highly infectious and contagious nature of Mtb[44].

Overall, data collected from a combination of various experimental models, such as in vitro, zebrafish, and mice, can be used to parameterize QSP models. QSP models can link the results from various experimental infection models, enabling predictions in humans.

Components of the qsp modelling framework

A QSP framework for HDTs should contain a combination of model components for PK of the drugs, host immune response, and pathogen dynamics, including their interactions **(Figure 7.2)**. Depending on the type of HDT drug studied, QSP models may be parameterized and adapted in specific ways, e.g., to capture the drug-specific parameters to induce specific immune system effects.

Pharmacokinetics

Consideration of drug concentrations-effect relationships, and therefore PK, is of essential value for design of HDT strategies. Physiologically based PK (PBPK) models describe the concentration profiles in specific tissues of interest and are informed by both drug- and system-specific parameters. PBPK models are of relevance to scale PK between preclinical species and humans in a mechanistic fashion. For TB, PBPK models describing lung exposure are of specific relevance. In the clinical phase, quantifying inter-patient variability in PK is important. Here, population PK models are of relevance, which capture inter-individual variation in underlying

parameters that can be explained by specific patient-specific covariates [45]. It is furthermore helpful that because many HDTs involve repurposed drugs, often PK models are available already to characterize their PK[46,47].

Figure 7.2 Components of the conceptual quantitative systems pharmacology framework to assess HDTs for treatment of Tuberculosis. A QSP framework for HDTs should contain a combination of model components for PK of the drugs, host immune response, and pathogen dynamics, including their interactions. Classical antibiotics and HDTs act by modulating pathogen dynamics and host immune response, respectively. Immune-mediated pathogen killing is dependent on interplay between the host immune response and pathogen evasion mechanisms, i.e., host-pathogen interactions. Key considerations for each model components are listed in green box. Types of studies and data that can be used to inform each model components are presented in purple box. Figure created with biorender.com

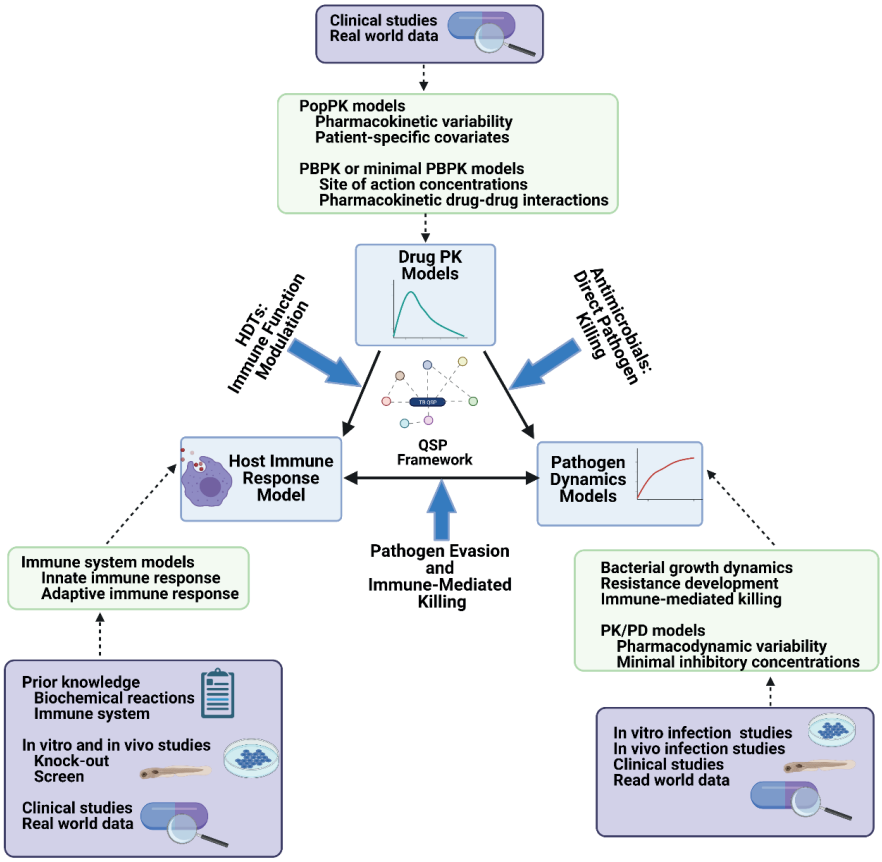

Immunodynamics

Models describing the key immune response components, such as dynamics of macrophage counts, cytokines, and CD4+ and CD8+ lymphocytes are essential for QSP models to study HDTs. Systems biology models describing the host-Mtb interactions within the lungs[48] have been previously developed, and later linked

with lymphatics[49] and blood circulations[50]. The states included in these models were resting-, activated-, and infected-macrophages, cytokines, such as IFN-γ, IL-10, and IL-12, dendritic cells, CD4+ lymphocytes, and intra- and extra-cellular Mtb. The key feature of this model was contributions of various immune components on intra- and extra-cellular Mtb. The above-developed model was later expanded to include CD8+ cells dynamics in lungs[51]. The parameters in these models were identified from published human derived or NHP experiments or model fitting to experimental data. These models can be expanded to include key drug targets involved in Mtb HDTs and their downstream effects on functional immune response changes and the quantitative interaction with Mtb.

There are currently no mathematical models available in literature describing HDT-relevant pathways, such as autophagy in Mtb infections; however, components and parameter estimates from single cell systems biology models[52] can be adapted and extended using experimental data. For example, a HDT model containing key biological features of autophagy[52] including HDAC1-related components **(Figure 7.1)** may be developed. The model parameters can be informed using prior data available in literature[52] and data from in vitro experiments[23]. The model may describe dynamics of the phagocytic cells and zebrafish infection with Mm load overtime in HDAC1 inhibitors exposed macrophage cell cultures as compared to controls to estimate the parameters relevant to HDAC1 effect. The simulations from the models may be compared with the experimental outcomes, preferably from different experimental conditions than the original experiments used for parameter estimation. This allows validation of the model structure and parameter estimates. In the above example, the simulations may be validated against data from zebrafish exposed to HDAC1 inhibitors (at various HDAC1 levels) experiments[23]. If multiple targets are affected by certain drugs, i.e., ATK inhibitors (Figure 1), all relevant mechanisms must be captured in such models.

Pathogen dynamics

Models for the dynamics of pathogens include the effect of antibiotic drug on the growth and elimination of Mtb and emergence of treatment resistance. In vitro and in vivo infection studies have enabled our understanding of parameters of Mtb growth rates, bactericidal and bacteriostatic effects of conventional anti-TB drugs[36], and resistance rates of bacteria[12]. The incorporation of immune cell effects on pathogen killing is a key required step to study the effects of HDTs on Mtb treatment. Published host-Mtb interaction models[49] can be updated to include contributions of key HDT components on pathogen killing, as well as pathogen evasion mechanisms. For example, an autophagy model may contain

quantitative relationship between bacterial load, mTOR, and autophagy. This will allow evaluations and predictions of various mTOR inhibitors on Mtb clearance by autophagy.

Applications of the qsp modelling framework

QSP modelling have successfully influenced various decision making at different stages starting from discovery to late-phase in various therapeutic areas[53] and offer potential for the challenges faced in translation and design of HDT strategies against Mtb **(Figure 7.3)**.

Figure 7.3 Applications of the conceptual quantitative systems pharmacology framework to assess host-directed therapies for treatment of Tuberculosis. QSP models can guide TB HDT drug discovery and development at various phases depending on the model attributes. For example, a model developed based on experimental in vitro and/or in vivo data can be useful to study various host-pathogen interactions, to screen for optimal HDT targets, and to guide in vitro and/or in vivo data experimental designs. Upon addition of various translational factors and inter-individual variability components, the models can be useful to design optimal clinical studies, to identify. Figure created with biorender.com.

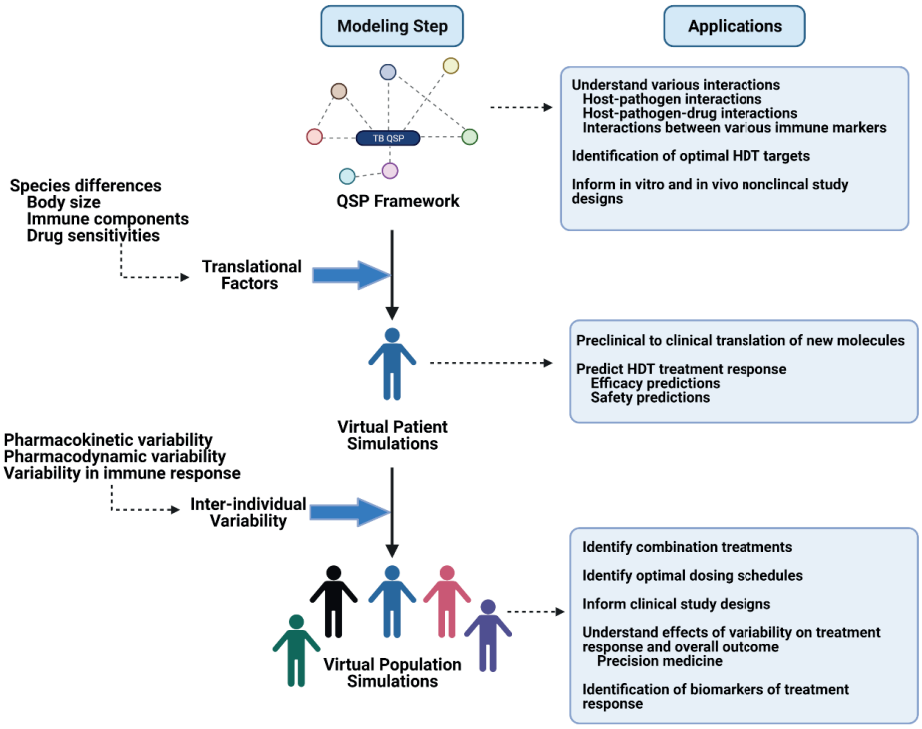

Target identification, drug discovery, and drug repurposing

QSP models integrate various host-pathogen interactions and drug PK/PD components; therefore, they can readily provide assessment of target engagement upon stimulation or inhibition of certain targets at various doses and affinities. This allows evaluations of the iterative process of hypotheses generation, designing new experiments, hypotheses validation and/or generation of new hypotheses. This approach can be applied to evaluate known HDT targets and molecules, to discover new HDT targets, and to discover new HDT molecules. With advances in technologies, applications of combining quantitative modelling and machine learning approaches are being evaluated to screen new virtual drug compounds with optimal characteristics[54]. For example, different ADME properties for a set of virtual compounds were used in a PBPK model combined with tumor dynamics model to simulate tumor size. Machine learning algorithms were then applied to the simulated dataset to identify the combination of ideal drug properties to provide desired outcome. This information may then be applied for lead prioritization[54]. Similar approaches can be applied to repurpose or reposition already marketed drugs using large scale drug-target interactions data[55]. Advanced target screening techniques, i.e., CRISPR-Cas9, can be also considered in combination with QSP models for HDT drug discovery and development in future.

Translational predictions

With increased complexity and innovation in design of new drugs within the last two decades, mechanistic models are increasingly being applied to inform translation of the results across different experimental conditions and species. The systematic incorporation of system-specific parameters not only for various species, but also incorporation of differences between in vitro systems and in vivo models, is crucial to enable translation towards clinical HDT treatment designs39. In some cases, i.e. for scaling from HFIM to humans, such scaling is well studied[36], whilst further studies are needed for the host's immune response components[56]. Consolidating immune-relevant differences between preclinical models and humans[56] may be challenging and resource intensive, as there may be varying strains of models used across different experiments depending on the objectives of the experiments. On the other hand, the shown evolutionary conservation of the metabolic responses to mycobacterial infection in human patients, mice, and zebrafish show that basic disease symptoms such as wasting syndrome are not depending on species or varying strains[57]. Gene expression analysis data across species may be used to inform parameters of expressions of genes responsible for certain immune functions[58]. Such expression data studies can be used to predict metabolism

using whole-genome metabolic network theoretical modelling approach in various organisms[59]. Factors such as severity of infection and sensitivity of drugs to bacterial strains (i.e., Mtb vs. Mm) may also be applied within the QSP framework.

Variability and precision medicine

The presentation and severity of TB is variable amongst patients, and thus treatment responses, especially to HDTs, are variable. Many factors such as age, sex, genotypes, comorbidities play role in determining the outcome of the disease and treatment. PopPK models have evaluated these factors' impact on variability in PK/PD of antibiotics[60] and can be included in QSP simulations. For example, known differences in PK and immune-response components for HIV co-infected TB patients may be incorporated in the framework, enabling extrapolation of results from studies in TB patients to HIV-TB patients[61]. In addition, considering immune-response relevant endotypes is important[62,63]. Technological advances within the last century enabled the generation of large-scale omics data. This data may enable us to better understand the inter-individual variations associated with the parameters of the QSP models. For example, parameters, together with inter-individual variations, describing the expression of baseline state of immune response components within lymph nodes and blood were estimated using data from a flow cytometry analysis of blood leukocytes and genome-wide DNA genotyping from humans[64]. Gene expression analysis of omics datasets from TB patients enabled stratification of the patients into two groups. One of the two groups was characterized by increased gene activity score for inflammatory response and decreased gene activity score for metabolism-relevant pathways, and patients in this group showed slower time to negative TB culture conversion and poor clinical outcome[62,63]. Similarly, gene expression data can be used to include variability in the QSP models and inform outcomes of certain HDT treatment.

Selection of optimal dosing regimens and combination therapies

QSP models are well-suited to efficiently evaluate combination therapies and dosing schedules, which is important to combination treatment strategies of HDTs and classical antibiotics against Mtb. In the field of immune-oncology, such QSP models have been widely applied to design optimal combination treatments of immune-targeting agents[65]. In the TB disease space, a QSP modelling approach for conventional antibiotic Mtb therapy has recently been applied to predict patient outcome with intensive dosing regimen and to explore shorter treatment duration scenarios[12].

Conclusions

HDTs offer a unique treatment strategy to combat Mtb infections but are challenged by complex and multiscale interactions between drug, host, and pathogen. Several key mechanisms are of interest to be exploited as HDTs but are facing challenges in translation towards clinically effective treatment strategies. The combined use of innovative experimental infection models with QSP modelling approaches can address these translational challenges and accelerate the design of novel HDT (combination) treatment strategies towards patients. QSP models supporting HDT design include model components describing biological system specific host-specific immunodynamics, pathogen dynamics and drug-specific models for PK and PK/PD for compounds of interest. Design of QSP models for HDTs relies on the availability of detailed mechanistic knowledge of relevant immunological and pharmacological aspects related to drug-host-pathogen interactions of Mtb infection, with significant knowledge gaps still present. Future work should focus on filling these knowledge gaps, which will require close and prospective coordination with such investigational efforts ensuring the correct data will be collected (see outstanding questions).

References

1. Parihar SP, Guler R, Khutlang R, Lang DM, Hurdayal R, Mhlanga MM, et al. Statin therapy reduces the mycobacterium tuberculosis burden in human macrophages and in mice by enhancing autophagy and phagosome maturation. J Infect Dis. 2014 Mar;209(5):754–63.
2. Jusko W. Foundations of Pharmacodynamic Systems Analysis. In: AAPS Advances in the Pharmaceutical Sciences Series. 2016. p. 161–75.
3. Nahid P, Dorman SE, Alipanah N, Barry PM, Brozek JL, Cattamanchi A, et al. Executive Summary: Official American Thoracic Society/ Centers for Disease Control and Prevention/ Infectious Diseases Society of America Clinical Practice Guidelines: Treatment of Drug-Susceptible Tuberculosis. Clin Infect Dis. 2016;63(7):853–67.
4. Young C, Walzl G, Du Plessis N. Therapeutic host-directed strategies to improve outcome in tuberculosis. Mucosal Immunol [Internet]. 2020;13(2):190–204. Available from: http://dx.doi.org/10.1038/s41385-019-0226-5
5. Tsenova L, Singhal A. Effects of host-directed therapies on the pathology of tuberculosis. J Pathol. 2020 Apr;250(5):636–46.
6. Kilinç G, Saris A, Ottenhoff THM, Haks MC. Host-directed therapy to combat mycobacterial infections. Immunol Rev. 2021 Feb;
7. Du Preez I, Loots DT. Novel insights into the pharmacometabonomics of first-line tuberculosis drugs relating to metabolism, mechanism of action and drug-resistance. Drug Metab Rev. 2018 Nov;50(4):466–81.
8. Walter ND, De Jong BC, Garcia BJ, Dolganov GM, Worodria W, Byanyima P, et al. Adaptation of Mycobacterium tuberculosis to Impaired Host Immunity in HIV-Infected Patients. J Infect Dis. 2016;214(8):1205–11.
9. van Hasselt JGC, Iyengar R. Systems Pharmacology: Defining the Interactions of Drug Combinations. Annu Rev Pharmacol Toxicol. 2019 Jan;59:21–40.
10. Aulin LBS, de Lange DW, Saleh MAA, van der Graaf PH, Völler S, van Hasselt JGC. Biomarker-Guided Individualization of Antibiotic Therapy. Clin Pharmacol Ther. 2021 Feb;
11. Bartelink IH, Zhang N, Keizer RJ, Strydom N, Converse PJ, Dooley KE, et al. New Paradigm for Translational Modeling to Predict Long-term Tuberculosis Treatment Response. Clin Transl Sci. 2017;10(5):366–79.
12. Fors J, Strydom N, Fox WS, Keizer RJ, Savic RM. Mathematical model and tool to explore shorter multi-drug therapy options for active pulmonary tuberculosis [Internet]. Vol. 16, PLoS Computational Biology. 2020. 1–36 p. Available from: http://dx.doi.org/10.1371/journal.pcbi.1008107
13. Singhal A, Jie L, Kumar P, Hong GS, Leow MKS, Paleja B, et al. Metformin as adjunct antituberculosis therapy. Sci Transl Med. 2014;6(263).
14. Lachmandas E, Eckold C, Böhme J, Koeken VACM, Marzuki MB, Blok B, et al. Metformin Alters Human Host Responses to Mycobacterium tuberculosis in Healthy Subjects. J Infect Dis. 2019 Jun;220(1):139–50.
15. Degner NR, Wang J-Y, Golub JE, Karakousis PC. Metformin Use Reverses the Increased Mortality Associated With Diabetes Mellitus During Tuberculosis Treatment. Clin Infect Dis an Off Publ Infect Dis Soc Am. 2018 Jan;66(2):198–205.
16. Ma Y, Pang Y, Shu W, Liu Y-H, Ge Q-P, Du J, et al. Metformin reduces the relapse rate of tuberculosis patients with diabetes mellitus: experiences from 3-year follow-up. Eur J Clin Microbiol Infect Dis Off Publ Eur Soc Clin Microbiol. 2018 Jul;37(7):1259–63.
17. Wallis RS, Ginindza S, Beattie T, Arjun N, Likoti M, Edward VA, et al. Adjunctive host-directed therapies for pulmonary tuberculosis: a prospective, open-label, phase 2, randomised controlled trial. Lancet Respir Med. 2021 Mar;
18. Hu Y, Wen Z, Liu S, Cai Y, Guo J, Xu Y, et al. Ibrutinib suppresses intracellular mycobacterium tuberculosis growth by inducing macrophage autophagy. J Infect. 2020 Jun;80(6):e19–26.
19. Tahir F, Bin Arif T, Ahmed J, Shah SR, Khalid M. Anti-tuberculous Effects of Statin Therapy: A Review of Literature. Cureus. 2020 Mar;12(3):e7404.

20. Dutta NK, Bruiners N, Zimmerman MD, Tan S, Dartois V, Gennaro ML, et al. Adjunctive Host-Directed Therapy With Statins Improves Tuberculosis-Related Outcomes in Mice. J Infect Dis [Internet]. 2020 Mar;221(7):1079—1087. Available from: https://doi.org/10.1093/infdis/jiz517

21. Tahir F, Bin Arif T, Ahmed J, Shah SR, Khalid M. Anti-tuberculous Effects of Statin Therapy: A Review of Literature. Cureus. 2020;12(3).

22. Chen Y-T, Kuo S-C, Chao P-W, Chang Y-Y. Use of lipid-lowering agents is not associated with improved outcomes for tuberculosis patients on standard-course therapy: A population-based cohort study. PLoS One. 2019;14(1):e0210479.

23. Moreira JD, Koch BE V, van Veen S, Walburg K V, Vrieling F, Mara Pinto Dabés Guimarães T, et al. Functional Inhibition of Host Histone Deacetylases (HDACs) Enhances in vitro and in vivo Anti-mycobacterial Activity in Human Macrophages and in Zebrafish. Front Immunol. 2020;11:36.

24. Mahadik K, Prakhar P, Rajmani RS, Singh A, Balaji KN. c-Abl-TWIST1 Epigenetically Dysregulate Inflammatory Responses during Mycobacterial Infection by Co-Regulating Bone Morphogenesis Protein and miR27a. Front Immunol [Internet]. 2018;9:85. Available from: https://www.frontiersin.org/article/10.3389/fimmu.2018.00085

25. Cox DJ, Coleman AM, Gogan KM, Phelan JJ, Ó Maoldomhnaigh C, Dunne PJ, et al. Inhibiting Histone Deacetylases in Human Macrophages Promotes Glycolysis, IL-1β, and T Helper Cell Responses to Mycobacterium tuberculosis. Front Immunol. 2020;11(July):1–15.

26. Wang X, Tang X, Zhou Z, Huang Q. Histone deacetylase 6 inhibitor enhances resistance to Mycobacterium tuberculosis infection through innate and adaptive immunity in mice. Pathog Dis. 2018 Aug;76(6).

27. Napier RJ, Rafi W, Cheruvu M, Powell KR, Zaunbrecher MA, Bornmann W, et al. Imatinib-Sensitive tyrosine kinases regulate mycobacterial pathogenesis and represent therapeutic targets against tuberculosis. Cell Host Microbe [Internet]. 2011;10(5):475–85. Available from: http://dx.doi.org/10.1016/j.chom.2011.09.010

28. Giver CR, Shaw PA, Fletcher H, Kaushal D, Pamela G, Omoyege D, et al. IMPACT-TB*: A Phase II Trial Assessing the Capacity of Low Dose Imatinib to Induce Myelopoiesis and Enhance Host Anti-Microbial Immunity Against Tuberculosis. *Imatinib Mesylate per Oral As a Clinical Therapeutic for TB. Blood [Internet]. 2019 Nov 13;134(Supplement_1):1050. Available from: https://doi.org/10.1182/blood-2019-130275

29. Marino S, Kirschner DE. A Multi-Compartment Hybrid Computational Model Predicts Key Roles for Dendritic Cells in Tuberculosis Infection. Comput (Basel, Switzerland). 2016;4(4).

30. Domingo-Gonzalez R, Prince O, Cooper A, Khader SA. Cytokines and Chemokines in Mycobacterium tuberculosis Infection. Microbiol Spectr. 2016 Oct;4(5).

31. Kolloli A, Subbian S. Host-directed therapeutic strategies for tuberculosis. Front Med. 2017;4(OCT).

32. Koh W-J, Kwon OJ, Suh GY, Chung MP, Kim H, Lee NY, et al. Six-month therapy with aerosolized interferon-gamma for refractory multidrug-resistant pulmonary tuberculosis. J Korean Med Sci. 2004 Apr;19(2):167–71.

33. Zhang R, Xi X, Wang C, Pan Y, Ge C, Zhang L, et al. Therapeutic effects of recombinant human interleukin 2 as adjunctive immunotherapy against tuberculosis: A systematic review and meta-analysis. PLoS One. 2018;13(7):1–14.

34. Van Der Vaart M, Korbee CJ, Lamers GEM, Tengeler AC, Hosseini R, Haks MC, et al. The DNA damage-regulated autophagy modulator DRAM1 links mycobacterial recognition via TLP-MYD88 to authophagic defense. Cell Host Microbe. 2014;15(6):753–67.

35. Korbee CJ, Heemskerk MT, Kocev D, van Strijen E, Rabiee O, Franken KLMC, et al. Combined chemical genetics and data-driven bioinformatics approach identifies receptor tyrosine kinase inhibitors as host-directed antimicrobials. Nat Commun. 2018 Jan;9(1):358.

36. Gumbo T, Pasipanodya JG, Nuermberger E, Romero K, Hanna D. Correlations Between the Hollow Fiber Model of Tuberculosis and Therapeutic Events in Tuberculosis Patients: Learn and Confirm. Clin Infect Dis [Internet]. 2015;61(suppl_1):S18–24. Available from: https://doi.org/10.1093/cid/civ426

37. Tezera LB, Bielecka MK, Chancellor A, Reichmann MT, Shammari B Al, Brace P, et al. Dissection of the host-pathogen interaction in human tuberculosis using a bioengineered 3-dimensional model. Elife. 2017;6:1–19.

38. Thacker V V., Dhar N, Sharma K, Barrile R, Karalis K, McKinney JD. A lung-on-chip model of early m. Tuberculosis infection reveals an essential role for alveolar epithelial cells in controlling bacterial growth. Elife. 2020;9:1–73.

39. Meijer AH. Protection and pathology in TB: learning from the zebrafish model. Semin Immunopathol. 2016;38(2):261–73.

40. H. Meijer A, P. Spaink H. Host-Pathogen Interactions Made Transparent with the Zebrafish Model. Curr Drug Targets. 2011;12(7):1000–17.

41. Johansen MD, Daher W, Roquet-Banères F, Raynaud C, Alcaraz M, Maurer FP, et al. Rifabutin Is Bactericidal against Intracellular and Extracellular Forms of Mycobacterium abscessus. Antimicrob Agents Chemother. 2020 Oct;64(11).

42. Ordas A, Raterink R-J, Cunningham F, Jansen HJ, Wiweger MI, Jong-Raadsen S, et al. Testing tuberculosis drug efficacy in a zebrafish high-throughput translational medicine screen. Antimicrob Agents Chemother. 2015 Feb;59(2):753–62.

43. van Wijk RC, Hu W, Dijkema SM, van den Berg DJ, Liu J, Bahi R, et al. Anti-tuberculosis effect of isoniazid scales accurately from zebrafish to humans. Br J Pharmacol. 2020;177(24):5518–33.

44. Yang H-J, Wang D, Wen X, Weiner DM, Via LE. One Size Fits All? Not in In Vivo Modeling of Tuberculosis Chemotherapeutics. Front Cell Infect Microbiol [Internet]. 2021;11:134. Available from: https://www.frontiersin.org/article/10.3389/fcimb.2021.613149

45. Mehta K, Ravimohan S, Pasipanodya JG, Srivastava S, Modongo C, Zetola NM, et al. Optimizing ethambutol dosing among HIV/tuberculosis co-infected patients: a population pharmacokinetic modelling and simulation study. J Antimicrob Chemother. 2019 Oct;74(10):2994–3002.

46. Hanke N, Türk D, Selzer D, Ishiguro N, Ebner T, Wiebe S, et al. A Comprehensive Whole-Body Physiologically Based Pharmacokinetic Drug–Drug–Gene Interaction Model of Metformin and Cimetidine in Healthy Adults and Renally Impaired Individuals. Clin Pharmacokinet [Internet]. 2020;59(11):1419–31. Available from: https://doi.org/10.1007/s40262-020-00896-w

47. Duong JK, Kumar SS, Kirkpatrick CM, Greenup LC, Arora M, Lee TC, et al. Population pharmacokinetics of metformin in healthy subjects and patients with type 2 diabetes mellitus: simulation of doses according to renal function. Clin Pharmacokinet. 2013 May;52(5):373–84.

48. Wigginton JE, Kirschner D. A Model to Predict Cell-Mediated Immune Regulatory Mechanisms During Human Infection with Mycobacterium tuberculosis . J Immunol. 2001;166(3):1951–67.

49. Marino S, Kirschner DE. The human immune response to Mycobacterium tuberculosis in lung and lymph node. J Theor Biol. 2004;227(4):463–86.

50. Palsson S, Hickling TP, Bradshaw-Pierce EL, Zager M, Jooss K, O'Brien PJ, et al. The development of a fully-integrated immune response model (FIRM) simulator of the immune response through integration of multiple subset models. BMC Syst Biol [Internet]. 2013;7(1):1. Available from: BMC Systems Biology

51. Sud D, Bigbee C, Flynn JL, Kirschner DE. Contribution of CD8 + T Cells to Control of Mycobacterium tuberculosis Infection . J Immunol. 2006;176(7):4296–314.

52. Holczer M, Hajdú B, Lőrincz T, Szarka A, Bánhegyi G, Kapuy O. A double negative feedback loop between MTORC1 and AMPK kinases guarantees precise autophagy induction upon cellular stress. Int J Mol Sci. 2019;20(22).

53. Bradshaw EL, Spilker ME, Zang R, Bansal L, He H, Jones RDO, et al. Applications of Quantitative Systems Pharmacology in Model-Informed Drug Discovery: Perspective on Impact and Opportunities. CPT Pharmacometrics \& Syst Pharmacol [Internet]. 2019;8(11):777–91. Available from: https://ascpt.onlinelibrary.wiley.com/doi/abs/10.1002/psp4.12463

54. Chen EP, Bondi RW, Michalski PJ. Model-based Target Pharmacology Assessment (mTPA): An Approach Using PBPK/PD Modeling and Machine Learning to Design Medicinal Chemistry and DMPK Strategies in Early Drug Discovery. J Med Chem. 2021;

55. Zhou Y, Wang F, Tang J, Nussinov R, Cheng F. Artificial intelligence in COVID-19 drug repurposing. Lancet Digit Heal [Internet]. 2020;2(12):e667–76. Available from: http://dx.doi.org/10.1016/S2589-7500(20)30192-8

56. Ernest JP, Strydom N, Wang Q, Zhang N, Nuermberger E, Dartois V, et al. Development of New Tuberculosis Drugs: Translation to Regimen Composition for Drug-Sensitive and Multidrug-Resistant Tuberculosis. Annu Rev Pharmacol Toxicol. 2021;61:495–516.

57. Ding Y, Raterink R-J, Marín-Juez R, Veneman WJ, Egbers K, van den Eeden S, et al. Tuberculosis causes highly conserved metabolic changes in human patients, mycobacteria-infected mice and zebrafish larvae. Sci Rep. 2020 Jul;10(1):11635.

58. Ahmed M, Thirunavukkarasu S, Rosa BA, Thomas KA, Das S, Rangel-Moreno J, et al. Immune correlates of tuberculosis disease and risk translate across species. Sci Transl Med [Internet]. 2020;12(528). Available from: https://stm.sciencemag.org/content/12/528/eaay0233

59. van Steijn L, Verbeek FJ, Spaink HP, Merks RMH. Predicting Metabolism from Gene Expression in an Improved Whole-Genome Metabolic Network Model of Danio rerio. Zebrafish. 2019 Aug;16(4):348–62.

60. McCallum AD, Pertinez HE, Else LJ, Dilly-Penchala S, Chirambo AP, Sheha I, et al. Intrapulmonary Pharmacokinetics of First-line Anti-tuberculosis Drugs in Malawian Patients With Tuberculosis. Clin Infect Dis. 2020;(Mic):1–9.

61. Walker NF, Meintjes G, Wilkinson RJ. HIV-1 and the immune response to TB. Future Virol. 2013 Jan;8(1):57–80.

62. DiNardo AR, Nishiguchi T, Grimm SL, Schlesinger LS, Graviss EA, Cirillo JD, et al. Tuberculosis endotypes to guide stratified host-directed therapy. Med [Internet]. 2021;2(3):217–32. Available from: https://doi.org/10.1016/j.medj.2020.11.003

63. DiNardo AR, Gandhi T, Heyckendorf J, Grimm SL, Rajapakshe K, Nishiguchi T, et al. Gene expression signatures identify biologically and clinically distinct tuberculosis endotypes. medRxiv [Internet]. 2021; Available from: https://www.medrxiv.org/content/early/2021/02/07/2020.05.13.20100776

64. Lazarou G, Chelliah V, Small BG, Walker M, van der Graaf PH, Kierzek AM. Integration of Omics Data Sources to Inform Mechanistic Modeling of Immune-Oncology Therapies: A Tutorial for Clinical Pharmacologists. Clin Pharmacol Ther. 2020;107(4):858–70.

65. Coletti R, Leonardelli L, Parolo S, Marchetti L. A QSP model of prostate cancer immunotherapy to identify effective combination therapies. Sci Rep [Internet]. 2020;10(1):9063. Available from: https://doi.org/10.1038/s41598-020-65590-0

66. Azer K, Kaddi CD, Barrett JS, Bai JPF, McQuade ST, Merrill NJ, et al. History and Future Perspectives on the Discipline of Quantitative Systems Pharmacology Modeling and Its Applications. Front Physiol. 2021;12(March).

Chapter 8

Quantitative systems pharmacology modeling framework of autophagy in tuberculosis: application to adjunctive metformin host-directed therapy

Krina Mehta, Tingjie Guo, Robert Wallis, Piet H. van der Graaf, J.G. Coen van Hasselt

Antimicrob Agents Chemother, 2022 July, Vol. 66, No. 8

Abstract

Background: Quantitative systems pharmacology (QSP) modeling of the host-immune response against Mtb can inform rational design of host-directed therapies (HDTs). We aimed to develop a QSP framework to evaluate the effects of metformin-associated autophagy-induction in combination with antibiotics.

Methods: A QSP framework for autophagy was developed by extending a model for host-immune response to include AMPK-mTOR-autophagy signalling. This model was combined with pharmacokinetic-pharmacodynamic models for metformin and antibiotics against Mtb. We compared the model predictions to mice infection experiments, and derived predictions for pathogen and host-associated dynamics in humans treated with metformin in combination with antibiotics.

Results: The model adequately captured the observed bacterial load dynamics in mice Mtb infection models treated with metformin. Simulations for adjunctive metformin therapy in newly diagnosed patients suggested a limited yet dose-dependent effect of metformin on reducing the intracellular bacterial load when overall bacterial load is low, late during antibiotic treatment.

Conclusions: We present the first QSP framework for HDTs against Mtb, linking cellular-level autophagy effects to disease progression and adjunctive HDT treatment response. This framework may be extended to guide the design of HDTs against Mtb.

Introduction

The increasing burden of *Mycobacterium tuberculosis* (Mtb) infections is a major global health concern associated with approximately 1.5-2 million deaths annually[1]. Current first-line treatment to active tuberculosis (TB) disease, include a two-month intensive phase with rifampicin, isoniazid, pyrazinamide, and ethambutol followed by a four-month continuation phase with rifampicin and isoniazid (HRZE). A long treatment duration, common treatment failure, relapse, and emergence of multi-drug resistant Mtb strains are key challenges to successful TB treatment[2].

Host-directed therapies (HDT) aim to exploit the interplay between the pathogen and the host immune response[3,4]. HDTs are increasingly being studied for treatment against Mtb infections. One of the most studied HDT strategies to date is autophagy induction[5]. Autophagy is an intracellular catabolic process involving delivery of excessive or damaged cellular components, including bacteria, to lysosome for degradation to maintain homeostasis. The AMPK-mTOR signaling pathway is an important regulator of autophagy. Mtb activates phosphorylation of Akt, which stimulates phosphorylation of mTORC1. Activation of mTORC1 inhibits autophagy by phosphorylation of various autophagy-related proteins[6]. Preclinical studies have demonstrated involvement of mTOR signaling pathway in the host response to Mtb, suggesting its relevance as therapeutic target[6,7]. Therefore, metformin, an antihyperglycemic agent and mTORC1 inhibitor, has been proposed as potential HDT against Mtb[6,7]. Metformin adjunctive therapy in diabetic TB patients was found to be associated with an improved therapy success rate and lowered mortality[8,9].

Quantitative systems pharmacology (QSP) models aim to capture mechanistic details of the interactions between a biological system and pharmacokinetic-pharmacodynamic (PKPD) properties of a drug[10]. QSP-based characterization of drug-host-pathogen interactions may allow evaluation of expected treatment responses upon perturbation of specific targets, which may help to identify promising HDT targets and to evaluate different potential combination treatment strategies. Within the TB field, the mathematical modeling approaches have primarily focused on PKPD modeling focusing mostly on design of antibiotics [11,12]. In addition, multiscale systems biology models of the host-immune response in response to Mtb infections have been developed[13,14]. The prior immune response model[13] have been combined with PKPD models of HRZE to explore the impact of patient immune response on the treatment outcomes[15–17]. Any of these models did not include HDT relevant pathways; however, established a strong basis for further developing QSP framework to enable design of HDTs.

To guide design and development of HDTs, relevant HDT pathways must be added to the QSP framework. The autophagy-regulating AMPK/mTOR pathway represents an important factor for HDTs. There are currently no mathematical models available in literature describing mTOR signaling-mediated autophagy in TB. The objectives of this work were, (1) to develop a QSP framework of host-immune response including autophagy-mediated interactions, and (2) to evaluate the effects of metformin-associated autophagy-induction in combination with HRZE treatment.

Methods

The developed QSP framework **(Figure 8.1)** included, (1) PK models for standard antibiotics and metformin, (2) TB host-immune response model including PD effects of HRZE, and (3) autophagy model including PD effects of metformin. The QSP model development was facilitated by adaptations of various models presented in literature[17–19]. A set of ODEs describing dynamics of intra- and extra-cellular bacteria in host lungs as functions of time, and dynamics of immune-response components, such as macrophages, cytokines, and lymphocytes as functions of time and bacterial load, form the core of our QSP framework [18]. The core model was then linked to a model describing the dynamics of AMPK-mTOR signaling proteins leading to autophagy[19]. The interactions between Mtb and autophagy connects these two models. Moreover, the combined TB host-immune response-autophagy model was linked with models capturing PKPD relationships of HRZE and metformin.

Model development

The details of the model development process are provided in supplementary materials (S8.1), and the key steps are presented below.

Pharmacokinetics

PK models of four antibiotics, HRZE, were reproduced from literature-based population PK models[20,21]. Plasma concentrations of HRZE following standard of care dosing were simulated using the PK models. HRZE intra- and extra-cellular lung concentrations were predicted by applying plasma to lung alveolar cells and plasma to lung epithelial lining fluid ratios respectively obtained from literature[22]. To predict lung concentrations of metformin, we developed a minimal physiologically based PK model for metformin including a lung compartment[23] (S8.1.1).

TB host-immune response and pharmacodynamics of standard antibiotics

A published model that captured the dynamics of the host-pathogen interactions following Mtb infection was implemented[18]. This host-immune response model contained host-pathogen interactions in lungs, and included three population of macrophage (resting-, activated-, and infected-), various cytokines (IFN-γ, TNF-α, IL-10, IL-4, IL-12) and lymphocytes, as well as intra- and extra-cellular Mtb populations. An update was made to this model to add the turn-over of IL-1b and IL-1b-mediated bacterial elimination[24] (S8.1.2).

We included two Mtb growth phases, fast and slow, as a simple implementation of initial rapid progression of active disease[13,18]. The switch from fast to slow growth rates was empirically set to 21 days post-infection based on mice infection experimental results[25,26]. We used the slow phase bacterial growth rate estimates same as the growth rate values from the reproduced TB host-immune response model[18]. The growth rates for the initial fast phase were optimized using digitized data from mice Mtb infection experiment[25](S8.1). Bactericidal effects on intra- and extra-cellular bacterial population and bacteriostatic effects on growth rates of bacteria driven by intra- and extra-cellular lung concentrations of HRZE were reproduced from the literature[17].

Autophagy and pharmacodynamics of metformin

The AMPK-mTOR cell signaling network model from literature was reproduced[19]. This model captured the dynamics of key proteins involved in AMPK-mTOR signaling pathway and includes relative interactions between proteins involved in AMPK-mTOR signaling pathway, such as, insulin receptor substrate, class I phosphatidylinositol 3-kinases, AMPK, mTORC1, and mTOR complex 2 (mTORC2). This model was updated to include various Mtb- and autophagy-related components. The updates can be categorized into: (1) the effect of Mtb Infection on autophagy inhibition due to activation of AMPK-mTOR signaling and (2) the effect of autophagy of Mtb elimination. Gene AKT3, a key upstream regulator of AMPK-mTOR signaling pathway, was found to be induced 1.38-fold in Mtb-infected vs. uninfected mice based on differential expression in lungs of Mtb infected vs. uninfected mice[6]. This ratio was added as a proportional scaling factor in the model on production of AKT to simulate the presence of Mtb and its impact on key down-stream proteins involved in AMPK-mTOR signaling, including mTORC1 (S8.1.3). Due to the limited data availability, time-course effects of progression of Mtb infection on autophagy is not included in the current model.

The effects of AMPK-mTOR signaling on autophagy were model using a direct effect saturable Emax model. Autophagy at time of Mtb infection was set to 100 % to represent a healthy state prior to infection. Then, the percent inhibition of autophagy due to Mtb infection and subsequent AMPK-mTOR signaling activation modeled. Next, the autophagy model was combined with TB host-immune response model by introducing autophagy-mediated intracellular bacterial killing and autophagy-mediated extracellular to intracellular bacterial uptake. These processes were incorporated as first-order processes, and the parameters were informed by Mtb survival data from in vitro infection experiments with and without metformin treatment[27](S1.3). The inhibitory effect of metformin on mTORC1 phosphorylation was incorporated using an indirect effect saturable Emax model, and the parameters were obtained from the literature[28,29].

Model evaluations

The combined TB-Autophagy QSP framework predictions were first compared to observed digitized lung bacterial load data from untreated and metformin-treated mice infected with Mtb[27]. To this end, the QSP model was scaled from humans to mice by applying volume differences between the species. To evaluate HRZE PKPD components of the combined QSP model, the predicted change in bacterial load over time after start of HRZE treatment was compared against reported values for TB patients[30–32].

Sensitivity analysis

High uncertainty existed in some parameters, especially for parameters related to autophagy model due to limited data availability. To further understand the impact of uncertainty in the parameters on model predictions, global uncertainty and sensitivity analysis using Latin hypercube sampling (LHS) and partial rank correlation coefficient method using 500 samples was performed[33,34]. The outcome used in this analysis was predicted total bacterial load. All parameters, except the PK and PD parameters, were evaluated in the global uncertainty and sensitivity analysis. The parameters ranges used for LHS were the same as the previous model for TB host-immune response model components and were varied by 20% for autophagy-related components[18].

Simulations of metformin-associated autophagy induction in humans

Typical TB patient simulations were conducted using the QSP framework to predict the effects of autophagy induction with metformin on overall treatment outcome. Typical TB patient simulations were performed using parameter values presented in S8.2. A typical virtual TB patient was defined as a 70 kg human. No random effects or uncertainty components were included in the simulations. An initial extracellular Mtb inoculum of 100 bacteria was introduced at day 0 in all simulations.

First, the simulations were performed to evaluate effects on bacterial load and on cytokine levels following HRZE therapy with and without adjunctive metformin treatment at three different dosing regimens starting at day 180 post-infection, i.e., upon diagnosis. Day 180 post-infection was selected as the approximate time to diagnosis and as such starting point for treatment based on prior model[17]. In these first set of simulations, metformin was added at the same time as starting HRZE treatment. Additional simulations were performed to predict the effects on total bacterial load if metformin was added at end of two months intensive HRZE treatment. Metformin dosing regimen used in the simulations included 250 mg, 500 mg, and 1000 mg, all BID. HRZE regimen in the simulations included 300 mg isoniazid, 600 mg rifampin, 1500 mg pyrazinamide, and 1100 mg ethambutol all QD for 2 months, followed by the same dose of isoniazid and rifampin for 4 months. Next, to understand the effects of metformin on the TB disease progression in scenarios where diabetic patients would be receiving metformin for their glycemic control at the time of infection with TB[8,9], simulations were performed to predict the effects of 500 mg BID metformin treatment starting at day 1 post-infection.

Software

All parameter optimization and model simulations were conducted in R and RStudio using nlmixr and RxODE packages[35]. Literature model for autophagy was converted from SBML file to ODEs in R using IQRsbml package [https://iqrsbml.intiquan.com/main.html].

Results

The QSP framework included combined host-pathogen interactions model, AMPK-mTORC1 signaling pathway model including autophagy, and PKPD models of HRZE and metformin **(Figure 8.1)**.

The QSP framework simulations recapitulate observed in vivo response to metformin

The model was evaluated by comparing predictions to the observed data. The model predictions for total bacterial load showed good agreement with observed digitized lung bacterial load data from untreated mice infected with Mtb[6] **(Figure 8.2A)**. The simulations with standard TB therapy starting at day 180 post-infection in TB patients predicted previously reported change in bacterial load from baseline with HRZE treatment reasonably well **(Figure 8.2B)**. Overall, these assessments suggested the reliability of the model for the objectives of this analysis.

Sensitivity analysis provides insights into the mechanistic details of the infection

The global uncertainty and sensitivity analysis suggested that the bacterial load was more sensitive to the parameters of host-pathogen interaction model compared to those of the autophagy model (S8.3). In general, the host-pathogen interaction model parameters that correlated with the bacterial load the most were related to macrophage recruitment, macrophage activation or deactivation, phagocytosis, IFN-y production, or IL-1b- or FAS-FAS-mediated apoptosis. Most of these parameters were identified in the sensitivity analysis in the prior models too[18]. In the prior models, these parameters were obtained either from literature or were estimated using in vitro or mice experiments' data and therefore, are considered relatively reliable. One parameter related to the autophagy model, AKT dephosphorylation rate, was found positively correlated with the bacterial load, and thus negatively correlated with infection control. This highlights the key role of Mtb evasion and inhibition of autophagy on disease progression. This parameter was unchanged in the current model from the previous AMPK-mTOR signaling model. In the previous work, this parameter was estimated using experimental data from immunoblots and thus deem reliable. This sensitivity analysis given uncertainty in the parameters provide a thorough picture of the current state of the model (Figure S8.3).

Figure 8.1 Combined TB-Autophagy QSP framework. The model captures the dynamics of host-immune response in the lungs because of Mtb infection. The model consists of various species of macrophages, lymphocytes, and the key cytokines involved in both innate and adaptive immune response against Mtb. The model includes the growth of Mtb as well as immune-mediated elimination of Mtb affecting the overall Mtb population. The immune-mediated bacterial killing include mainly cytokine- and lymphocytes- mediated apoptosis as well as autophagy. The model also consists of Mtb evasion mechanism, such as, induction of AMPK-mTOR pathway and inhibition of autophagy. Bi=intracellular Mtb, Be=extracellular Mtb, Ma=activated macrophage, Mi=infected macrophage, Mr=resident macrophage, T80=precursor-activated CD8+ T cells, T8=sub-class (IFN-y producing) of activated CD8+ T-cells, Tc=subclass (cytotoxic lymphocytes) of activated CD8+ T-cells, Th0=naïve T-cells, Th1=type 1 helper T-cells, Th2=type 2 helper T-cells. Figure created with biorender.com

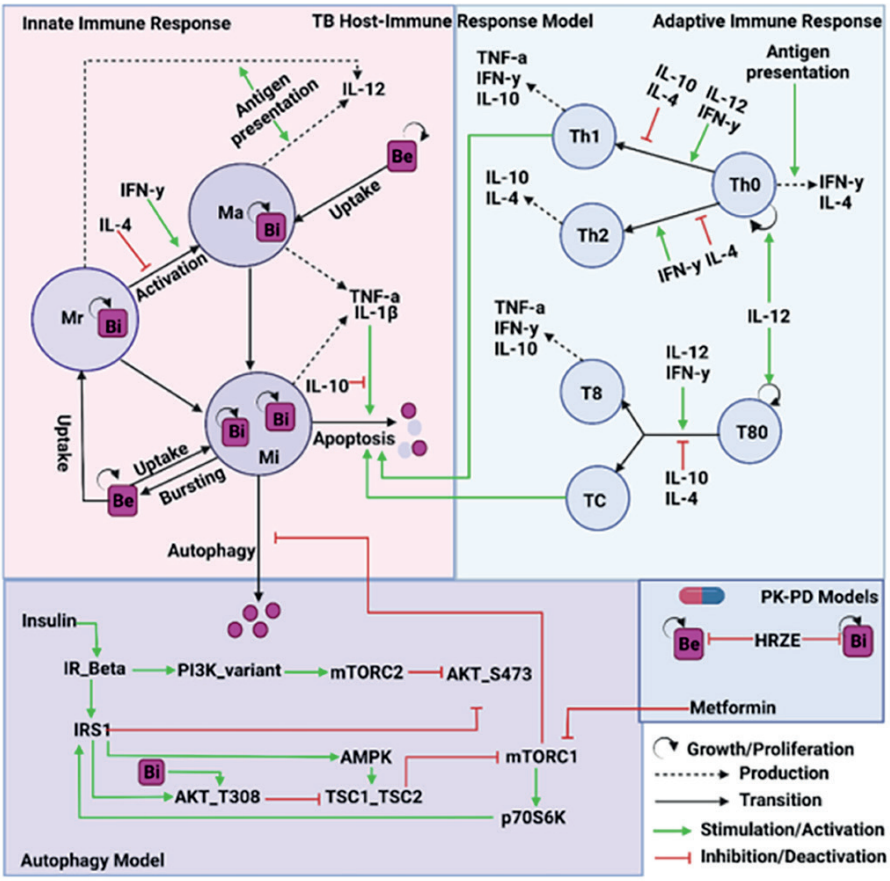

Figure 8.2 Time course of predicted and observed lung bacterial load: (A) Mtb-infected mice treated or untreated with Metformin, (B) Tuberculosis patients treated with standard antibiotic regimen. The model predictions for total bacterial load agree well with the observed mice data treated with or without metformin. Additionally, model predictions for effects of standard antibiotics therapy reasonable agree observed change in bacterial load from baseline data from TB patients. CFU=colony-forming unit, Metformin was administered daily from day 7 through 35 with six days on, one day off regimen in mice, points represent observed and lines represent model predictions.

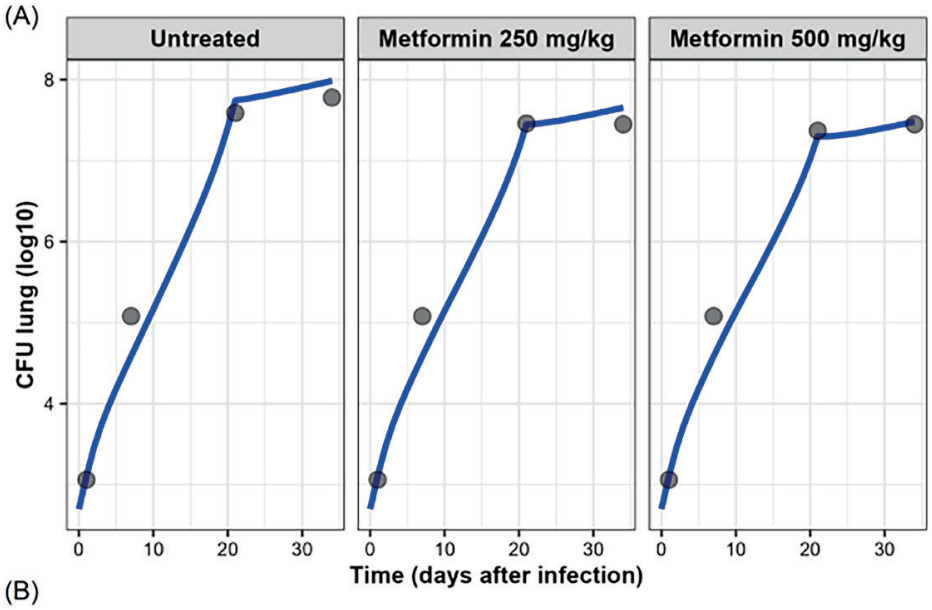

Metformin-associated autophagy induction is predicted to provide dose-dependent reduction in intracellular bacterial load

The simulations for TB disease progression, i.e., prior to the start of treatment suggested that Mtb infection is predicted to reduce autophagy by 55% in a typical subject. We compared the effects of HRZE with or without adjunctive metformin treatment on bacterial load and cytokine levels in a typical virtual TB patient. These simulations considered a typical scenario where the treatment was started upon diagnosis of TB, which was considered around day 180 after initial infection. Adjunctive metformin with HRZE treatment was predicted to show limited yet apparent dose-dependent increase in autophagy-mediated intracellular and total bacterial elimination when total bacterial burden is relatively low after first two months of treatment **(Figure 8.3a)**. No significant impact was predicted on cytokine levels in the adjunctive metformin with HRZE scenario compared to HRZE only scenario **(Figure 8.3B)**. The simulations for a scenario where metformin was added two-months after the start of intensive phase treatment with HRZE predicted that adjunctive metformin may reduce overall treatment duration by 3-5 days (Figure S8.4). Overall, we conclude that adjunctive metformin treatment may provide modest benefit in reducing Mtb bacterial load in TB patients during the continuation phase of HRZE treatment.

Metformin may delay disease progression in diabetic tb patients

We assessed if metformin would delay TB disease progression if metformin was administered prior to TB diagnosis, i.e., in scenarios where diabetic patients would be receiving metformin for their glycemic control at the time of infection with Mtb **(Figure 8.4a)**. For these simulations, metformin input was added at the same time as initial bacterial infection. We found that metformin use in diabetic TB patients would delay TB disease progression as assessed by intra-, extra-, and total-bacterial load. Lower levels of pro-inflammatory cytokines, IL-1b, TNF-α, IFN-y, and IL-12, were also predicted in metformin-treated vs. no metformin-treated typical patient **(Figure 8.4b)**. Overall, these simulations suggest some protective effects over tissue damage of metformin use in diabetic TB patients. As these simulations represent scenarios prior to TB diagnosis, thy do not provide guidance in metformin treatment for TB patients. However, these simulations provide mechanistic insights into the role of autophagy on the dynamics of TB infection.

Figure 8.3 Typical patient simulations for adjunctive Metformin to atandard antibiotics treatment at various dosing regimen starting at day 180 post-infection: (A) Bacterial load, (B) Cytokines. The simulations suggest dose-dependent effects of metformin on reduction of intracellular bacterial load. The reduction in intracellular bacterial elimination with adjunctive metformin treatment; however, does not significantly affect extracellular and thus total bacterial load compared to standard antibiotics only treatment when total bacterial burden is high. HRZE refers to 2 months of rifampicin, isoniazid, pyrazinamide, and ethambutol + 4 months of rifampicin and isoniazid regimen; vertical dashed line refers to end of 2 months regimen.

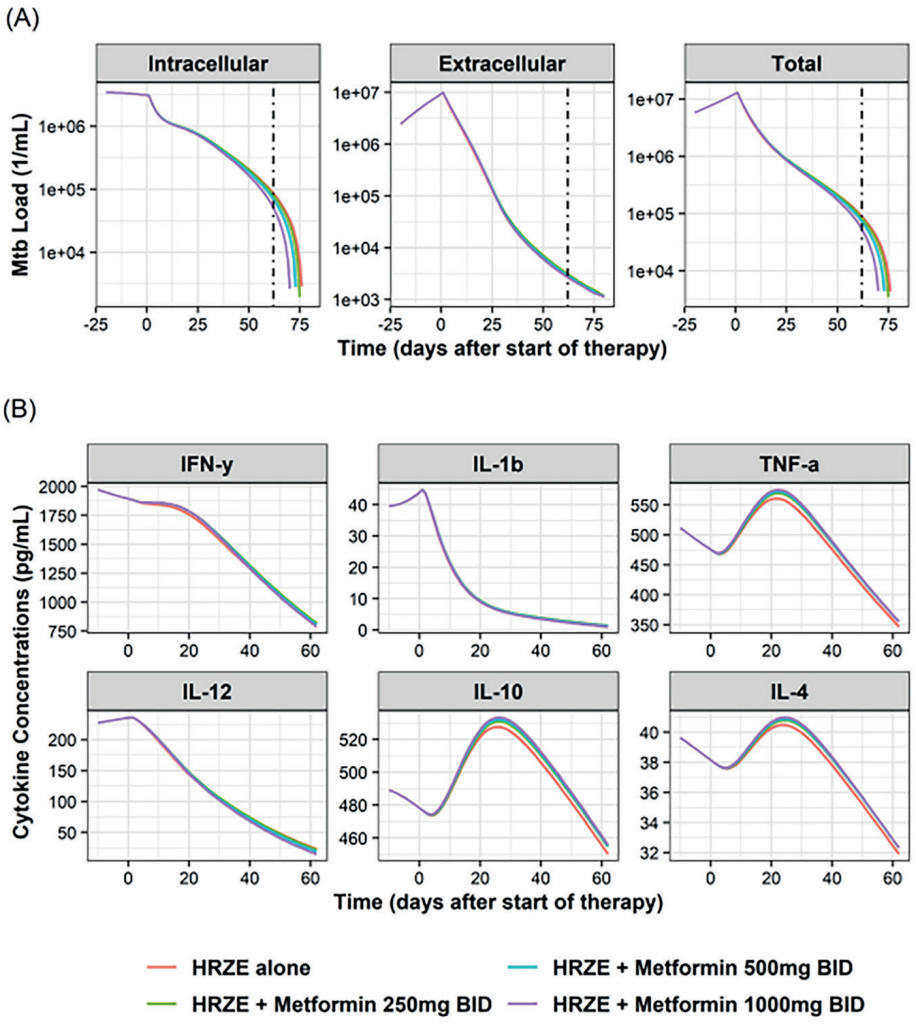

Figure 8.4 Typical patient simulations with or without 500 mg twice daily Metformin starting at day 1 post-infection: (A) Bacterial load, (B) Cytokines. The model predicted some benefits of metformin use in delaying the disease progression in virtual diabetic patients receiving metformin as compared to non-treated patients.

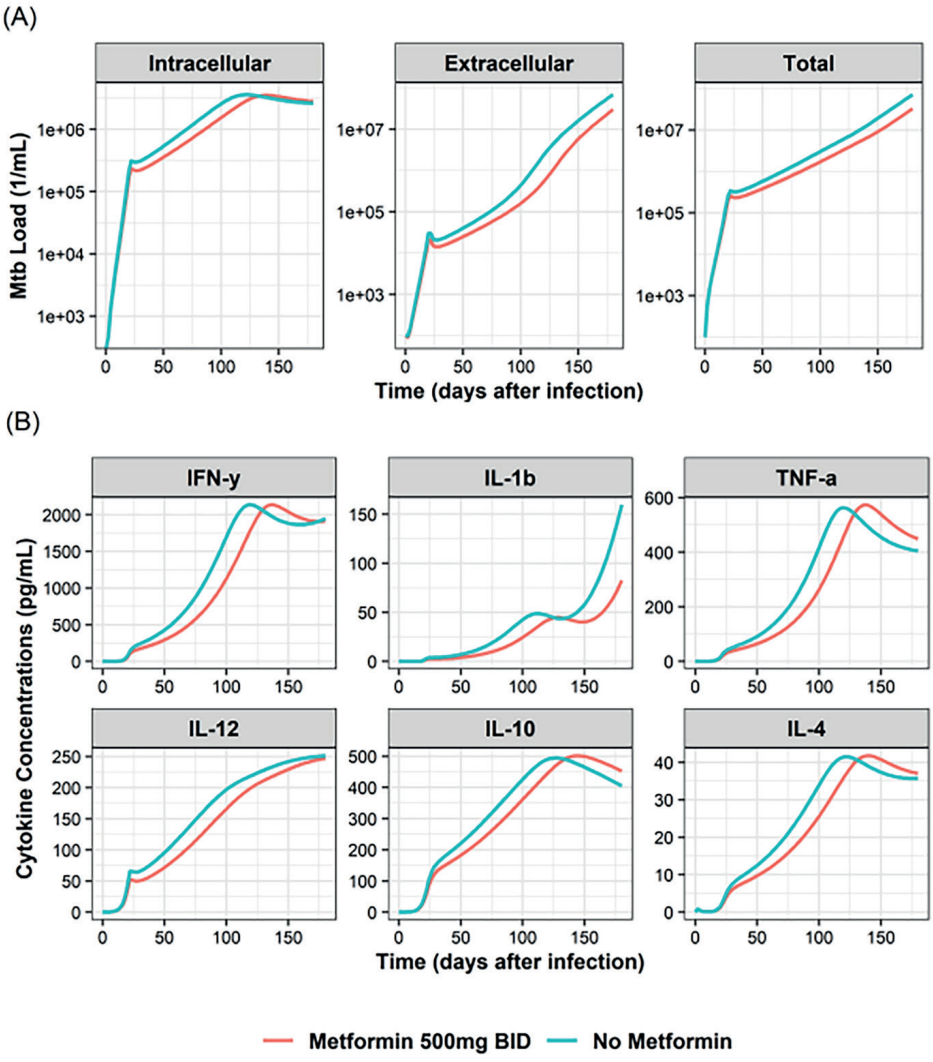

Discussions and conclusions

Here, we developed a first QSP framework for design and evaluation of HDTs focusing on autophagy. Our model was able to recapitulate results from an in vivo study evaluating metformin as a HDT in Mtb-infected mice. We applied the framework to predict treatment effects of autophagy induction by metformin in a typical TB patient.

Our analysis identified a modest beneficial effect of adjunctive metformin treatment in a typical TB patient, after intensive phase antibiotics treatment when total bacillary load is predicted to be relatively low. The predictions suggested that overall effects of treatment with metformin would depend on extracellular-to-intracellular bacteria ratio, which may depend on the stage of infection. The model also predicted some benefits of metformin use in delaying the disease progression in virtual diabetic patients receiving metformin. Our results agree with the clinical reports where lowered mortality rates were reported in diabetic patients receiving metformin[8,9]. A key Mtb survival strategy depends on provoking a non-sterilizing immune response, allowing for Mtb to replicate beyond reach of most immune mechanisms. As part of host-pathogen interactions, granuloma formation limits Mtb growth, but also provide niche for replication by disseminating Mtb to other areas[36]. Metformin, and HDTs in general, may provide beneficiary effects early after initial infection, i.e., in newly infected TB household contacts, or late during treatment, i.e., after sputum has been sterilized but when small numbers of persisting bacteria are still present. In these scenarios, small changes in the survival of a rather small bacterial population may have a large effect on infection outcome, and future studies may consider evaluating this.

Our model provides relevant quantitative insight into the mechanistic details of factors contributing to autophagy-mediated bacterial elimination. Lack of predicted effects of metformin at doses up to 1000 mg BID on total bacterial load can also be attributed to its potency on AMPK-mTORC1-autophagy signaling and its distribution in lungs, in addition to extracellular-to-intracellular bacterial ratio. Previously, metformin dose-ranging study that evaluated effects of metformin at doses 100–10000 uM on Mtb survival in human monocyte-derived macrophages showed no increased Mtb survival at doses up to 500 uM. In the same study, approximately 4% reduction in total bacterial load on day 35 was noted in mice treated with 250 mg/kg and 500 mg/kg metformin daily from day 7-35 (6 days on, 1 day off)[6]. Our mPBPK model predicted mice lungs Cmax 668 uM and 1336 uM in 250 mg/kg and 500 mg/kg metformin dose groups, respectively. When these body weight-based

doses of metformin that were evaluated in mice are compared to clinically feasible doses, predicted lungs Cmax in humans are approximately 10- to 15-fold lower than those predicted in mice. As such, it would be no surprise that our predictions showed no significant effects of metformin on the reduction of bacterial load. In fact, a recently completed clinical trial evaluating adjunctive metformin treatment to standard treatment in TB patients reported that metformin treatment did not significantly reduce time to sputum conversion as compared to controls[37].

The integrated QSP framework connects the complex intracellular process, autophagy, to disease outcome at organism-level. The model can be easily adapted to perform evaluations of other mTORC1 inhibitors mTORC1-independent autophagy inducers in the future using similar approach as ours. Some candidate drugs include, everolimus, statins, PI3K inhibitors, and tyrosine kinase inhibitor. The model can also facilitate in silico evaluations of perturbations of various proteins involved in autophagy and predict their effects on the outcome, as such enable target identification for optimal autophagy induction. For example, the model may be used in combination with screening assays to prioritize further development of potential HDTs.

One of the limitations of our model was that it built upon a prior relatively simple TB host-immune response model[18]. In our model, we added empirical transition from fast- to slow- Mtb growth phase to resemble initial log-phase increase in bacterial load. However, growth and treatment effects on different subpopulations of Mtb, i.e., non-persisters and persisters, at a given time is not included in the model. Future work may integrate a mechanistic model with various subpopulations of both intra- and extra-cellular Mtb into the QSP framework. For this, measurements of various Mtb subpopulation from sputum or bronchoalveolar lavage fluid of TB patients are required. The proposed integration may also require applying antibiotics' bacterial kill rates specific to the subpopulation. In general, the current construct of TB host-immune response model is relevant for our primary objective, i.e., to evaluate different treatment scenarios with and without metformin in TB patients when bacterial load has already reached relatively high.

Our model includes relative activity of the key proteins involved in the AMPK-mTOR-autophagy signaling, and however, do not consider total concentrations of these proteins. The original data-driven AMPK-mTOR model that was adapted in this work was developed using immunoblot data from HeLa cells, and therefore considered relative activity of the proteins[19]. Direct measurements of these are not available to date. As such, uncertainty exist in parameters impacting effects of

AMPK-mTOR signaling on autophagy and treatment effect predictions. However, the current approach of using relative activities of the AMPK-mTOR signaling proteins to evaluate their downstream effects on autophagy provides a useful alternative in absence of absolute proteins data.

To summarize, we developed a QSP framework for autophagy-inducing HDT by integrating a previously developed models for AMPK-mTOR signaling, host-pathogen interactions, and PKPD. We extended the framework to include autophagy to enable in silico evaluations of adjunctive metformin to antibiotics in TB patients. Our predictions suggest that metformin may provide some beneficiary effects when overall bacterial load, or extracellular-to-intracellular bacterial ratio is low. Overall, this is the first QSP that links cellular-level events affecting autophagy to disease progression and may further be developed to guide HDT design and development for treatment of TB.

References

1. Nahid P, Dorman SE, Alipanah N, Barry PM, Brozek JL, Cattamanchi A, Chaisson LH, Chaisson RE, Daley CL, Grzemska M, Higashi JM, Ho CS, Hopewell PC, Keshavjee SA, Lienhardt C, Menzies R, Merrifield C, Narita M, O'Brien R, Peloquin CA, Raftery A, Saukkonen J, Schaaf HS, Sotgiu G, Starke JR, Migliori GB, Vernon A. 2016. Executive Summary: Official American Thoracic Society/Centers for Disease Control and Prevention/Infectious Diseases Society of America Clinical Practice Guidelines: Treatment of Drug-Susceptible Tuberculosis. Clin Infect Dis 63:853–867.
2. Ginsberg AM, Spigelman M. 2007. C O M M E N TA RY Challenges in tuberculosis drug research and development. Nat Med 13:290–294.
3. Mehta K, Spaink HP, Ottenhoff THM, van der Graaf PH, van Hasselt JGC. 2021. Host-directed therapies for tuberculosis: quantitative systems pharmacology approaches. Trends Pharmacol Sci 1–12.
4. Kilinç G, Saris A, Ottenhoff THM, Haks MC. 2021. Host-directed therapy to combat mycobacterial infections. Immunol Rev https://doi.org/10.1111/imr.12951.
5. Young C, Walzl G, Du Plessis N. 2020. Therapeutic host-directed strategies to improve outcome in tuberculosis. Mucosal Immunol 13:190–204.
6. Singhal A, Jie L, Kumar P, Hong GS, Leow MK-S, Paleja B, Tsenova L, Kurepina N, Chen J, Zolezzi F, Kreiswirth B, Poidinger M, Chee C, Kaplan G, Wang YT, De Libero G. 2014. Metformin as adjunct antituberculosis therapy. Sci Transl Med 6:263ra159.
7. Lachmandas E, Eckold C, Böhme J, Koeken VACM, Marzuki MB, Blok B, Arts RJW, Chen J, Teng KWW, Ratter J, Smolders EJ, Van den Heuvel C, Stienstra R, Dockrell HM, Newell E, Netea MG, Singhal A, Cliff JM, Van Crevel R. 2019. Metformin Alters Human Host Responses to Mycobacterium tuberculosis in Healthy Subjects. J Infect Dis 220:139–150.
8. Degner NR, Wang J-Y, Golub JE, Karakousis PC. 2018. Metformin Use Reverses the Increased Mortality Associated With Diabetes Mellitus During Tuberculosis Treatment. Clin Infect Dis an Off Publ Infect Dis Soc Am 66:198–205.
9. Yu X, Li L, Xia L, Feng X, Chen F, Cao S, Wei X. 2019. Impact of metformin on the risk and treatment outcomes of tuberculosis in diabetics: a systematic review. BMC Infect Dis 19:859.
10. van der Graaf PH, Benson N. 2018. The Role of Quantitative Systems Pharmacology in the Design of First-in-Human Trials. Clin Pharmacol Ther. United States https://doi.org/10.1002/cpt.1145.
11. Gumbo T, Angulo-Barturen I, Ferrer-Bazaga S. 2015. Pharmacokinetic-Pharmacodynamic and Dose-Response Relationships of Antituberculosis Drugs: Recommendations and Standards for Industry and Academia. J Infect Dis 211:S96–S106.
12. Gaohua L, Wedagedera J, Small BG, Almond L, Romero K, Hermann D, Hanna D, Jamei M, Gardner I. 2015. Development of a Multicompartment Permeability-Limited Lung PBPK Model and Its Application in Predicting Pulmonary Pharmacokinetics of Antituberculosis Drugs. CPT Pharmacometrics Syst Pharmacol 4:605–613.
13. Marino S, Kirschner DE. 2004. The human immune response to Mycobacterium tuberculosis in lung and lymph node. J Theor Biol 227:463–486.
14. Kirschner D, Pienaar E, Marino S, Linderman JJ. 2017. A review of computational and mathematical modeling contributions to our understanding of Mycobacterium tuberculosis within-host infection and treatment. Curr Opin Syst Biol 3:170–185.
15. Goutelle S, Bourguignon L, Jelliffe RW, Conte JE, Maire P. 2011. Mathematical modeling of pulmonary tuberculosis therapy: Insights from a prototype model with rifampin. J Theor Biol 282:80–92.
16. Lyons MA, Lenaerts AJ. 2015. Computational pharmacokinetics/pharmacodynamics of rifampin in a mouse tuberculosis infection model. J Pharmacokinet Pharmacodyn 42:375–389.
17. Fors J, Strydom N, Fox WS, Keizer RJ, Savic RM. 2020. Mathematical model and tool to explore shorter multi-drug therapy options for active pulmonary tuberculosisPLoS Computational Biology.

18. Sud D, Bigbee C, Flynn JL, Kirschner DE. 2006. Contribution of CD8+ T cells to control of Mycobacterium tuberculosis infection. J Immunol 176:4296–4314.

19. Sonntag AG, Dalle Pezze P, Shanley DP, Thedieck K. 2012. A modelling-experimental approach reveals insulin receptor substrate (IRS)-dependent regulation of adenosine monosphosphate-dependent kinase (AMPK) by insulin. FEBS J 279:3314–3328.

20. Svensson RJ, Aarnoutse RE, Diacon AH, Dawson R, Gillespie SH, Boeree MJ, Simonsson USH. 2018. A Population Pharmacokinetic Model Incorporating Saturable Pharmacokinetics and Autoinduction for High Rifampicin Doses. Clin Pharmacol \& Ther 103:674–683.

21. Denti P, Jeremiah K, Chigutsa E, Faurholt-Jepsen D, PrayGod G, Range N, Castel S, Wiesner L, Hagen CM, Christiansen M, Changalucha J, McIlleron H, Friis H, Andersen AB. 2015. Pharmacokinetics of Isoniazid, Pyrazinamide, and Ethambutol in Newly Diagnosed Pulmonary TB Patients in Tanzania. PLoS One 10:1–19.

22. McCallum AD, Pertinez HE, Else LJ, Dilly-Penchala S, Chirambo AP, Sheha I, Chasweka M, Chitani A, Malamba RD, Meghji JZ, Gordon SB, Davies GR, Khoo SH, Sloan DJ, Mwandumba HC. 2020. Intrapulmonary Pharmacokinetics of First-line Anti-tuberculosis Drugs in Malawian Patients With Tuberculosis. Clin Infect Dis 73:e3365–e3373.

23. Jermain B, Hanafin PO, Cao Y, Lifschitz A, Lanusse C, Rao GG. 2020. Development of a Minimal Physiologically-Based Pharmacokinetic Model to Simulate Lung Exposure in Humans Following Oral Administration of Ivermectin for COVID-19 Drug Repurposing. J Pharm Sci 109:3574–3578.

24. Jayaraman P, Sada-Ovalle I, Nishimura T, Anderson AC, Kuchroo VK, Remold HG, Behar SM. 2013. IL-1β promotes antimicrobial immunity in macrophages by regulating TNFR signaling and caspase-3 activation. J Immunol 190:4196–4204.

25. Reiling N, Homolka S, Walter K, Brandenburg J, Niwinski L, Ernst M, Herzmann C, Lange C, Diel R, Ehlers S, Niemann S. 2013. Clade-specific virulence patterns of Mycobacterium tuberculosis complex strains in human primary macrophages and aerogenically infected mice. MBio 4.

26. Musuka S, Srivastava S, Siyambalapitiyage Dona CW, Meek C, Leff R, Pasipanodya J, Gumbo T. 2013. Thioridazine pharmacokinetic-pharmacodynamic parameters "wobble" during treatment of tuberculosis: A theoretical basis for shorter-duration curative monotherapy with congeners. Antimicrob Agents Chemother 57:5870–5877.

27. Singhal A, Jie L, Kumar P, Hong GS, Leow MKS, Paleja B, Tsenova L, Kurepina N, Chen J, Zolezzi F, Kreiswirth B, Poidinger M, Chee C, Kaplan G, Wang YT, De Libero G. 2014. Metformin as adjunct antituberculosis therapy. Sci Transl Med 6.

28. Howell JJ, Hellberg K, Turner M, Talbott G, Kolar MJ, Ross DS, Hoxhaj G, Saghatelian A, Shaw RJ, Manning BD. 2017. Metformin Inhibits Hepatic mTORC1 Signaling via Dose-Dependent Mechanisms Involving AMPK and the TSC Complex. Cell Metab 25:463–471.

29. Hawley SA, Gadalla AE, Olsen GS, Hardie DG. 2002. The antidiabetic drug metformin activates the AMP-activated protein kinase cascade via an adenine nucleotide-independent mechanism. Diabetes 51:2420–2425.

30. Wallis RS, Vinhas SA, Johnson JL, Ribeiro FC, Palaci M, Peres RL, Sá RT, Dietze R, Chiunda A, Eisenach K, Ellner JJ. 2003. Whole blood bactericidal activity during treatment of pulmonary tuberculosis. J Infect Dis 187:270–278.

31. Sabiiti WS, Bowness RB, Gillespie SHG, Consortium P. 2016. Rapid monitoring of tuberculosis treatment response: A multi-centre study. Eur Respir J 48:OA1513.

32. Hai HT, Vinh DN, Thu DDA, Hanh NT, Phu NH, Srinivasan V, Thwaites GE, T T Thuong N. 2019. Comparison of the Mycobacterium tuberculosis molecular bacterial load assay, microscopy and GeneXpert versus liquid culture for viable bacterial load quantification before and after starting pulmonary tuberculosis treatment. Tuberculosis (Edinb) 119:101864.

33. Alden K, Read M, Timmis J, Andrews PS, Veiga-Fernandes H, Coles M. 2013. Spartan: A Comprehensive Tool for Understanding Uncertainty in Simulations of Biological Systems. PLoS Comput Biol 9.

34. Marino S, Hogue IB, Ray CJ, Kirschner DE. 2008. A methodology for performing global uncertainty and sensitivity analysis in systems biology. J Theor Biol 254:178–196.

35. Fidler M, Wilkins JJ, Hooijmaijers R, Post TM, Schoemaker R, Trame MN, Xiong Y, Wang W. 2019. Nonlinear Mixed-Effects Model Development and Simulation Using nlmixr and Related R Open-Source Packages. CPT pharmacometrics Syst Pharmacol 8:621–633.

36. Ehlers S, Schaible UE. 2012. The granuloma in tuberculosis: dynamics of a host-pathogen collusion. Front Immunol 3:411.

37. Padmapriydarsini C, Mamulwar M, Mohan A, Shanmugam P, Gomathy NS, Mane A, Singh UB, Pavankumar N, Kadam A, Kumar H, Suresh C, Reddy D, Devi P, Ramesh PM, Sekar L, Jawahar S, Shandil RK, Singh M, Menon J, Guleria R. 2021. Randomized Trial of Metformin With Anti-Tuberculosis Drugs for Early Sputum Conversion in Adults With Pulmonary Tuberculosis. Clin Infect Dis 1–30.

Supplementary Materials

The supplementary material can be accessed from the following GitHub repository: https://github.com/krinaj/TB_Autophagy_Metformin_Model

Section V.

Summary and General Discussion

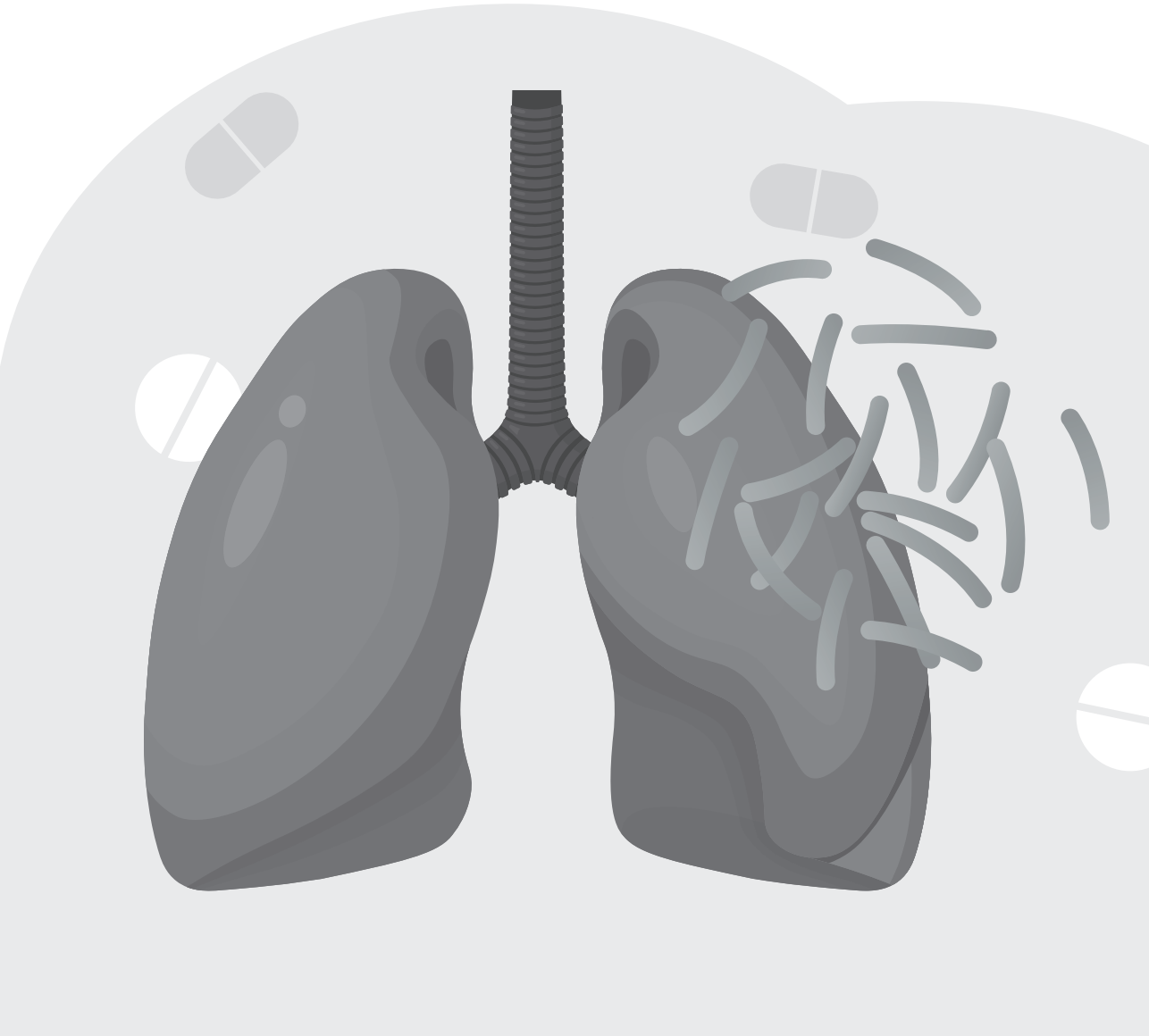

Chapter 9

Summary and General discussion

Tuberculosis (TB) is associated with high morbidity and mortality[1]. Current key challenges against treatment of TB include variability in treatment response, evasion of host immune response, and development of drug resistance. Quantitative pharmacology methods are valuable tools for developing innovative approaches to optimize treatment against Mtb infections to address the challenges effectively and efficiently[2]. In this thesis, we utilized diverse modeling and simulation approaches tailored to specific contexts of use, aiming to tackle the challenges associated with treatment of TB. Key learnings and future perspectives are discussed below divided into themes based on applications of modeling and simulation.

Predictions of drug exposures at sites of action

Understanding the distribution of anti-TB drugs at site-of-action tissues is essential to predict and optimize treatment effects. Lungs and cavitary lung lesion concentrations of bedaquiline and pretomanid have not been collected yet from humans. In **Chapter 4**, translational minimal physiologically-based pharmacokinetic (mPBPK) models of bedaquiline and pretomanid were developed using serum and site-of-action concentrations data from preclinical studies, and serum concentrations data from TB patients. Our model-based simulations suggested that although the currently approved dosing of bedaquiline and pretomanid may achieve lung exposures to exhibit bactericidal activity against replicating bacteria, additional treatment optimization may be required for the eradication of non-replicating bacteria from cavitary lung lesions[3]. In **Chapter 6**, a whole-body PBPK model including central nervous system (CNS) distribution for bedaquiline and its active metabolite, M2, was developed to predict exposures within cerebrospinal fluid (CSF), brain interstitial, and brain intracellular. Bedaquiline and M2 unbound concentrations at target sites, brain interstitial and intracellular, for TB meningitis (TBM) patients, were predicted to be significantly lower than predicted lung intracellular unbound concentrations, suggesting that bedaquiline may not provide an effective treatment option for patients with drug-resistant TBM. In **Chapter 3**, whole-body PBPK models allowed predictions of unbound rifampin and isoniazid exposures at target sites, brain interstitial and intracellular, to evaluate the probability of target attainment for TBM patients. For the drug-susceptible strains, our predictions suggested a high probability (>80%) of target attainment in brain interstitial and intracellular with standard dosing of rifampin and isoniazid, respectively[4]. Consistent with our work, there has been a growing focus on measurement and modeling of lungs and lesion drug concentrations data for anti-TB drugs. For example, mechanistic modeling of seven anti-TB drugs data obtained

from nine different lung lesion types from TB patients demonstrated application of such approach to improve TB treatment outcomes[5,27]. On the other hand, although PBPK models have been applied to predict brain drug concentrations in other therapeutic areas[28], PBPK approach to predict brain drug concentrations of anti-TB drugs have not been published prior to our work.

In the absence of observed relevant target site concentrations data, our models could not be compared against observed data, highlighting a key limitation of such modeling approach. For example, the translational mPBPK models for bedaquiline and pretomanid developed using mice data assumed relatively comparable drug partition coefficients in lungs amongst mice and humans. The CNS PBPK models developed for bedaquiline, rifampin, and isoniazid are reliant on serum and CSF data from patients, and drug distribution to brain interstitial and intracellular compartments is informed by physiological understanding of CNS.

Quantitative pharmacology analyses are reliant on appropriate assumptions and accurate data. In general, the current standard methods for pharmacokinetic (PK) and pharmacodynamic (PD) data collection generally do not include site-of-action measurements; thus, future work could focus more on innovative sampling and measurement methods to obtain relevant and accurate site-of-action PK and PD data[5]. It is not feasible to collect site-of-action samples from large cohorts of patients. Quantitative pharmacology approaches may be used to link data measured using different sampling methods. For example, PK data from a relatively small but significant cohort of patients may be used along with PBPK model-based analyses to quantify the relationships between vascular and site-of-action drug concentrations of anti-TB drugs. Similarly, more refined and precise quantitative relationships could be developed between sputum and site of action Mtb bacterial load data using measurements from a larger pool of patient data than currently available[6,7]. Advancements in newer measurement techniques, for example, imaging techniques capable of measuring PK and PD at the site of action can be very valuable to increasingly support the development of quantitative pharmacology approaches to advance anti-TB therapeutics[8,9].

To summarize, the translational minimal PBPK and whole-body PBPK modeling and simulations performed in this thesis provided insight into target site exposures and target attainment for two first-line, rifampin and isoniazid, and two newer, bedaquiline and pretomanid, anti-TB drugs. These findings can be used to rationally select treatment options for pulmonary TB and TBM patients, as appropriate.

Future advancements in data collection methods combined with quantitative pharmacology approaches are crucial.

Addressing interindividual variability

It is crucial to quantify the interindividual variability affecting PK and PD properties of drugs, as well as the factors influencing this variability. PK of drugs can be affected by various intrinsic factors, e.g., body weight, age, host genotype, and comorbidities, and extrinsic factors, e.g., drug-drug interactions, and smoking status. The PD of drugs is affected by drug exposure at the site-of-action, pathogen genotype, disease severity, etc. Modeling and simulation of anti-TB drugs provide valuable insights into factors affecting interindividual variability to inform treatment optimization approaches[2]. In **Chapter 2**, a top-down population PK modeling approach of ethambutol suggested significant impact of human immunodeficiency virus (HIV) co-infection on reduction in oral bioavailability of ethambutol in pulmonary TB patients. Model-based simulations suggested that a supplementary 400 mg QD ethambutol dosing among HIV/TB co-infected patients may provide a strategy to optimize anti-TB treatment regimens in this high-risk population[10].

In **Chapter 3**, using a bottom-up modeling approach, whole-body PBPK models for rifampin and isoniazid were developed to predict the impact of solute carrier organic anion transporter family member 1B1 (SLCO1B1) genotype on rifampin and N-acetyltransferase 2 (NAT2) genotype on isoniazid, and minimum inhibitory concentrations (MIC) on CNS target attainment following standard and intensified dosing regimen in patients with TBM. The combined effects of genotype and MIC were potent determinants of CNS target attainment of rifampin and isoniazid, providing a direction for future evaluations of precision dosing of rifampin and isoniazid in TBM patients[4]. In **Chapter 4,** translational mPBPK model–based simulations for bedaquiline and pretomanid suggested no significant effects of the size of cavitary lung lesions and body weight on target attainment within lungs and lung lesions in pulmonary TB patients[3]. In **Chapter 5**, the translational mPBPK models of bedaquiline and pretomanid were incorporated within a mechanistic modeling framework to simulate the anti-bacterial efficacy of the combination regimen BPaL. The framework included the dynamics of TB disease progression, drug distribution and available effective fraction into lung and lesions, individual drug effects, PD drug interactions, and the effect of MIC. Our framework predicted no significant impact of covariates, body weight, and MIC, on the overall efficacy of the BPaL combination[11]. In the recent years, mechanistic model-based evaluations

of variability in anti-TB drugs' PK and effects have been performed[27,29-31]. For example, similar to our findings, a published mechanistic model including TB granuloma size predicted no significant impact of granuloma size on duration to granuloma sterilization[31].

The majority of approaches for quantification of covariate effects and interindividual variability have relied on top-down empirical modeling[2]. In this thesis, we also explored how mechanistic model-based approaches can be used to identify covariates that may affect the variability in PK and anti-TB treatment outcome. A key constraint to using mechanistic modeling approach to evaluate interindividual variability is that full mechanistic details of factors that may affect interindividual variability are often not understood a priori. Additionally, models to identify factors affecting interindividual variability are best developed when a large amount of patient level data is available. Moreover, analysis of larger pool of data within mechanistic modeling framework is computationally costly. Future work may consider applications of advanced computational methods, such as Bayesian approaches and machine learning methods using a larger pool of relevant clinical data, along with mechanistic models for robust characterization of covariate–parameter relationships[12,13]. Additionally, various patient data collection methods, including the incorporation of real-world evidence, electronic health records, wearables, etc may be used to support the development of the proposed models. Predictions using such models can be used to rationally guide treatment optimization approaches against TB.

To conclude, the evaluations of the factors affecting PK and PD of anti-TB drugs were demonstrated using top-down and bottom-up modeling approaches depending on available data. These results can be useful to evaluate model-informed precision dosing options. Future efforts should increasingly consider evaluations of data from a variety of sources using mechanistic modeling approaches to guide treatment optimization approaches based on patient factors affecting variability.

Translation from experiments to patients

Accurate translation of PK and PD of new anti-TB drugs from preclinical experiments to patients is essential to rationally design clinical studies. In **Chapter 4**, predictions of exposures in lungs and lesions of TB patients were performed using data from PK studies in mice[3]. This demonstrated the usefulness of the PBPK model-based approach to predict the site of action distribution of anti-TB

drugs, although the predictive power of these models could not be evaluated due to the lack of human lungs and lesion PK data for bedaquiline and pretomanid to date. In **Chapter 5**, translational mPBPK models were extended into a quantitative modeling framework for bedaquiline, pretomanid, and linezolid (BPaL) combination regimen using a variety of in vitro experimental data, such as time-kill experiments in culture, hollow-fiber infection model (HFIM)m, and in vitro PD interaction studies, and PK and early-bactericidal activities data from clinical studies in TB patients. The quantitative framework–based simulations for the combination therapy effects in multidrug resistant TB (MDR-TB) patients matched reasonably well with the observed clinical trial data[11]. In **Chapter 8**, lung bacterial load data from a mice infection study were used to inform metformin-induced autophagy effects within the host-pathogen interactions model. The model-based simulations suggested that adjunctive metformin therapy to first-line anti-TB therapy in TB patients would provide limited effect on reducing the bacterial load. More importantly, the model provided insights into the differences in the overall effects of adjunctive metformin therapy between mice and TB patients (**Chapter 8** Section 8.4)[14]. Similar to our work, application of quantitative framework has also recently been published to efficiently translate effects of anti-TB drugs effects from preclinical to clinical[32,33].

Efficient and accurate preclinical data collection methods are crucial to study the PK and PD of anti-TB drugs and to construct a quantitative framework. Data from preclinical in vivo studies, for example, site of action distribution and immunodynamics data for host-directed therapy (HDTs), sometimes do not directly translate to patients; thus, increasing evaluations of alternative experimental methods combined with modeling and simulations may be beneficial in future. For example, multiple vascularized organ chips may be developed, and data from such a model along with PBPK modeling can be used to predict human serum and target site of action PK of anti-TB drugs efficiently and accurately[15]. Target site PK predictions can then be used along with time-kill experiments at varying drug concentrations from HFIM or in vitro culture experiments to predict early bactericidal activities in patients. Omics experimental data combined with artificial intelligence methods may be evaluated to parameterize QSP models of host-pathogen interactions[16].

In conclusion, we demonstrated the importance of quantitative approaches to compile the findings from various preclinical data into a decision-making framework. It is important to continue to develop innovative data collection methods and to use model-informed approaches to overcome preclinical to patient translational challenges.

Treatment of multi-drug resistant tuberculosis

MDR-TB is caused by Mtb strains resistant against both rifampin and isoniazid, two key first-line anti-TB drugs. The recent approval of the new combination regimen BPaL against MDR-TB has been a key step towards the resolution of the global health challenge of drug-resistant tuberculosis. Some safety and adherence concerns remain with the BPaL-approved dosing schedules[17,18]. In **Chapter 5**, a quantitative modeling framework was developed for the BPaL combination regimen. The framework adequately described the observed antibacterial activity data in patients following monotherapy for each drug and approved BPaL dosing. The simulations for approved and alternative dosing regimens suggested that similar efficacy could be attained by using alternative dosages of bedaquiline and linezolid in the BPaL combination. The alternative dosage has the potential to enhance safety and adherence. Additionally, the simulations provided insights into the approximate treatment duration required for the eradication of both replicating and non-replicating Mtb from lung lesions. The BPaL quantitative platform can be used to assess treatment optimization approaches, including dosing regimen and duration of treatment predictions to eradicate both replicating- and non-replicating bacteria from lungs and lesions to ensure appropriate treatment and to avoid relapse of MDR-TB patients.[11] In alignment with our predictions, recently published clinical data and top-down model-based analysis of the data evaluating the approved and alternative linezolid dosing predicted no significant difference in efficacy between the approved and alternative linezolid doses in MDR-TB patients[18,29].

To eradicate TB in the future, treatment approaches should consider not only treatment of drug-resistant TB but also prevention of resistance development. To accomplish this goal, exploration of rigorous treatment approaches could be employed. As discussed, quantitative platforms could be used to guide the optimization of dosing regimens and treatment duration based on patient factors. For example, individual drugs' MIC, could be used to guide dosing and treatment duration to ensure eradication of both replicating- and non-replicating Mtb. Models can be used to ensure optimal exposures at the target site of action to ensure adequate efficacy, to prevent the development of drug resistance, and to manage safety concerns[19,20]. This may help increase patient adherence and avoid treatment interruptions that play a crucial role in achieving overall positive treatment outcomes in MDR-TB patients. Additionally, future work could consider extension of our BPaL quantitative framework to include PK and PD of additional drugs to guide the selection of optimal combination regimens based on patient factors[21].

To summarize, we presented a quantitative framework for predicting dosing regimens of BPaL combination treatment in MDR-TB patients. The framework can be used to evaluate treatment optimization approaches for the BPaL combination. We propose future development and use of quantitative frameworks to support the development of new treatment approaches against MDR-TB.

Treatment of tuberculosis meningitis

Relatively rare but the most severe form of TB, TBM, is associated with high morbidity and mortality rates to date. In this thesis, model-based approaches to predict PK exposures within CNS to evaluate intensified dosing schedules were explored (Section 91.1). As discussed in **Chapter 3**, intensified dosing schedules of rifampin and isoniazid are required for a subset of patients based on pharmacogenetics and Mtb MIC to achieve therapeutically desirable exposures within the brain for the treatment of TBM. Additionally, the cases of rifampin- and isoniazid-resistant TBM are on the rise and there is no standard-of-care treatment regimen that is safe and efficacious for those patients. Therefore, newer anti-TB drugs, such as bedaquiline, are being evaluated as a treatment option for such cases[9,22]. In **Chapter 6**, we predicted bedaquiline unbound concentrations within brain intracellular compartments to be significantly lower than predicted lung intracellular concentrations range using a whole-body PBPK modeling approach. This suggested that bedaquiline may not be suitable for the treatment of drug-resistant TBM and that additional newer anti-TB drugs should be evaluated for this population.

In this thesis, we introduced PBPK approach to predict brain drug concentrations of anti-TB drugs for the treatment of TBM. A limitation of this approach is that it is not feasible to collect samples from patients to be able to compare model predictions against. However, as we showcased, observed CSF drug concentrations combined with PBPK approach and in vitro MIC data may provide a broader view of overall effects of anti-TB drugs for treatment of TBM.

The current first-line treatment regimen against TBM is ineffective in a high number of patients and intensified rifampin and/or isoniazid dosing is often required[23,24]. Future work may focus on the implementation of a PBPK-based modeling framework to guide dose and dosing regimen optimization, including intensified dosing as needed, to ensure optimal CNS exposure based on patient factors, such as patient genotype, individual MIC, body weight, etc. Although intensified

rifampin and isoniazid dosing provide improved efficacy in TBM patients compared to standard dosing, they can be associated with increased safety concerns. There seems to be an apparent need to further evaluate current newer anti-TB drugs for TBM patients, and increasing the use of quantitative pharmacology methods could offer an efficient and reliable strategy. In silico approaches can also help identify desired physicochemical and kinetic properties to guide the discovery of new anti-TB drugs with high CNS penetration and anti-TB efficacy.

To conclude, the use of PBPK models to predict brain target attainment for rifampin and isoniazid to identify TBM patient populations who may require intensified treatment approaches. Additionally, the use of the PBPK approach to predict the suitability of newer drugs, such as bedaquiline, for the treatment of TBM was demonstrated. Further efforts in the discovery and development of treatment approaches for the effective treatment of TBM, especially drug-resistant TBM, are essential.

Host-directed therapies to harness the power of immune response to fight against tuberculosis

HDTs that modulate host-pathogen interactions to enhance the effect of host immune response against Mtb offer innovative treatment options and are being evaluated. In **Chapter 7**, key HDT mechanisms were reviewed, such as autophagy induction, regulation of host epigenetics, and modulation of cytokine and T-cell responses. Next, the use of QSP modeling approaches was proposed to facilitate the design of novel HDT combination treatment strategies and discussed the components of QSP models[14]. In **Chapter 8**, we exhibited an example of using QSP modeling with experimental data to predict the effects of metformin-associated autophagy induction combined with first-line anti-TB treatment in patients. The model-based simulations for adjunctive metformin therapy in newly diagnosed patients suggested a limited yet dose-dependent effect of metformin on reducing the intracellular bacterial load when overall bacterial load is low, and late during antibiotic treatment[14]. This framework may be extended to guide the design of HDTs against Mtb. Literature-based examples of evaluations of host-pathogen interactions mathematical models to evaluate vaccine candidates are available; however, such models have not been utilized to support evaluations of HDTs prior to our work[34].

Future work could consider an extension of the QSP framework (**Chapter 8**) with additional HDT pathways as illustrated in **Chapter 7**. Simulations using such models can be used to identify HDT targets to evaluate and design treatment approaches. Moreover, integrating the HDT QSP model with the extended multistate tuberculosis pharmacometrics model - PKPD quantitative framework (**Chapter 5**) may be valuable in designing optimal HDT and anti-TB antibiotic combinations to fight against MDR-TB and to prevent the development of resistance against anti-TB drugs[25,26]. As the development of QSP models for HDTs in the context of drug-host-pathogen interactions is contingent upon comprehensive mechanistic understanding, future work could focus on addressing the current knowledge gaps through efforts to collect relevant experimental data and using QSP in learn-and-confirm paradigm[35].

In conclusion, the content and applications of QSP models to efficiently evaluate HDT treatment approaches against Mtb were discussed. Then, an example of the proposed QSP model-based approach was demonstrated using metformin as an autophagy induced combined with first-line anti-TB treatment.

Conclusions

In this thesis, we demonstrated that it is imperative to increasingly employ model-informed drug development and treatment optimization methodologies to effectively combat TB. We applied modeling and simulation approaches to tackle key TB treatment challenges, including target site exposures, factors affecting interindividual variability, translation of experimental findings to patients, and enhancing treatment of drug resistance TB and TBM. Several takeaways were derived from this work. For instance, PBPK model-based predictions of target site exposures after accounting for intrinsic and extrinsic factors affecting interindividual variability in PK can be useful to optimize dosing schedules anti-TB drugs to attain optimal Mtb killing. PBPK models are also well suited to understand tissue distribution and binding characteristics of drugs enabling translational prediction of a drug's viability for treating different forms of TB, including, pulmonary TB and TBM. Similarly, quantitative frameworks, e.g., BPaL combination framework, can be useful to develop new combination regimens and to evaluate treatment optimization approaches for combination regimens against TB, especially drug-resistant TB. Moreover, we discussed leveraging host-pathogen interactions for treatment of TB and showcased the use of QSP for evaluating adjunctive HDTs for TB treatment. A key limitation to applying quantitative

pharmacology approaches to inform anti-TB treatment approaches is often the availability of relevant mechanistic information and data. Future efforts should consider collecting and incorporating data from diverse sources into mechanistic modeling frameworks to guide treatment approaches against TB more effectively and efficiently.

References

1. Nahid P, Dorman SE, Alipanah N, et al. Executive Summary: Official American Thoracic Society/Centers for Disease Control and Prevention/Infectious Diseases Society of America Clinical Practice Guidelines: Treatment of Drug-Susceptible Tuberculosis. *Clinical Infectious Diseases*. 2016;63(7):853-867. doi:10.1093/cid/ciw566
2. Wilkins JJ, Svensson EM, Ernest JP, Savic RM, Simonsson USH, McIlleron H. Pharmacometrics in tuberculosis: progress and opportunities. *International Journal of Antimicrobial Agents*. 2022;60(3). doi:10.1016/j.ijantimicag.2022.106620
3. Mehta K, Guo T, van der Graaf PH, van Hasselt JGC. Predictions of Bedaquiline and Pretomanid Target Attainment in Lung Lesions of Tuberculosis Patients using Translational Minimal Physiologically Based Pharmacokinetic Modeling. *Clin Pharmacokinet*. 2023;62(3):519-532. doi:10.1007/s40262-023-01217-7
4. Mehta K, Narayanan N, Heysell SK, et al. Pharmacogenetic variability and the probability of site of action target attainment during tuberculosis meningitis treatment: A physiologically based pharmacokinetic modeling and simulations study. *Tuberculosis*. 2022;137:102271. doi:10.1016/j.tube.2022.102271
5. Strydom N, Gupta SV, Fox WS, et al. Tuberculosis Drugs' Distribution and Emergence of Resistance in Patient's Lung Lesions: A Mechanistic Model and Tool for Regimen and Dose Optimization. Vol 16.; 2019. doi:10.1371/journal.pmed.1002773
6. Bowness R, Boeree MJ, Aarnoutse R, et al. The relationship between mycobacterium tuberculosis mgit time to positivity and cfu in sputum samples demonstrates changing bacterial phenotypes potentially reflecting the impact of chemotherapy on critical sub-populations. *Journal of Antimicrobial Chemotherapy*. 2015;70(2):448-455. doi:10.1093/jac/dku415
7. Svensson RJ, Sabiiti W, Kibiki GS, et al. Model-Based Relationship between the Molecular Bacterial Load Assay and Time to Positivity in Liquid Culture. Published online 2019. doi:10.1128/AAC
8. Mota F, Ruiz-Bedoya C, Tucker E, De Jesus P, Flavahan K, Turner M E, C, Bahr M, Kim J, Farina M, Peloquin CA, Ordonez A JSK. Noninvasive Assessment of Intralesional Antimicrobial Concentration- Time Profiles in Pulmonary and Central Nervous System Tuberculosis using Dynamic 18F-Pretomanid Positron Emission Tomography. *OFID 2021:8 Session: P-80 Tuberculosis and other Mycobacterial Infections*. Published online 2021:789-790.
9. Mota F, Ruiz-Bedoya CA, Tucker EW, et al. Dynamic 18F-Pretomanid PET imaging in animal models of TB meningitis and human studies. *Nature Communications*. 2022;13(1):7974. doi:10.1038/s41467-022-35730-3
10. Mehta K, Ravimohan S, Pasipanodya JG, et al. Optimizing ethambutol dosing among HIV/tuberculosis co-infected patients: a population pharmacokinetic modelling and simulation study. *J Antimicrob Chemother*. 2019;74(10):2994-3002. doi:10.1093/jac/dkz265
11. Mehta K, Guo T, van der Graaf PH, van Hasselt JGC. Model-based dose optimization framework for bedaquiline, pretomanid and linezolid for the treatment of drug-resistant tuberculosis. *British Journal of Clinical Pharmacology*. 2023;n/a(n/a). doi:10.1111/bcp.15925
12. Libiseller-Egger J, Wang L, Deelder W, Campino S, Clark TG, Phelan JE. TB-ML-a framework for comparing machine learning approaches to predict drug resistance of Mycobacterium tuberculosis. *Bioinform Adv*. 2023;3(1):vbad040. doi:10.1093/bioadv/vbad040
13. Keutzer L, You H, Farnoud A, et al. Machine Learning and Pharmacometrics for Prediction of Pharmacokinetic Data: Differences, Similarities and Challenges Illustrated with Rifampicin. *Pharmaceutics*. 2022;14(8). doi:10.3390/pharmaceutics14081530
14. Mehta K, Guo T, Wallis RS, van der Graaf PH, van Hasselt JGC. Quantitative Systems Pharmacology Modeling Framework of Autophagy in Tuberculosis: Application to Adjunctive Metformin Host-Directed Therapy. *Antimicrob Agents Chemother*. 2022;66(8):e0036622. doi:10.1128/aac.00366-22

15. Herland A, Maoz BM, Das D, et al. Quantitative prediction of human pharmacokinetic responses to drugs via fluidically coupled vascularized organ chips. *Nat Biomed Eng*. 2020;4(4):421-436. doi:10.1038/s41551-019-0498-9

16. Mehta K, Spaink HP, Ottenhoff THM, van der Graaf PH, van Hasselt JGC. Host-directed therapies for tuberculosis: quantitative systems pharmacology approaches. *Trends in Pharmacological Sciences*. 2022;43(4):293-304. doi:10.1016/j.tips.2021.11.016

17. Conradie F, Diacon AH, Ngubane N, et al. Treatment of Highly Drug-Resistant Pulmonary Tuberculosis. *New England Journal of Medicine*. 2020;382(10):893-902. doi:10.1056/nejmoa1901814

18. Conradie F, Bagdasaryan TR, Borisov S, et al. Bedaquiline–Pretomanid–Linezolid Regimens for Drug-Resistant Tuberculosis. *New England Journal of Medicine*. 2022;387(9):810-823. doi:10.1056/nejmoa2119430

19. Alffenaar JWC, Akkerman OW, Kim HY, Tiberi S, Migliori GB. Precision and personalized medicine and anti-TB treatment: Is TDM feasible for programmatic use? *International Journal of Infectious Diseases*. 2020;92:S5-S9. doi:10.1016/j.ijid.2020.01.041

20. Sturkenboom MGG, Märtson AG, Svensson EM, et al. Population Pharmacokinetics and Bayesian Dose Adjustment to Advance TDM of Anti-TB Drugs. *Clinical Pharmacokinetics*. 2021;60(6):685-710. doi:10.1007/s40262-021-00997-0

21. Gumbo T, Chapagain M, Magombedze G, et al. Novel tuberculosis combination regimens of two and three-months therapy duration. doi:10.1101/2022.03.13.484155

22. Davis A, Meintjes G, Wilkinson RJ. Treatment of Tuberculous Meningitis and Its Complications in Adults. *Current Treatment Options in Neurology*. 2018;20(3). doi:10.1007/s11940-018-0490-9

23. Cresswell FV, Meya DB, Kagimu E, et al. High-Dose Oral and Intravenous Rifampicin for the Treatment of Tuberculous Meningitis in Predominantly Human Immunodeficiency Virus (HIV)-Positive Ugandan Adults: A Phase II Open-Label Randomized Controlled Trial. *Clinical Infectious Diseases*. 2021;73(5):876-884. doi:10.1093/cid/ciab162

24. Seddon JA, Wilkinson R, van Crevel R, et al. Knowledge gaps and research priorities in tuberculous meningitis. *Wellcome Open Research*. 2019;4:1-18. doi:10.12688/wellcomeopenres.15573.1

25. Abreu R, Giri P, Quinn F. Host-Pathogen Interaction as a Novel Target for Host-Directed Therapies in Tuberculosis. *Frontiers in Immunology*. 2020;11(July):1-14. doi:10.3389/fimmu.2020.01553

26. Allué-Guardia A, Garcia-Vilanova A, Olmo-Fontánez AM, et al. Host- and Age-Dependent Transcriptional Changes in Mycobacterium tuberculosis Cell Envelope Biosynthesis Genes after Exposure to Human Alveolar Lining Fluid. *International Journal of Molecular Sciences*. 2022;23(2). doi:10.3390/ijms23020983

27. Yun HY, Chang V, Radtke KK, Wang Q, Strydom N, Chang MJ, Savic RM. Model-Based Efficacy and Toxicity Comparisons of Moxifloxacin for Multidrug-Resistant Tuberculosis. Open Forum Infect Dis. 2021 Dec 29;9(3):ofab660. doi: 10.1093/ofid/ofab660.

28. Gaohua L, Neuhoff S, Johnson TN, Rostami-Hodjegan A, Jamei M. Development of a permeability-limited model of the human brain and cerebrospinal fluid (CSF) to integrate known physiological and biological knowledge: Estimating time varying CSF drug concentrations and their variability using in vitro data, Drug Metab. Pharmacokinet. 2016, Vol31, Issue3, Pages 224-233. doi: 10.1016/j.dmpk.2016.03.005.

29. Belén P Solans, Marjorie Z Imperial, Morounfolu Olugbosi, Rada M Savic, Analysis of Dynamic Efficacy Endpoints of the Nix-TB Trial, Clinical Infectious Diseases, Volume 76, Issue 11, 1 June 2023, Pages 1903–1910, https://doi.org/10.1093/cid/ciad051

30. Humphries, H, Almond, L, Berg, A, et al. Development of physiologically-based pharmacokinetic models for standard of care and newer tuberculosis drugs. CPT Pharmacometrics Syst Pharmacol. 2021; 10: 1382–1395. https://doi.org/10.1002/psp4.12707

31. Cicchese, JM, Dartois V, Kirschner DE, Linderman JJ. Both Pharmacokinetic Variability and Granuloma Heterogeneity Impact the Ability of the First-Line Antibiotics to Sterilize Tuberculosis Granulomas. Frontiers in Pharmacology. Vol11, 2020. doi: 10.3389/fphar.2020.00333

32. Ernest JP, Goh JJ, Strydom N, Wang Q, Wijk R, Zhang N, Deitchman A, Nuermberger E, Savic RM. Translational predictions of phase 2a first-in-patient efficacy studies for antituberculosis drugs. European Respiratory Journal Aug 2023, 62 (2) 2300165; DOI: 10.1183/13993003.00165-2023

33. Ernest JP, Strydom N, Wang Q, Zhang N, Nuermberger E, Dartois V, Savic RM. Development of New Tuberculosis Drugs: Translation to Regimen Composition for Drug-Sensitive and Multidrug-Resistant Tuberculosis. Annu Rev Pharmacol Toxicol. 2021 Jan 6;61:495-516. doi: 10.1146/annurev-pharmtox-030920-011143.

34. Joslyn LR, Linderman JJ, and Kirschner DE. A virtual host model of Mycobacterium tuberculosis infection identifies early immune events as predictive of infection outcomes. Journal of Theoretical Biology. 2022; Vol539. https://doi.org/10.1016/j.jtbi.2022.111042.

35. Lesko LJ. Perspective on model-informed drug development. CPT Pharmacometrics Syst Pharmacol. 2021 Oct;10(10):1127-1129. doi: 10.1002/psp4.12699.

Hoofdstuk 10.

Nederlandse samenvatting

Tuberculose (TB) wordt jaarlijks in verband gebracht met 1,5 miljoen sterfgevallen. TB-infecties vereisen een behandeling met een combinatie van meerdere antibiotica gedurende ten minste 6 tot 9 maanden. Niet alle patiënten reageren optimaal op de bestaande behandelingsschema's, wat veroorzaakt kan worden door verschillende factoren, zoals de hoeveelheid geneesmiddelen die de plaats van infectie bereiken, zoals de longen. Bovendien veroorzaken sommige geneesmiddelen die voor de behandeling van TB worden gebruikt ernstige bijwerkingen, en ten slotte worden TB-bacteriën steeds vaker resistent tegen de meest gebruikte antibiotica, waardoor ze minder effectief zijn of niet meer werken. Er bestaat daarom behoefte aan het optimaliseren van zowel de huidige als nieuwe antibioticacombinatiebehandelingsstrategieën om de effectiviteit van behandelingen van TB te verbeteren.

Wiskunde modellen in de kwantitatieve farmacologie beschrijven zowel de farmacokinetiek (PK), d.w.z. het proces waarbij geneesmiddelen zich in het lichaam verspreiden en worden geëlimineerd, en de farmacodynamiek (PD), d.w.z. het tijdsverloop van de effecten van geneesmiddelen, zoals het effect van antibiotica op TB-pathogenen. Wiskunde PK-PD modellen kunnen worden gebruikt om behandelingsschema's met TB-geneesmiddelen te bestuderen en te optimaliseren om het succespercentage van de behandeling te verbeteren en het risico op bijwerkingen te verminderen.

Om een succesvolle behandeling te garanderen, is het belangrijk om te begrijpen hoeveel anti-TB-geneesmiddelen de plaats van infectie bereiken. In hoofdstuk 3 vonden wij dat het medicijn rifampicine en isoniazide beide voldoende hoge concentraties in de hersenen kunnen bereiken om TB-meningitispatiënten effectief te behandelen. In hoofdstuk 6 vonden wij echter dat het TB-medicijn bedaquiline mogelijk niet de vereiste concentraties in de hersenen bereikt na standaarddosering bij TB-meningitispatiënten die resistent zijn tegen rifampine of isoniazide. In hoofdstuk 4 laten onze modelvoorspellingen aan dat standaarddoses van bedaquiline en pretomanide geneesmiddelconcentraties in de longen kunnen bereiken voor voldoende werkzaamheid. Aanpassing van de dosering kan mogelijk echter het risico op resistentieontwikkeling verlagen.

Het is cruciaal om de factoren te identificeren die kunnen leiden tot variabele responses op anti-TB-geneesmiddelen bij verschillende soorten patiënten. In hoofdstuk 2 ontdekten we dat een hogere dosis ethambutol bij TB-patiënten met co-infectie met hiv een beter behandelingsresultaat kan opleveren. In hoofdstuk 3 brachten wij de invloed van het genotype van patiënten en de

bacteriestam op de concentraties van rifampine en isoniazide in de hersenen van TB-meningitispatiënten. In hoofdstuk 4 en 5 vinden wij met modellen voor bedaquiline en pretomanide dat er geen duidelijke effecten van lichaamsgewicht, bacteriestam en TB-cavitygrootte op het resultaat van de combinatiebehandeling met bedaquiline, pretomanide en linezolid (BPaL).

Nauwkeurige vertaling van gegevens over nieuwe geneesmiddelen tegen TB van preklinische experimenten naar patiënten is essentieel voor het goed ontwerpen van klinische studies. In hoofdstuk 4 en 5 hebben we laten zien hoe modellering gebruikt kan worden om de bevindingen van verschillende preklinische gegevens te combineren, met BPaL-combinatietherapie als voorbeeld. De BPaL-combinatietherapie is van bijzonder belang voor de behandeling van TB-infecties die resistent zijn tegen twee belangrijke eerstelijns geneesmiddelen, rifampicine en isoniazide. Er zijn echter zorgen over de veiligheid en therapietrouw bij standaard BPaL doseringsschema's. In hoofdstuk 5 ontwikkelden we een model voor het BPaL-combinatieschema. Dit model werd gebruikt om alternatieve BPaL-doseringsschema's te simuleren die mogelijk de veiligheid en therapietrouw verbeteren. Daarnaast verschaften onze simulaties inzicht in de behandelingsduur die nodig is om TB-bacteriën volledig te elimineren, om te voorkomen dat de symptomen terugkeren of dat resistentie zich ontwikkelt.

Gastheergestuurde therapieën (HDT's) proberen de immuunrespons van de gastheer (d.w.z. de patiënt) tegen TB-bacteriën te stimuleren. HDT's worden beschouwd als een potentiële nieuwe behandelingsstrategie voor TB, hoewel hun effectiviteit nog niet duidelijk is aangetoond in klinische studies. In hoofdstuk 7 bespreken we hoe modelgebaseerde voorspellingen kunnen helpen om de ontwikkeling van HDT's te ondersteunen. In hoofdstuk 8 onderzochten wij met een modelgedreven benadering de toepassing van metformine als autofagie-inducerend middel in combinatie met eerstelijns anti-TB-behandeling. Het ontwikkelde model kan verder worden uitgebreid om de ontwikkeling van andere HDT's tegen TB te ondersteunen.

Samenvattend beschrijft dit proefschrift hoe kwantitatieve farmacologische modelvoorspellingen kunnen bijdragen aan de verdere ontwikkeling en optimalisatie van zowel bestaande als nieuwe therapieën en behandelstrategieën tegen TB.

Section VI.

Appendices

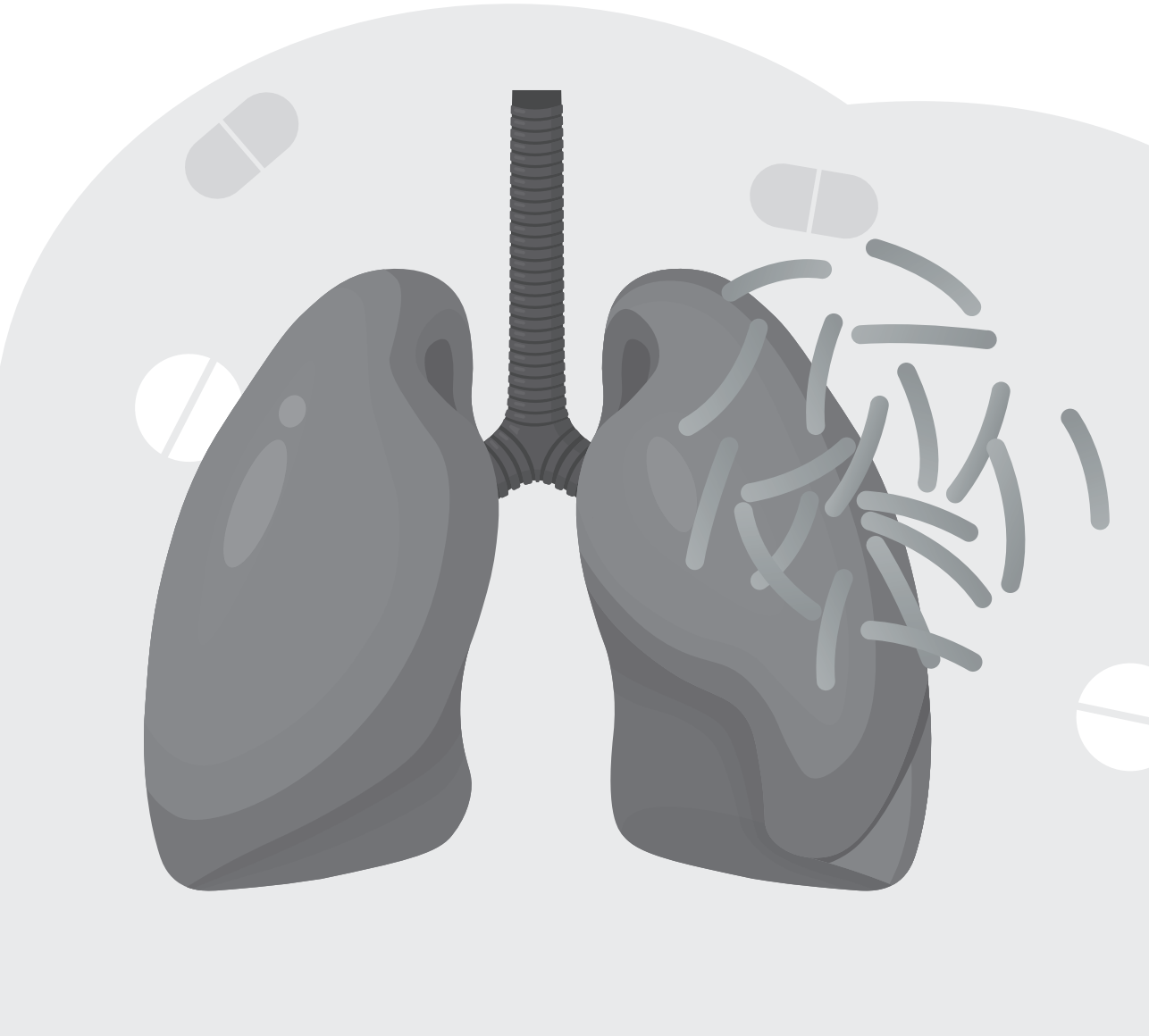

Curriculum vitae

Krina Mehta (1983, Bhavnagar, Gujarat, India) obtained her Bachelor of Pharmacy (BPharm) degree from the Saurashtra University, Gujarat, in 20004. Krina moved to the United States in 2005 and worked as a pharmacovigilance scientist and regulatory documentation scientist for approximately 10 years. Her work in these areas helped her gain a deep understanding of drug development, clinical trials and regulatory processes. In 2015, Krina enrolled in a Master's program in Pharmacometrics program at the University of Maryland, where she received broad training in the field of pharmacometrics, with a focus on strategic applications of pharmacometrics in drug development. In 2016, while pursuing her master's degree, Krina started working as a pharmacometrics contractor, where she performed population PK modeling, R shiny application development, first-in-human dose predictions, and exposure-response modeling. In 2018, Krina joined qPharmetra LLC as an a pharmacometrics consultant and contributed to several projects by utilizing pharmacometrics approaches to support decision making and regulatory submissions.

In 2021, Krina started her PhD program at Leiden University, The Netherlands, under supervision of Coen van Hasselt and Piet van der Graaf, in parallel to her main positions at qPharmetra. Here, the project was focused on the use of model-based approaches in optimization of treatments against tuberculosis. Krina joined Kyowa Kirin Inc as a pharmacometrics scientist in 2020, and as of January 2024, Krina became Director, Pharmacometrics at Kyowa Kirin Inc. In her role at Kyowa Kirin, she has supported incorporation of pharmacometric and quantitative systems pharmacology (QSP) approaches for effective and efficient drug development for innovative modalities in oncology and rare disease.

List of publications

Journal Publications

1. Mehta, K, Balazki P, van der Graaf, PH, Guo, T,van Hasselt, JGC. Predictions of bedaquiline central nervous system exposure in tuberculosis meningitis patients using physiologically-based pharmacokinetic modeling. Clin Pharmacokinet. 2024 Mar 26. doi: 10.1007/s40262-024-01363-6.
2. Mehta, K, Guo, T, van der Graaf, PH, van Hasselt, JGC. Model-based dose optimization framework for bedaquiline, pretomanid and linezolid for the treatment of drug-resistant tuberculosis. Br J Clin Pharmacol. 2023; 1-12. doi:10.1111/bcp.15925.
3. Mehta, K., Guo, T., van der Graaf, P.H. et al. Predictions of Bedaquiline and Pretomanid Target Attainment in Lung Lesions of Tuberculosis Patients using Translational Minimal Physiologically Based Pharmacokinetic Modeling. Clin Pharmacokinet 62, 519–532 (2023). doi:10.1007/s40262-023-01217-7.
4. Mehta K, Narayanan N, Heysell SK, Bisson GP, Subbian S, Kurepina N, Kreiswirth BN, Vinnard C. Pharmacogenetic variability and the probability of site of action target attainment during tuberculosis meningitis treatment: A physiologically based pharmacokinetic modeling and simulations study. Tuberculosis (Edinb). 2022 Dec; 137:102271. doi: 10.1016/j.tube.2022.102271.
5. Mehta K, Guo T, Wallis RS, van der Graaf PH, van Hasselt JGC. Quantitative Systems Pharmacology Modeling Framework of Autophagy in Tuberculosis: Application to Adjunctive Metformin Host-Directed Therapy. Antimicrob Agents Chemother. 2022 Aug 16;66(8):e0036622. doi: 10.1128/aac.00366-22.
6. Mehta K, Spaink HP, Ottenhoff THM, van der Graaf PH, van Hasselt JGC. Host-directed therapies for tuberculosis: quantitative systems pharmacology approaches. Trends Pharmacol Sci. 2022 Apr;43(4):293-304. doi: 10.1016/j.tips.2021.11.016.
7. Oni-Orisan, A., Srinivas, N., Mehta, K., Das, J.L., Nguyen, T.T., Tison, G.H., Bauer, S.R., Burian, M., Funk, R.S., Graham, R.A. and (2021), Leveraging innovative technology to generate drug response phenotypes for the advancement of biomarker-driven precision dosing. Clin Transl Sci, 14: 784-790. doi: 10.1111/cts.12973.
8. Mehta K, Ravimohan S, Pasipanodya J, et al. (2019). Optimizing ethambutol dosing among HIV/tuberculosis co-infected patients: a population pharmacokinetic modelling and simulation study. The Journal of antimicrobial chemotherapy. doi: 10.1093/jac/dkz265.

Conference Posters

1. Mehta K, Storopoli J, Ramwani N, et al., Burosumab treatment-induced increases in serum phosphate are associated with reduction in fracture counts in adults with x-linked hypophosphatemia as assessed with graded item response analysis. Poster ACoP · Nov 11, 2023.
2. Mehta K, Barriere O, Gosselin NH, et al., Burosumab treatment-induced increases in serum phosphate provide improvements in patient reported outcomes in adults with x-linked hypophosphatemia as assessed with graded item response analysis. Poster ACoP · Nov 2, 2022.
3. Mehta K, Patel D, Vupugalla R, et al., Rationale for the clinical use of less frequent dosing of mogamulizumab for T-cell lymphomas using population pharmacokinetic and exposure response analysis. Poster American Society of Hematology 2021 Conference. Abstract 2475 · Dec 12, 2021.
4. Mehta K, Koshiba S, Hasegawa M, et al., Population pharmacokinetic-pharmacodynamic analysis of KHK2455 in patients with locally advanced or metastatic solid tumors. Abstract 1368. Poster AACR 2021, July 01, 2021.
5. Mehta K and Vinnard C. Impact of SLCO1B1 genotype and single nucleotide polymorphism on rifampin pharmacokinetics using linkage analysis and physiologically-based pharmacokinetic (PBPK) modeling approach. Poster ACoP10, October 2019.

Acknowledgements

Pursuing this PhD has been a remarkable journey of learning for me. I would like to thank many people who supported or inspired me throughout my academic, professional, and personal journey that shaped me to be who I am today.

Foremost, I thank my promoters, Prof. Dr. J. G. Coen van Hasselt and Prof. Dr. Piet Hein van der Graaf, for the opportunity and guidance. Coen, your insightful feedback and unwavering support has been instrumental in achieving this key milestone for me. Your guidance has especially equipped me with the skills to formulate research strategies and to articulate the research results clearly and efficiently, and I will use these skills throughout my professional journey. Piet Hein, your mentorship and constructive criticism has empowered me to focus on overarching goals and has driven me to pursue excellence in my endeavors. I am truly grateful to both of you for everything.

I thank all our co-authors and collaborators on various projects in this thesis. I would like to sincerely thank Tingjie Guo for reviewing and discussing the model codes and manuscripts. I express my gratitude to Christopher Vinnard, Herman Spaink, Tom Ottenhoff, Robert Wallis, and Pavel Balaski for dedicating their time and expertise in reviewing the manuscripts in their respective areas. I also thank Joga Gobburu for introducing me to the career in pharmacometrics and mentorship.

I am grateful for my parents, Ullas and Haresh Shah, for their unconditional love and for always believing in me. I thank my children, Krisha and Keval Mehta, for their love and enthusiasm as I pursued this PhD. Lastly but most importantly, I want to express gratitude to my husband, Jinesh Mehta, for being by my side and providing unwavering support through all the highs and lows. Jinesh, you always encouraged me to push the limits, whether conquering challenging mountain hikes or embarking on this ambitious journey of pursuing a PhD alongside other responsibilities.

Thank you,

Krina